Ministry of Higher Education and Scientific Research
Babylon University
College of Engineering
Department of Mechanical Engineering

Design of Axisymmetric Supersonic Air Intake

A Thesis

Submitted to the College of Engineering of the University of Babylon in Partial Fulfillment of the Requirements for the Degree of Master of Science in Mechanical Engineering

By

Hussain Kadhim Al-Shukri

B. SC. ٢٠٠٠

Supervisors

Dr.	**Dr.**
Arkan K. Al-Taie	**Abdul Kareem A. Wahab**

September ٢٠٠٣

وزارة التعليم العالي والبحث العلمي
جامعة بابل
كلية الهندسة
قسم الهندسة الميكانيكية

تصميم أخذة هواء فوق صوتية متناضرة حول محورها

أطروحة

مقدمة إلى كلية الهندسة في جامعة بابل
كجزء من متطلبات نيل درجة الماجستير علوم
في الهندسة الميكانيكية

أعدت من قبل

حسين كاظم الشكري

بكالوريوس ٢٠٠٠

المشرفون

د. أركان خلخال الطائي　　　　د. عبد الكريم عبد الوهاب

أيلول ٢٠٠٣

الخلاصـــــــــــة

تمت دراسة أخذة هواء فوق صوتية, ذات شكل هندسي ثابت, متناضر حول المحور, وذات أنضغاط خارجي بمخروطين (ثنائية المخروط) (نضام ثلاثي الصدمة). في هذا البحث, تم تقسيم أخذة الهواء إلى جزئين خارجي وداخلي, بحيث أن كل جزء حلّل وصمّم مثالياً بمعزل عن الأخر.

ظروف التصميم كانت عند (رقم ماخ (M_∞ = ٢), الارتفاع (H = ١٠٠٠٠ m), و معدل تدفق الكتلة($\dot{m} = 30 Kg/sec$).

الجزء الخارجي، يتكون هذا الجزء من مخروطين مبتدأ من راس المخروط الأول وصولا إلى مدخل الأخذة , حيث بداية الجزء الداخلي. افترض الجريان انضغاطي, مخروطي, غير لزج, مستقر, وشبه ثلاثي الأبعاد (متناظر حول محوره). استخدمت طريقة (Taylor-Maccoll) والمعتمدة على طريقة (Runge-Kutta) للتكامل العددي لحل معادلات الجريان (الزخم والاستمرارية) بالإحداثيات الكروية. تم تحليل هذا الجزء لعدة أرقام لماخ (٥ to ١.١~) وزوايا مخروط (°٥٠ to °١٠), بحيث تم حساب زوايا الصدمة المخروطية و كذلك كافة خواص الجريان ابتداءً من موجة الصدمة المخروطية وصولاً إلى سطح المخروط. تم إثبات صحة النتائج بمقارنتها مع معادلات ذات صيغ تجريبية وكانت الدقة مقبولة. تم تصميم هذا الجزء مثالياً للحصول على أعلى ضغط إرجاعي كلي.

الجزء الداخلي، يتكون هذا الجزء من ناشر ملتمّ-منفرج مبتدأ مباشرةً من نهاية الجزء الخارجي وصولاً إلى وجه الضاغط. ظروف الخروج من الجزء الخارجي سوف تكون ظروف الدخول للجزء الداخلي. افترض الجريان انضغاطي, غير لزج, مستقر, وشبه ثلاثي الأبعاد (متناظر حول محوره(ناشر حلقي)). استخدمت طريقة الحل العددي المعتمدة على تكنولوجيا الفروقات المحددة (Finite Difference) لحل معادلات الجريان (الزخم, الاستمرارية, الطاقة, والحالة) بالإحداثيات الأسطوانية حلاً تكرارياً بواسطة استخدام طريقة (Newton-Raphson). عمليات التصميم ركّزت على الجزء المنفرج من الأخذة, بينما أستخدم الجزء الملتم كضاغط أيسنتروبي لتقليل الجريان الفوق صوتي إلى جريان صوتي أو صوتي تقريباً, حيث انه الصدمة العمودية في الشروط التصميمية تعمل على فصل الجزئين عند منطقة العنق. تم تحليل الجزء المنفرج لعدة نسب مساحة و زوايا ميلان الجدار.

النتائج العددية للجزء الخارجي بينت بأن الجريان حول المخروط والمبتدأ بفوق صوتي مباشرةً خلف الصدمة أما يبقى فوق صوتي أو ينتهي بجريان دون صوتي عند سطح معين (مخروط صوتي), حيث أن مجال الجريان في الحالة الثانية هو خليط فوق ودون صوتي. أخيراً الجريان والمبتدأ بدون صوتي مباشرةً خلف الصدمة, سيُلزم بالبقاء دون صوتي.

الضغط الكلي الرجوعي يزداد مع زيادة زاوية المخروط الأول بثبوت زاوية المخروط الثاني, حتى يصل إلى أعلى قيمه عند ($\delta_{c١} = ٢٠°$) بعدها يقل, كذلك يزداد مع زيادة زاوية المخروط الثاني بثبوت زاوية المخروط الأول حتى يصل إلى أعلى قيمة عند ($\delta_{c٢} = ١٨°$) بعدها يقل.

النتائج العددية للجزء الداخلي بينت بأن مركبة السرعة الخطية تتناقص مع المسافة وتزداد مع زيادة الزاوية لنفس نسبة المساحة قرب المدخل وتقريباً نفس قيمة السرعة عند المخرج, كذلك تتناقص مع زيادة نسبة المساحة لنفس الزاوية.

مركبة السرعة الشعاعية تزداد مع المسافة لنفس الزاوية وتزداد مع زيادة الزاوية ومع زيادة نسبة المساحة.

رقم ماخ يتصرف كمركبة السرعة الخطية مع المسافة. رقم ماخ عند مقطع الخروج يتناقص من قيم عالية إلى واطئة (دون صوتي) مع زيادة المسافة من الجدار الأفقي إلى المائل لنفس نسبة المساحة ويتناقص مع زيادة نسبة المساحة. أبعاد الشكل الهندسي للتصميم الأفضل لهذا الجزء هو عند, ($AR = ١.٣٥$ و $\theta = ٧^{\circ}$), حيث تم إثبات صحة قيمة الزاوية عن طريق المصدر [٣٩].

قيم التصميم الكلي للأخذة فوق الصوتية هي: -

$\delta_{c١} = ٢٠^{\circ}$, $\delta_{c٢} = ١٨^{\circ}$, $L_N = ٢٣.٥٢٤٧١$ cm, $L_W = ١٧.٦٦٣٨٠٥٥$ cm, $h_{co} = ٢٣.٥٢٤٧١$ cm, $r_١ = ٧.٢٧٧٩٨$ cm, $r_{th} = ٧.٠٨٢٦٣$ cm, $r_٢ = ١١.٠٤٦٣١$ cm, $L_١ = ٢.٥$ mm, $L_٢ = ٣٢.٢٨١٣٥$ cm, $\theta = ٧^{\circ}$, $L_{overall} = ٥٦.٠٥٦٠٦$ cm.

تم فحص هذا التصميم للارتفاعات و لأرقام ماخ مختلفة.

ABSTRACT

A theoretical investigation for a supersonic air intake was made, in which the type of supersonic air intake considered was a fixed geometric axisymmetry external compression with two-cone (bicone) (٣-shock system). In this investigation, air intake was divided into two parts, external and internal parts, each part was analyzed and designed optimally separated from the other.

The design conditions was at (M_∞ = ٢, altitude (H) = ١٠٠٠٠ m, and mass flow rate $(\dot{m}) = 30\,\mathrm{Kg/sec}$).

For the external part, this part consists of two- cones, began with the vertex of the first cone up to inlet of intake, where the internal part was begun. The flow is assumed inviscid conical compressible, steady state, and quasi three-dimensional (axisymmetric). The flow equations (Momentum and continuity) in spherical coordinate system, was solved by using Taylor- Maccoll method which depended on the numerical integral Runge-Kutta method. This part was analyzed for several Mach numbers (~١.١ to ٥) and cone angles (١٠° to ٥٠°). Where the conical shock wave angle and all flow properties are determined from the conical shock wave to the surface of cone. The accuracy of the results is very high, where validated by comparison with empirical formula equations. This part optimized to get on a maximum total pressure recovery.

For the internal part, this part consists of a converge-diverge diffuser, began immediately down of external part up to the face of compressor. The exit conditions from the external part will be the inlet conditions for internal part. The flow is assumed inviscid compressible, steady state, and quasi three-dimensional (axisymmetric (annular diffuser)). The flow equations (Momentum, continuity, energy, and state) in cylindrical coordinate system, was solved by using numerical solution based on a finite difference technique, where the set of equations governing the problem is to be solved iteratively by using Newton-Raphson method. The designing process was concentrated on the diverge portion of the diffuser, while the converge portion was used as isentropic compression to

decrease supersonic flow to sonic or nearly sonic flow, where at on design condition the normal shock separated these two portions at the throat section. The diverge portion was analyzed for different area ratios and angles of diverge wall.

The numerical results for external part showed that, the flow over cone which is initially supersonic just behind the shock front may either remain supersonic or go over to a subsonic flow at some surface (sonic surface), where in the latter case, the flow field is mixing supersonic and subsonic. Finally, a flow, which is initially subsonic behind the shock, will necessary remain subsonic.

The total pressure recovery increases with increase the first cone angle for constant second cone angle until it reaches to maximum value at ($\delta_{c١}$ = ٢٠°) then decreases, also increases with increase the second cone angle for constant first cone angle until it reach maximum value at ($\delta_{c٢}$ = ١٨°) then drop.

The numerical results for the internal part showed that, the axial velocity component decreases with distance and increases with the increase angle for the same area ratio near the inlet and approximately the same value at the exit, also decreases with increase area ratio for the same angle.

The radial velocity component increases with distance for the same angle and increases with increase angle and with increase area ratio.

Mach number behaves as axial velocity components with distance. Also Mach number at the exit section decreases with increase distance from straight to diverge wall for the same area ratio. The geometry for optimum design of this part is a [AR = ١.٣٥ and θ = ٧°], where the latter value is validated from ref. [٣٩].

The overall design data for supersonic air intake are: -
$\delta_{c١}$ = ٢٠°, $\delta_{c٢}$ = ١٨°, L_N = ٢٣.٥٢٤٧١ cm, L_W = ١٧.٦٦٣٨٠٥٥ cm, h_{co} = ٢٣.٥٢٤٧١ cm, $r_١$ = ٧.٢٧٧٩٨ cm, r_{th} = ٧.٠٨٢٦٣ cm, $r_٢$ = ١١.٠٤٦٣١ cm, $L_١$ = ٢.٥ mm, $L_٢$ = ٣٢.٢٨١٣٥ cm, θ = ٧°, $L_{overall}$ = ٥٦.٠٥٦٠٦ cm.

This design was tested for different Mach numbers and altitudes.

بسم الله الرحمن الرحيم

يؤتي الحكمة من يشاء ومن يؤت

الحكمة فقد أوتي خيرا كثيرا وما

يذكر إلا أولو الألباب

صدق الله العلي العظيم

سورة البقرة ٢٦٩

ACKNOWLEDGMENTS

(In The Name of Allah, The Gracious, The Merciful)

Praise be to "**ALLAH**" and his prophet **"Mohammed**". This research has been completed under their benediction.

I would like to express my deepest thanks and gratitude to my supervisors, **Dr. Arkan K. AL-Taie** and **Dr. Abdul Kareem A. Wahab** for their great support, guidance, advice and assistance throughout the various stages of the present work.

I am also indebted to the head (Dr. Ala M. Hosain) and staff of Mechanical Engineering Department, and advanced computer laboratory for their facilities during my work.

I record my sincere gratitude to my family and especially to my father and mother for his assistance, encouragement and support during the period of preparing this work.

Finally, I would also like to thank all my friends in Babylon University and out of it especially **Miss. Sahar** in library of Technology University for their helpful and encouragement during the entire period of this research.

Hussain Kadhim Holwass

٢٠٠٣

APPENDIX – A

DERIVATION OF EQUATIONS (٣.١٥) AND (٣.٢٨): -

Equation (٣.١٥) is drove as follows: -

By applying the differential form of the energy equation for a steady one-dimensional flow, between two-points for adiabatic, no external work (dQ = dw = ٠) and negligible a potential energy term (g (z٢-z١)), so.

$$h_1 + \frac{V_1^2}{2} = h_2 + \frac{V_2^2}{2} = \text{constant} \quad \textbf{...(A١.١)}$$

For a perfect gas flow, dh = c_P T

Assume that "c_P" is not a function of " T ".

Hence,

$$c_P T_1 + \frac{V_1^2}{2} = c_P T_2 + \frac{V_2^2}{2} = c_P T + \frac{V^2}{2} = \text{constant} \quad \textbf{...(A١.٢)}$$

Also for a perfect gas,

$$c_P = \frac{\gamma R}{(\gamma - 1)} \quad \textbf{...(A١.٣)}$$

$$a^2 = \gamma RT \quad \textbf{...(A١.٤)}$$

Substitute equations (A١.٣), (A١.٤) in equation (A١.٢) to get,

$$\frac{a_1^2}{\gamma - 1} + \frac{V_1^2}{2} = \frac{a_2^2}{\gamma - 1} + \frac{V_2^2}{2} = \frac{a^2}{\gamma - 1} + \frac{V^2}{2} = \text{constant} \quad \textbf{...(A١.٥)}$$

$$M = \frac{V}{a} \quad \textbf{...(A١.٦)}$$

So,

Then,

$$a_1^2\left(1+\frac{\gamma-1}{2}M_1^2\right)=a_2^2\left(1+\frac{\gamma-1}{2}M_2^2\right)=a^2\left(1+\frac{\gamma-1}{2}M^2\right)=\text{constant} \qquad \textbf{...(A١.٧)}$$

If the station (٢) is sonic flow $\Longrightarrow$ $M_٢ = ١$ $\longrightarrow$ $a_٢ = a^*$

Where V٢ = $a_٢$

Then,

$$a^2\left(1+\frac{\gamma-1}{2}\frac{V^2}{a^2}\right)=\frac{\gamma+1}{2}a^*$$

$$a^2+\frac{(\gamma-1)}{2}V^2=\frac{\gamma+1}{2}a^*$$

Then,

$$\left(\frac{a}{a^*}\right)^2=\frac{\gamma+1}{2}-\frac{(\gamma-1)}{2}\left(\frac{V}{a^*}\right)^2=\frac{\gamma+1}{2}-\frac{\gamma-1}{2}M^{*2} \textbf{...(A١.٨)}$$

Equation of (M^*) as function of local Mach number (M) , is drived as follows: -

$$M^{*2}=\left(\frac{V}{a^*}\right)^2*\left(\frac{a}{a}\right)^2=M^2\left(\frac{a}{a^*}\right)^2 \textbf{...(A٢.١)}$$

Then,

$$\left(\frac{a}{a^*}\right)^2=\left(\frac{M^*}{M}\right)^2 \qquad \textbf{...(A٢.٢)}$$

Substitute equation (A٢. ٢) in equation (A١. ٨), to get: -

$$\frac{\gamma-1}{2}M^{*2}+\left(\frac{M^*}{M}\right)^2=\frac{\gamma+1}{2}$$

Then,

$$M^{*2}=\frac{(\gamma+1)M^2}{2+(\gamma-1)M^2} \textbf{..(A٢.٣)}$$

APPENDIX – B

Runge-Kutta Integration Method: -

Runge-Kutta Integration Method is one of many numerical methods for solving of the ordinary differential equation, but this method has more accuracy than other method. Runge-Kutta method may be driven for any order. The most popular Runge-Kutta method is the fourth-order, which presented as follows: -

$$y_{n+١} = y_n + \frac{1}{6}(k_١ + ٢k_٢ + ٢k_٣ + k_٤)$$

$$k_١ = f_١(x_n , y_n , z_n) h$$

$$k_٢ = f_١(x_n+ \frac{h}{2}, y_n+ \frac{k_1}{2}, z_n + \frac{l_1}{2}) h$$

$$k_٣ = f_١(x_n+ \frac{h}{2}, y_n+ \frac{k_2}{2}, z_n + \frac{l_2}{2}) h$$

$$k_٤ = f_١(x_n+ h , y_n+ k_3 , z_n + l_3) h$$

$$z_{n+١} = z_n + \frac{1}{6}(l_١ + ٢l_٢ + ٢l_٣ + l_٤)$$

$$l_١ = f_٢(x_n , y_n , z_n)$$

$$l_٢ = f_٢(x_n+ \frac{h}{2}, y_n+ \frac{k_1}{2}, z_n + \frac{l_1}{2}) h$$

$$l_٣ = f_٢(x_n+ \frac{h}{2}, y_n+ \frac{k_2}{2}, z_n + \frac{l_2}{2}) h$$

$$l_٤ = f_٢ (x_n+ h , y_n+ k_3, z_n + l_3) h$$

Where,

h …. Step.

APPENDIX – C

Newton-Raphson method for system of equations: -

Consider the following system of nonlinear algebraic equations, evaluated at $x_1,\ldots,x_n$: -

$$
\begin{aligned}
&F_1(x_1,x_2,\ldots,x_n)=F_1(x_i)\\
&F_2(x_1,x_2,\ldots,x_n)=F_2(x_i)\\
&\qquad\vdots\\
&F_n(x_1,x_2,\ldots,x_n)=F_n(x_i)
\end{aligned}
$$

Using Taylor series, where the functions $F_{١}$, $F_{٢}$, …, F_n can be evaluated at $x_{١}+h_{١}$, $x_{٢}+h_{٢}$, …, x_n+h_n by expanding about the initial values $x_{١}$, …,x_n. Thus,

$$
\begin{aligned}
&F_1(x_1+h_1,x_2+h_2,\ldots,x_n+h_n)=F_1(\bar{x}_i)\\
&F_2(x_1+h_1,x_2+h_2,\ldots,x_n+h_n)=F_2(\bar{x}_i)\\
&\qquad\qquad\vdots\\
&F_n(x_1+h_1,x_2+h_2,\ldots,x_n+h_n)=F_n(\bar{x}_i)
\end{aligned}
$$

$$
\left.
\begin{aligned}
&F_1(\bar{x}_i)=F_1(x_i)+\sum_{j=1}^{n}h_j\frac{\partial F_1(x_i)}{\partial x_j}\\
&F_2(\bar{x}_i)=F_2(x_i)+\sum_{j=1}^{n}h_j\frac{\partial F_2(x_i)}{\partial x_j}\\
&\qquad\qquad\vdots\\
&F_n(\bar{x}_i)=F_n(x_i)+\sum_{j=1}^{n}h_j\frac{\partial F_n(x_i)}{\partial x_j}
\end{aligned}
\right\}
\qquad \textbf{...(C.١)}
$$

Equations (C.١) represent a truncated Taylor series in which only the linear terms are retained, which is why this method is sometimes referred to as the "linear method". Therefore, forcing the functions $F_1(\bar{x}_i),\ldots,F_n(\bar{x}_i)$ to be zeros permits the derivation of an iterative formula for determining roots of nonlinear algebraic equations, that is,

$$0 = F_1(x_i) + \sum_{j=1}^{n} h_j \frac{\partial F_1(x_i)}{\partial x_j}$$

$$0 = F_2(x_i) + \sum_{j=1}^{n} h_j \frac{\partial F_2(x_i)}{\partial x_j}$$

$$\vdots$$

$$0 = F_n(x_i) + \sum_{j=1}^{n} h_j \frac{\partial F_n(x_i)}{\partial x_j}$$

Expanding, then using the matrix form yields:

$$\begin{bmatrix} \frac{\partial F_1(x_i)}{\partial x_1} & \frac{\partial F_1(x_i)}{\partial x_2} & \cdots & \frac{\partial F_1(x_i)}{\partial x_n} \\ \frac{\partial F_2(x_i)}{\partial x_1} & \frac{\partial F_2(x_i)}{\partial x_2} & \cdots & \frac{\partial F_2(x_i)}{\partial x_n} \\ \vdots & \vdots & & \vdots \\ \frac{\partial F_n(x_i)}{\partial x_1} & \frac{\partial F_n(x_i)}{\partial x_2} & \cdots & \frac{\partial F_n(x_i)}{\partial x_n} \end{bmatrix} \begin{Bmatrix} h_1 \\ h_2 \\ \vdots \\ h_n \end{Bmatrix} = -\begin{Bmatrix} F_1(x_i) \\ F_2(x_i) \\ \vdots \\ F_n(x_i) \end{Bmatrix} \qquad \textbf{...(C.٢)}$$

Or more simply

$$[J]\{h\} = -\{F\}$$

Where:

$\{h\}$… Increments vector.

$\{F\}$… Function matrix.

$\{J\}$… Jacobian matrix (matrix of partial derivatives).

Solving for the increments vector gives:

$$\{h\} = -[J]^{-1}\{F\} \qquad \textbf{...(C.٣)}$$

However, since $h_1 = \bar{x}_1 - x_1,\ h_2 = \bar{x}_2 - x_2,\ ...,\ h_n = \bar{x}_n - x_n$ substitute into equation (C.٣) yields: -

$$\{\bar{x}\} = \{x\} - [J]^{-1}\{F\} \qquad \textbf{...(C.٤)}$$

CHAPTER ONE

1

INTRODUCTION

١.١ GENERAL: -

Aircraft propulsion systems can be classified according to flight speed into subsonic (M<١) and supersonic (M≥ ١), Fig. (١.١) illustrates the major types of propulsion systems and their types of intakes.

The subsonic propulsion system can be classified into four types according to the value of Mach number.

The piston-prop (M<٠.٥) was the first form of air craft propulsion system, where today piston-props are mainly limited to light airplanes and some agricultural aircrafts.

The turbo-prop and turbofan propulsion systems both use a turbine to extract mechanical power from the exhaust gases.

For the turbo-prop propulsion system (M≤ ٠.٥), the outside air is accelerated by a conventional propeller.

For the by pass turbofan propulsion system (M<١), the air is accelerated with a ducted fan of one or several stages.

The "By pass ratio" is the mass-flow ratio of the bypassed air to the air that goes into the core of the engine, the value of high-bypass-ratio can be equaled to "٦". The type of intake used for prop-fan, and high by pass ratio-turbofan (M≤ ١), propulsion system is a pitot intake type as shown in Fig. (١.٢.a).

The supersonic propulsion system can also be classified into five types according to the value of Mach number.

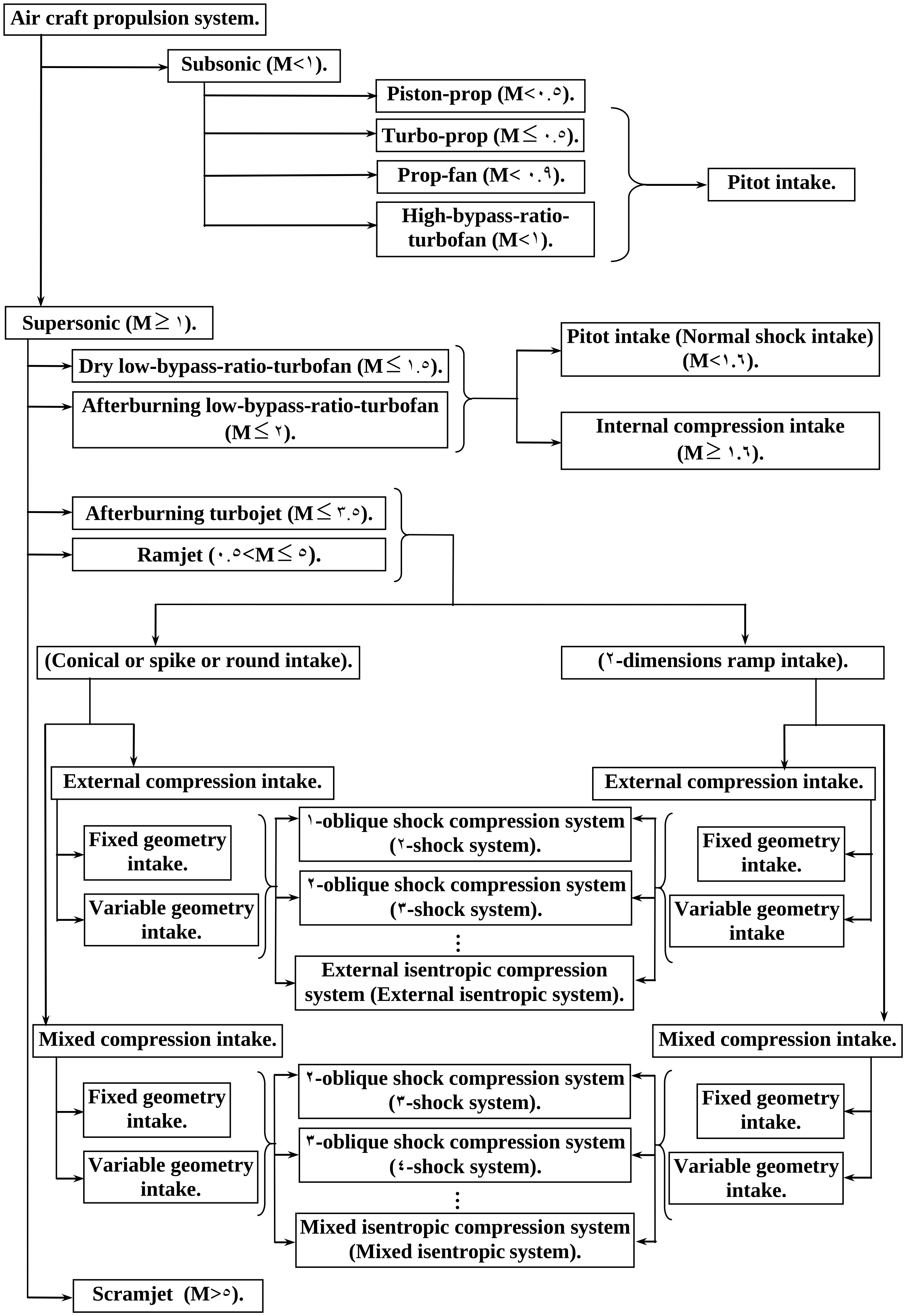

Fig. (١.١) Aircraft propulsion systems and its types of intakes.

In some of supersonic propulsion systems air to fuel mixture ratio is about (٦٠ to ١), where only about a quarter of this ratio is used for combustion and the remaining is for cooling. If fuel is injected into this largely uncombusted hot air, it will mix and burn, this will raise the thrust as much as a factor of two and is known as “afterburning“, this process used in some of low-bypass-ratio turbofan and turbojet. The type of intake of (dry low-bypass-ratio turbofan (M<١.٥) and afterburning low-bypass-ratio turbofan (M≤٢)) is either a pitot intake or an internal compression intake, according to the value of design Mach number. Where for (M<١.٦) used a pitot intake type (normal shock type) Fig. (١.٢.b), and for (M≥ ١.٦) used internal compression intake type Fig. (١.٢.c).

The ramjet propulsion system (٠.٥<M≤٥) is used for fast traveling aircraft. There are two types of intakes used for afterburning turbojet (M<٣.٥) and ramjet propulsion system, they are (two-dimensions ramp intake) and (conical or spike or round intake), as shown in Fig. (١.٢.d and e), respectively. Each of these two types of intakes may be subdivided to two another types, (fixed and variable geometry intakes). Where variable geometry, can be achieved by changing the angles of, and/or translating, the supersonic compression surfaces, as shown in Fig. (١.٣). External and mixed fixed and variable geometry intakes may be divided into a number of types according to the numbers of shock waves, which may be generated on the surface of compression as in Figs. ((١.٤) and (١.٥)).

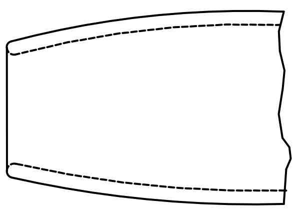

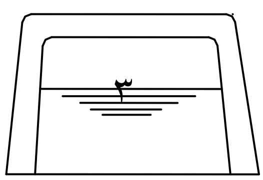

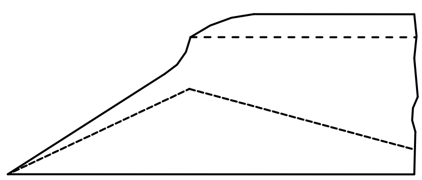

a. Pitot intake

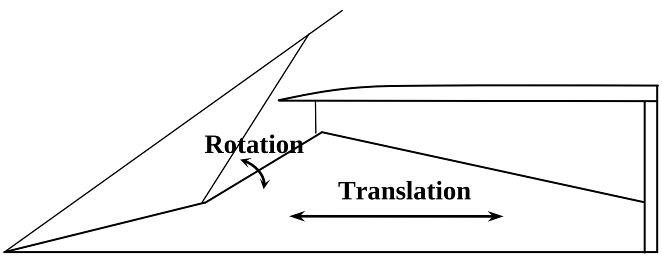

Fig. (١.٣) Supersonic variable geometry intake, [٢٩].

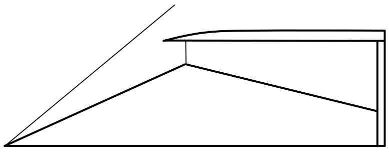

١-Oblique shock compression system (٢-shock system).

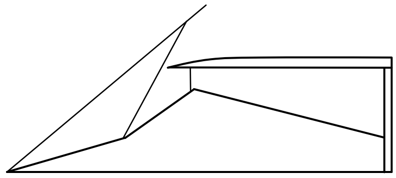

٢-Oblique shock compression system (٣-shock system).

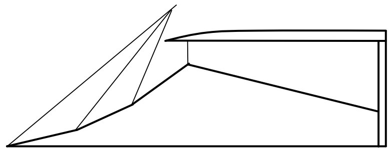

٣-Oblique shock compression system (٤-shock system).

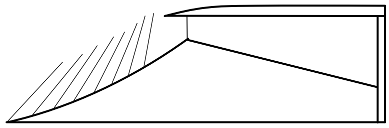

External isentropic compression system (External isentropic system).

Fig. (١.٤) Supersonic intake-external compression, [٤٢].

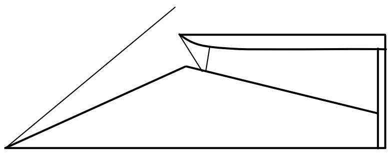

٢-Oblique shock compression system (٣-shock system).

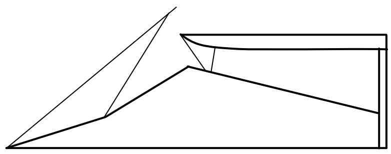

٣-Oblique shock compression system (٤-shock system).

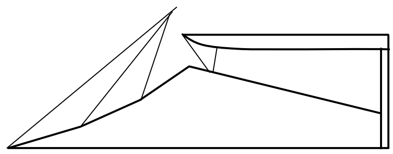

٤-Oblique shock compression system (٥-shock system).

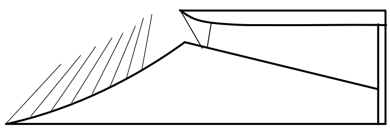

Mixed isentropic compression system (Mixed isentropic system).

Fig. (١.٥) Supersonic intake-mixed compression, [٤٢].

١.٢ SUPERSONIC INTAKE: -

The supersonic intakes have been developed since the Second World War, in parallel with the development of the jet engine itself, so due to this development supersonic intakes have many different shapes, but for the same basic function. The intake consists of a duct (rectangular, cylindrical or conical) with fixed or variable geometry depending on the surface of compression or spike moving inside the intake Fig. (١.٣). The supersonic intake consists of two parts, supersonic part (shock wave part) which consists of number of shock waves (oblique or conical) and finished with a weak or a strong normal shock wave depending on its position from intake, the another is subsonic part (shockless part), where this part consists of divergent walls (diffuser). Where the subsonic flow will be further slowed down to the speed required by the engine. Thus, a diffuser is increasing in a cross-sectional area from front to back, as shown in Fig. (١.٦).

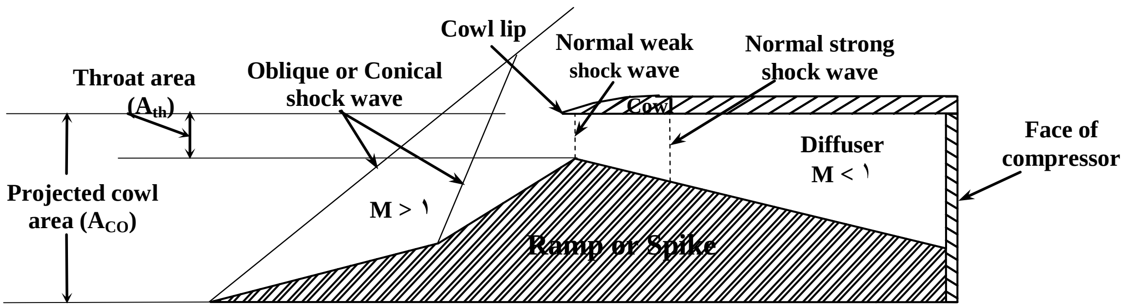

Fig. (١.٦) Supersonic intake.

The basic function of a supersonic air intake is to supply the correct quantity and quality of air to the compressor face of the engine. The correct mass flow of air must be delivered to the compressor face at about Mach ٠.٣~٠.٥, with acceptable velocity distribution with as little loss of stagnation pressure (P_o) as possible. Consequently the intake delivers air to the compressor at a static pressure considerably greater than ambient and it is, therefore, able to contribute significantly to the cycle compression process Fig. (١.٧) [٢٩], where the intake is required to do this at all flight conditions and at least weight, cost, and drag.

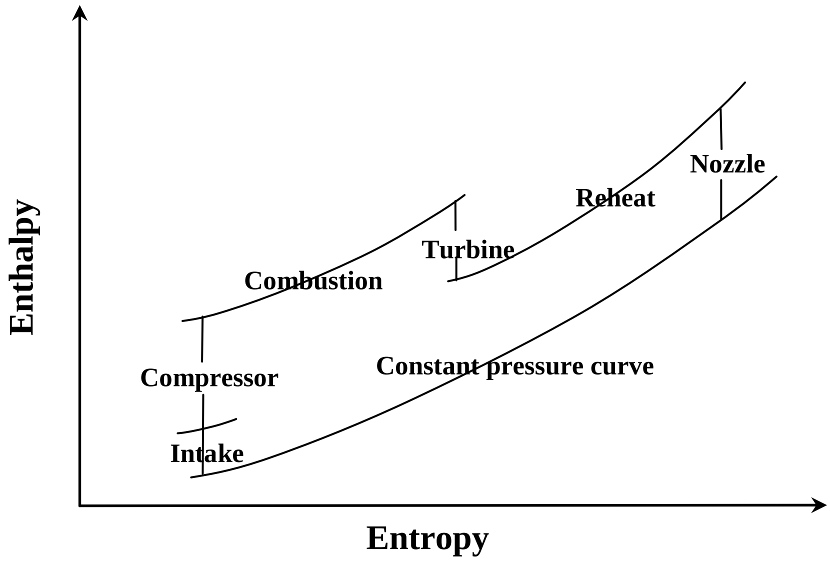

Fig. (١.٧) Supersonic gas turbine cycle [٢٩].

١.٣ THE AIM OF THE WORK: -

A- The aim of the present work is to design an axisymmetric bicone supersonic air intake, as follows: -

١- Design the geometry of the external part and analyze the supersonic flow around the cone.

٢- Design the geometry of the internal part.

B- Performance study: -

i- On design.

The on design conditions are Mach number (M = ٢), ($\dot{m} = 30$ kg/sec), and the flow properties are at an altitude of (H = ١٠٠٠٠ m).

ii- Off design.

The values of Mach number and flow properties are then changed to predict the intake flight envelope.

The analysis requires establishment of master computer program, which has the ability to analyze the flow structure in supersonic and subsonic airflow. To achieve this goal, a preliminary program is to be implemented to state the inlet boundary condition to the master program, by taking into account the conical shock system. The system of equations (momentum and continuity) in spherical coordinate is applicable to flow behind a shock wave, where the properties of flow are calculated at the nose of the intake.

The results are to be obtained at a different flow Mach number, different angles of cone, different altitudes, and at different area ratios for subsonic portion, where optimization is the final goal.

CHAPTER TWO

LITERATURE REVIEW

2

٢.١ General: -

This chapter consists of a brief review of the related works on design and analysis of supersonic intakes. A difficulty is met in getting up to date detailed informations of intake design and analysis necessary for verification of the results.

٢.٢ EXPERIMANTAL INVESTIGATION: -

The first serious work on supersonic inlets was done by **Oswatitsch, ١٩٤٤, [١],** in Germany during the World War II when he performed a series of pioneering analytical and experimental investigations.

The work was on a single and double-wedge intake and showed that for such a system in two dimensions, the maximum shock recovery is obtained when the oblique shocks are of equal strength. This means that Mach numbers perpendicular to the shocks are equal, as shown in Fig. (٢.١).

$\mathbf{M_{\infty} \sin\sigma_{١} = M_{١} \sin\sigma_{٢}} \ldots$

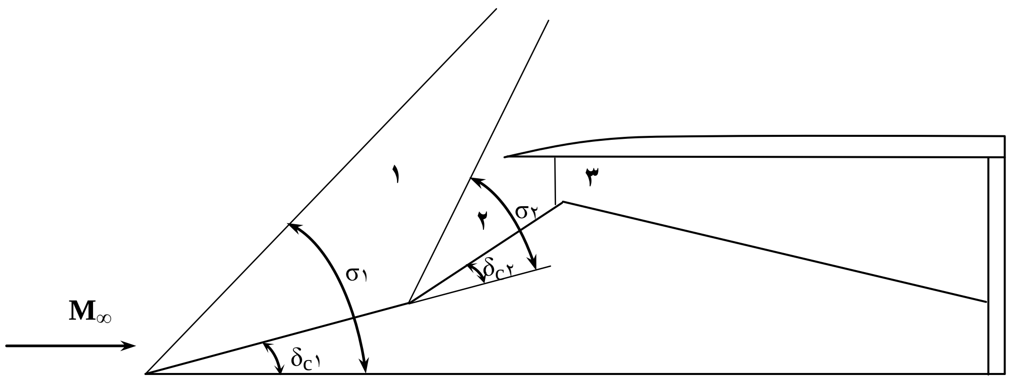

Fig. (٢.١) ٣-Shock intake showing wedge angles.

Brajnikoff, ١٩٤٨, [٢], used a model of an annular inlet having a ramp to create a single oblique shock wave in the ٨-by ٨-inch supersonic wind tunnel in the range of Mach numbers between ١.٣٦ and ٢.٠١. The results of the tests showed that the maximum total pressure recovery of the model investigated was considerably improved through the addition of a ramp where it is approximately equal to four~fifths of that of a normal shock wave occurring at the same free stream Mach number.

Ferri and **Nucci, ١٩٤٨, [٣],** presented a discussion of inlets having a circular cross section and a central body, designed for high Mach numbers. The optimum relationship between external and internal supersonic compression has been discussed with respect to the external drag and the maximum pressure recovery. Many models were tested at three streams Mach numbers of ٣.٣, ٢.٧٥, and ٢.٤٥ at zero angle of attach. Value of maximum pressure recovery and shadowgraphs for different combinations of central body relative to cowling have been given. The results of the tests have been analyzed and show that, with the proper selection of geometric and aerodynamic parameter, high pressure recovery and low drag can be obtained. Pressure recoveries of ٠.٥٧, ٠.٦٧, and ٠.٧٨ at Mach numbers of ٣.٣, ٢.٧٥, and ٢.٤٥ respectively have been obtained with very low external drag.

Ferri and **Nucci, ١٩٥٢, [٤],** presented a theoretical analysis on supersonic axisymmetric inlet with external compression fixed geometry, ٢-shock system. And showed that this type of inlet gives high-pressure recovery for a large range of Mach number and mass flow, and therefore it is practical for use on supersonic airplanes and missile. For some Mach numbers the drag coefficient for this type of inlet is larger than that for internal compression inlets, but the pressure recovery is larger for all flight conditions. Experimental results confirm the results of the theoretical analysis and show that pressure recoveries of (٩٥٪) for a Mach number of ١.٧٢ and (٨٦٪) for a Mach number of ٢.١ are possible with the configurations considered. If the mass flow decreases, the total drag coefficient increases gradually and the pressure recovery does not change appreciably.

Conners and **Meyer, ١٩٥٥, [٥],** presented an experimental investigation at Mach (١.٩). To determine the overall performance capabilities of axisymmetric two-cone (semi-angles of first and second cone are (٢٠^o) and (٢٨^o) respectively). And isentropic ((٢٠^o) tip cone semi-angle followed by isentropic surface to (٣٠.٢^o)), nose inlets in terms of total-pressure recovery, mass flow, and external drags. The test was done in ١٨-by ١٨-inch supersonic wind tunnel. The air was maintained at (T_O = ٨٣.٣٣٣∓٢.٧٧٨ ^{o}C), the simulated pressure altitude was approximately (١٣٧١٩.٥١٢٢ m). Schlieren photographs of the two models of the inlets airflow patterns are presented for different operations (supercritical, critical, and subcritical) and for different angles of attack (٠^o, ٤^o, and ٨^o). One of the results of investigation is critical total-pressure recovery for two-cone and isentropic inlets are ٠.٩٢ and ٠.٩٤ respectively.

McGregor, ١٩٧١, [٦], presented a study of theoretical parameter relevant to the performance of rectangular double ramp compression surface air intake at supersonic speeds. He stated that the principle of breaking down an external shock system could be extended to any desired number of stages. The theoretical shock pressure recovery of one oblique and one normal shock system (٢-shock system) and two obliques and one normal shock system (٣-shock system) constitute useful standards. One of results of study is the total pressure recovery, which is improved when the external part of supersonic intake extended to more than one stage.

Tindell, ١٩٨١, [٧], presented a testing of a semiconical and two-dimensional external compression inlets at Mach number (٢) in ١٥ by ١٥ inch supersonic wind tunnel at zero angle of attack. Both inlets have three-shock system with the same pressure recovery approximately. The first and second semicone angles are (١٩°) and (٢٩°) respectively, and the first and second two dimensions semi angles are (١٠°) and (٣٠°) respectively, where the effect of the compression system shock structure upon the inlet drag and stability was determined with other parameters for both inlets. The drag of semiconical inlet is found higher than that of the two-dimensional inlet and the stability of semiconical inlet is found higher than that of the two-dimensional inlet.

Shaikh, et al. ٢٠٠٠, [٨], designed a two-dimensional air intake for a ramjet propelled missile. The design takes into consideration the varying cruise Mach number, at a different altitude of flight. The design has been done to ensure an adequate air capture for a different missile operation. The half scale two-dimension intake model was tested in supersonic blowdown wind tunnel at Mach (٢) and (٢.٥) at zero angle of attack, the operation characteristic of the intake, i.e. pressure recovery vs. air mass capture ratio, was studied and presented for different back pressures.

Sandip Chattopadhyay, et al. ٢٠٠٠, [٩], presented an experimental investigation of two-dimensional, mixed-compression variable geometry supersonic air intake, by using supersonic wind tunnel at Mach (٢). Experiments mainly consist of flow visualization by shadowgraph and colour schlieren using transparent side plates made of perspex. The basic objective was to capture the details of flow field inside the intake. Tests have been conducted at different back pressure. Schlieren flow field has been compared with the pressure data and a good agreement is obtained.

٢.٣ NUMERICAL INVESTIGATION: -

Connors and **Meyer, ١٩٥٦, [١٠],** presented design charts for Mach numbers up to ٤, for single and double-oblique and conical-shock inlets and for isentropic axisymmetric and two-dimensional surfaces having theoretically focused Mach lines. Compression limits for isentropic inlets are presented. A comparison of optimum performance for various inlet configurations (normal shock, convergent-divergent (internal compression), single cone, double cone, and isentropic) is presented .The geometric angles of the single-and double cone inlets were optimized in terms of pressure recovery by using Taylor-Maccoll method.

Steger, ١٩٧٨, [١١], solved Euler equations by using finite-difference procedures which subjected to an arbitrary boundary condition. An automatic grid generation program is employed. Computational efficiency and compatibility to vectorized computer processors is maintained by the use of approximate factorization technique. Computer results for inviscid-flow about airfoils are described and compared to known solution.

Chen, et al. ١٩٨٠, [١٢], presented a method for calculating inviscid supercritical flow fields about axisymmetric inlet cowls with centerbodies. A finite-difference approximation to the full-potential equation is solved under a general coordinate transformation. The difference equations are solved by relaxation numerical method. Numerical results for pressure distributions are generally agreed well with the experiment.

Knight, ١٩٨١, [١٣], developed a numerical code to calculate the flow field in two-dimensional high-speed inlets using the Navier-Stokes equations. The code has applied to calculate the flow in a simulated high-speed inlet operating at a Mach (٢.٥) and Reynolds number of $1.4*10^7$ based on the inlet length. The computed results are compared with detailed measurements of the ramp and cowl static pressure. The agreement with the experimental data is generally good.

Bangert, et al. ١٩٨٢, [١٤], conducted an analytical study to determine the impact of flight Mach number on inlet type for a supersonic cruise aircraft. External and mixed-compression axisymmetric (two cone (bicone) and isentropic external compression) and two-dimensional (two wedge and isentropic external compression) inlets, were considered. The study was done at Mach (٢, ٢.٣, and ٢.٥٥). At Mach (٢) axisymmetric mixed-compression inlet provided the best aircraft range. At Mach (٢.٣), the two-dimensional mixed-compression inlet was the most attractive if enough variable geometry was incorporated to minimize the spillage during subsonic cruise.

Shimabukuro, et al. ١٩٨٢, [١٥], conducted an analysis study for various inlet-engine combinations for a Mach (٢.٢), to select a preferred inlet type for single-engine pod installations. These types of inlets included two-dimensional and axisymmetric with either mixed or external compression. The results of the study indicated that the axisymmetric mixed compression inlet was preferred. Detailed design studies of single and double cone axisymmetric mixed compression inlets types are discussed.

Lavante and, **Thompkins Jr., ١٩٨٣, [١٦],** presented a numerical method for solving the Navier-Stokes equations. This method is very similar to the MacCormack method. This method was tested on a number of numerical examples, including incompressible and compressible Coutte flow and a supersonic diffuser. The supersonic diffuser results were presented at free stream Mach number equal to (٢).

Biringen, ١٩٨٤, [١٧], outlines a time-implicit, finite-difference solution procedure for the Euler equations, to calculate two-dimensional inlet flow fields. This work focuses on the calculation of inviscid inlet flow fields with uniform and non-uniform inflow boundary condition. All the calculations were preformed at the design Mach number of the inlet (٣.٥). Results for a practical inlet configuration are presented. The method can be used for a flow field with both subsonic and supersonic regions and is found to converge rapidly for supercritical, and subcritical inlet operations. Convergence to steady state is slow.

Walters, et al. ١٩٨٦, [١٨], presented a numerical method for solving the compressible Navier-Stokes equations in conservative form. This method was tested on a number of numerical examples, one of them was a supersonic inlet. The supersonic inlet results were presented for (٥^{o}) wedge inlet at free stream Mach number equal to (٣). The results were in a good agreement with other methods, and/or experiments.

Bradley, et al. ١٩٨٦, [١٩], developed an artificial density method to determine full-potential equation for steady supersonic conical flow. Grid generation and transformation of coordinate are presented. The results were presented for circular and elliptic cones at different supersonic Mach numbers and angle of attack.

Moretti, ١٩٨٨, [٢٠], presented an efficient Euler computational technique for two-dimensional Euler equations at any number of shock of any shape and type, whose interaction can be treated by this technique. He presented the results for a number of examples, such as transonic airfoils, shocks in ducts, intake flows, multiple Mach reflections. The results for intake were at free stream Mach number equal to (٢), ended at outlet of duct of (٠.٣) Mach.

Gilding, ١٩٨٨, [٢١], presented a technique for the generation of boundary-fitted curvilinear coordinate system, for the numerical solution of partial differential equations in two-space dimensions. The technique is algebraic. Applications of numerical grid generation for problems in the field of computational fluid dynamics are presented.

Dimitri, ١٩٨٩, [٢٢], presented a simple theoretical method to determine the inviscide, steady state diffuser performance of a tunnel with two plane, parallel supersonic streams that come into contact downstream of a splitter plane and form an infinitely thin interface. The model predictions can be useful to the design and operation of supersonic wind tunnels and of aircraft engine.

Mittal, et al. ٢٠٠٠, [٢٣], presented a numerical method to solve compressible Euler equations for two-dimension mixed compression supersonic inlet. A stabilized finite-element method is employed. The computations are capable of simulating the start-up problems associated with mixed compression supersonic inlets. If the diffuser throat is not large enough to allow the start-up normal shock wave to pass through the inlet it unstarts. The computation method is presented for design Mach number (٣). The results were the start-up problem of inlet, which can be solved with either an increase of the throat area (variable geometry) or by increasing the free stream Mach number (fixed geometry).

Singh Th., et al. ٢٠٠٠, [٢٤], presented a studied of the field of axisymmetric, mixed-compression, supersonic air intakes for viscous flows. The governing equations of mass, momentum, energy, and state equation have been solved to obtain the complete flow field using the commercial software package (**FLUENT**). A comparative study is presented for different values of inlet Mach numbers. Critical, subcritical, and supercritical operations of the spike type air intake have been predicted accurately. The cowl inner wall static pressure distribution was in a good agreement with the experimental.

Geetha, et.al ٢٠٠٠, [٢٥], presented a study to optimize the turning angles of scramjet engine inlet, by using Lagrange multipliers for a maximum total pressure recovery at the inlet entry at the design Mach number condition (٧). The effect of number of forebody ramps and their turning angles on precompression effects. Intake parameters and aerodynamic characteristics are studied. One of the results obtained by the study is that the optimum design has shocks of equal strength.

٢.٤ SUMMARY: -

Summary of the literature cited yield that most types of supersonic air intake are investigated. But these investigations are concentrated solely on supersonic portion of air intake and ignore the subsonic portion, especially the experimental and some of numerical investigations. Also most of exposition results of these investigations are the variation of mass flow ratio with total-pressure recovery and ignore the effect of other properties of flow such as (pressure variation, temperature, density, velocity, Mach … etc). So,

١. To design the external part, the Taylor-Maccoll method will be used.

٢. To design the internal part, a numerical solution will be employed based on a finite difference technique, where the set of equations governing the problem will be solved iteratively by using Newton-Raphson method.

٣. The work will include writing a master program, which will solved iterativelly (momentum, continuity, energy, and state) equations in cylindrical coordinate.

٤. Due to the geometrical nature of the flow inside the intake. An axis transformation is required from the stream wise axis to numerical axis, i.e. regular mesh.

CHAPTER THREE

3

THEORY

٣.١: INTRODUCTION: -

The supersonic intake type considered as a fixed geometry axisymmetric external compression with two-cone (٣-shock system). When running on-design Mach number, the supersonic part consists of two conical shock waves, followed by a normal shock wave.

This chapter includes a description of the selected supersonic intake, and its operation conditions, also the formulation of the basic equations, which describe the flow in supersonic and subsonic portions.

٣.٢: OPERATIONAL DISCRIPTION OF SUPERSONIC INTAKE: -

Supersonic air intake considered as illustrated in Fig. (٣.١). It consists of two distinct portions, a supersonic and a subsonic. The supersonic part is formed between a two step spike and a cowl, while the subsonic part is essentially a divergent annular ducting.

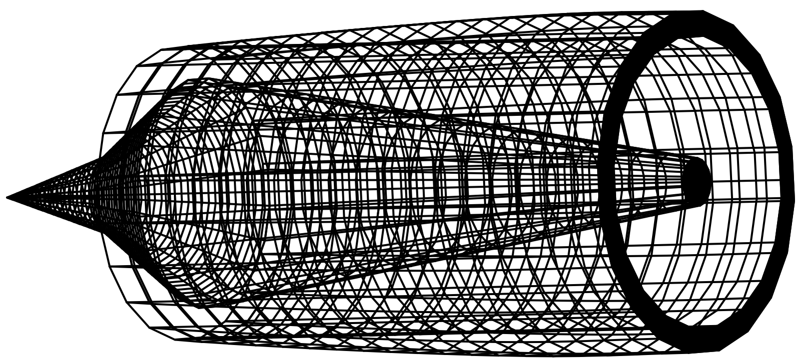

Fig. (٣.١) External compression supersonic air intake.

٣.٢.١: INTAKE OPERATING CONDITIONS: -

There are three distinct operating conditions under which the intake for an air-breathing engine can operate depending upon the backpressure, [٨].

a- **Critical Operation: -** when the pressure inside the compressor is such that the back pressure at the exit of the subsonic diffuser causes the normal shock to be positioned at the intake lip, it said to be critical Fig. (٣.٢.a). Other characteristics of this operation are:

- **i-** High total pressure recovery.
- **ii-** Full capture area ratio.
- **iii-** Low flow distortions.
- **iv-** Low drag.

b- **Super-critical Operation: -** when the compressor pressure drops to a value less than the static pressure at the exit of the subsonic diffuser causes the normal shock is swallowed, and the air flow in the subsonic diffuser becomes supersonic. This operating condition is called supercritical Fig. (٣.٢.b). Other characteristics of this operation are: -

- **i-** Low total pressure recovery.
- **ii-** Full capture area ratio.
- **iii-** High flow distortions.
- **iv-** Low drag.

c- **Sub-critical Operation: -** when the compressor pressure is higher than the static pressure at the exit of the subsonic diffuser, The flow becomes choked and the normal shock wave is expelled out from the intake and there is spill over of the incoming air over the intake lip. Operating under this condition is said to be subcritical Fig. (٣.٢.c). Other characteristics of this operation are: -

i- High total pressure recovery (if stable).

ii- Reduce capture area.

iii- High drag.

iv- The flow may be unstable i.e. buzz.

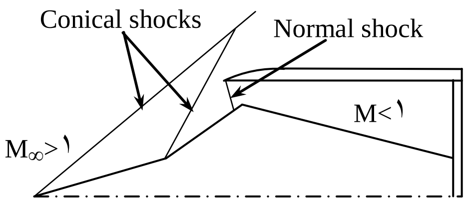

a- Critical operation.

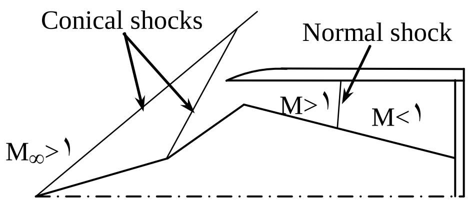

b- Supercritical operation.

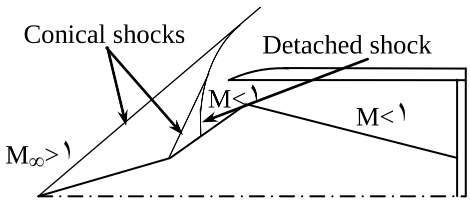

c- Subcritical operation.

Fig. (٣.٢) Intake operation conditions.

Fig. (٣.٣) depicts the various modes of intake operation on a plot of total pressure versus airflow. The total pressure recovery is shown ratioed to freestream total pressure, and the airflow is shown referenced to the airflow that would be captured by the cowl at freestream conditions, [٣٩].

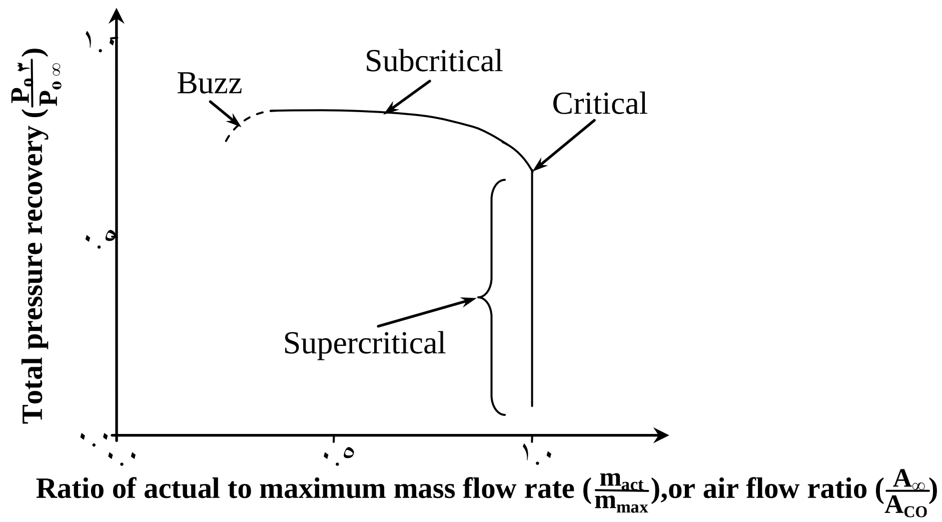

Fig. (٣.٣) Air-intake characteristic curve, [٢٥].

٣.٢.٢: MACH NUMBER: -

Intake under consideration is of a fixed geometry. Hence it operates on "on design" at only one Mach number, it's the design Mach number.

٣.٢.٢.١:DESIGN MACH NUMBER: -

At design Mach number, Fig. (٣.٤.a). The supersonic intake is characterized by: -

- All external compression shock waves are attached to the cowl lip.
- Freestream tube is equal to intake cowl area.
- No spillage air and the drag are small.

٣.٢.٢.٢:OFF-DESIGN MACH NUMBER: -

Off design Mach number may be interpreted as lower or higher than design Mach numbers.

At a lower Mach number, Fig. (٣.٤.b). The supersonic intake is characterized by: -

- All external shock waves move ahead of the cowl lip.
- Freestream tube of air is less than intake cowl area.
- High spillage air and drag.

At a higher Mach number, Fig. (٣.٤.c). The supersonic intake is characterized by: -

- All external shock waves move inside the cowl lip.
- Freestream tube of air capture is equal to intake cowl area.
- No spillage air and the drag is small.

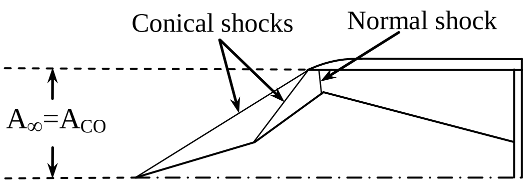

a- On design Mach number.

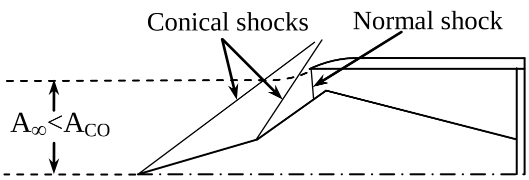

b- Below design Mach number.

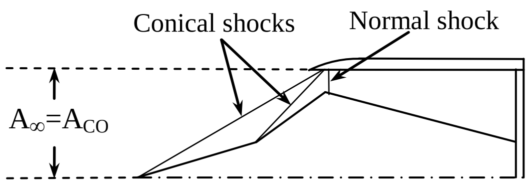

c- Above design Mach number.

Fig. (٣.٤) Intake flowfield characteristics.

The entry area (A_{CO})(streamtube 'capture' area at entry) is defined as the area enclosed by the leading edge, or 'highlight' of the intake cowl, including the cross-sectional area of the forebody in that plane. The maximum flow ratio achievable at supersonic speed occurs when the boundary of the freestream (A_∞) arrives undisturbed at the lip. This means that,

$$\frac{A_{\infty}}{A_{co}} = 1$$

The condition will be termed 'full flow'. Hence, the maximum flow occurs when the flow remains supersonic up to the entry. This means that the normal shock is at the lip or inside, [٣٨].

٣.٣:EXTERNAL PART: -

This part consists of a sharp cone with semi-vertex angle ($\delta_{C١}$), followed by a second cone with semi-angle ($\delta_{C٢}$) as in Fig. (٣.٥). The shocks generated due to the sharp cones in supersonic flow are called 'conical shock waves'. The flow behind the conical shock wave is itself conical, and called as 'conical flow', in such flows, the flow properties are constant along rays from the vertex

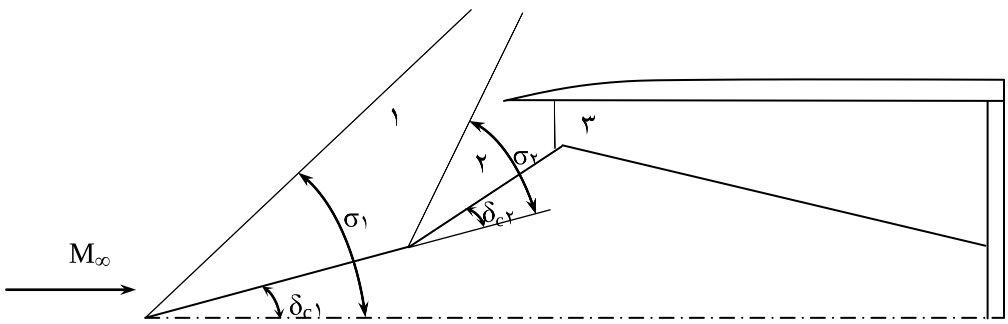

Fig. (٣.٥) ٣-Shock intake showing cone angles.

of a cone but varies along a streamline. The flow field between the shock and the cone surface is no uniform, where the flow area increases with increasing the distance from the centerline of the cone as in Fig. (٣.٦). The conservation of mass will require that the streamlines of flow downstream of a conical shock wave be curved as in Fig. (٣.٧),([٢٦], [٢٧], [٣٠], [٣١], [٣٢], [٣٣], [٣٥], [٤٤], and [٤٥]).

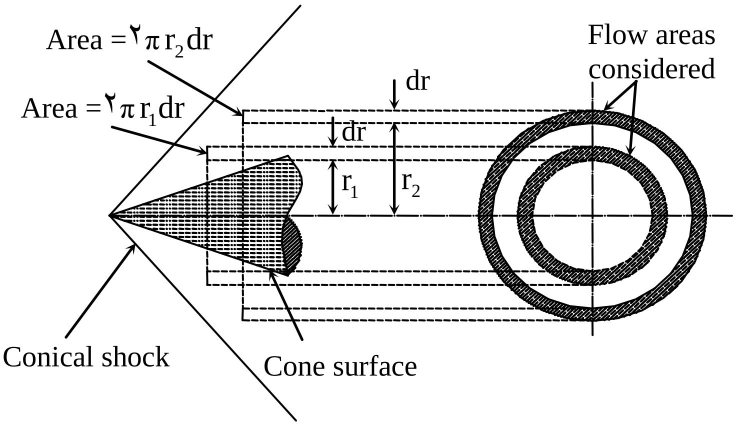

Fig. (٣.٦) Flow area between cone surface and conical shock.

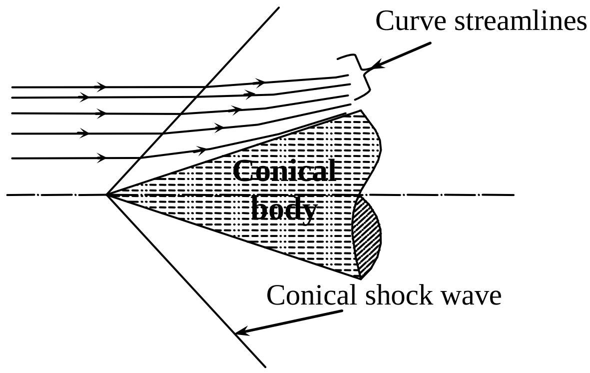

Fig. (٣.٧) Curved streamlines downstream of conical shock wave.

٣.٣.١ : MATHEMATICAL MODEL: -

The external part of intake consists of: -

١- Adiabatic compression system.

a- Conical shock waves system.

b- Normal shock waves system.

٢- Isentropic compression system.

For the conical flow it is convenient to express the governing equations in the spherical coordinate system as in Fig. (٣.٨).

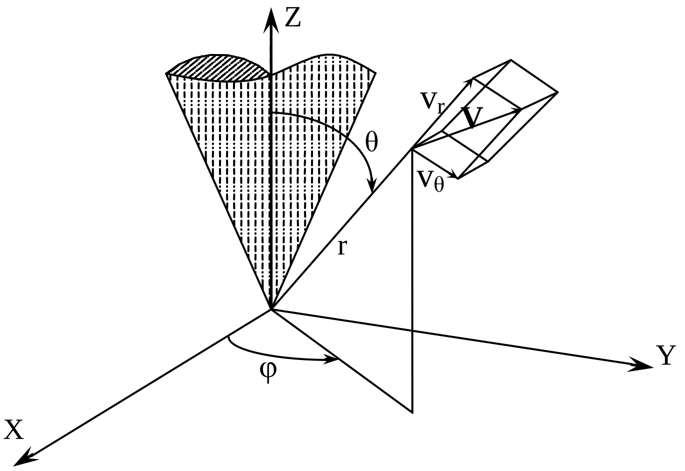

Fig. (٣.٨) The spherical coordinate system.

Calculation of the angle of the conical shock wave (θ_S), necessary to calculate the flow properties between the cone with a semi vertex angle (δ_C) and the conical shock in front of it. For this purpose the system of equations applicable to flow behind a shock wave is considered. It will be assumed that thermodynamic equilibrium is established in the perturbed flow region. The gas parameters are constant on any intermediate conical surface (including those with angles $\theta = \theta_S$ and $\theta = \delta_C$) Fig. (٣-٩). And change only from one surface to another, then on the basis of this property, any partial derivative with respect to r-coordinate Fig. (٣.٨) is equal to zero, also the flow properties are independent of the angle (φ) due to the axial symmetry of the flow field (angle of attack is zero), so the flow properties depend only on the spherical angle (θ) and the governing partial differential equations reduced to the ordinary differential equations.

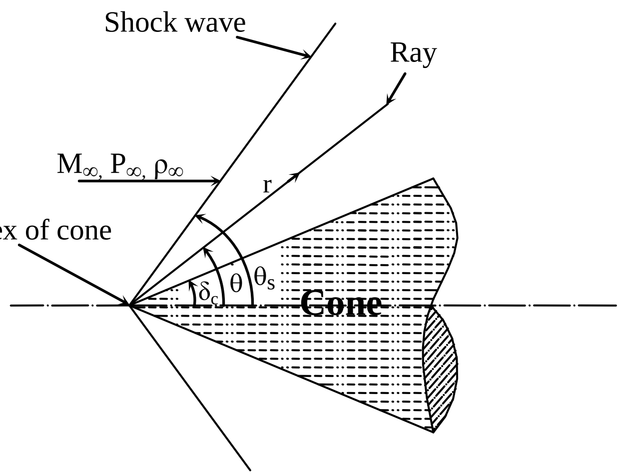

Fig. (٣.٩) Relationship between θ , θ_S, δ_C and ray (r).

٣.٣.٢: ASSUMPTIONS: -

The following assumptions are made: -

١- The airflow is treated as a perfect gas.

٢- Zero angle of attack (Axisymmetric flow).

٣- Non-viscous flow.

٤- The cone has straight surface.

٥- Steady flow.

٣.٣.٣: THE GOVERNING EQUATIONS: -

According to the assumptions, the system of governing equations in spherical coordinate system are [٣١]: -

١-Mass balance: -

$$\frac{1}{r^2}\frac{\partial\left(\rho r^2 v_r\right)}{\partial r}+\frac{1}{r\sin\theta}\frac{\partial\left(\rho v_\theta \sin\theta\right)}{\partial\theta}=0 \qquad \text{...(٣.١)}$$

By drive it,

$$\frac{1}{r^2}\left(2\rho v_r r\frac{\partial r}{\partial r}+r^2\frac{\partial \rho v_r}{\partial r}\right)+\frac{1}{r\sin\theta}\left(v_\theta \sin\theta\frac{\partial \rho}{\partial \theta}+\rho\left(v_\theta\cos\theta+\sin\theta\frac{\partial v_\theta}{\partial \theta}\right)\right)=0$$

$\frac{\partial}{\partial r}=0$ (Properties are constant along (r)),

$$\frac{2\rho\, v_r}{r}+\frac{v_\theta \sin\theta}{r\sin\theta}\frac{\partial\rho}{\partial\theta}+\frac{\rho v_\theta}{r\sin\theta}\cos\theta+\frac{\rho}{r\sin\theta}\sin\theta * \frac{\partial v_\theta}{\partial\theta}=0 \qquad \text{...(٣.٢)}$$

Multiplying both side of equation (٣.٢) by (r) to get,

$$2\rho\, v_r+v_\theta\frac{\partial\rho}{\partial\theta}+\rho v_\theta\cot\theta+\rho\frac{\partial v_\theta}{\partial\theta}=0$$

Now $\partial \longrightarrow d$.

So,

$$2\rho\, v_r+v_\theta\frac{d\rho}{d\theta}+\rho\frac{dv_\theta}{d\theta}+\rho v_\theta\cot\theta=0 \qquad \text{...(٣.٣)}$$

٢- Momentum balance: -

i. r-momentum.

$$v_r\frac{\partial v_r}{\partial r}+\frac{v_\theta}{r}\frac{\partial v_r}{\partial\theta}-\frac{{v_\theta}^2}{r}=-\frac{1}{\rho}\frac{\partial P}{\partial r} \qquad \text{...(٣.٤)}$$

$$\because \frac{\partial}{\partial r}=0$$

Then,

$$\frac{v_\theta}{r}\frac{\partial v_r}{\partial\theta}=\frac{{v_\theta}^2}{r}$$

$$\therefore \frac{dv_r}{d\theta}=v_\theta \qquad \text{...(٣.٥)}$$

ii. θ-momentum.

$$v_r\frac{\partial v_\theta}{\partial r}+\frac{v_\theta}{r}\frac{\partial v_\theta}{\partial\theta}+\frac{v_r v_\theta}{r}=-\frac{1}{r\rho}\frac{\partial P}{\partial\theta} \qquad \text{...(٣.٦)}$$

Also $\because \dfrac{\partial}{\partial r} = 0$

Then,

$$\frac{v_\theta}{r}\frac{\partial v_\theta}{\partial \theta} + \frac{v_r v_\theta}{r} = -\frac{1}{r\rho}\frac{\partial P}{\partial \theta}$$

Multiply the last equation by (rρ) to get to,

$$\rho v_\theta \frac{dv_\theta}{d\theta} + \rho v_r v_\theta + \frac{dP}{d\theta} = 0 \qquad \text{...(٣.٧)}$$

From sonic velocity equation,

$$a^2 = \frac{dP}{d\rho} = \frac{dP}{d\theta} * \frac{d\theta}{d\rho} \qquad \text{(Chain rule).}$$

$$\therefore \frac{dP}{d\theta} = a^2\left(\frac{d\rho}{d\theta}\right) \qquad \text{...(٣.٨)}$$

Substituting equation (٣.٨) into (٣.٧) to get,

$$\rho v_\theta \frac{dv_\theta}{d\theta} + \rho v_r v_\theta + a^2\left(\frac{d\rho}{d\theta}\right) = 0$$

$$\therefore \frac{d\rho}{d\theta} = \frac{-\rho v_\theta \dfrac{dv_\theta}{d\theta} - \rho v_r v_\theta}{a^2} \qquad \text{...(٣.٩)}$$

By substituting equation (٣.٩) in (٣.٣) then,

$$2\rho v_r + v_\theta\left(\frac{-\rho v_\theta \dfrac{dv_\theta}{d\theta} - \rho v_r v_\theta}{a^2}\right) + \rho \frac{dv_\theta}{d\theta} + \rho v_\theta \cot\theta = 0$$

$$2\rho v_r a^2 - \rho v_\theta^2 \frac{dv_\theta}{d\theta} - \rho v_r v_\theta^2 + \rho a^2 \frac{dv_\theta}{d\theta} + \rho a^2 v_\theta \cot\theta = 0$$

$$2v_r a^2 - v_\theta^2 \frac{dv_\theta}{d\theta} - v_r v_\theta^2 + a^2 \frac{dv_\theta}{d\theta} + a^2 v_\theta \cot\theta = 0$$

$$(a^2 - \nu_\theta^2)\frac{d\nu_\theta}{d\theta} = \nu_r\nu_\theta^2 - 2\nu_r a^2 - a^2\nu_\theta \cot\theta$$

$$(a^2 - \nu_\theta^2)\frac{d\nu_\theta}{d\theta} = \nu_r\nu_\theta^2 - \nu_r a^2 - \nu_r a^2 - a^2\nu_\theta \cot\theta$$

$$\frac{d\nu_\theta}{d\theta} = \frac{\nu_r(\nu_\theta^2 - a^2) - a^2(\nu_r - \nu_\theta \cot\theta)}{(a^2 - \nu_\theta^2)}$$

$$\frac{d\nu_\theta}{d\theta} = \frac{\nu_r(\frac{\nu_\theta^2}{a^2} - 2) + \nu_\theta \cot\theta}{(1 - \frac{\nu_\theta^2}{a^2})} \qquad \text{...(٣.١٠)}$$

Equation (٣.٥) and (٣.١٠) may be written in dimensionless form by dividing by the "critical speed of the free stream (a^*)".

Thus,

$$\nu_r^* = \frac{\nu_r}{a^*} = M_r^* \qquad \text{...(٣.١١)}$$

$$\nu_\theta^* = \frac{\nu_\theta}{a^*} = M_\theta^* \qquad \text{...(٣.١٢)}$$

So equation (٣.٥) and (٣.١٠) becomes,

$$\frac{d\nu_r^*}{d\theta} = \nu_\theta^* \qquad \text{...(٣.١٣)}$$

$$\frac{d\nu_\theta^*}{d\theta} = \frac{\nu_r^*(\frac{\nu_\theta^{*2}}{a^{\sim 2}} - 2) - \nu_\theta^* \cot\theta}{(1 - \frac{\nu_\theta^{*2}}{a^{\sim 2}})} \qquad \text{...(٣.١٤)}$$

Where,

$$a^{\sim 2} = \left(\frac{a}{a^*}\right)^2 = \frac{\gamma + 1}{2} - \frac{(\gamma - 1)}{2}M^{*2} \qquad \text{...(٣.١٥)}$$

$$M^* = \frac{V}{a^*}$$

$$V = \sqrt{\nu_r^2 + \nu_\theta^2}$$

So,

$$M^{*2} = \frac{\nu_r^2 + \nu_\theta^2}{a^{*2}} = \frac{\nu_r^2}{a^{*2}} + \frac{\nu_\theta^2}{a^{*2}}$$

Then,

$$M^{*2} = \nu_r^{*2} + \nu_\theta^{*2} \qquad \text{...(٣.١٦)}$$

$$u^* = \nu_r^* \cos\theta - \nu_\theta^* \sin\theta \qquad \text{...(٣.١٧)}$$

$$v^* = \nu_r^* \sin\theta + \nu_\theta^* \cos\theta \qquad \text{...(٣.١٨)}$$

$$\Phi = \theta - \tan^{-1}\left(\frac{\nu_\theta^*}{\nu_r^*}\right) = \tan^{-1}\left(\frac{u^*}{v^*}\right) \qquad \text{...(٣.١٩)}$$

Where equation (٣.١٥) is derived in Appendix (A). Fig. (٣.١٠) shows the flow nomenclature on cone.

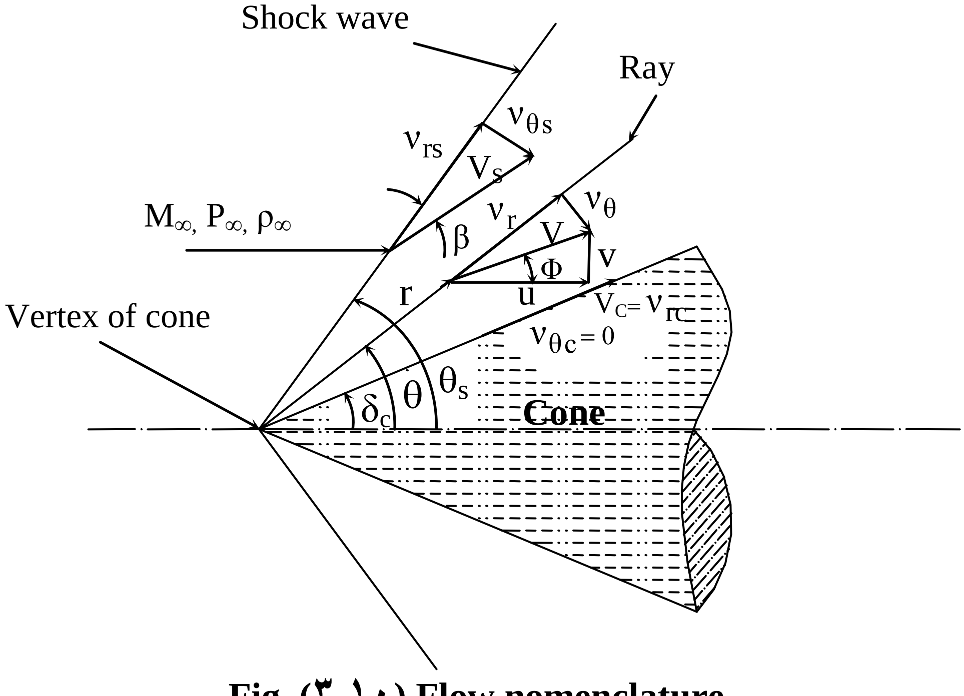

Fig. (٣.١٠) Flow nomenclature.

Equation (٣.١٣) and (٣.١٤) comprise a set of two coupled ordinary differential equations, for the determination of the non-dimensional velocity components (v_r^*) and (v_θ^*) in a steady conical flow. Those equations may be integrated by any standard integration method, such as, the fourth order Range-Kutta method that presented in Appendix (B).

٣.٣.٤: PROPERTY RATIOS ACROSS AN OBLIQUE SHOCK WAVE: -

From Fig. (٣.٩) the properties ratios according to ref. [٤٦] are: -

$$\frac{P_s}{P_\infty} = \frac{2\gamma}{\gamma+1} M_\infty^2 \sin^2\theta_s - \frac{\gamma-1}{\gamma+1} \qquad ...(٣.٢٠)$$

$$\frac{\rho_s}{\rho_\infty} = \frac{\tan\theta_s}{\tan\beta} = \frac{(\gamma+1) M_\infty^2 \sin^2\theta_s}{2+(\gamma-1) M_\infty^2 \sin^2\theta_s} \qquad ...(٣.٢١)$$

$$\frac{Vs}{V_\infty} = \frac{\left(Vs / a^* \right)}{\left(V_\infty / a^* \right)} = \frac{M_s^*}{M_\infty^*} = \frac{\sin\theta_s}{\sin\beta} \left(\frac{2}{(\gamma+1) M_\infty^2 \sin^2\theta_s} + \frac{\gamma-1}{\gamma+1} \right) \qquad ...(٣.٢٢)$$

$$v_{rs}^* = M_s^* \cos\beta \qquad ...(٣.٢٣)$$

$$v_{\theta s}^* = M_s^* \sin\beta \qquad ...(٣.٢٤)$$

٣.٣.٥: PROPERTY RATIOS FOR ISENTROPIC FLOW: -

The isentropic flow property ratios are as in ref. [٤٦].

$$\frac{T_o}{T} = \frac{\gamma+1}{(\gamma+1) - (\gamma-1) M^{*2}} \qquad ...(٣.٢٥)$$

$$\frac{P_o}{P} = \left(\frac{T_o}{T} \right)^{\gamma/(\gamma-1)} \qquad ...(٣.٢٦)$$

$$\frac{\rho_o}{\rho} = \left(\frac{T_o}{T}\right)^{1/(\gamma-1)} \qquad ...(٣.٢٧)$$

Where in general form,

$$M^{*2} = \frac{(\gamma+1)M^2}{2+(\gamma-1)M^2} \qquad ...(٣.٢٨)$$

Where equation (٣.٢٨) is derived also in Appendix (A).

٣.٤: INTERNAL PART: -

This part starting immediately downstream of the external part of intake, this part of intake has axisymmetric convergence-divergence form, as shown in Fig. (٣.١١).

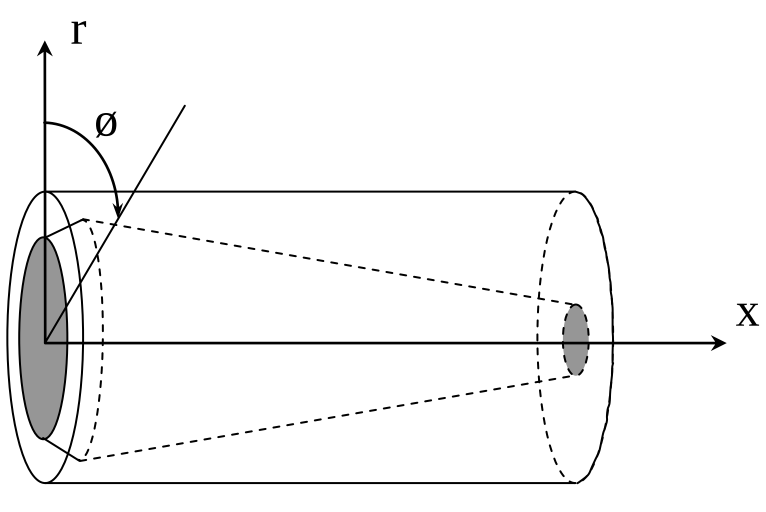

Fig. (٣.١١) Internal part of intake.

٣.٤.١: ASSUMPTIONS: -

The following assumptions are made: -

١- The airflow is treated as a perfect gas.

٢- The flow is treated as quasi-three dimensional (Axisymmetric flow).

٣- Non-viscous flow.

٤- The flow is steady.

٣.٤.٢: THE GOVERNING EQUATIONS: -

For the internal part of supersonic air intake it is convenient to express the governing equations in the cylindrical coordinate system, as in Fig. (٣.١١).

According to the assumptions, the systems of equations in cylindrical coordinate system are [٣٠]: -

١-Mass balance: -

$$\frac{\partial(\rho v_x)}{\partial x} + \frac{\partial(\rho v_r)}{\partial r} + \frac{\rho v_r}{r} = 0 \qquad \text{...(٣.٢٩)}$$

٢- Momentum balance: -

i. x-momentum.

$$\rho v_x \frac{\partial v_x}{\partial x} + \rho v_r \frac{\partial v_x}{\partial r} = -\frac{\partial P}{\partial x} \qquad \text{...(٣.٣٠)}$$

ii. r-momentum.

$$\rho v_x \frac{\partial v_r}{\partial x} + \rho v_r \frac{\partial v_r}{\partial r} = -\frac{\partial P}{\partial r} \qquad \text{...(٣.٣١)}$$

٣- Energy balance: -

$$v_x \frac{\partial}{\partial x}\left(cpT + \left(\frac{v_x^2 + v_r^2}{2}\right)\right) + v_r \frac{\partial}{\partial r}\left(cpT + \left(\frac{v_x^2 + v_r^2}{2}\right)\right) = 0 \qquad \text{...(٣.٣٢)}$$

٤- State equation: -

The equation of state for perfect gas is: -

$$P = \rho R T \qquad \text{...(٣.٣٣)}$$

i. x-direction.

$$\frac{\partial P}{\partial x} = R\left(\rho\frac{\partial T}{\partial x} + T\frac{\partial \rho}{\partial x}\right) \qquad ...(٣.٣٤)$$

ii. r-direction.

$$\frac{\partial P}{\partial r} = R\left(\rho\frac{\partial T}{\partial r} + T\frac{\partial \rho}{\partial r}\right) \qquad ...(٣.٣٥)$$

The set of equations ((٣.٢٩) to (٣.٣٥)) in partial differential form (conservation form) may be expressed in finite difference form, but in beginning generate grid on domain of flow must be established of suitable computational geometry, i.e. regular nodal mesh.

٣.٤.٣: FINITE DIFFERENCE TECHNIQUE: -

The philosophy of finite difference solutions is to replace the partial derivatives of the conservation equations, by algebraic difference quotients, yielding algebraic equations for the flow field variables at the specific grid points.

The type of finite difference, which is used to replace the partial derivatives, can be selected from a number of different forms, depending on the desired accuracy of the solution, convergence behavior, stability and convenience. However, the most common forms are forward, backward, and central differences, all of which stem from the Taylor's-series expansion, [٣٥]. In the present analysis only the backward difference expression used for all the nodes, due to the nature of boundary.

٣.٤.٤: GRID GENERATION TECHNIQUES: -

One of the first steps to be taken in establishing a finite difference procedure for solving of partial differential equations (PDEs) is to replace the continuous problem domain by a finite difference grid. The creation of grid points within the physical domain, as well as the boundaries of the domain is known as grid generation. When the physical domain has non-uniform shape such as converge-diverge diffuser, leads to non-uniform grid mesh, i.e. unequal grid space. Where this creates complications with the finite difference equations (FDEs), since approximations with non-equal stepsize must be used. This form of the FDEs changes from node to node, creating cumbersome programming details. In order to eliminate difficulties, the complex physical domain is transformed into a rectangular constant stepsize computational domain. Grid generation techniques may be classified into three categories:

١- Algebraic method.

٢- Partial differential method.

٣- Conformal mapping based on complex variables (complex variable method).

In addition, the grid system may be classified into two categorized:

a- Fixed grid system.

b- Adaptive grid system.

Details on these classifications are presented in (**Anderson (١٩٨٤) [٣٦]**, and **Hoffman (١٩٨٩) [٤١]**). For the present study, algebraic methods are used to produce a boundary fitted computational mesh. A general numerical mapping procedure is required in computing the complex flow field, where algebraic transformation equations cannot be established easily.

٣.٤.٥: TRANSFORMATION OF PHYSICAL TO COMPUTATIONAL DOMAIN: -

The physical domain of the problem under investigation must be manipulated in some how to a suitable form of computational domain. The coordinate (x) and (r) specify each node in the flow field. In the computational domain the nodal points are specified by (ξ) and (η) coordinates.

A completely general two-dimensional transformation function for a fixed grid is: -

$$\left.\begin{aligned}\xi &= \xi(x, r)\\ \eta &= \eta(x, r)\end{aligned}\right\} \quad \text{...(٣.٣٦)}$$

For any property, the variations in the physical plane, with respect to the spatial coordinates, can be expressed in the computational plane using the chain rule of partial differentiation as follows: -

$$\frac{\partial(\,)}{\partial x} = \frac{\partial(\,)}{\partial \xi}\frac{\partial \xi}{\partial x} + \frac{\partial(\,)}{\partial \eta}\frac{\partial \eta}{\partial x} = \frac{\partial(\,)}{\partial \xi}\xi_x + \frac{\partial(\,)}{\partial \eta}\eta_x \quad \text{...(٣.٣٧)}$$

$$\frac{\partial(\,)}{\partial r} = \frac{\partial(\,)}{\partial \xi}\frac{\partial \xi}{\partial r} + \frac{\partial(\,)}{\partial \eta}\frac{\partial \eta}{\partial r} = \frac{\partial(\,)}{\partial \xi}\xi_r + \frac{\partial(\,)}{\partial \eta}\eta_r \quad \text{...(٣.٣٨)}$$

The quantities ($\xi_x, \eta_x, \xi_r, \eta_r$) appearing in the above equations are called the metrics of transformation. Consequently, the matrices of transformation are computed numerically. The method of such analysis is described in **Anderson (١٩٨٤)**. However in the two dimensions symmetric converge-diverge diffuser, simple normalized analytical expressions may be used. Thus, determination of the metrics of transformation is readily done. One type of such transformation is given by:

$$\left.\begin{aligned}\xi &= x\\ \eta &= \frac{r}{r_w(x)}\end{aligned}\right\} \quad \text{...(٣.٣٩)}$$

Where $r_w(x)$ is the function describing the wall of a diffuser. Expressions for the metrics of transformation are simply obtained by differentiation as follows: -

$$\left.\begin{aligned}\xi_x &= 1\\ \xi_r &= 0\\ \eta_x &= -\eta\eta_r\bar{r}_w(x)\end{aligned}\right\} \quad \text{...(٣.٤٠)}$$

$$\eta_r = \frac{1}{r_w(x)}$$

The transformation creteria is shown in Fig. (٣.١٢).

٣.٤.٦: TRANSFORMATION OF GOVERNING EQUATIONS: -

The governing equations (contenuty, momentum, energy, and state) in cylinderical coordinate for steady two-dimensions symmetrical compressible fluid flow, can be expressed in terms of generalized orthoginal coordinates system (ξ, η), for the application of converge-diverge diffuser, by substituting the metrics of transformations for fixed grid given in equation (٣.٣٩) the general partial differential for any property equations (٣.٣٧) and (٣.٣٨) yields:

$$\frac{\partial(\ )}{\partial x} = \frac{\partial(\ )}{\partial \xi} + \frac{\partial(\ )}{\partial \eta}\eta_x$$ **...(٣.٤١)**

$$\frac{\partial(\ )}{\partial r} = \frac{\partial(\ )}{\partial \eta}\eta_r$$ **...(٣.٤٢)**

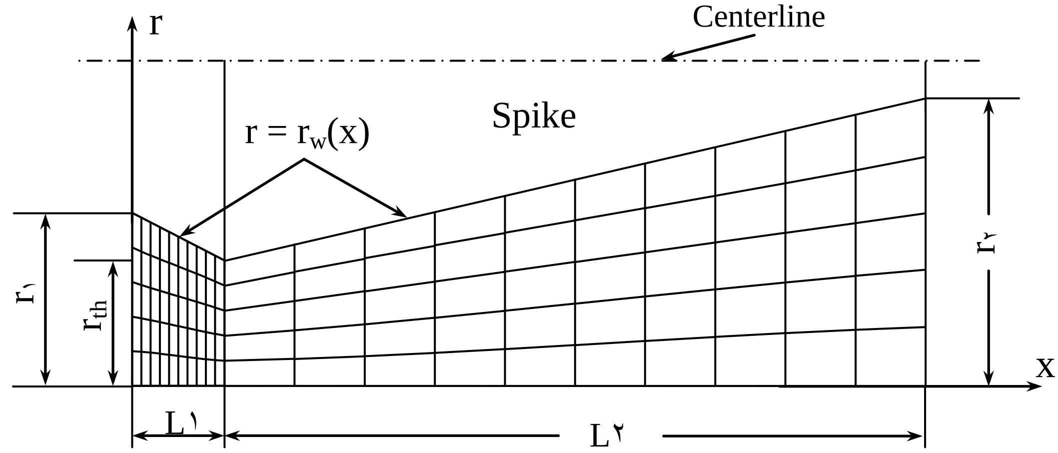

A- (x, r) Physical Domain.

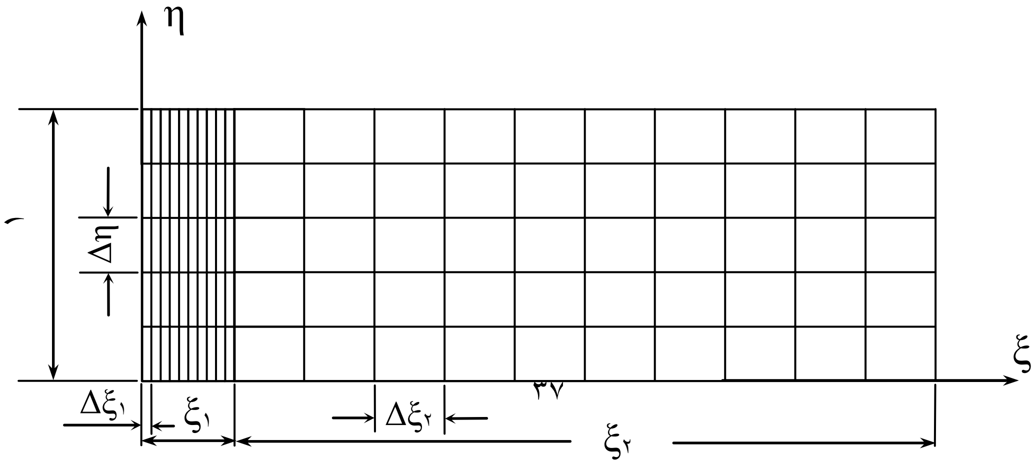

B- (ξ, η) Computational Domain.

quations (٣.٤١) and (٣.٤٢) may be used to transform the original set of governing equations (٣.٢٩) to (٣.٣٥) from cylinderical symmetry coordinate (x, r) to computational coordinate (ξ, η), as follows: -

٣.٤.٦.١:Continuty equation: -

The continuty equation (٣.٢٩) my be drived and become as follows:

$$\rho\frac{\partial v_x}{\partial x}+v_x\frac{\partial \rho}{\partial x}+\rho\frac{\partial v_r}{\partial r}+v_r\frac{\partial \rho}{\partial r}+\frac{\rho v_r}{r}=0 \qquad \text{...(٣.٤٣)}$$

Which may be transformed to computational coordinate by using equations (٣.٤١) and (٣.٤٢) as follows: -

$$\frac{\partial v_x}{\partial x}=\frac{\partial v_x}{\partial \xi}+\frac{\partial v_x}{\partial \eta}\eta_x \qquad \text{...(٣.٤٤)}$$

$$\frac{\partial \rho}{\partial x}=\frac{\partial \rho}{\partial \xi}+\frac{\partial \rho}{\partial \eta}\eta_x \qquad \text{...(٣.٤٥)}$$

$$\frac{\partial v_r}{\partial r}=\frac{\partial v_r}{\partial \eta}\eta_r \qquad \text{...(٣.٤٦)}$$

$$\frac{\partial \rho}{\partial r}=\frac{\partial \rho}{\partial \eta}\eta_r \qquad \text{...(٣.٤٧)}$$

By substituting equations (٣.٤٤) to (٣.٤٧) into equation (٣.٤٣) yields: -

$$\rho\left(\frac{\partial v_x}{\partial \xi}+\frac{\partial v_x}{\partial \eta}\cdot\eta_x\right)+v_x\left(\frac{\partial \rho}{\partial \xi}+\frac{\partial \rho}{\partial \eta}\cdot\eta_x\right)+\rho\left(\frac{\partial v_r}{\partial \eta}\cdot\eta_r\right)+v_r\left(\frac{\partial \rho}{\partial \eta}\cdot\eta_r\right)+ \frac{\rho v_r}{r}=0 \qquad \text{...(٣.٤٨)}$$

٣.٤.٦.٢: Momentum equation (Euler equation): -

i. x-momentum: -

The pressure term into equation (٣.٣٠) may be substituted from state equation in x-direction (٣.٣٤) and the resulting equation becomes: -

$$\rho v_x \frac{\partial v_x}{\partial x} + \rho v_r \frac{\partial v_x}{\partial r} + R\left(\rho \frac{\partial T}{\partial x} + T\frac{\partial \rho}{\partial x}\right) = 0 \qquad \text{...(٣.٤٩)}$$

By combinning equations (٣.٤٤) and (٣.٤٦) with equation (٣.٤٩) and by setting: -

$$\frac{\partial T}{\partial x} = \frac{\partial T}{\partial \xi} + \frac{\partial T}{\partial \eta} \cdot \eta_x \qquad \text{...(٣.٥٠)}$$

$$\frac{\partial v_x}{\partial r} = \frac{\partial v_x}{\partial \eta} \eta_r \qquad \text{...(٣.٥١)}$$

$\therefore$ The momentum equation in computational coordinate then becomes: -

$$\rho v_x \left(\frac{\partial v_x}{\partial \xi} + \frac{\partial v_x}{\partial \eta} \cdot \eta_x\right) + \rho v_r \left(\frac{\partial v_x}{\partial \eta} \cdot \eta_r\right) + R\left(\begin{array}{l} \rho\left(\dfrac{\partial T}{\partial \xi} + \dfrac{\partial T}{\partial \eta} \cdot \eta_x\right) \\ + T\left(\dfrac{\partial \rho}{\partial \xi} + \dfrac{\partial \rho}{\partial \eta} \cdot \eta_x\right) \end{array}\right) = 0 \qquad \text{...(٣.٥٢)}$$

ii. r-momentum: -

Also the pressure term into equation (٣.٣١) may be substituted from state equation in r-direction (٣.٣٥) and the resulting equation becomes: -

$$\rho v_x \frac{\partial v_r}{\partial x} + \rho v_r \frac{\partial v_r}{\partial r} + R\left(\rho \frac{\partial T}{\partial r} + T\frac{\partial \rho}{\partial r}\right) = 0 \qquad \text{...(٣.٥٣)}$$

By combinning equations (٣.٤٦) and (٣.٤٧) with equation (٣.٥٣) and by setting: -

$$\frac{\partial T}{\partial r} = \frac{\partial T}{\partial \eta} \cdot \eta_r \qquad \text{...(٣.٥٤)}$$

$$\frac{\partial v_r}{\partial x} = \frac{\partial v_r}{\partial \xi} + \frac{\partial v_r}{\partial \eta} \cdot \eta_x \qquad \text{...(٣.٥٥)}$$

$\therefore$ The momentum equation in computational coordinate then becomes: -

$$\rho\, v_x\left(\frac{\partial v_r}{\partial \xi} + \frac{\partial v_r}{\partial \eta} \cdot \eta_x\right) + \rho\, v_r\left(\frac{\partial v_r}{\partial \eta} \cdot \eta_r\right) + R\begin{pmatrix} \rho\left(\frac{\partial T}{\partial \eta} \cdot \eta_r\right) + \\ T\left(\frac{\partial \rho}{\partial \eta} \cdot \eta_r\right) \end{pmatrix} = 0 \qquad \text{...(٣.٥٦)}$$

٣.٤.٦.٣: Energy equation: -

The energy equation (٣-٣٢), may be written as follows: -

$$v_x\left(c_P \frac{\partial T}{\partial x} + v_x \frac{\partial v_x}{\partial x} + v_r \frac{\partial v_r}{\partial x}\right) + v_r\left(c_P \frac{\partial T}{\partial r} + v_x \frac{\partial v_x}{\partial r} + v_r \frac{\partial v_r}{\partial r}\right) = 0 \qquad \text{...(٣.٥٧)}$$

By combination of equations ((٣.٤٤), (٣.٤٦), (٣.٥٠), (٣.٥١), (٣.٥٤) and (٣.٥٥)) with equation (٣.٥٧) to get energy equation in computational coordinate as follows: -

$$\begin{aligned} & v_x\left(c_P\left(\frac{\partial T}{\partial \xi} + \frac{\partial T}{\partial \eta} \cdot \eta_x\right) + v_x\left(\frac{\partial v_x}{\partial \xi} + \frac{\partial v_x}{\partial \eta} \cdot \eta_x\right) + v_r\left(\frac{\partial v_r}{\partial \xi} + \frac{\partial v_r}{\partial \eta} \cdot \eta_x\right)\right) + \\ & v_r\left(c_P\left(\frac{\partial T}{\partial \eta} \cdot \eta_r\right) + v_x\left(\frac{\partial v_x}{\partial \eta} \cdot \eta_r\right) + v_r\left(\frac{\partial v_r}{\partial \eta} \cdot \eta_r\right)\right) = 0 \end{aligned} \qquad \text{...(٣.٥٨)}$$

٣.٤.٦.٤: State equations: -

i. x-direction: -

In computational coordinate, the equation of state may be written as follows after combination of equations (٣.٤٥) and (٣.٥٠), with equation (٣.٣٤) and by setting: -

$$\frac{\partial P}{\partial x} = \frac{\partial P}{\partial \xi} + \frac{\partial P}{\partial \eta} \cdot \eta_x \quad \text{...(٣.٥٩)}$$

The equation of state become as follows:

$$\frac{\partial P}{\partial \xi} + \frac{\partial P}{\partial \eta} \cdot \eta_x = R\left(\rho\left(\frac{\partial T}{\partial \xi} + \frac{\partial T}{\partial \eta} \cdot \eta_x\right) + T\left(\frac{\partial \rho}{\partial \xi} + \frac{\partial \rho}{\partial \eta} \cdot \eta_x\right)\right) \quad \text{...(٣.٦٠)}$$

ii. r-direction.

In computational coordinate, equation of state in r-direction may be written as follows after combination of equations (٣.٤٧) and (٣.٥٤), with equation (٣.٣٥) and by setting: -

$$\frac{\partial P}{\partial r} = \frac{\partial P}{\partial \eta} \cdot \eta_r \quad \text{...(٣.٦١)}$$

The equation of state become as follows:

$$\frac{\partial P}{\partial \eta} \cdot \eta_r = R\left(\rho\left(\frac{\partial T}{\partial \eta} \cdot \eta_r\right) + T\left(\frac{\partial \rho}{\partial \eta} \cdot \eta_r\right)\right) \quad \text{...(٣.٦٢)}$$

Equations (٣.٤٨), (٣.٥٢), (٣.٥٦), (٣.٥٨), (٣.٦٠), and (٣.٦٢) are partial differential equations in regular constant stepsize computational coordinate domain (ξ, η). The set of these equations may be expressed in algebraic form by using finite defference technique.

٣.٤.٧: INITIAL VALUES AND BOUNDARY CONDITIONS: -

The set of equations ((٣.٤٨), (٣.٥٢), (٣.٥٦), and (٣.٥٨)) is used to compute the flow field properties inside the intake.

The initial distributions of flow variables (ρ, T, v_x, v_r, p) are obtained from the steady one-dimension variable area, isentropic flow. This is decoded as two-dimensional distributions.

All stagnation properties of flow field of intake are assumed constant (isentropic flow) except at shock waves, where the flow is assumed adiabatic only.

The Mach number in one dimensional solution should be evaluated at each axial station, [٤٥] where:

$$\frac{dM^2}{M^2} = -\frac{2\left(1+\frac{\gamma-1}{2}M^2\right)}{1-M^2}\frac{dA}{A} \qquad ...(٣.٦٣)$$

Integration between two ends of state gives: -

$$\frac{M_2}{M_1} = \left(\frac{1+(\gamma-1)M_2^2}{1+(\gamma-1)M_1^2}\right)^{\frac{(\gamma+1)}{2(\gamma-1)}}\frac{A_1}{A_2} \qquad ...(٣.٦٤)$$

The isentropic flow properties are calculated from the following equations: -

$$\frac{T_o}{T} = 1+\frac{\gamma-1}{2}M^2 \qquad ...(٣.٦٥)$$

The pressure and density ratios are calculated from equations (٣.٢٦) and (٣.٢٧) respectively.

٣.٤.٨: PREPARATIONS OF GOVERNING EQUATIONS IN FINITE DIFFEREANCE FORM (ALGEBRAIC FORM): -

The finite difference approximations for the partial derivatives of the dependent variables are expressed in terms of the values of the variables at the nodal points. These nodal points can be located according to the value of i and j. So difference equations are usually written in terms of the general points (i, j) and its neighbors. This labeling is illustrated in Fig. (٣.١٣), where $\Delta\xi$ and $\Delta\eta$ represents the pivotal spacing step in ξ and η respectively as a computational plane, [٣٦].

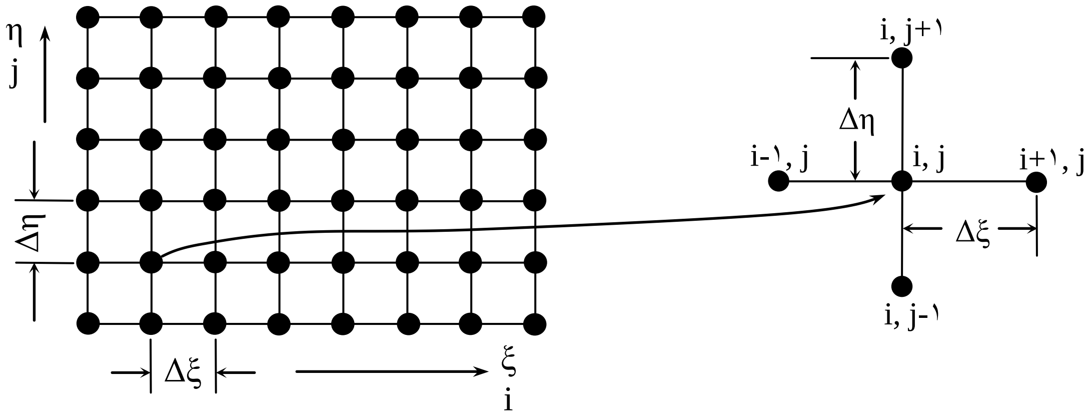

Fig. (٣.١٣) Finite difference grid

The governing equations of section (٣.٤.٦) in computational coordinate may be converted to algebraic form by expressing it in finite difference form. Where according to mesh configuration and nature of boundary conditions, the backward differences must be used.

Substituting backward difference expression into the governing equations in section (٣.٤.٦) gives: -

❖ **The equation of continuity (٣.٤٨) as : -**

$$\rho_{(i,\,j)}\left[\frac{v_{x(i,\,j)}-v_{x(i-1,\,j)}}{\Delta\xi}+\left(\frac{v_{x(i,\,j)}-v_{x(i,\,j\text{-}1)}}{\Delta\eta}\right)\eta_{x(i,\,j)}\right]+v_{x\,(i,\,j)}$$
$$\left[\frac{\rho_{(i,\,j)}-\rho_{(i-1,\,j)}}{\Delta\xi}+\left(\frac{\rho_{(i,\,j)}-\rho_{(i,\,j-1)}}{\Delta\eta}\right)\eta_{x(i,\,j)}\right]+\rho_{(i,\,j)} \qquad \text{...(٣.٦٦)}$$
$$\left[\left(\frac{v_{r(i,\,j)}-v_{r(i,\,j-1)}}{\Delta\eta}\right)\eta_{r(i,\,j)}\right]+v_{r\,(i,\,j)}\left[\left(\frac{\rho_{(i,\,j)}-\rho_{(i,\,j-1)}}{\Delta\eta}\right)\eta_{r(i,\,j)}\right]+$$
$$\frac{\rho_{(i,\,j)}\,v_{r\,(i,\,j)}}{r}=0$$

The left-hand side of equation (٣.٦٦) is abbreviated as (F_C).

❖ **The equations of momentum : -**

- **in ξ direction (٣.٥٢) : -**

$$\rho_{(i,j)}\, v_{x(i,j)} \left[\frac{v_{x(i,j)} - v_{x(i-1,j)}}{\Delta\xi} + \left(\frac{v_{x(i,j)} - v_{x(i,j-1)}}{\Delta\eta} \right) \eta_{x(i,j)} \right] + \rho_{(i,j)}\, v_{r(i,j)} \left[\left(\frac{v_{x(i,j)} - v_{x(i,j-1)}}{\Delta\eta} \right) \eta_{r(i,j)} \right] + R\,\rho_{(i,j)} \left[\frac{T_{(i,j)} - T_{(i-1,j)}}{\Delta\xi} + \left(\frac{T_{(i,j)} - T_{(i,j-1)}}{\Delta\eta} \right) \eta_{x(i,j)} \right] + R\,T_{(i,j)} \left[\frac{\rho_{(i,j)} - \rho_{(i-1,j)}}{\Delta\xi} + \left(\frac{\rho_{(i,j)} - \rho_{(i,j-1)}}{\Delta\eta} \right) \eta_{x(i,j)} \right] = 0 \quad \text{...(٣.٦٧)}$$

The left-hand side of equation (٣.٦٧) is abbreviated as (F_{MX}).

- **in η direction (٣.٥٦) : -**

$$\rho_{(i,j)}\, v_{x(i,j)} \left[\frac{v_{r(i,j)} - v_{r(i-1,j)}}{\Delta\xi} + \left(\frac{v_{r(i,j)} - v_{r(i,j-1)}}{\Delta\eta} \right) \eta_{x(i,j)} \right] + \rho_{(i,j)}\, v_{r(i,j)} \left[\left(\frac{v_{r(i,j)} - v_{r(i,j-1)}}{\Delta\eta} \right) \eta_{r(i,j)} \right] + R\,\rho_{(i,j)} \left[\left(\frac{T_{(i,j)} - T_{(i,j-1)}}{\Delta\eta} \right) \eta_{r(i,j)} \right] + R\,T_{(i,j)} \left[\left(\frac{\rho_{(i,j)} - \rho_{(i,j-1)}}{\Delta\eta} \right) \eta_{r(i,j)} \right] = 0 \quad \text{...(٣.٦٨)}$$

The left-hand side of equation (٣.٦٨) is abbreviated as (F_{Mr}).

❖ **The equation of energy (٣.٥٨) : -**

$$v_{x(i,\ j)}\, c_P \left[\frac{T_{(i,\ j)} - T_{(i-1,\ j)}}{\Delta\xi} + \left(\frac{T_{(i,\ j)} - T_{(i,\ j\text{-}1)}}{\Delta\eta} \right) \eta_{x(i,\ j)} \right] + v^2_{x\,(i,\ j)}$$

$$\left[\frac{v_{x(i,\ j)} - v_{x(i-1,\ j)}}{\Delta\xi} + \left(\frac{v_{x(i,\ j)} - v_{x(i,\ j\text{-}1)}}{\Delta\eta} \right) \eta_{x(i,\ j)} \right] + v_{x(i,\ j)} v_{r(i,\ j)}$$

$$\left[\frac{v_{r(i,\ j)} - v_{r(i-1,\ j)}}{\Delta\xi} + \left(\frac{v_{r(i,\ j)} - v_{r(i,\ j\text{-}1)}}{\Delta\eta} \right) \eta_{x(i,\ j)} \right] + v_{r(i,\ j)} c_P \qquad \text{...(٣.٦٩)}$$

$$\left[\left(\frac{T_{(i,\ j)} - T_{(i,\ j\text{-}1)}}{\Delta\eta} \right) \eta_{r(i,\ j)} \right] + v_{r\,(i,\ j)}\, v_{x(i,\ j)} \left[\left(\frac{v_{x(i,\ j)} - v_{x(i,\ j-1)}}{\Delta\eta} \right) \eta_{r(i,\ j)} \right] +$$

$$v^2_{r(i,\ j)} \left[\left(\frac{v_{r(i,\ j)} - v_{r(i,\ j\text{-}1)}}{\Delta\eta} \right) \eta_{r(i,\ j)} \right] = 0$$

The left-hand side of equation (٣.٦٩) is abbreviated as (F_E).

CHAPTER FOUR

METHOD OF SOLUTION

4

٤.١: INTRODUCTION: -

In any numerical simulation the choice of numerical algorithm and flow field model are dictated by considerations of computer cost, type of problem solved, flow regime and whether a very precise solution or an approximate solution is needed. These have spawned a vast array of simulation techniques (e.g. finite differences, finite elements, integral method …etc). The use of special approximations (e.g., incompressible or compressible, steady or unsteady, rotational or irrotational, boundary layer or Navier-Stokes) and a variety of ways to impose geometric boundaries (e.g., thin airfoil theory, special boundary operators, curvilinear and conformal coordinates, finite elements).

It seems that, even if one has a definite problem to solve, it is difficult or impossible to select the best or most efficient numerical method. For example, a procedure that runs very efficiently on a conventional serial computer processor may run poorly on a particular vector computer processor, [١١].

The true effectiveness of any numerical process used for approximating in these instances differential equations can only be done by comparison with analytical solution, others have well proven numerical techniques or experimental results.

The problem under consideration is divided into two distinct parts: -

٤.٢: EXTERNAL PART ANALYSIS: -

In the Taylor-Maccoll flow, the free stream flow properties $M_\infty, P_\infty, T_\infty$, and δ_C are specified, and θ_S and the velocity distributions $(\nu_r(\theta))$ and $(\nu_\theta(\theta))$ are determined. An iterative procedure is required to determine initial value condition for ν_r^* and ν_θ^* behind the shock wave, since (θ_S) is unknown.

Several iterative approaches are possible, where in the beginning (θ_S) is assumed, by equation (٤.١). And $(\nu_{r_S}^*)$ and $(\nu_{\theta_S}^*)$, are calculated from the properties ratios across an oblique shock wave, section (٣.٣.٤), where these values are the initial conditions for initiating the numerical integration of equation (٣.١٣) and (٣.١٤) by fourth-order Range-Kutta numerical method which is presented in Appendix (B). $(\nu_r^*(\theta))$ and $(\nu_\theta^*(\theta))$ are calculated from the governing equation downstream of the shock wave reaching to the surface of the cone according to chosen step $(\Delta\theta)$, which is determined by equation (٤.٣), where (δ_C) is determined.

$$\theta_s = \delta_c + \frac{\alpha}{2} \qquad \text{...(٤.١)}$$

Where (α) is the free stream Mach angle.

$$\alpha = \sin^{-1}\left(\frac{1}{M_\infty}\right) \qquad \text{...(٤.٢)}$$

$$\Delta\theta = -\frac{\theta_s - \delta_c}{N} \qquad \text{...(٤.٣)}$$

Where (N) is the desired number of steps between the shock wave and the surface of cone.

The condition that limits the solution is, when (δ_C) determined is equal to (δ_C) specified and $(\nu_r^*(\delta_C))$ is nearly or equal to zero (according to error tolerance (TOL)), where the solution is considered complete. The flow properties (V(θ), Φ(θ), P(θ), T(θ), ρ(θ), …etc) may be calculated from equations of sections (٣.٣.٣), (٣.٣.٤), and (٣.٣.٥). But when (δ_C) that determine is not equal to (δ_C) that specified, and/or ($v_r^*(\delta_C)$) is not equal to or nearly zero, then the new value of (θ_S) is assumed and the procedure is repeated again and so on, [٢٦][٢٧][٣٠][٣١][٣٢][٣٣][٤٤][٤٥].

For the second angle of cone, the procedure that used in the calculation of first cone may be repeated for the calculations of second cone, but some of assumptions were used on it. The Mach number of the conical flow field of the initial cone was considered to be the arithmetic average of the Mach number immediately behinds of the tip shock wave up to the Mach number along the first cone surface [١٠]. The second conical-shock wave was calculated by considering that this averaged flow would undergo a two-dimensional flow deflection equals to the summations of first and second cone angles subtracted by the average angles of flow stream line immediately behind the tip shock wave up to the first cone surface as in Fig. (٤.١).

$$\text{def.angle} = \delta_{c1} + \delta_{c2} - \Phi_{\text{average}} \qquad \text{...(٤.٤)}$$

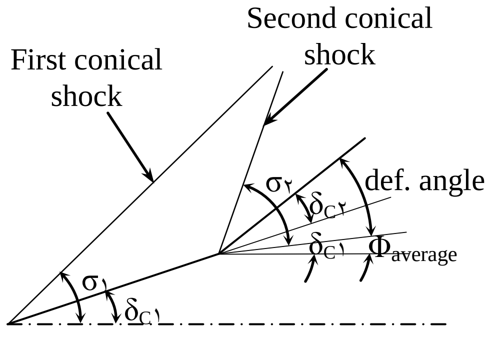

Fig. (٤.١) Angles nomenclature.

Flow chart of the program for analysis of external part of intake is presented in Fig. (٤.٣).

٤.٢.١: DESIGN PROCEDURE: -

The design elements of this part are $\delta_{C١}$, $\delta_{C٢}$, L_W, L_N, and h_{co}, the geometric angles of first and second angles of cone may be optimized in terms of pressure recovery. Where all pressure recoveries are based on shock losses. In the intake under consideration the total pressure losses, occur across the two conical shock waves and the normal shock wave. On design conditions are (M_∞ = ٢, H = ١٠ km, and $\dot{m}$ = ٣٠ kg/sec).

After optimized the first and second cone angles. The geometry of external part of intake Fig. (٤.٣) may be limited to the follows, [٣٨]: -

The continuity equation for the capture area mass flow (full flow) may be expressed as, [٨].

$$\dot{m}_{max} = \rho_\infty A_{co} V_\infty = \frac{P\infty}{RT_\infty} A_{co} V_\infty \qquad \text{...(٤.٥)}$$

The pressure and temperature may be expressed as function of altitude as follows [٣٤]: -

$$P_\infty = \frac{101.325}{10^{\left(H/19200\right)}} \qquad \text{...(٤.٦)}$$

$$T_\infty = 288.16 - 0.0065H \qquad \text{...(٤.٧)}$$

The free stream Mach number may be expressed as follows: -

$$M_\infty = \frac{V_\infty}{a} \qquad \text{...(٤.٨)}$$

$$a = \sqrt{\gamma RT_\infty} \qquad \text{...(٤.٩)}$$

$$A_{co} = \pi h_{co}^2 \qquad \text{...(٤.١٠)}$$

By substituting equations (٤.٦), (٤.٧), (٤.٨), (٤.٩), and (٤.١٠) into equation (٤.٥) and arrange it to get to h_{co} as a function of design conditions as follows: -

$$h_{co} = \sqrt{\frac{2\dot{m}\sqrt{R(288.16-0.0065H)} * 10^{\left(H/19200\right)}}{\pi\sqrt{\gamma} * 101.325 M_{\infty}}} \qquad \text{...(٤.١١)}$$

Where: -

$\dot{m} = 30\,\text{kg/sec}$.

$M_{\infty} = 2$

R = ٠.٢٨٧ kJ/kg. K

H = ١٠,٠٠٠ m

$\gamma = 1.4$

$$L_N = \frac{h_{co}}{\tan\sigma_1} \qquad \text{...(٤.١٢)}$$

$$\frac{L_W}{L_N} = \frac{L_W}{h_{co}}\tan(\sigma_1) = \frac{\tan(\sigma_2 + \Phi_{average}) - \tan(\sigma_1)}{\tan(\sigma_2 + \Phi_{average}) - \tan(\delta_{c1})} \qquad \text{...(٤.١٣)}$$

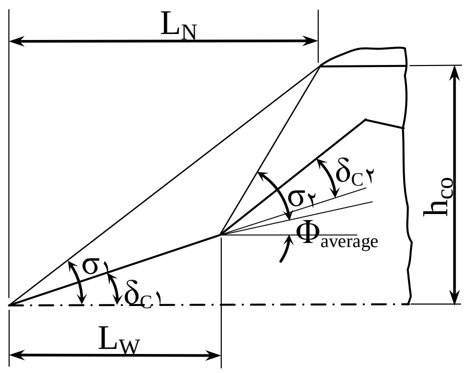

Fig. (٤.٢) External part geometry.

Flow chart of the program for design of external part of intake is presented in Fig. (٤.٤).

٤.٣: INTERNAL PART ANALYSIS: -

This part consists of convergent duct followed by a divergent one as in Fig. (٣.١١), so this part has non-uniform shape, hence the grid generation on it has non- uniform grid space, section (٣.٤.٤). So it needs to be transformed to uniform grid space, section (٣.٤.٥).

Equation (٣.٦٤) must be solved first to get Mach number at each axial node step. Where this equation must be solved iteratively, by trail and error, using Newton-Raphson formula as in equation (٤.١٤), where the output data of the external part may be used as inlet boundary condition for the internal part of intake. So all flow properties obtained as one-dimension decoded as two-dimension guess values distributions, which are necessary for iteration.

$$x_{i+1} = x_i - \frac{f(x_i)}{f'(x_i)} \qquad \text{...(٤.١٤)}$$

Where: -

x_i … approximate root after i iterations.

$x_{i+١}$ … approximate root after i+١ iterations.

$f(x_i)$ … functional value at x_i.

$f'(x_i)$ … first derivative value of the function at x_i.

Then equations (٣.٦٦) to (٣.٦٩) may be solved simultaneously in ξ and η coordinate at each node of mesh, using Newton-Raphson iteration technique, section (٤.٣.٢).

In on design condions, the normal shock wave seperates the converge part from the diverge part (throatle section), hence each part is solved sperately.

For the converge part: -

- The length of this part is signal by ($L_١$) which equal to (٢.٥ mm), with inclination wall angle equal to ($\delta_{c1} + \delta_{c2}$), as in Fig. (٣.١٢.A).

- The number of grids along (i) is equal to (١١). And the number of grids along (j) equals (٦), hence this part consists of (٦٦) nodal mesh points, Fig. (٣.١٢).
- The station (i = ٠) is considered as inlet boundary conditions to the finite difference solution of nodal mesh, these inlet boundary conditions represents the output of the solution of the external part analysis.
- The nodes (i = ٠, j = ٠ to i = ١١, j = ٠) are considered as duct horizantol wall boundary conditions to the finite difference solution of the nodal mesh, these wall boundary conditions are calculated as in section (٣.٤.٧).
- The iteration is started at the node i = ١, j = ١, and go to i = ١, j = ٢ after achieving the limiting tolerance (percent relative error (P.E) ≤Tol), and so on reaching to (i = ١١, j = ٦).

At the end of the converge part, the weak normal shock wave is generated,and the properties of flow across it are calculated according to section (٤.٣.٤).

The value of inlet gap of flow of converge part (r_1), and throat gap of flow (r_{th}) are calculated as the following equations: -

$$r_1 = h_{co} - \left[(L_N - L_{NW}) \tan\delta_{c1} + L_{NW} * \tan(\delta_{c1} + \delta_{c2}) \right] \quad \textbf{...(٤.١٥)}$$

Where:

$$L_{NW} = L_N - L_W \quad \textbf{...(٤.١٦)}$$

$$r_{th} = r_1 - L_1 * \tan(\delta_{c1} + \delta_{c2}) \quad \textbf{...(٤.١٧)}$$

For the diverge part : -

- This part starts immediately downstream of the normal shock wave, where Mach number is less than unity.

- This part will be subjected to optimization latter. Hence the length of this part is designated by ($L_٢$), and the inclination wall angle designated by (θ), as in Fig. (٣.١٢.A).
- The number of grids along (i) is equal to (١١). And the number of grids along (j) is equals to (٦), hence this part consists of (٦٦) nodal mesh points, Fig. (٣.١٢).
- The station (i = ٠) is considered as inlet boundary conditions to the finite difference solution of nodal mesh. These inlet boundary conditions represent the output of, the solution of the weak normal shock wave at on design condition,and the converge part at off design condition (M ≠٢ and/or H ≠ ١٠ km).
- The nodes (i = ٠, j = ٠ to i = ١١, j = ٠) are considered as duct horizantol wall boundary conditions to the finite difference solution of the nodal mesh, these wall boundary conditions are calculated as in section (٣.٤.٧).
- The iteration is started at the node i = ١, j = ١, and go to i = ١, j = ٢ after achieving the limiting tolerance (percent relative error (P.E) ≤Tol), and so on reaching to (i = ١١, j = ٦).

٤.٣.١: DESIGN PROCEDURE: -

The design elements of this part are area ratio (AR), length ($L_٢$), and angle of inclination wall (θ). These elements must be optimized to get intake with the following characteristics: -

- Short enough to keep weight and drag to minimum.
- Long enough to give Mach equals to (٠.٣ ~ ٠.٥) at the face of compressor.
- The air has uniform flow with high pressure ratios.

The value of exit gap of flow of diverge part ($r_٢$) is calculated by the followind equation.

$$r_2 = r_{th} + L_2 * \tan\theta \qquad ...(٤.١٨)$$

Flow chart of the program for analysis and design of internal part of intake is presented in Fig. (٤.٥).

٤.٣.٢: NEWTON-RAPHSON ITERATIVE METHOD: -

The solutions of non-linearity system of governing differential equations of the internal part flow field of intake form a difficult task. After transforming these equations from their differential forms to the finite difference form and substituting each node of the mesh, a system of non-linear simultaneous algebraic equations will be generated. To determine the variables in the internal part flow field, the number of the algebraic equations must be equal to the number of the mesh nodes. This system of equations can be solved by Newton-Raphson iterative method, as suggested by Al-Khafaji, (١٩٨٦)[٤٠]. This procedure is shown in Appendix (C).

Where the x in that illustration refers to the field variable which are (P, T, ρ, v_x, and v_r).

The construction of Newton-Raphson equation (C.٤) has the form as that for the single linear algebraic equation (٤.١٤). Therefore, (i) is used to designate the number of iterations performed. Equation (C.٤) can be expressed in the following general form: -

$$\{x\}_{i+1} = \{x\}_i - [J]_i^{-1}\{F\}_i \qquad , i = 1,2,... \qquad ...(٤.١٩)$$

The solution procedure consists of making initial approximations for each of the n variables, then evaluating the Jaciobian and the n equations so that,

det[J] $\neq$ ٠.

٤.٣.٣: ELEMENTS OF JACOBIAN MATRICES: -

Consider section (٣.٤.٨), where the F functions are constructed for the internal part of intake. The Jacobian matrices elements of the solution are the derivatives of these functions with respect the flow field variables (P, ρ, T, v_x, and v_r), at the considered point (node) in the finite difference mesh.

❖ **Continuity equation (٣.٦٦): -**

$$\frac{\partial F_c}{\partial \rho_{(i,\,j)}} = \frac{v_{x(i,\,j)} - v_{x(i-1,\,j)}}{\Delta\xi} + \left(\frac{v_{x(i,\,j)} - v_{x(i,\,j-1)}}{\Delta\eta}\right)\eta_{x(i,\,j)} + \frac{v_{x(i,\,j)}}{\Delta\xi} + v_{x(i,\,j)} * \frac{\eta_{x(i,\,j)}}{\Delta\eta} + \left(\frac{v_{r(i,\,j)} - v_{r(i,\,j-1)}}{\Delta\eta}\right)\eta_{r(i,\,j)} + v_{r(i,\,j)}\left[\frac{\eta_{r(i,\,j)}}{\Delta\eta} + \frac{1}{r}\right] \quad \text{...(٤.٢٠)}$$

$$\frac{\partial F_c}{\partial v_{x(i,\,j)}} = \rho_{(i,\,j)}\left[\frac{1}{\Delta\xi} + \frac{\eta_{x(i,\,j)}}{\Delta\eta}\right] + \left(\frac{\rho_{(i,\,j)} - \rho_{(i-1,\,j)}}{\Delta\xi}\right) + \left(\frac{\rho_{(i,\,j)} - \rho_{(i,\,j-1)}}{\Delta\eta}\right) * \eta_{x(i,\,j)} \quad \text{...(٤.٢١)}$$

$$\frac{\partial F_c}{\partial v_{r(i,\,j)}} = \rho_{(i,\,j)}\left(\frac{\eta_{r(i,\,j)}}{\Delta\eta}\right) + \left(\frac{\rho_{(i,\,j)} - \rho_{(i,\,j-1)}}{\Delta\eta}\right) * \eta_{r(i,\,j)} + \frac{\rho_{(i,\,j)}}{r} \quad \text{...(٤.٢٢)}$$

$$\frac{\partial F_c}{\partial T_{(i,\,j)}} = 0 \quad \text{...(٤.٢٣)}$$

❖ **Momentum equation: -**

i. in ξ direction (٣.٦٧): -

$$\frac{\partial F_{Mx}}{\partial \rho_{(i,j)}} = v_{x(i,j)}\left[\frac{v_{x(i,j)} - v_{x(i-1,j)}}{\Delta\xi} + \left(\frac{v_{x(i,j)} - v_{x(i,j-1)}}{\Delta\eta}\right)\eta_{x(i,j)}\right] + v_{r(i,j)}\left[\left(\frac{v_{x(i,j)} - v_{x(i,j-1)}}{\Delta\eta}\right)\eta_{r(i,j)}\right] + R\left[\frac{T_{(i,j)} - T_{(i-1,j)}}{\Delta\xi} + \left(\frac{T_{(i,j)} - T_{(i,j-1)}}{\Delta\eta}\right)\eta_{x(i,j)}\right] + R\left[T_{(i,j)}\left(\frac{1}{\Delta\xi} + \frac{\eta_{x(i,j)}}{\Delta\eta}\right)\right] \quad \text{...(٤.٢٤)}$$

$$\frac{\partial F_{Mx}}{\partial v_{x(i,j)}} = \rho_{(i,j)}\left[\left(\frac{2v_{x(i,j)} - v_{x(i-1,j)}}{\Delta\xi}\right) + \left(\frac{2v_{x(i,j)} - v_{x(i,j-1)}}{\Delta\eta}\right)\eta_{x(i,j)}\right] + \rho_{(i,j)} * v_{r(i,j)}\left(\frac{\eta_{r(i,j)}}{\Delta\eta}\right) \quad \text{...(٤.٢٥)}$$

$$\frac{\partial F_{Mx}}{\partial v_{r(i,j)}} = \rho_{(i,j)}\left[\left(\frac{v_{x(i,j)} - v_{x(i,j-1)}}{\Delta\eta}\right)\eta_{r(i,j)}\right] \quad \text{...(٤.٢٦)}$$

$$\frac{\partial F_{Mx}}{\partial T_{(i,j)}} = R\left[\rho_{(i,j)}\left(\frac{1}{\Delta\xi} + \frac{\eta_{x(i,j)}}{\Delta\eta}\right)\right] + R\left[\left(\frac{\rho_{(i,j)} - \rho_{(i-1,j)}}{\Delta\xi}\right) + \left(\frac{\rho_{(i,j)} - \rho_{(i,j-1)}}{\Delta\eta}\right)\eta_{x(i,j)}\right] \quad \text{...(٤.٢٧)}$$

ii. in η direction (٣.٦٨): -

$$\frac{\partial F_{Mr}}{\partial \rho_{(i,j)}} = v_{x(i,j)}\left[\frac{v_{r(i,j)} - v_{r(i-1,j)}}{\Delta\xi} + \left(\frac{v_{r(i,j)} - v_{r(i-1,j)}}{\Delta\eta}\right)\eta_{x(i,j)}\right] + v_{r(i,j)}\left[\left(\frac{v_{r(i,j)} - v_{r(i,j-1)}}{\Delta\eta}\right)\eta_{r(i,j)}\right] + R\left[\left(\frac{T_{(i,j)} - T_{(i,j-1)}}{\Delta\eta}\right) * \eta_{r(i,j)} + T_{(i,j)}\left(\frac{\eta_{r(i,j)}}{\Delta\eta}\right)\right] \quad \text{...(٤.٢٨)}$$

$$\frac{\partial F_{Mr}}{\partial v_{x(i,j)}} = \rho_{(i,j)}\left[\left(\frac{v_{r(i,j)} - v_{r(i-1,j)}}{\Delta\xi}\right) + \left(\frac{v_{r(i,j)} - v_{r(i,j-1)}}{\Delta\eta}\right)\eta_{x(i,j)}\right] \quad \text{...(٤.٢٩)}$$

$$\frac{\partial F_{Mr}}{\partial v_{r(i,j)}}=\rho_{(i,j)}*v_{x(i,j)}\left[\frac{1}{\Delta\xi}+\frac{\eta_{x(i,j)}}{\Delta\eta}\right]+\rho_{(i,j)}\left[\left(\frac{2v_{r(i,j)}-v_{r(i,j-1)}}{\Delta\eta}\right)*\eta_{r(i,j)}\right] \quad ...(٤.٣٠)$$

$$\frac{\partial F_{Mr}}{\partial T_{(i,j)}}=R\left[\rho_{(i,j)}\left(\frac{\eta_{r(i,j)}}{\Delta\eta}\right)+\left(\frac{\rho_{(i,j)}-\rho_{(i,j-1)}}{\Delta\eta}\right)\eta_{r(i,j)}\right] \quad ...(٤.٣١)$$

❖ **Energy equation: -**

$$\frac{\partial F_E}{\partial \rho_{(i,j)}}=0 \quad ...(٤.٣٢)$$

$$\frac{\partial F_E}{\partial v_{x(i,j)}}=c_P\left[\left(\frac{T_{(i,j)}-T_{(i-1,j)}}{\Delta\xi}\right)+\left(\frac{T_{(i,j)}-T_{(i,j-1)}}{\Delta\eta}\right)\eta_{x(i,j)}\right]+\frac{3v_{x(i,j)}^2}{\Delta\xi}$$
$$-\left(\frac{v_{x(i-1,j)}*2v_{x(i,j)}}{\Delta\xi}\right)+\left(\frac{3v_{x(i,j)}^2}{\Delta\eta}-\left(\frac{v_{x(i,j-1)}*2v_{x(i,j)}}{\Delta\eta}\right)\right)* \quad ...(٤.٣٣)$$
$$\eta_{x(i,j)}+\left(\frac{2v_{x(i,j)}-v_{x(i,j-1)}}{\Delta\eta}\right)\eta_{r(i,j)}*v_{r(i,j)}+$$
$$v_{r(i,j)}\left[\left(\frac{v_{r(i,j)}-v_{r(i-1,j)}}{\Delta\xi}\right)+\left(\frac{v_{r(i,j)}-v_{r(i,j-1)}}{\Delta\eta}\right)\eta_{x(i,j)}\right]$$

$$\frac{\partial F_E}{\partial v_{r(i,j)}}=v_{x(i,j)}\left[\frac{2v_{r(i,j)}-v_{r(i,j-1)}}{\Delta\xi}+\left(\frac{2v_{r(i,j)}-v_{r(i,j-1)}}{\Delta\eta}\right)\eta_{x(i,j)}\right]+$$
$$c_P\left[\left(\frac{T_{(i,j)}-T_{(i,j-1)}}{\Delta\eta}\right)\eta_{r(i,j)}\right]+v_{x(i,j)}\left[\left(\frac{v_{r(i,j)}-v_{r(i,j-1)}}{\Delta\eta}\right)*\eta_{r(i,j)}\right]+ \quad ...(٤.٣٤)$$
$$\left(\frac{3v_{r(i,j)}^2-v_{r(i,j-1)}*2v_{r(i,j)}}{\Delta\eta}\right)\eta_{r(i,j)}$$

$$\frac{\partial F_E}{\partial T_{(i,\,j)}} = c_P * v_{x(i,\,j)}\left[\frac{1}{\Delta\xi}+\frac{\eta_{x(i,\,j)}}{\Delta\eta}\right]+c_P * v_{r(i,\,j)}\left(\frac{\eta_{r(i,\,j)}}{\Delta\eta}\right) \qquad ...(٤.٣٥)$$

٤.٣.٤: PROPERTY RATIOS ACROSS A NORMAL SHOCK WAVE: -

The flow properties up stream of the normal shock wave are defined by subscript (x), and the flow properties immediately down stream of the normal shock are defined by subscript (y), so: -[Fox ١٩٩٨ [٤٦]],

$$M_y = \sqrt{\frac{M_x^2+\frac{2}{\gamma+1}}{\frac{2\gamma}{\gamma-1}M_x^2-1}} \qquad ...(٤.٣٦)$$

$$\frac{P_{oy}}{P_{ox}} = \left(\frac{\frac{\gamma+1}{2}M_x^2}{1+\frac{\gamma-1}{2}M_x^2}\right)^{\gamma/(\gamma-1)} * \left(\frac{2\gamma}{\gamma+1}M_x^2-\frac{\gamma-1}{\gamma+1}\right)^{-1/(\gamma-1)} \qquad ...(٤.٣٧)$$

$$\frac{T_y}{T_x} = \frac{1+\frac{\gamma-1}{2}M_x^2}{1+\frac{\gamma-1}{2}M_y^2} \qquad ...(٤.٣٨)$$

$$\frac{p_y}{p_x} = \frac{1+\gamma M_x^2}{1+\gamma M_y^2} = \frac{2\gamma}{\gamma+1}M_x^2-\frac{\gamma-1}{\gamma+1} \qquad ...(٤.٣٩)$$

$$\frac{\rho_y}{\rho_x} = \frac{V_x}{V_y} = \frac{M_x}{M_y}\left[\frac{1+\frac{\gamma-1}{2}M_y^2}{1+\frac{\gamma-1}{2}M_x^2}\right]^{1/2} \qquad ...(٤.٤٠)$$

٤.٣.٥: CONVERGENCE CRITERIA: -

In order to decide when the iterative processes should be terminated, convergence criteria are required. The convergence criterion, adopted for the computational courses of Newton-Raphson method, was presented as "percent relative error (P.E)", [٤٥].

$$P.E = \frac{\text{current approximation} - \text{previous approximation}}{\text{current approximation}}$$

or in other form,

$$١٠٠\%\ P.E = \left| \frac{x^{m} - x^{m-1}}{x^{m}} \right| * \qquad ...(٤.٤١)$$

Where m and m-١ are the present and previous iterations. And x refers to the field variables, P, ρ, T, v_x, and v_r.

The convergence can be checked by the follows: -

$$P.E \leq Tol. \qquad ...(٤.٤٢)$$

٤.٣.٧: IMPROVEMENT OF CONVERGENCE USING RELAXATION: -

Relaxation represents a slight modification of the Newton-Raphson method and it is designed to enhance convergence. After each new value of x computed using equation (٤.١٥), that value is modified by a weighted average of the results of the previous and the present iterations:

$$x_i^{new} = \lambda x_i^{new} + (1-\lambda) x_i^{old} \qquad ...(٤.٤٣)$$

Where λ is a weighting factor that is assigned a value between ٠ and ٢.

If λ=١, (١- λ) is equal to ٠ and the result is unmodified. However, if λ is set at a value between ٠ and ١, the result is a weighted average of the present and the previous result. This type of modofication is called underrelaxation. It is typically employed to make a non-convergent system converge or to hasten convergence by damping out oscillations.

For values of λ from ١ to ٢, extra weight is placed on the present value. In this instance, there is an implicit assumption that the new value is moving in the correct direction toward the true solution but at too slow rate. Thus, the added weight of λ is intended to improve the estimate by pushing it closer to the truth. Hence, this type of modification, which is called overrelaxation, is desiged to accelerate the convergence of an already convergent system. The approach is also called successive or simultaneous overrelaxation, or SOR.

The choice of a proper value for λ is often determined empirically, [٤٥]. In the present study λ = (٠ ~ ١).

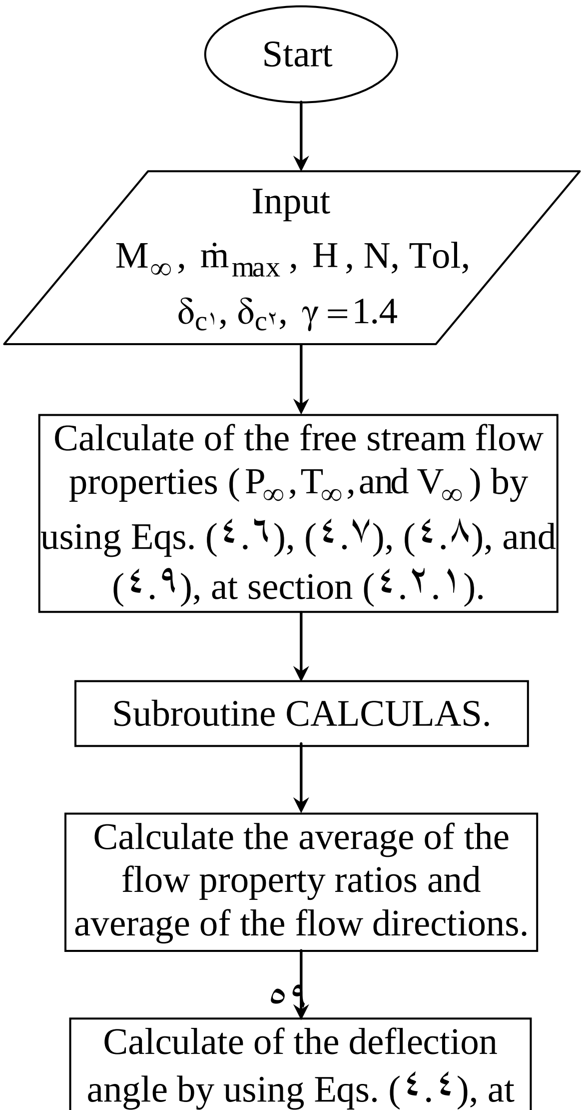

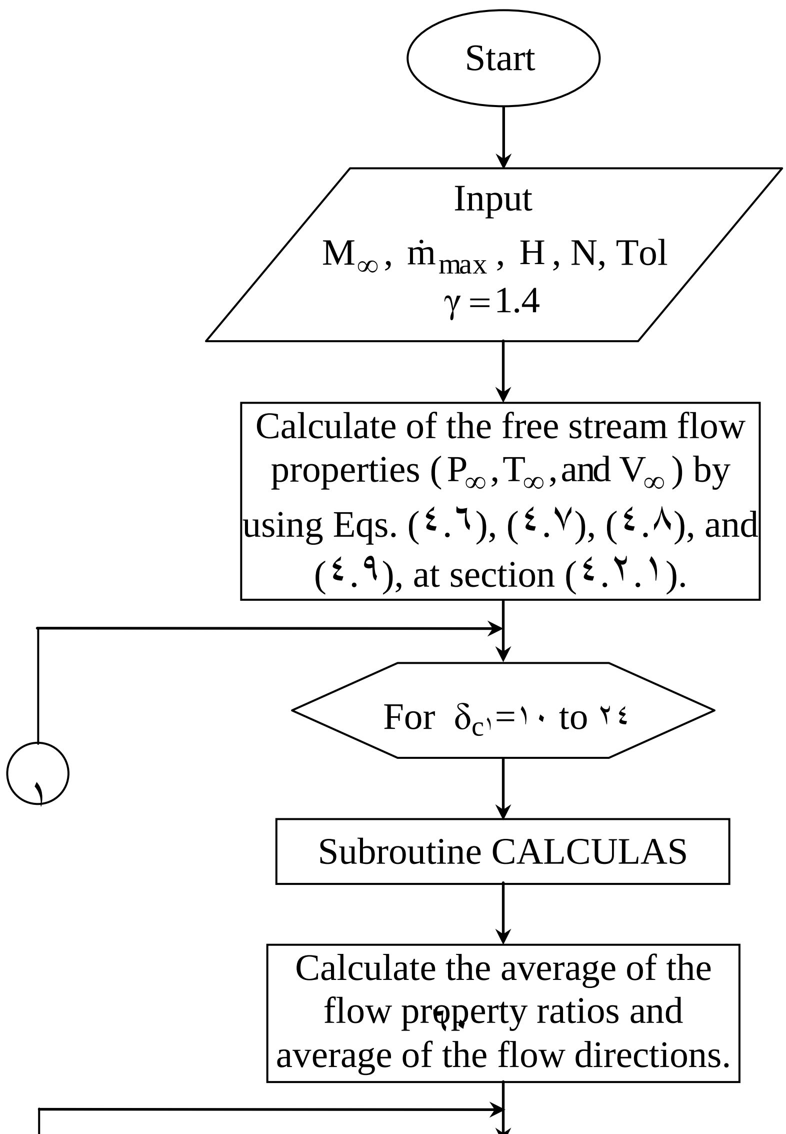
Start
Input
M_∞ , $\dot{m}_{max}$, H , N, Tol
$\gamma = 1.4$
Calculate of the free stream flow properties (P_∞ , T_∞ , and V_∞) by using Eqs. (٤.٦), (٤.٧), (٤.٨), and (٤.٩), at section (٤.٢.١).
For $\delta_{c١}$=١٠ to ٢٤
١
Subroutine CALCULAS
Calculate the average of the flow property ratios and average of the flow directions.

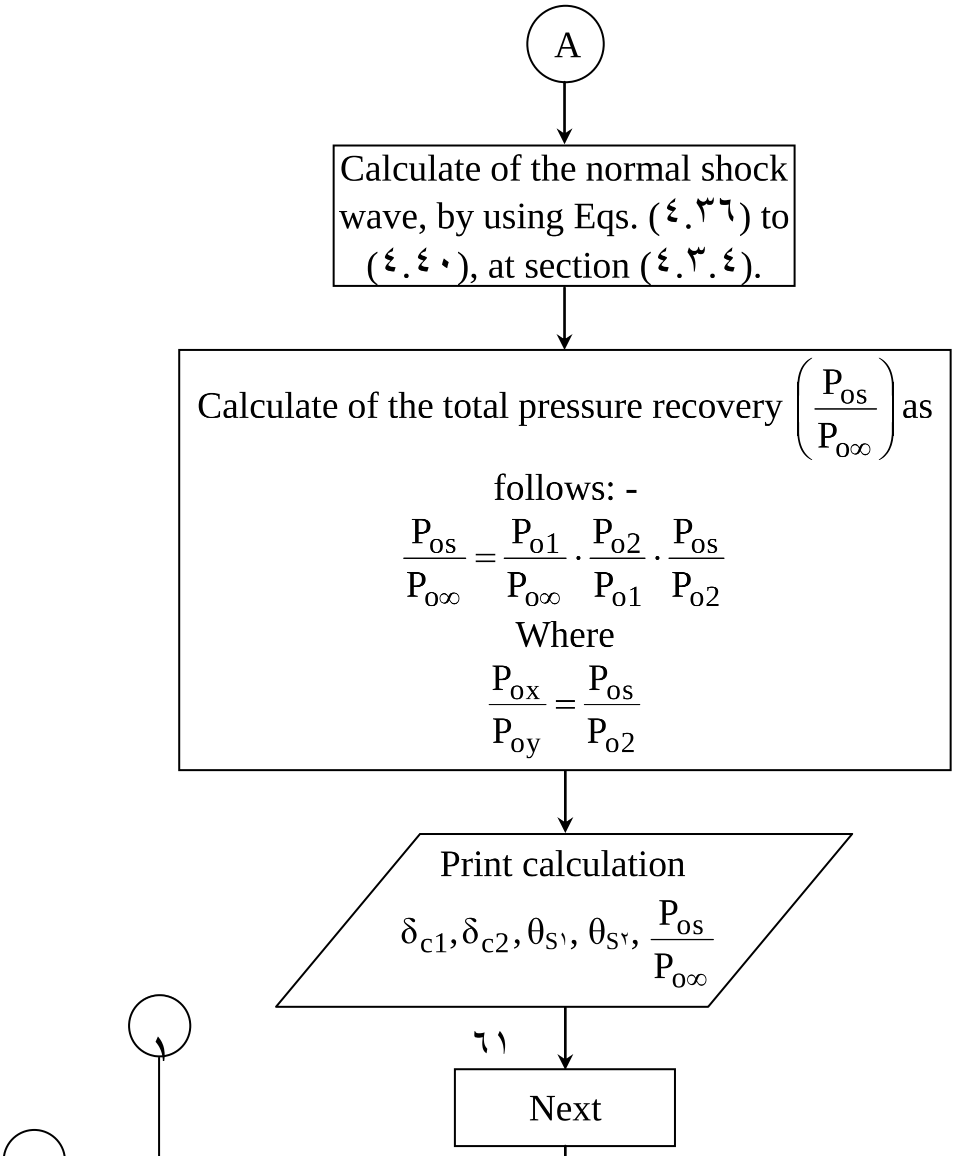
A
Calculate of the normal shock wave, by using Eqs. (٤.٣٦) to (٤.٤٠), at section (٤.٣.٤).
Calculate of the total pressure recovery $\left(\frac{P_{os}}{P_{o\infty}}\right)$ as follows: -
$\frac{P_{os}}{P_{o\infty}} = \frac{P_{o1}}{P_{o\infty}} \cdot \frac{P_{o2}}{P_{o1}} \cdot \frac{P_{os}}{P_{o2}}$
Where
$\frac{P_{ox}}{P_{oy}} = \frac{P_{os}}{P_{o2}}$
Print calculation
$\delta_{c1}, \delta_{c2}, \theta_{S١}, \theta_{S٢}, \frac{P_{os}}{P_{o\infty}}$
Next
١

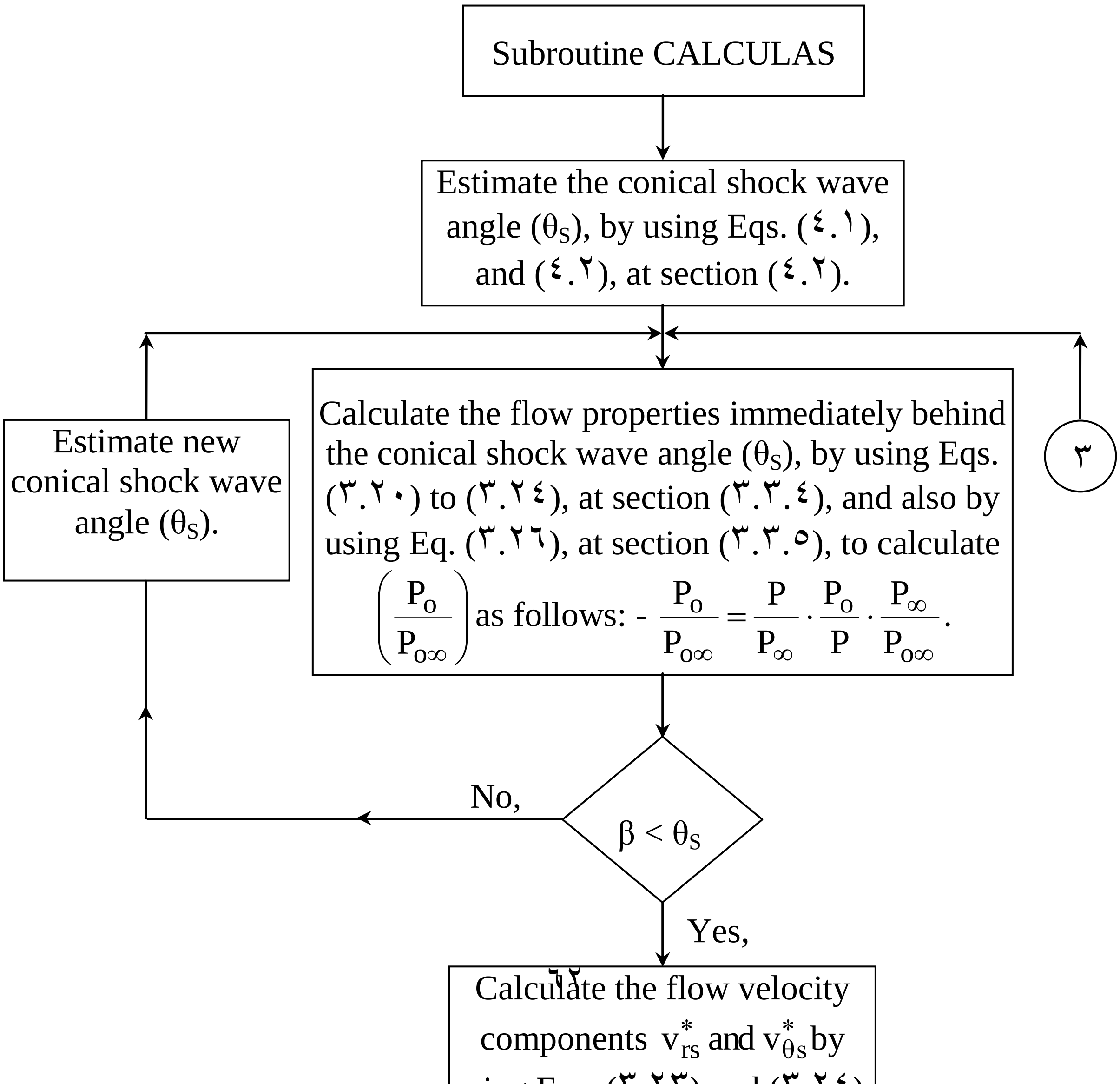
Subroutine CALCULAS
Estimate the conical shock wave angle (θ_S), by using Eqs. (٤.١), and (٤.٢), at section (٤.٢).
Calculate the flow properties immediately behind the conical shock wave angle (θ_S), by using Eqs. (٣.٢٠) to (٣.٢٤), at section (٣.٣.٤), and also by using Eq. (٣.٢٦), at section (٣.٣.٥), to calculate $\left(\frac{P_o}{P_{o\infty}}\right)$ as follows: - $\frac{P_o}{P_{o\infty}} = \frac{P}{P_\infty} \cdot \frac{P_o}{P} \cdot \frac{P_\infty}{P_{o\infty}}$.
٣
Estimate new conical shock wave angle (θ_S).
$\beta < \theta_S$
No,
Yes,
Calculate the flow velocity components v^*_{rs} and $v^*_{\theta s}$ by

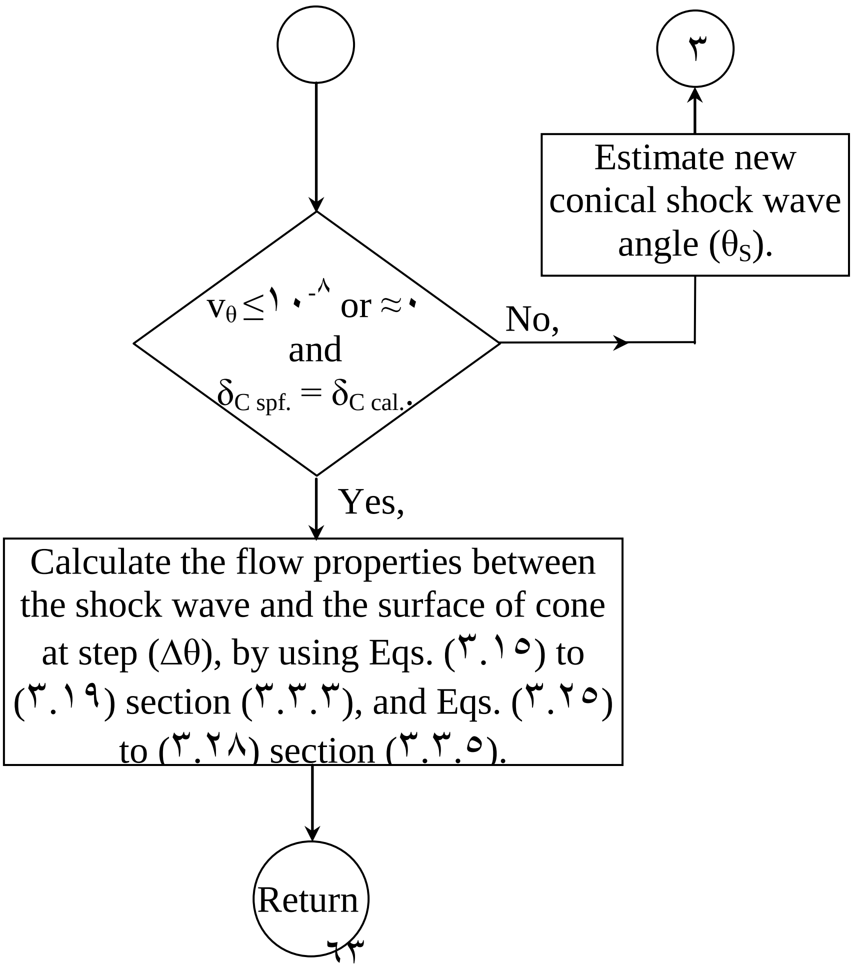
٣
Estimate new conical shock wave angle (θS).
vθ ≤ ١٠-٨ or ≈٠
and
δC spf. = δC cal..
No,
Yes,
Calculate the flow properties between the shock wave and the surface of cone at step (Δθ), by using Eqs. (٣.١٥) to (٣.١٩) section (٣.٣.٣), and Eqs. (٣.٢٥) to (٣.٢٨) section (٣.٣.٥).
Return

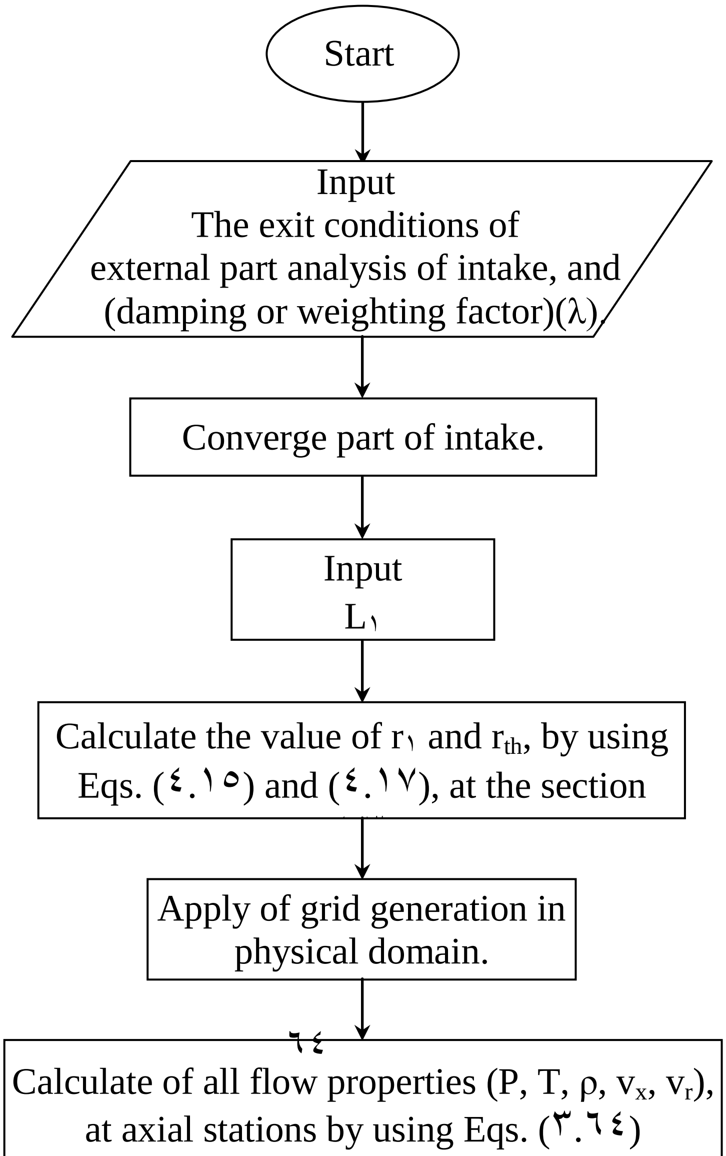
Start
Input
The exit conditions of
external part analysis of intake, and
(damping or weighting factor)(λ).
Converge part of intake.
Input
L١
Calculate the value of r١ and rth, by using
Eqs. (٤.١٥) and (٤.١٧), at the section
Apply of grid generation in
physical domain.
Calculate of all flow properties (P, T, ρ, vx, vr),
at axial stations by using Eqs. (٣.٦٤)

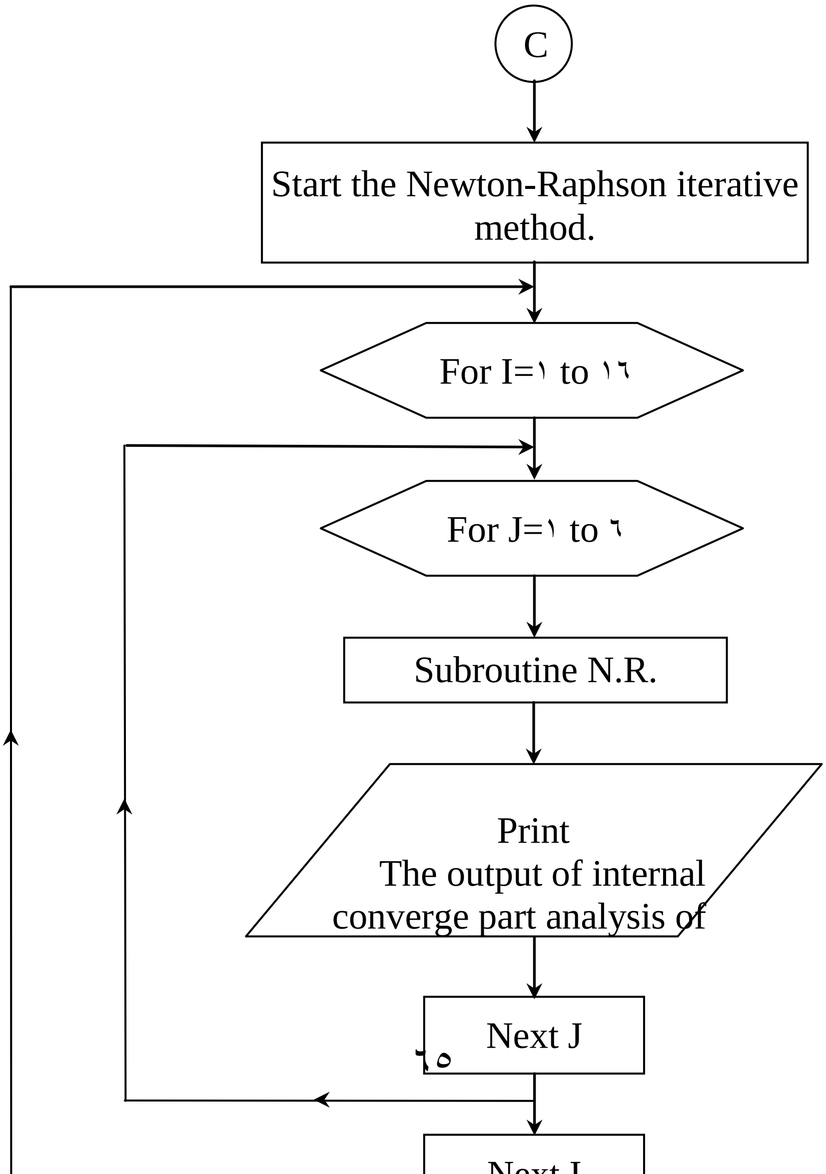
C
Start the Newton-Raphson iterative method.
For I=١ to ١٦
For J=١ to ٦
Subroutine N.R.
Print
The output of internal converge part analysis of
Next J

D

Calculate the value of $r_{٢}$, by using Eqs. (٤.١٨), at the section (٤.٣.١).

Apply of grid generation in physical domain.

Calculate of all flow properties (P, T, ρ, v_x, and v_r), at axial stations by using Eqs. (٣.٦٤) iteratively by using Newton-Raphson formula Eq. (٤.١٤), at the section (٤.٣).

Decoded all flow properties at one-dimension into two-dimensions.

Transformation of physical domain (x, r) to computational domain (ξ,η), by using Eqs. (٣.٣٧) to (٣.٤٠), at the section (٣.٤.٥).

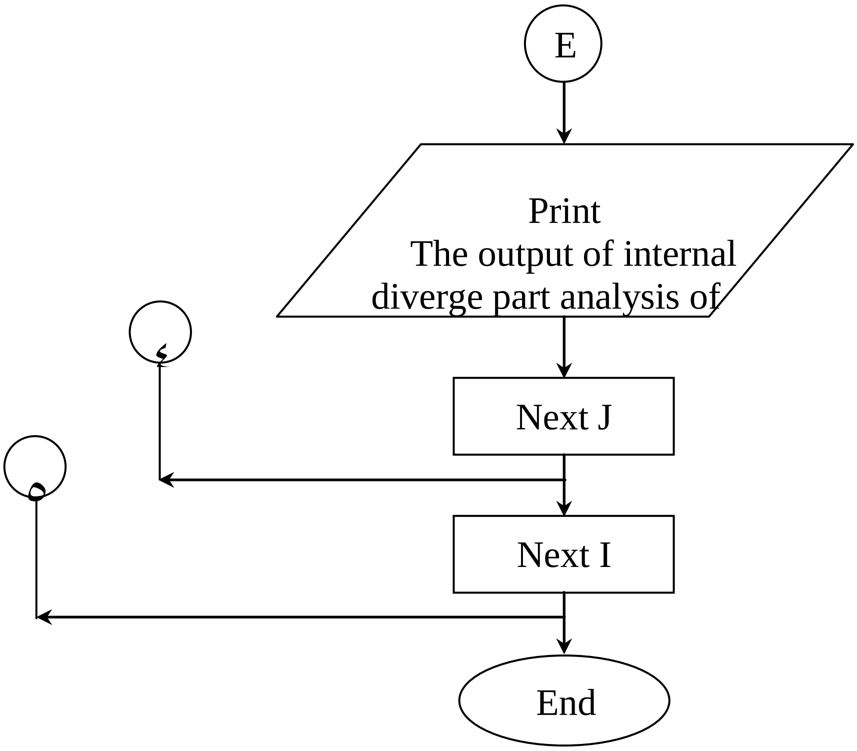

Fig. (٤.٥) Flow chart of the program for analysis and design of intake “Internal Part”.

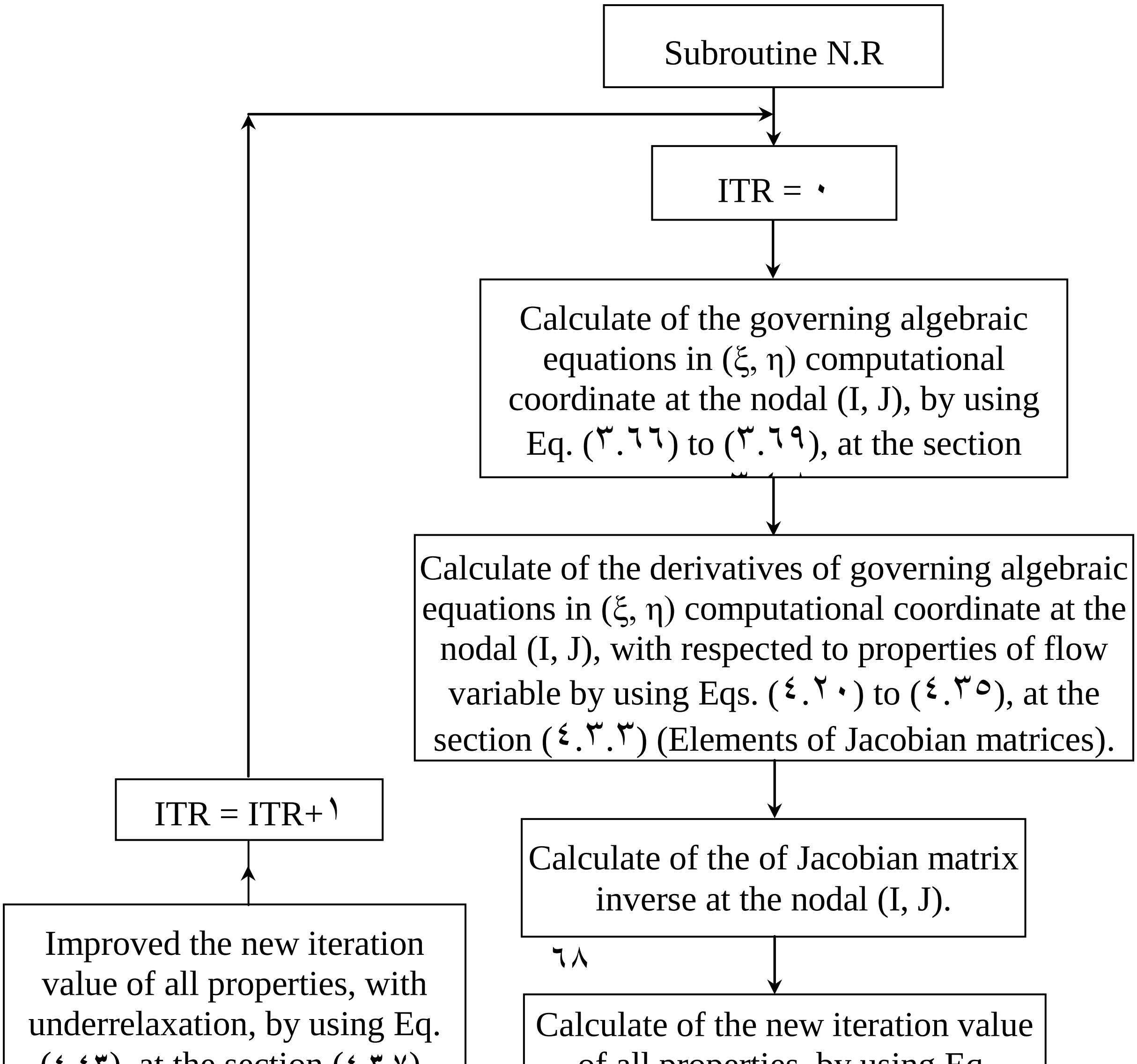
Subroutine N.R
ITR = ٠
Calculate of the governing algebraic equations in (ξ, η) computational coordinate at the nodal (I, J), by using Eq. (٣.٦٦) to (٣.٦٩), at the section
Calculate of the derivatives of governing algebraic equations in (ξ, η) computational coordinate at the nodal (I, J), with respected to properties of flow variable by using Eqs. (٤.٢٠) to (٤.٣٥), at the section (٤.٣.٣) (Elements of Jacobian matrices).
Calculate of the of Jacobian matrix inverse at the nodal (I, J).
Calculate of the new iteration value
ITR = ITR+١
Improved the new iteration value of all properties, with underrelaxation, by using Eq.

CHAPTER FIVE 5

RESULTS AND DISCUSSION

٥.١: INTRODUCTION: -

The results are the output of the computer programs. These computer programs are built to analyze and then design of the two-parts of intake (external and internal flow parts). Hence, so as to obtain deep understanding, the results will be presented for each two parts separately and then the collection takes place.

٥.٢: RESULTS OF THE EXTERNAL PART: -

A Taylor-Maccoll method was employed to analyze the supersonic inviscid flow around the cone by solves the equations of continuity and momentum in spherical coordinate system. In this section the results are concerned on presented of flow properties over a cone in supersonic Mach number for different angle of cone (١٠° to ٥٠°) with different free stream Mach number (~١.١ to ٥). Finally the optimization takes place to design this part as mentioned in section (٤.٣.١).

Fig. (٥.١) presents Mach number behind shock wave and at surface of cone as a function of free stream Mach number for different angles of cone. Where Mach numbers behind shock wave is bigger than that at surface of cone due to the isentropic compression region behind the shock wave. Both of them increase with increasing of free stream Mach number for constant angle of cone due to decrease of the shock wave angle (decrease of shock strength), and decrease with increasing angle of cone for constant free stream Mach number due to increase the angle of shock (increase of shock strength).

Fig. (٥.٢) presents the angle of shock wave as a function of free stream Mach number for different angles of cone. Where the angle of shock wave decreases with increasing of free stream Mach number for constant angle of cone, and increases with increasing angle of cone for constant free stream Mach number, where the relation is contrary.

Figs. (٥.٣), (٥.٤), and (٥.٥) present the static pressure, density, and temperature ratios respectively behind shock wave and at surface of cone to static free stream pressure, density, and temperature respectively as a function of free stream Mach number for different angles of cone. Where these properties behind shock wave is smaller than that at surface of cone due to the same reason mentioned in Fig. (٥.١). Both of these properties are increased with increasing of the free stream Mach number for constant angle of cone, and increased with increasing angle of cone for constant free stream Mach number but at different ratios due to the same reasons mentioned in Fig. (٥.١).

Figs. (٥.٦), (٥.٧), and (٥.٨) present the total pressure, density, and temperature ratios respectively to static free stream pressure, density, and temperature respectively as a function of free stream Mach number for different angles of cone. Where these properties are increased with the increasing of free stream Mach number for constant angle of cone, and decreased with increasing angle of cone for constant free stream Mach number due to the same reasons mentioned in Fig. (٥.١), except the total temperature ratio which remains constant for all angle of cone with constant free stream Mach number, where the process is adiabatic.

Fig. (٥.٩) presents the total pressure ratio of total pressure behind shock wave to free stream total pressure as a function of free stream Mach number for different angles of cone. Where this property decreases with the increase of free stream Mach number for constant angle of cone, and decreases with increasing angle of cone for constant free stream Mach number due to the same reason mentioned in Fig. (٥.١).

The flow over cone may be supersonic, subsonic or mixing between supersonic and subsonic. The data presented in table (١.١) give the minimum values of the freestream Mach number for which flow between the cone and the shock remains supersonic. At lesser Mach numbers, subsonic regions appear and cause deviations from conical flow.

δ_C°	١	٢	٣
١٠	١.٠٥٣٨	١.٠٥٨٨	١.١١٦
١٢.٥	١.٠٨٢٨	١.٠٨٤٨	١.١٦٤٥
١٥	١.١١٩٣	١.١٢٣	١.٢١٨٧
١٧.٥	١.١٦٢٢	١.١٦٨٨	١.٢٧٨١
٢٠	١.٢١١٥	١.٢٢٢٧	١.٣٤٢٨
٢٢.٥	١.٢٦٧٣	١.٢٨٥٣	١.٤١٣٥
٢٥	١.٣٣٠١	١.٣٥٧٢	١.٤٩١١
٣٠	١.٤٨٢	١.٥٣٣٦	١.٦٧٣٦
٣٥	١.٦٨١٤	١.٧٦٨٦	١.٩١١٤
٤٠	١.٩٥٨٢	٢.٠٩٩٥	٢.٢٤٨٦
٤٥	٢.٣٢١	٢.٦٢١٦	٢.٧٩٥
٥٠	٣.١٥٥	٣.٦٧٩١	٣.٩٥٦٩

Notes: -

Col. ١: Minimum value of (M_∞) for which conical flow is possible.

Col. ٢: Maximum value of (M_∞) for completely subsonic flow between the cone and the shock wave.

Col. ٣: Minimum value of (M_∞) for completely supersonic flow between the cone and the shock wave.

Table (٥.١) Values of freestream Mach number for various flow regimes for supersonic conical flow.

In order to validate the present study, some of empirical formulas, in which the properties of flow and the conical shock wave angle can be found with small different on the values that calculated from present study, are presented down, [٣١].

$$K_1 = M_\infty \sin \delta_c \quad \textbf{...(٥.١)}$$

$$M_\infty \sin\theta_s = \left(1 + \frac{(\gamma+1)}{2} K_1^2\right)^{\frac{1}{2}} \quad \textbf{...(٥.٢)}$$

$$\frac{P_c}{P_\infty} = 1.493(K_1)^{1.98} + 1.302 \qquad ...(٥.٣)$$

$$\frac{T_c}{T_\infty} = 0.2403(K_1)^{1.97} + 1.119 \qquad ...(٥.٤)$$

Fig. (٥.١٠) presents the total pressure recovery (the ratio of stagnation pressure behind the two conical and one normal shock wave to free stream stagnation pressure ($\frac{P_{o3}}{P_{o\infty}}$)) as a function of the second cone angle for a series of values of the first cone angle, for design Mach number ($M_\infty = 2$). Where this ratio increases for all values of first cone semi angles (δ_{c1}), with the increase of the values of second cone semi angle (δ_{c2}), but for different increase ratios. And at different values of (δ_{c2}), these increases in total pressure ratio will decrease. Hence, to get on the highest total pressure recovery, the optimum values of first and second semi cone angles are (20^o) and (18^o) respectively, where at these values the value of total pressure recovery is equal to (٠.٩٧٣٤٨٢٥).

٥.٣: RESULTS OF THE INTERNAL PART: -

A finite difference method was employed to solve the equations of continuity, momentum and energy for an axisymmetric flow. In this section the results of diverge part are presented. These results present the optimum design annular diverge part diffuser for several area ratios (AR) and angle of diverge wall (θ). For each area ratio the angle was increased until circulation takes place. And for each area ratio, Mach numbers distribution at the exit section for a series of angles are presented.

Fig. (٥.١١) shows the results for a diffuser for three paths. Path (١) is at the row (J = ١), path (٢) is at the row (J = ٤), and path (٣) is at the row (J = ٥).

Fig. (٥.١٢) presents the axial velocity component (v_x) distribution along the divergent portion of internal part of intake, for area ratio (AR = ١.٣) at path

(١) and different inclination wall angles (θ). The velocity decreases along the divergent portion for the same angle and approximately the same velocity for all angles, except a small different in the beginning of this portion due to the increase in the divergent wall angle.

Fig. (٥.١٣) presents the axial velocity component (v_x) distribution along the divergent portion of internal part of intake, at path (٢). The velocity decreases with the distance for the same angle, except for angle ($\theta = 13^\circ$), where the velocity decreases for (X/L=٠.٠ to ٠.٦) and then slightly increases and then drops. The reason of this response at flow axial velocity is due to the fact that the input condition for this part is the output of the normal shock wave. Where the value of (v_x) at path (١) is smaller than its value at path (٢) and the value of (v_x) at path (٢) is smaller than its value at path (٣). So the flow at path (٢) is under effect of other two paths one of them is path (١), which is not affected by the increase of the divergent wall due to far from diverge wall (nearly of the horizontal). The other, path (٣) which is affected by the increase of the divergent wall due to nearly of it. Hence for small values of (θ), the flow at path (١) has more effected on the flow at path (٢) than the flow at path (٣). And for high values of (θ), the flow at path (٣) has more effected on flow at path (٢) than the flow at path (١).

Fig. (٥.١٤) presents the axial velocity component (v_x) distribution along the divergent portion of internal part of intake, at path (٣). The velocity decreases with distance for the same angle, except for angles ($\theta = 9^\circ$ to 13°), where the velocity decreases for (X/L=٠.٠ to between (٠.٥~٠.٦٤)) and then increases and after this may be decreased due to the same reason mentioned in Fig. (٥.١٣).

Fig. (٥.١٥) presents the radial velocity component (v_r) distribution along the divergent portion of internal part of intake, at path (١). It shows that the velocity in the initial section increases with distance and then slightly decreases and then levels out for all angles due to the sudden change in flow direction as the flow enter to the diverge portion. Also the velocity increases with the increase angle values due to the increase in the divergent wall.

Fig. (٥.١٦) presents the radial velocity component (v_r) distribution along the divergent portion of internal part of intake, at path (٢). It shows that in range (3° to 9°) the velocity increases with distance and then slightly decreases and then levels out due to the same reason mentioned in Fig. (٥.١٥). And in range (11° to 13°) velocity increases with distance and then drops as it is approach circulation and then increases due to the same reason mentioned in Fig. (٥.١٣).

Fig. (٥.١٧) presents the radial velocity component (v_r) distribution along the divergent portion of internal part of intake, at path (٣). It shows that in range (3° to 9°) the velocity increases with distance and then slightly decreases and then levels out due to the same reason mentioned in Fig. (٥.١٥). And in range (11° to 13°) the velocity increases in strong form with distance and then falling in strong form to negative value at distance (X/L = ٠.٦٢~٠.٧٦) for angle (11^o) and at distance (X/L = ٠.٦٧~٠.٩٣) for angle (13^o) and then increases to reasonable value at the exit section due to the same reason mentioned in Fig. (٥.١٣).

Fig. (٥.١٨) presents the Mach number (M) distribution along the divergent portion of internal part of intake, for path (١). The Mach number decreases along the diverge portion for the same angle and approximately the same Mach number for all angles except a small different in the beginning of this portion due to the increase in the divergent wall angle.

Fig. (٥.١٩) presents the Mach number (M) distribution along the divergent portion of internal part of intake, for path (٢). The Mach number decreases with distance for the same angle, except for angle ($\theta = 13^{\circ}$) where the Mach number decreases for (X/L = ٠.٠ to ٠.٦) and then slightly increases and then decreases due to the same reason mentioned in Fig. (٥.١٣).

Fig. (٥.٢٠) presents the Mach number (M) distribution along the divergent portion of internal part of intake, for path (٣). The Mach number decreases along this part for the same angle, except for range (9° to 13°) where the Mach number decrease for (X/L = ٠.٠ to between (٠.٥٥~٠.٦٤)) and then increases to reasonable value at the exit section due to the same reason mentioned in Fig. (٥.١٣).

Fig. (٥.٢١) presents the Mach number (M) distribution at the exit section of the divergent portion of internal part of intake, for area ratio (AR = ١.٣). The Mach number near the horizontal wall has the same values for all angles due to the fact that at the horizontal wall or near from it, the Mach number is far from divergent wall effects. But at the diverge wall or near from it, the Mach number has different values for different angles due to the effect of divergent wall, where Mach number decreases with the increase of angle. For this area ratio the values of Mach numbers at the exit section lies between (٠.٤٣٥ to ٠.١٦) for all angles.

Fig. (٥.٢٢) presents the axial velocity component (v_x) distribution along the divergent portion of internal part of intake, for area ratio (AR = ١.٣٥) at path (١) and different inclination wall angles (θ). The velocity decreases along this part for the same angle and approximately the same velocity for all angles, except a small different in the beginning of this portion due to the same reason mentioned in Fig. (٥.١٢).

Fig. (٥.٢٣) presents the axial velocity component (v_x) distribution along the divergent portion of internal part of intake, at path (٢). The velocity decreases with distance for the same angle, except for angle ($\theta = 13^{\circ}$). Where the velocity decreases for (X/L=٠.٠ to ٠.٥) and then slightly increases and then decreases. The velocity at the exit section (X/L = ١) has the same value for all angles due to the same reason mentioned in Fig. (٥.١٣).

Fig. (٥.٢٤) presents the axial velocity component (v_x) distribution along the divergent portion of internal part of intake, at path (٣). The velocity decreases with distance for the same angle, except for angles ($\theta = 11^{\circ}$ to 13°), where the velocity increases at (X/L=٠.٥ to ٠.٦) then decreases due to the same reason mentioned in Fig. (٥.١٤).

Fig. (٥.٢٥) presents the radial velocity component (v_r) distribution along the divergent portion of internal part of intake, at path (١). It shows that the velocity in the initial section increases with distance and then decreases and then levels out for all angles due to the same reason mentioned in Fig. (٥.١٥).

Fig. (٥.٢٦) presents the radial velocity component (v_r) distribution along the divergent portion of internal part of intake, at path (٢). It shows that in range (3° to 9°) velocity increases with distance and then slightly decreases and then levels out due to the same reason mentioned in Fig. (٥.١٥). And in range (11° to 13°) the velocity increases with distance and then drops as it is approach circulation and then increases due to the same reason mentioned in Fig. (٥.١٣).

Fig. (٥.٢٧) presents the radial velocity component (v_r) distribution along the divergent portion of internal part of intake, at path (٣). It shows that in range (3° to 9°) the velocity increases with distance and then slightly decreases and then levels out due to the same reason mentioned in Fig. (٥.١٥). And in range (11° to 13°) the velocity increases in strong form with distance and then falling in strong form to negative value for angle (13°) at distance (X/L = ٠.٧) and then increases to reasonable value at the exit section due to the same reason mentioned in Fig. (٥.١٣).

Fig. (٥.٢٨) presents the Mach number (M) distribution along the divergent portion of internal part of intake, for path (١). The Mach number decreases along the diverge portion for the same angle and approximately the same Mach number for all angles except a small different in the beginning of this portion due to the same reason mentioned in Fig. (٥.١٨).

Fig. (٥.٢٩) presents the Mach number (M) distribution along the divergent portion of internal part of intake, for path (٢). The Mach number decreases with distance for the same angle, except for angle ($\theta = 13^{\circ}$) where the Mach number decreases for (X/L = ٠.٠ to ٠.٦) and then slightly increases and then decreases due to the same reason mentioned in Fig. (٥.١٣).

Fig. (٥.٣٠) presents the Mach number (M) distribution along the divergent portion of internal part of intake, for path (٣). The Mach number decreases with distance for the same angle, except for angles (11° and 13°) where the Mach number decreases for (X/L = ٠.٠ to between (٠.٥~٠.٦)) and then increases and after this decreases due to the same reason mentioned in Fig. (٥.١٣).

Fig. (٥.٣١) presents the Mach number (M) distribution at the exit section of the divergent portion of internal part of intake, for area ratio (AR = ١.٣٥). The Mach number near the horizontal wall has the same values for all angles. But at the diverge wall or near from it, the Mach number has different values for different angles due to the same reason mentioned in Fig. (٥.٢١). For this area ratio the values of Mach numbers at the exit section lies between (٠.٤ to ٠.١٣) for all angles.

Fig. (٥.٣٢) presents the axial velocity component (v_x) distribution along the divergent portion of internal part of intake, for area ratio (AR = ١.٤) at path (١) and different inclination wall angles (θ). The velocity decreases along this part for the same angle and approximately the same velocity for all angles, except a very small different in the beginning of this portion due to the same reason mentioned in Fig. (٥.١٢).

Fig. (٥.٣٣) presents the axial velocity component (v_x) distribution along the divergent portion of internal part of intake, at path (٢). The velocity decreases with distance for the same angle, but at different range especially for angles ($\theta = 11^\circ$ and 13°) at distance (X/L = ٠.٠ to ٠.٦). The velocity at the exit section (X/L = ١) has approximately the same value for all angles due to the same reason mentioned in Fig. (٥.١٣).

Fig. (٥.٣٤) presents the axial velocity component (v_x) distribution along the divergent portion of internal part of intake, at path (٣). The velocity decreases with distance for the same angle, except for angles ($\theta = 11^\circ$ and 13°), where the velocity increases at (X/L=٠.٥ to ٠.٥٥) then decreases due to the same reason mentioned in Fig. (٥.١٤).

Fig. (٥.٣٥) presents the radial velocity component (v_r) distribution along the divergent portion of internal part of intake, at path (١). It shows that the velocity in the initial section increases with distance and then decreases and then levels out for all angles due to the same reason mentioned in Fig. (٥.١٥).

Fig. (٥.٣٦) presents the radial velocity component (v_r) distribution along the divergent portion of internal part of intake, at path (٢). It shows that in range (3° to 9°) the velocity increases with distance and then slightly decreases and then levels out due to the same reason mentioned in Fig. (٥.١٥). And in range (11° to 13°) the velocity increases with distance and then drops at different range as it is approach circulation and then increases to levels out due to the same reason mentioned in Fig. (٥.١٣).

Fig. (٥.٣٧) presents the radial velocity component (v_r) distribution along the divergent portion of internal part of intake, at path (٣). It shows that in range (3° to 9°) the velocity increases with distance and then slightly decreases and then levels out due to the same reason mentioned in Fig. (٥.١٥). And in range (11° to 13°) the velocity increases in strong form with distance and then falling in strong form to negative value for angle (13°) at distance (X/L = ٠.٦٤) and then increases then levels out due to the same reason mentioned in Fig. (٥.١٣).

Fig. (٥.٣٨) presents the Mach number (M) distribution along the divergent portion of internal part of intake, for path (١). The Mach number decreases along the diverge portion for the same angle and approximately the same Mach number for all angles except a very small different in the beginning of this portion due to the same reason mentioned in Fig. (٥.١٨).

Fig. (٥.٣٩) presents the Mach number (M) distribution along the divergent portion of internal part of intake, for path (٢). The Mach number decreases with distance for the same angle, but at different range especially for angles (θ = 11° and 13°) at distance (X/L = ٠.٠ to ٠.٦). And then decreases, where the Mach number at the exit section (X/L = ١) has approximately the same value for all angles due to the same reason mentioned in Fig. (٥.١٣).

Fig. (٥.٤٠) presents the Mach number (M) distribution along the divergent portion of internal part of intake, for path (٣). The Mach number decreases with distance for the same angle, except for angles (11° and 13°) where the Mach number decreases for (X/L = ٠.٠ to between (٠.٥~٠.٥٤)) and then increases and after this decrease due to the same reason mentioned in Fig. (٥.١٣).

Fig. (٥.٤١) presents the Mach number (M) distribution at the exit section of the divergent portion of internal part of intake, for area ratio (AR = ١.٤). The

Mach number near the horizontal wall has the same values for all angles. But at the diverge wall or near from it, the Mach number has different values for different angles due to the same reason mentioned in Fig. (٥.٢١). For this area ratio the values of Mach numbers at the exit section lies between (٠.٣٧ to ٠.٠٦) for all angles.

Fig. (٥.٤٢) presents the axial velocity component (v_x) distribution along the divergent portion of internal part of intake, for area ratio (AR = ١.٤٥) at path (١) and different inclination wall angles (θ). The velocity decreases along this part for the same angle and approximately the same velocity for all angles, except a very small different in the beginning of this portion due to the same reason mentioned in Fig. (٥.١٢).

Fig. (٥.٤٣) presents the axial velocity component (v_x) distribution along the divergent portion of internal part of intake, at path (٢). The velocity decreases with distance for the same angle, but at different range especially for angles (θ = 11° and 13°) at distance (X/L = ٠.٠ to ٠.٦). The velocity at the exit section (X/L = ١) has approximately the same value for all angles due to the same reason mentioned in Fig. (٥.١٣).

Fig. (٥.٤٤) presents the axial velocity component (v_x) distribution along the divergent portion of internal part of intake, at path (٣). The velocity decreases with distance for the same angle, except for angle (θ = 13°), where the velocity increases at (X/L=٠.٥) then decreases due to the same reason mentioned in Fig. (٥.١٤).

Fig. (٥.٤٥) presents the radial velocity component (v_r) distribution along the divergent portion of internal part of intake, at path (١). It shows that the velocity in the initial section increases with distance and then decreases and then levels out for all angles due to the same reason mentioned in Fig. (٥.١٥).

Fig. (٥.٤٦) presents the radial velocity component (v_r) distribution along the divergent portion of internal part of intake, at path (٢). It shows that in range (3° to 9°) the velocity increases with distance and then slightly decreases and then levels out due to the same reason mentioned in Fig. (٥.١٥). In angles (11° and 13°) the velocity increases in strong form then falls with strong form also at different range as it is approach circulation and then increases to levels out due to the same reason mentioned in Fig. (٥.١٣).

Fig. (٥.٤٧) presents the radial velocity component (v_r) distribution along the divergent portion of internal part of intake, at path (٣). It shows that in range (3° to 7°) the velocity increases with distance and then slightly decreases and then levels out due to the same reason mentioned in Fig. (٥.١٥). And in angle (9°) the velocity increase with distance and drops then slightly increases at distance (X/L = ٠.٤٧) to levels out. In angles (11° and 13°) the velocity increases in strong form then falls with strong form also at different range and then increases at distance (X/L = ٠.٥ to ٠.٦) to decrease again with little range at the exit section due to the same reason mentioned in Fig. (٥.١٣).

Fig. (٥.٤٨) presents the Mach number (M) distribution along the divergent portion of internal part of intake, for path (١). The Mach number decreases along the diverge portion for the same angle and approximately the same Mach number for all angles except a very small different in the beginning of this portion due to the same reason mentioned in Fig. (٥.١٨).

Fig. (٥.٤٩) presents the Mach number (M) distribution along the divergent portion of internal part of intake, for path (٢). The Mach number decreases with distance for the same angle, but at different range especially for angles ($\theta = 11^\circ$ and 13°) at distance (X/L = ٠.٠ to ٠.٥٨). And then decreases, where the

Mach number at the exit section (X/L = ١) has approximately the same value for all angles due to the same reason mentioned in Fig. (٥.١٣).

Fig. (٥.٥٠) presents the Mach number (M) distribution along the divergent portion of internal part of intake, for path (٣). The Mach number decreases with distance for the same angle, except for angles (13°) where the Mach number decreases for (X/L = ٠.٠ to between ٠.٥) and then increases and after this decreases due to the same reason mentioned in Fig. (٥.١٣).

Fig. (٥.٥١) presents the Mach number (M) distribution at the exit section of the divergent portion of internal part of intake, for area ratio (AR = ١.٤٥). The Mach number near the horizontal wall has the same values for all angles. But at the diverge wall or near from it, the Mach number has different values for different angles due to the same reason mentioned in Fig. (٥.٢١). For this area ratio the values of Mach numbers at the exit section lies between (٠.٣٤٢ to ٠.٠٤١٥) for all angles.

٥.٤: RESULTS OF THE PERFORMANCE STUDY: -

The performance study was done at on and off design conditions by offer of properties of flow along the intake that designed in previous section. Where the parameter of intake that designed are:

$\delta_{c١}$ = ٢٠°.

$\delta_{c٢}$ = ١٨°. → **Calculated From numerical method for "external part".**

h_{co} = ٢٣.٥٢٤٧١ cm. → **Calculated From equation (٤.١١).**

L_N = ٢٣.٥٢٤٧١ cm. → **Calculated From equation (٤.١٢).**

L_W = ١٧.٦٦٣٨٠٥٥ cm. → **Calculated From equation (٤.١٣).**

$r_١$ = ٧.٢٧٧٩٨ cm. → **Calculated From equation (٤.١٥).**

→ **Calculated From numerical method for internal part "converge portion" to get sonic or nearly sonic flow at throat section.**

→ **Calculated From equation (٤.١٧).**

Calculated From numerical method for internal part

$L_{١}$ = ٢.٥ mm.

r_{th} = ٧.٠٨٢٦٣ cm.

$L_{٢}$ = ٣٢.٢٨١٣٥ cm.

θ = ٧°.

$r_{٢}$ = ١١.٠٤٦٣١ cm.

The overall length of supersonic air intake ($L_{overall}$) = L_N + $L_{١}$ + $L_{٢}$ = ٢٣.٥٢٤٧١ + ٠.٢٥ + ٣٢.٢٨١٣٥ = ٥٦.٠٥٦٠٦ cm.

Fig. (٥.٥٢) presents the vector plot distribution along the supersonic air intake at design conditions, this figure shows the direction and the values of the absolute velocity. Where the velocity distribution has high values behind the conical shock wave and drop gradually to small values at the end of intake due to the shock waves (conical and normal) and the diverge wall which starting at (٢٣.٥٢٤٧١ cm).

Fig. (٥.٥٣) presents the contour lines of the Mach number (M) distribution along the supersonic air intake at design conditions. Where the Mach distribution has high values behind the conical shock wave and drop gradually to small values at the end of intake due to the same reasons mentioned in Fig. (٥.٥٢).

Fig. (٥.٥٤) presents the contour lines of the pressure ratio (P/P_∞) distribution along the supersonic air intake at design conditions. Where the pressure ratio distribution has small values behind the conical shock wave and increases gradually to high values at the end of intake due to the same reasons mentioned in Fig. (٥.٥٢).

Fig. (٥.٥٥) presents the contour lines of the temperature ratio (T/T_∞) distribution along the supersonic air intake at design conditions. Where the temperature ratio distribution has small values behind the conical shock wave and increases gradually to high values at the end of intake due to the same reasons mentioned in Fig. (٥.٥٢).

Fig. (٥.٥٦) presents the vector plot distribution along the supersonic air intake at off-design condition (H = ١١٠٠٠ m), this figure shows the direction and the values of the absolute velocity. Where the velocity distribution has high values behind the conical shock wave and drops gradually to small values at the end of intake due to the same reasons mentioned in Fig. (٥.٥٢).

The other graphs of Mach and flow property ratios are the same graphs of design conditions in Figs. (٥.٥٣), (٥.٥٤), and (٥.٥٥) respectively.

Fig. (٥.٥٧) presents the vector plot distribution along the supersonic air intake at off-design condition (H = ٠ m), this figure shows the direction and the values of the absolute velocity. Where the velocity distribution has high values behind the conical shock wave and drops gradually to small values at the end of intake due to the same reasons mentioned in Fig. (٥.٥٢).

The other graphs of Mach and flow property ratios are the same graphs of design conditions in Figs. (٥.٥٣), (٥.٥٤), and (٥.٥٥) respectively.

Fig. (٥.٥٨) presents the vector plot distribution along the supersonic air intake at off-design condition (M = ١.٥), this figure shows the direction and the values of the absolute velocity. Where the velocity distribution has high values behind the conical shock wave and drops gradually to small values at the end of intake due to the same reasons mentioned in Fig. (٥.٥٢). Also this figure shows that the conical shock wave moves ahead of the cowl lip, and the normal shock wave expelled out at (X ≈ ١٥.٨ cm) due to the drop in Mach number (١.٥).

Fig. (٥.٥٩) presents the contour lines of the Mach number (M) distribution along the supersonic air intake at off-design condition (M = ١.٥). Where the Mach distribution has high values behind the conical shock wave and drops gradually to small values at the end of intake due to the same reasons mentioned in Fig. (٥.٥٢). Also this figure shows that the conical shock wave moves ahead of the cowl lip, and the normal shock wave expelled out at (X ≈ ١٥.٨ cm) due to the same reason mentioned in Fig. (٥.٥٧).

Fig. (٥.٦٠) presents the contour lines of the pressure ratio (P/P_{∞}) distribution along the supersonic air intake at off-design condition (M = ١.٥). Where the pressure ratio distribution has small values behind the conical shock wave and increases gradually to high values at the end of intake due to the same reasons mentioned in Fig. (٥.٥٢). Also this figure shows that the conical shock wave moves ahead of the cowl lip, and the normal shock wave expelled out at (X ≈ ١٥.٨ cm) due to the same reason mentioned in Fig. (٥.٥٧).

Fig. (٥.٦١) presents the contour lines of the temperature ratio (T/T_{∞}) distribution along the supersonic air intake at off-design condition (M = ١.٥). Where the temperature ratio distribution has small values behind the conical shock wave and increases gradually to high values at the end of intake due to the same reasons mentioned in Fig. (٥.٥٢). Also this figure shows that the conical shock wave moves ahead of the cowl lip, and the normal shock wave expelled out at (X ≈ ١٥.٨ cm) due to the same reason mentioned in Fig. (٥.٥٧).

Fig. (٥.٦٢) presents the vector plot distribution along the supersonic air intake at off-design condition (M = ٢.٢), this figure shows the direction and the values of the absolute velocity. Where the velocity distribution has high values behind the conical shock wave and drops gradually to small values at the end of intake due to the same reasons mentioned in Fig. (٥.٥٢). Also this figure shows that the conical shock wave moves inside of the cowl lip, and the normal shock wave go to diverge section at (X ≈ ٢٧ cm) due to the increase in Mach number (٢.٢).

Fig. (٥.٦٣) presents the contour lines of the Mach number (M) distribution along the supersonic air intake at off-design condition (M = ٢.٢). Where the Mach distribution has high values behind the conical shock wave and drops gradually to small values at the end of intake due to the same reasons mentioned in Fig. (٥.٥٢). Also this figure shows that the conical shock wave moves inside of the cowl lip, and the normal shock wave go to diverge section at (X ≈ ٢٧ cm) due to the same reason mentioned in Fig. (٥.٦٢).

Fig. (٥.٦٤) presents the contour lines of the pressure ratio (P/P_{∞}) distribution along the supersonic air intake at off-design condition (M = ٢.٢). Where the pressure ratio distribution has small values behind the conical shock wave and increases gradually to high values at the end of intake due to the same reasons mentioned in Fig. (٥.٥٢). Also this figure shows that the conical shock wave moves inside of the cowl lip, and the normal shock wave go to diverge section at (X ≈ ٢٧ cm) due to the same reason mentioned in Fig. (٥.٦٢).

Fig. (٥.٦٥) presents the contour lines of the temperature ratio (T/T_{∞}) distribution along the supersonic air intake at off-design condition (M = ٢.٢). Where the temperature ratio distribution has small values behind the conical shock wave and increases gradually to high values at the end of intake due to the same reasons mentioned in Fig. (٥.٥٢). Also this figure shows that the conical shock wave moves inside of the cowl lip, and the normal shock wave go to diverge section at (X ≈ ٢٧ cm) due to the same reason mentioned in Fig. (٥.٦٢).

CHAPTER SIX

CONCLUSIONS AND RECOMMENDATION

6

٦.١: CONCLUSIONS: -

The conclusions of this study may be classified into two parts according to parts of intake under study: -

٦.١.١: EXTERNAL PART: -

The part of intake consists of a sharp cone with angle ($\delta_{C١}$) follows by a second cone with angle ($\delta_{C٢}$).

The following conclusions can be withdrawn for the cone are: -

١. The flow over the cone is complex, where this flow has curve form, so it is non-uniform, thus, its properties are non-uniform, so it needs to three dimensions to study (or quasi-three dimensions (axisymmetric)).

٢. The flow which is initially supersonic just behind the shock front may either remain supersonic or go over to a subsonic flow at some surface (θ = constant (the sonic cone or sonic line)). Where in the latter case, the flow field is mixing supersonic and subsonic. Finally, a flow, which is initially subsonic behind the shock, will necessarily remain subsonic.

٣. The total pressure recovery ($\frac{P_{o3}}{P_{o\infty}}$) increases with increasing the first cone angle for range $(10^o - 20^o)$ for constant second cone angle until it reaches to maximum value then decreases for range $(21^o - 24^o)$. Also total pressure recovery increases with increasing the second cone angle for constant first cone angle but at different range then drop. So the optimum first and second cone angle was (20^o) and (18^o) respectively, as shown in Fig. (٥.١٠).

٦.١.٢: INTERNAL PART: -

This part of intake consists of a converge diverge diffuser, the designing process was concentrated on the diverge portion of diffuser, while the converge portion was used as isentropic compression to decrease supersonic flow to sonic or nearly sonic flow.

The following conclusions can be withdrawn for the diverge portion of internal part of supersonic air intake are: -

١. The results indicated that the axial velocity component (v_x) for paths (١) and (٢) decreases with distance and increases with increase of the angle for the same area ratio near inlet and approximately the same value at exit. Also these values decreases with the increase area ratio for the same angle. For path (٣) and for angles $(3^o - 7^o)$ the velocity behave as in paths (١) and (٢), and for larger than these angles the velocity decreases with the distance until it reaches to minimum value at large angle then increases to normal value at diffuser exit for the same area ratio. This behavior eliminates gradually with the increase area ratio for the same angle.

٢. The radial velocity component (v_r) for path (١) increases with distance until it reaches to maximum value near the inlet, then decreases then level out, at the same angle for all area ratio. Also the velocity increases with increase of the angle for the same area ratio. For paths (٢) and (٣) and for angle $(3^o - 7^o)$ the velocity behaves as in path (١). For large than these angles the velocity increases with distance then decreases until it reaches minimum value at large angle then increases to normal value at diffuser exit for the same area ratio. This behavior eliminate gradually with increase of the area ratio for the same angle

٣. Mach number (M) behaves as axial velocity in paragraph (٢). Mach number at the exit section decreases from high to low values (subsonic) with the increase distance from straight to diverge wall.

٤. From studying the results of the analysis of flow through the divergent portion for several models, the geometry data for optimum design found are: -

AR = ١.٣٥,

$\theta = 7^{o}$

٦.١.٣: GEOMETRY DATA FOR OPTIMUM DESIGN OF SUPERSONIC AIR INTAKE: -

From studying the results of the analysis of the flow through the external and internal parts of supersonic air intake for several models at design conditions (M_∞ = ٢, H = ١٠٠٠٠ m, and $\dot{m} = 30\,kg/sec$), the geometry data for optimum design found are: -

$\delta_{c١}$ = ٢٠°.

$\delta_{c٢}$ = ١٨°.

L_N = ٢٣.٥٢٤٧١ cm.

L_W = ١٧.٦٦٣٨٠٥٥ cm.

h_{co} = ٢٣.٥٢٤٧١ cm.

$r_١$ = ٧.٢٧٧٩٨ cm.

r_{th} = ٧.٠٨٢٦٣ cm.

$r_٢$ = ١١.٠٤٦٣١ cm.

$L_١$ = ٢.٥ mm.

$L_٢$ = ٣٢.٢٨١٣٥ cm.

θ = ٧°.

$L_{overall}$ = ٥٦.٠٥٦٠٦ cm.

The intake selected was tested under variable altitude and Mach numbers, and gave a good performance.

٦.٢: RECOMMENDATIONS: -

The following recommendations are suggested for a further work to achieve a complete analysis and design of supersonic air intake: -

١. Developing the work by employing non- zero angle of attack (non-axisymmetric).

٢. Design of the transient section (Throat section), which includes the cowl lip and the surface of spike.

٣. Developing the work by employing viscous flow, and comparing the results with the present (unviscous).

٤. Change the geometry of the spike as the follows: -

- ٤-shock system (Three - cone).
- Isentropic compression system.

٥. Employing another technique to solve the governing differential equations, such as characteristic method, finite element method and MacCormack method.

CERTIFICATION

We certify that we have read this thesis, entitled ***"Design of axisymmetric supersonic air intake",*** and as examining committee, examined the student "**Hussain Kadhim Holwass"** in its contents and in what is connected with it, and that in our opinion it meets the standard of a thesis for the degree of Master of Science in Mechanical Engineering.

Signature:

Name: Asst. Prof. Dr.Ihsan Y. Hussain
(Member)
Date: / /٢٠٠٣

Signature:

Name: Asst. Prof Dr. Ikhlas Mohammed Fayed
(Member)
Date: / /٢٠٠٣

Signature:

Name: Prof. Dr. Ghaniem Kadhem Abdul Sada
(Chairman)
Date: / /٢٠٠٣

Signature:

Name: Asst. Prof. Dr. Arkan K. Al-Taie
(Supervisor)
Date: / /٢٠٠٣

Signature:

Name: Asst. Prof. Dr. Abdul-Kareem A Wahab.
(Supervisor)
Date: / /٢٠٠٣

Approval of the Mechanical Engineering Department

Signature:

Name: Lecturer Dr. Ala M. Hosain
Head of the Mechanical Engineering Department
Date: / /٢٠٠٣

Approval of the Deanery of the College of Engineering in Babylon University.

Signature:

Name: Asst. Prof. Dr. Haroun A. K. Shahad
Dean of the College of Engineering

Date: / /٢٠٠٣

SUPERVISORS CERTIFICATE

We certify that the preparation of this thesis entitled ***"Design of axisymmetric supersonic air intake"*** was prepared by **"Hussain Kadhim Holwass"** under our supervision at Babylon University, College of Engineering in partial fulfillment of the requirements for the degree of Master of Science in Mechanical Engineering.

Signature:	**Signature:**
Name: Asst. Prof.	**Name:** Asst. Prof.
Dr. Arkan K. Al-Taie	**Dr. Abdul Kareem A. Wahab**
(Supervisor)	(Supervisor)
Date: / / ٢٠٠٣	**Date:** / / ٢٠٠٣

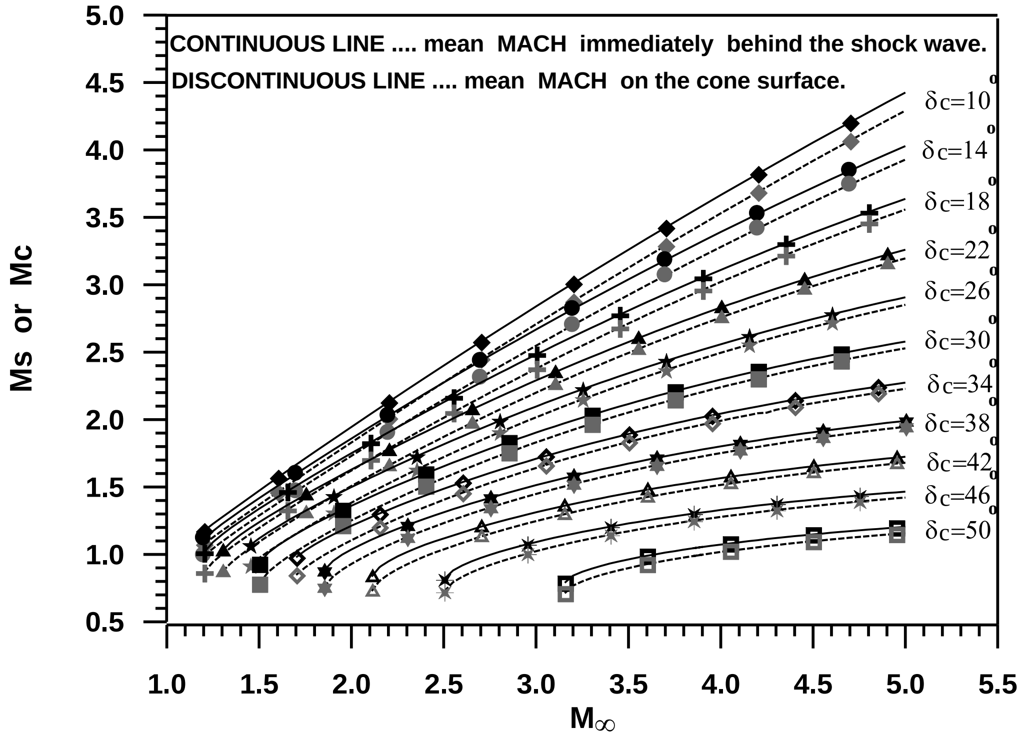

Fig. (٥. ١) Mach number behind the shock wave and at the surface of cone versus free stream Mach number for different cone angles.

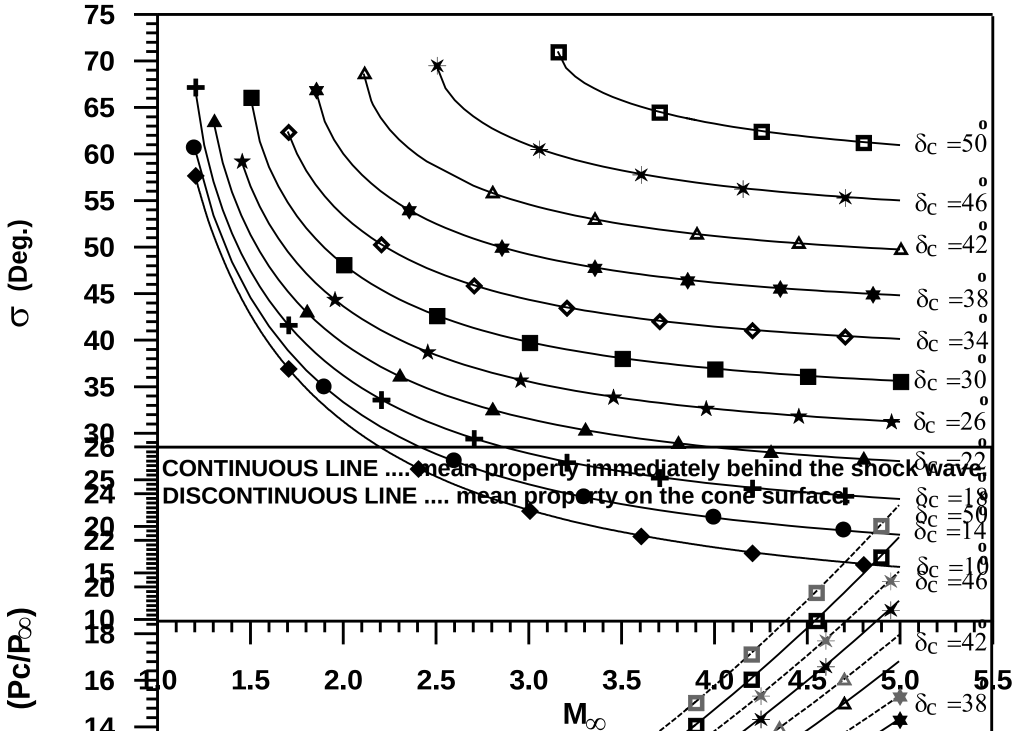

Fig. (٥. ٢) Angle of the shock wave versus free stream Mach number for different cone angles.

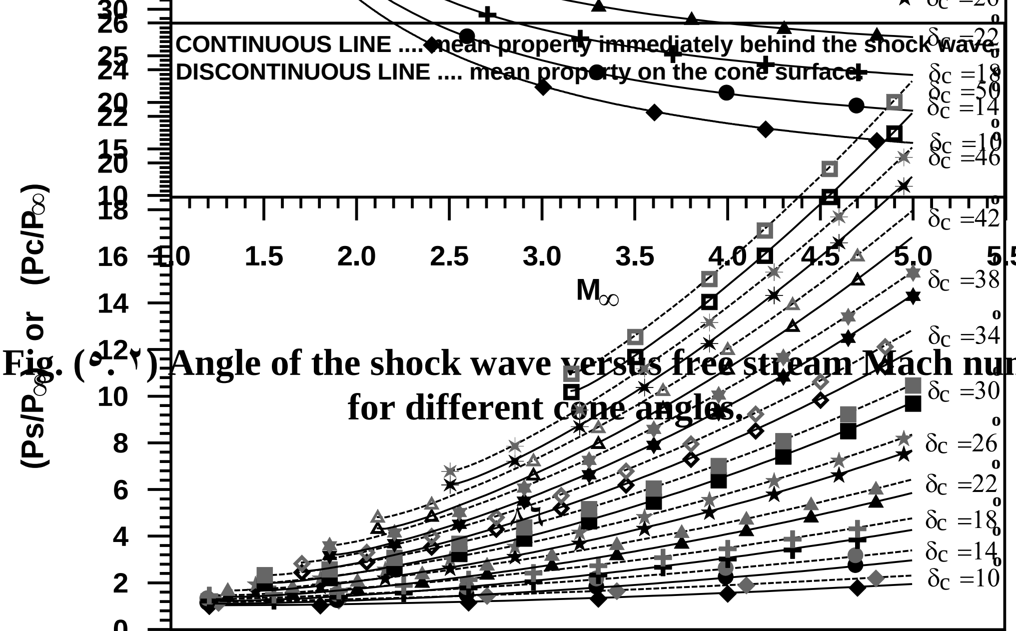

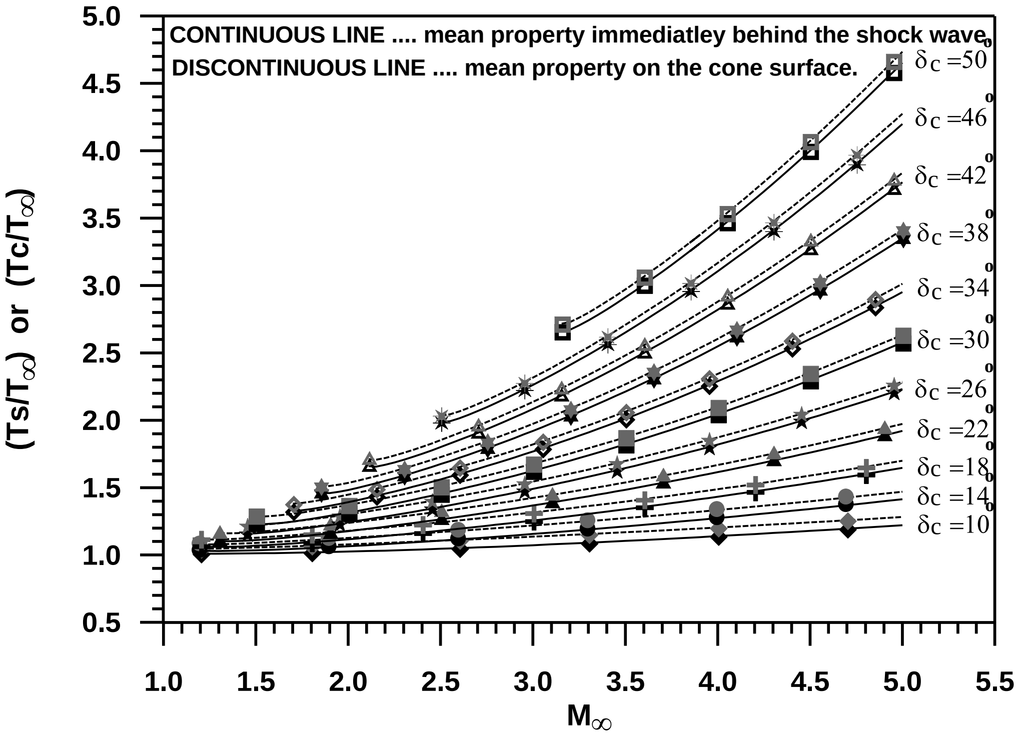

Fig. (٥. ٥) Temperature ratio behind the shock wave and at the surface of cone versus free stream Mach number for different cone angles.

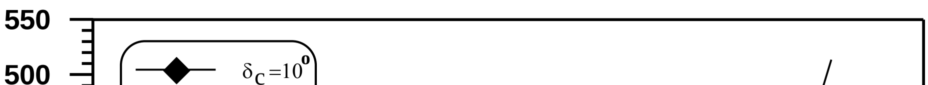

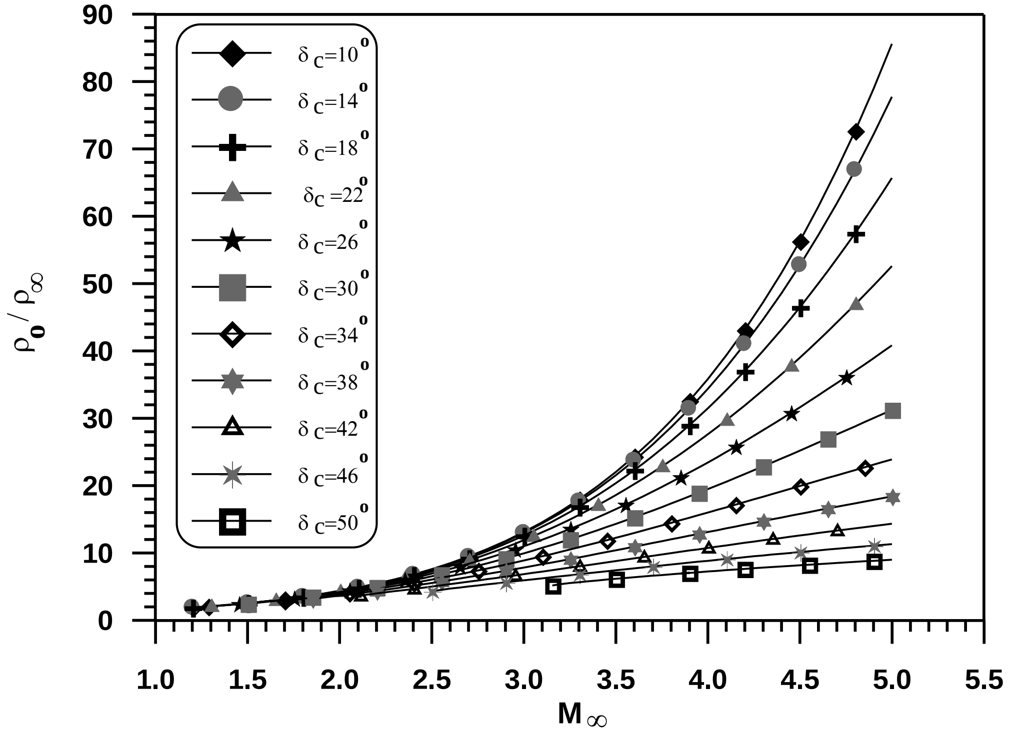

Fig. (٥. ٧) Density ratio of total density behind the shock wave to free stream static density versus free stream Mach number for different cone angles.

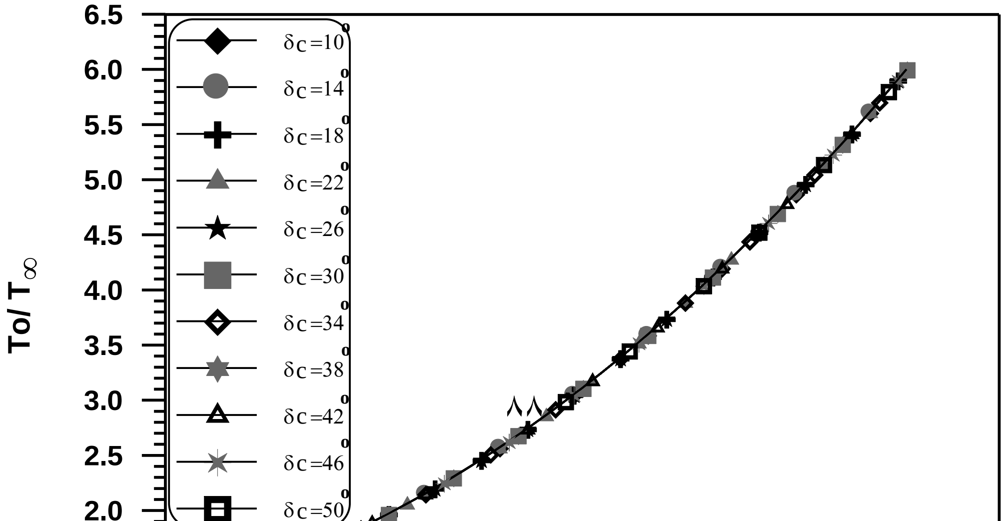

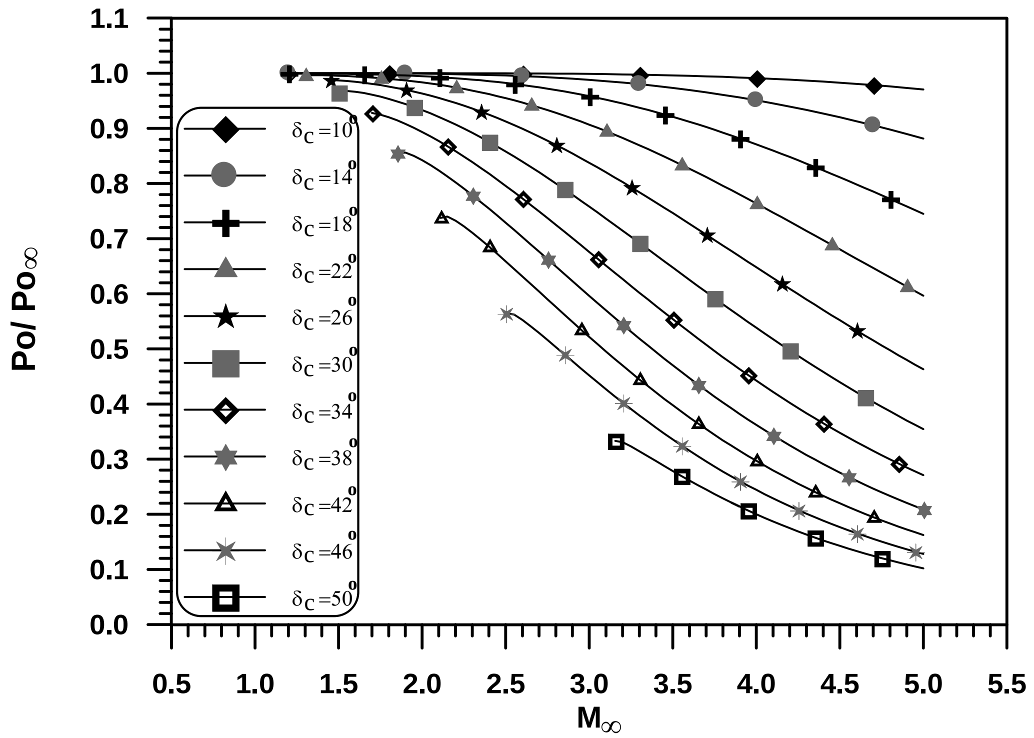

Fig. (٥. ٩) Total Pressure ratio of total pressure behind the shock wave to free stream total pressure versus free stream Mach number for different cone angles.

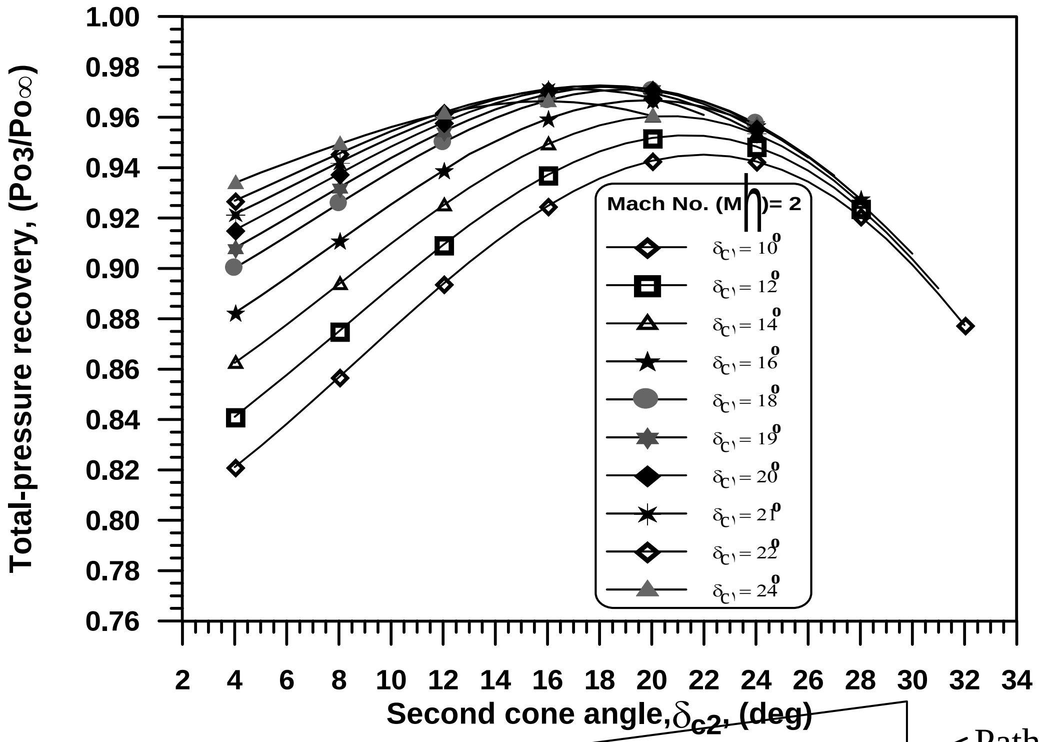

Fig. (٥.١٠) Total pressure recovery of total pressure behind the normal shock to free stream total pressure versus second cone angle for different first cone angles.

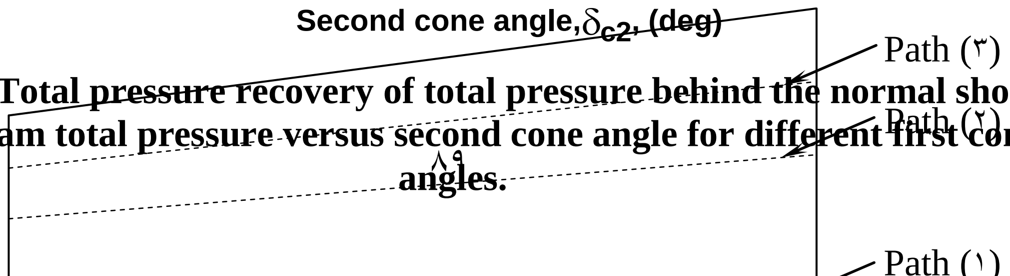

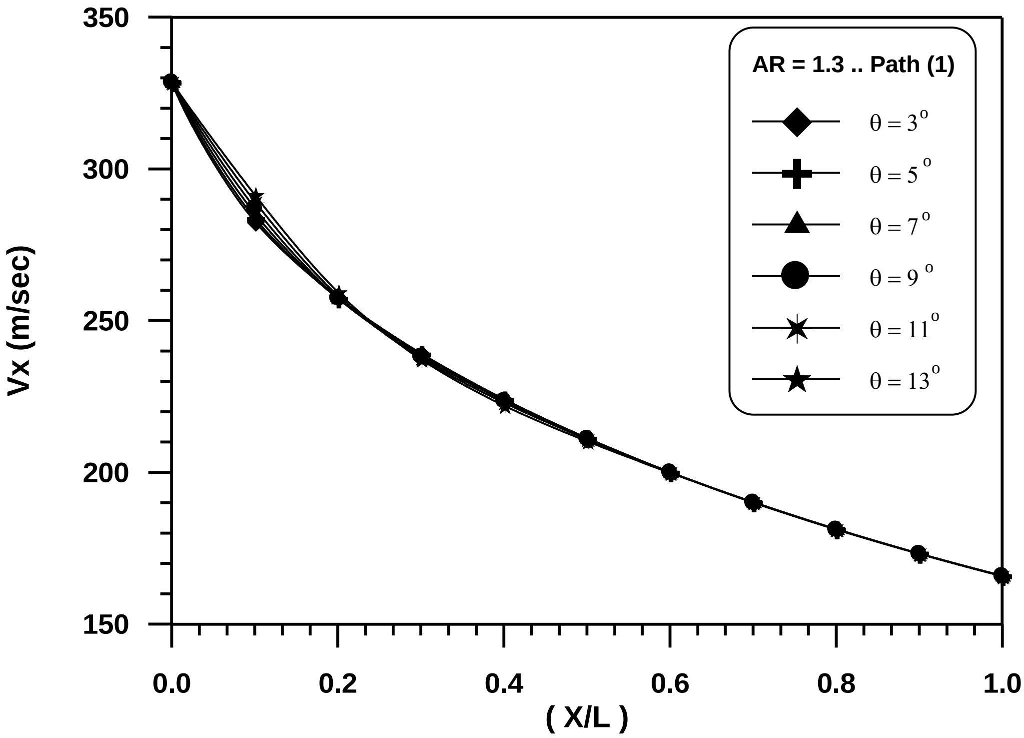

Fig. (٥.١٢) Flow axial velocity component across the diverge portion of intake.

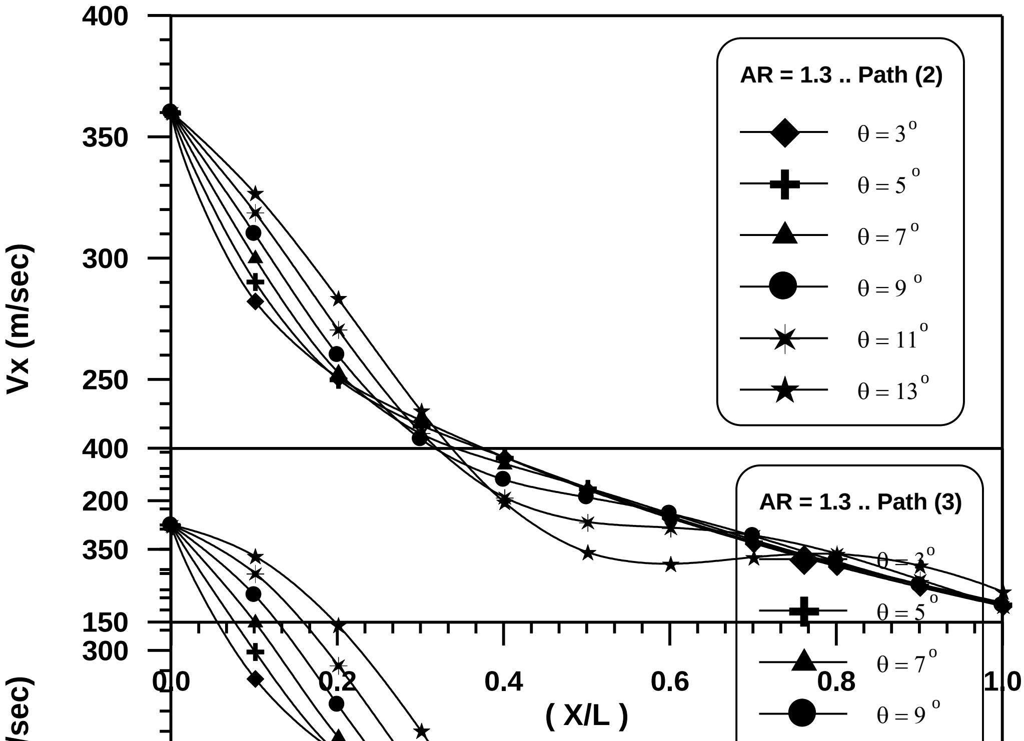

Fig. (٥.١٣) Flow axial velocity component across the diverge portion of intake.

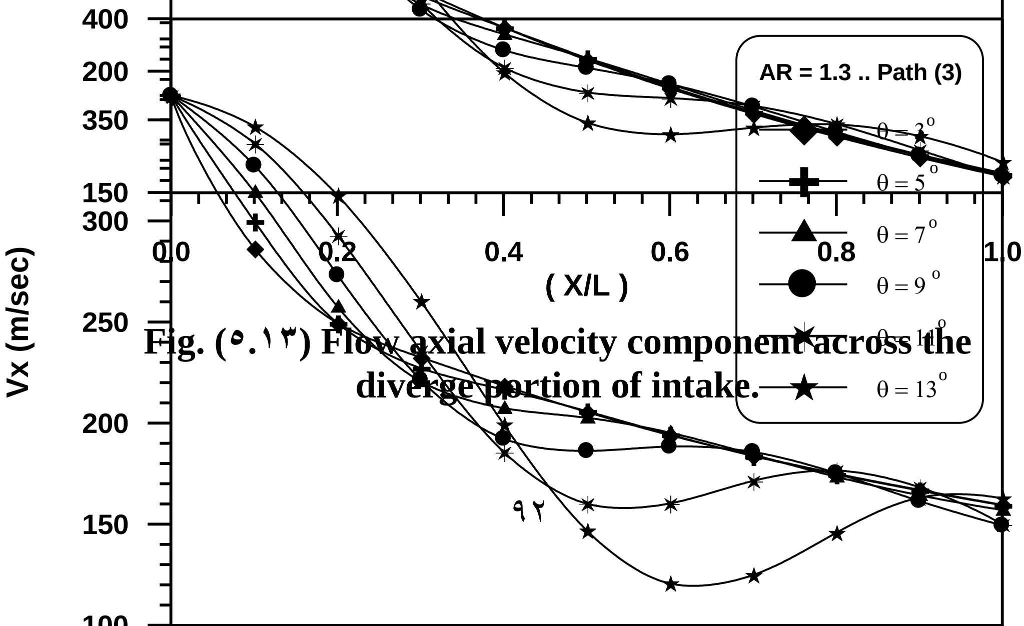

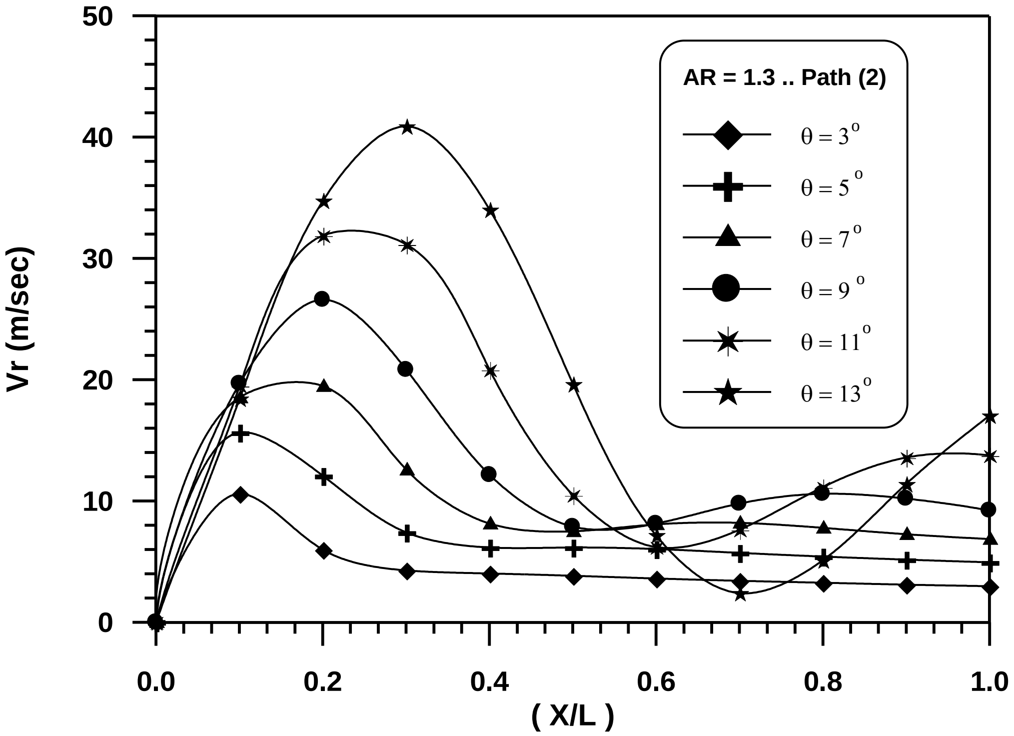

Fig. (٥.١٦) Flow radial velocity component across the diverge portion of intake.

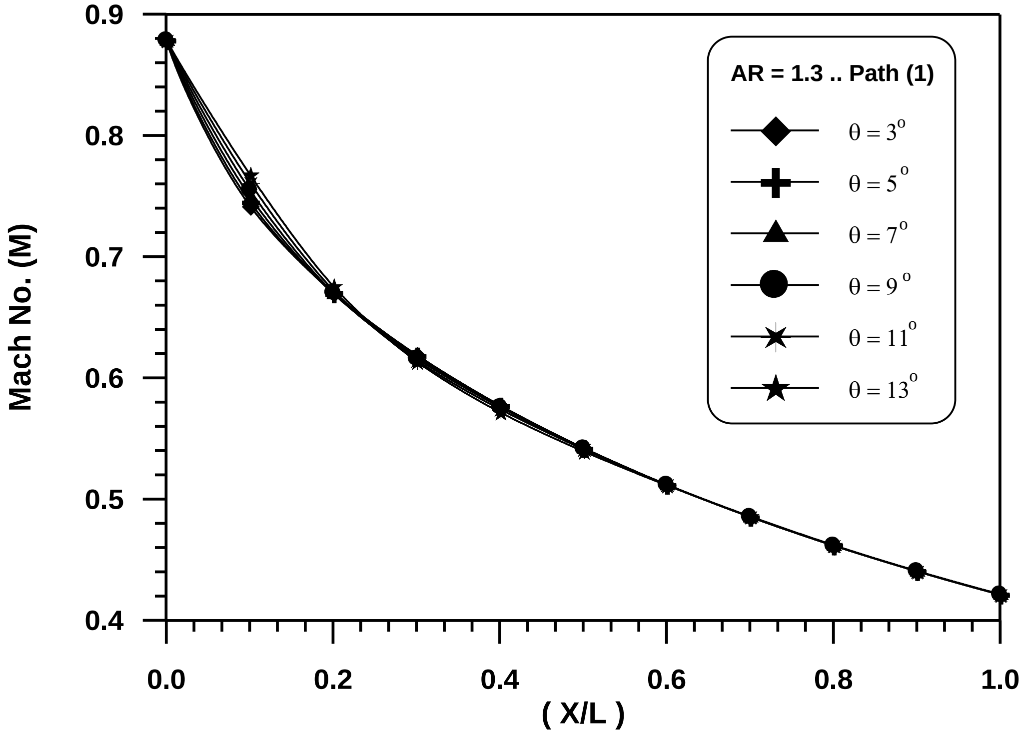

Fig. (٥.١٨) Mach number distribution across the diverge portion of intake.

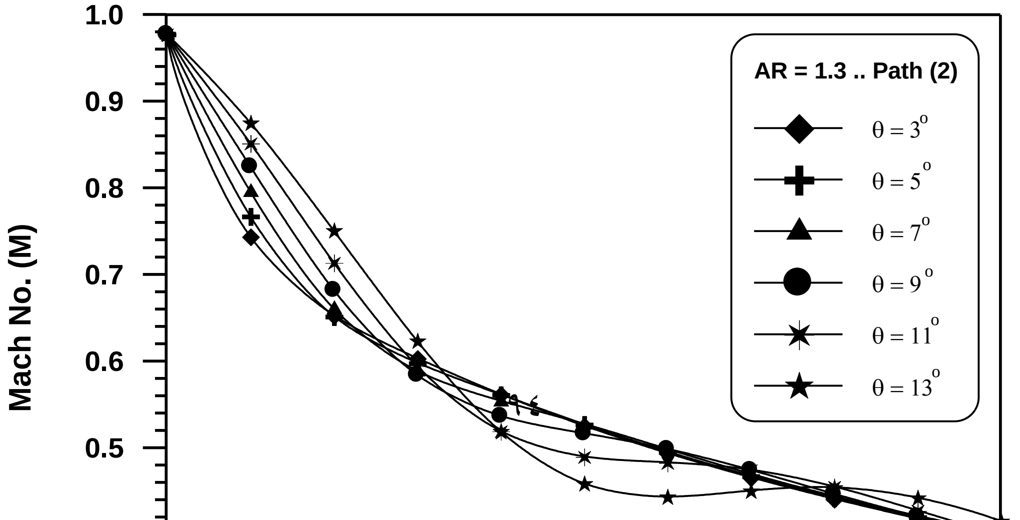

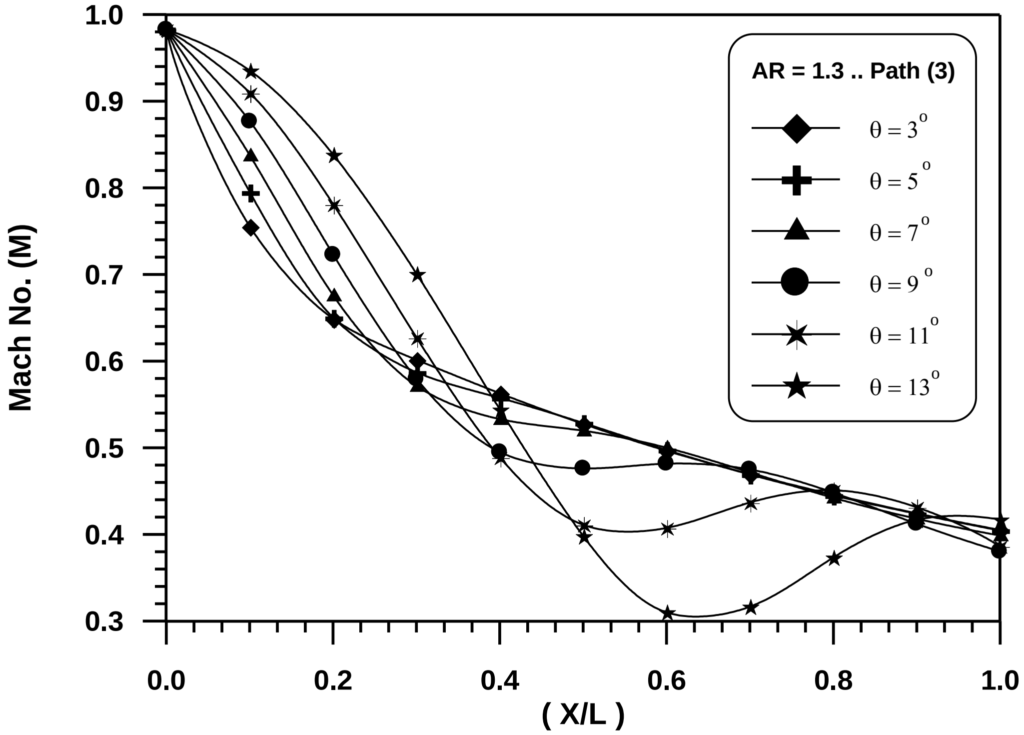

Fig. (٥.٢٠) Mach number distribution across the diverge portion of intake.

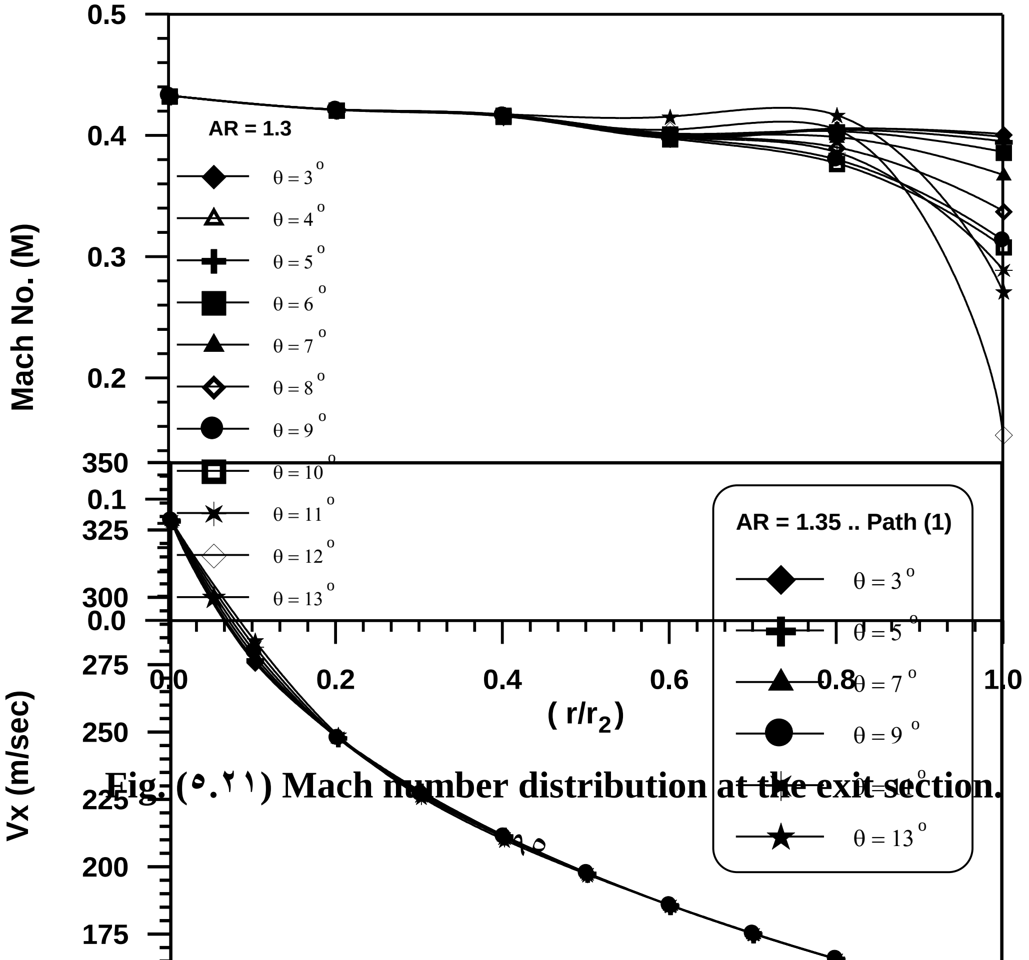

Fig. (٥.٢١) Mach number distribution at the exit section.

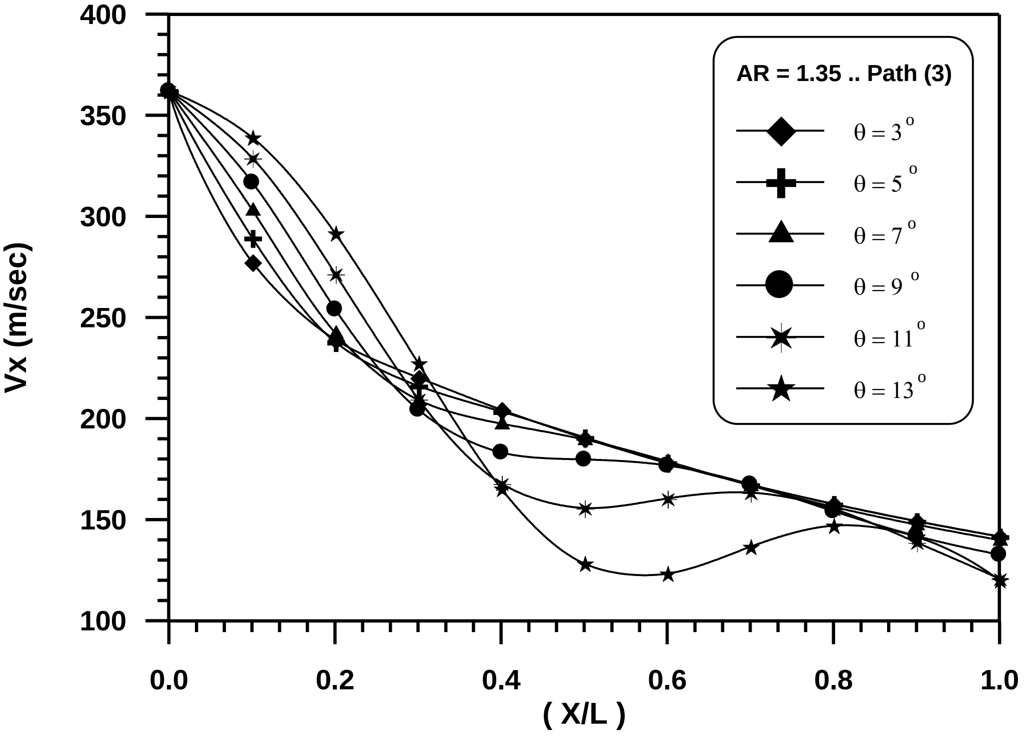

Fig. (٥.٢٤) Flow axial velocity component across the diverge portion of intake.

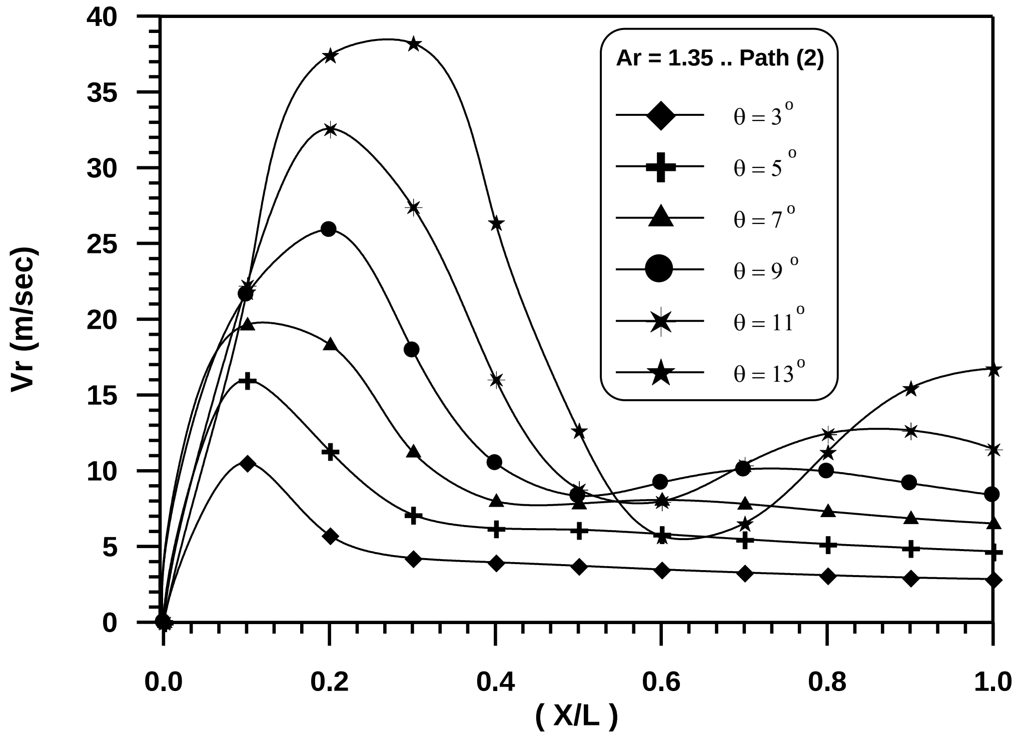

Fig. (٥.٢٦) Flow radial velocity component across the diverge portion of intake.

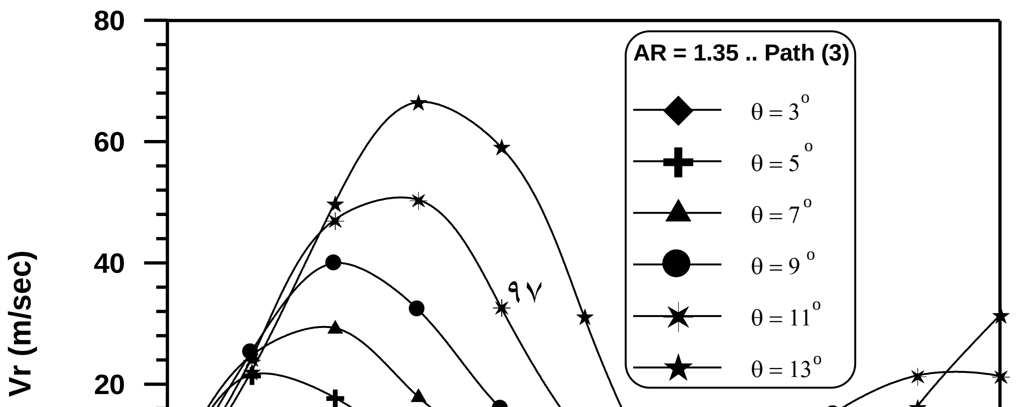

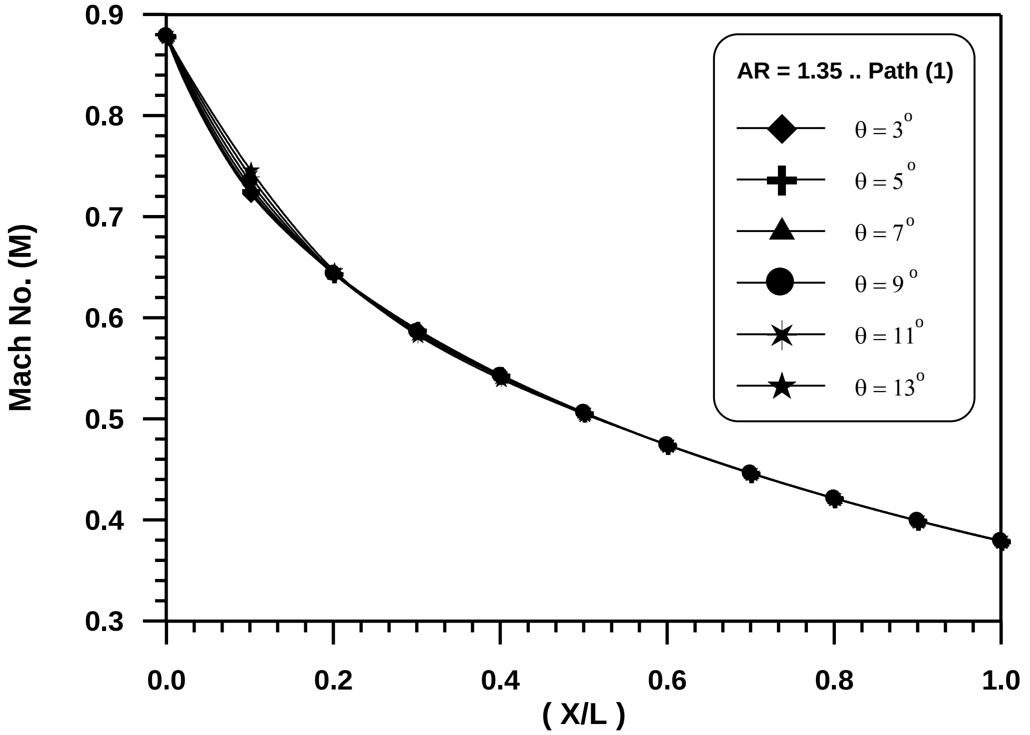

Fig. (٥.٢٨) Mach number distribution across the diverge portion of intake.

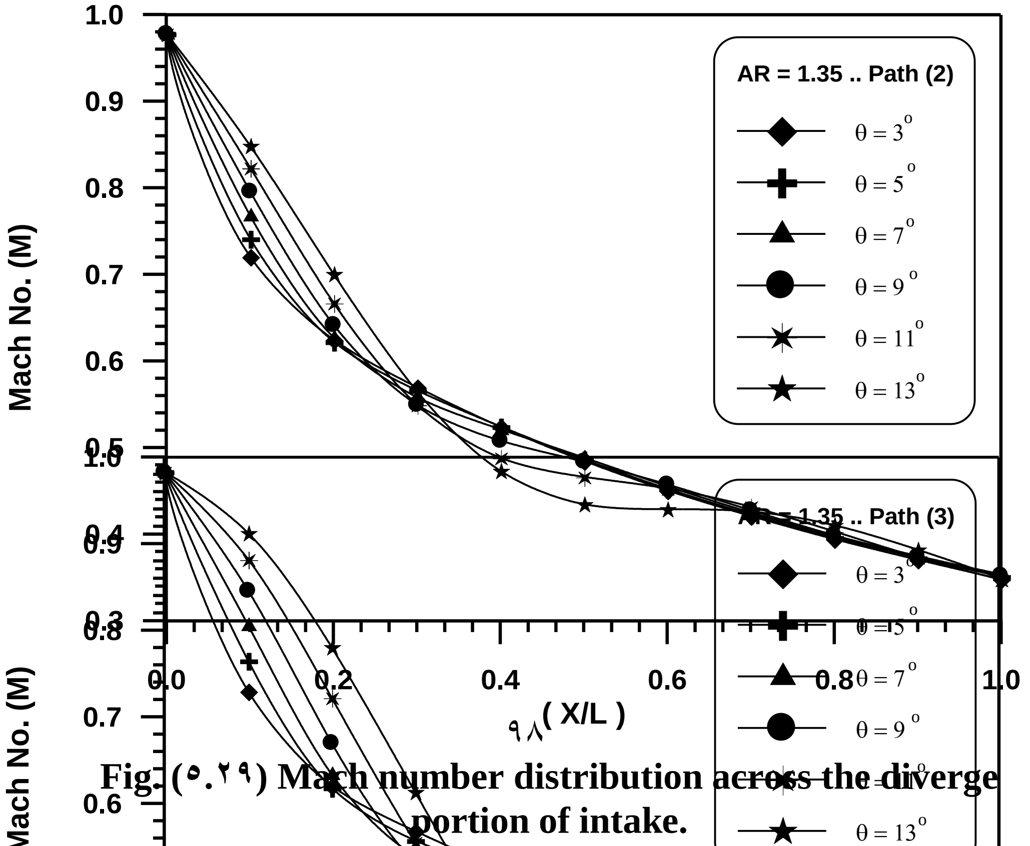

Fig. (٥.٢٩) Mach number distribution across the diverge portion of intake.

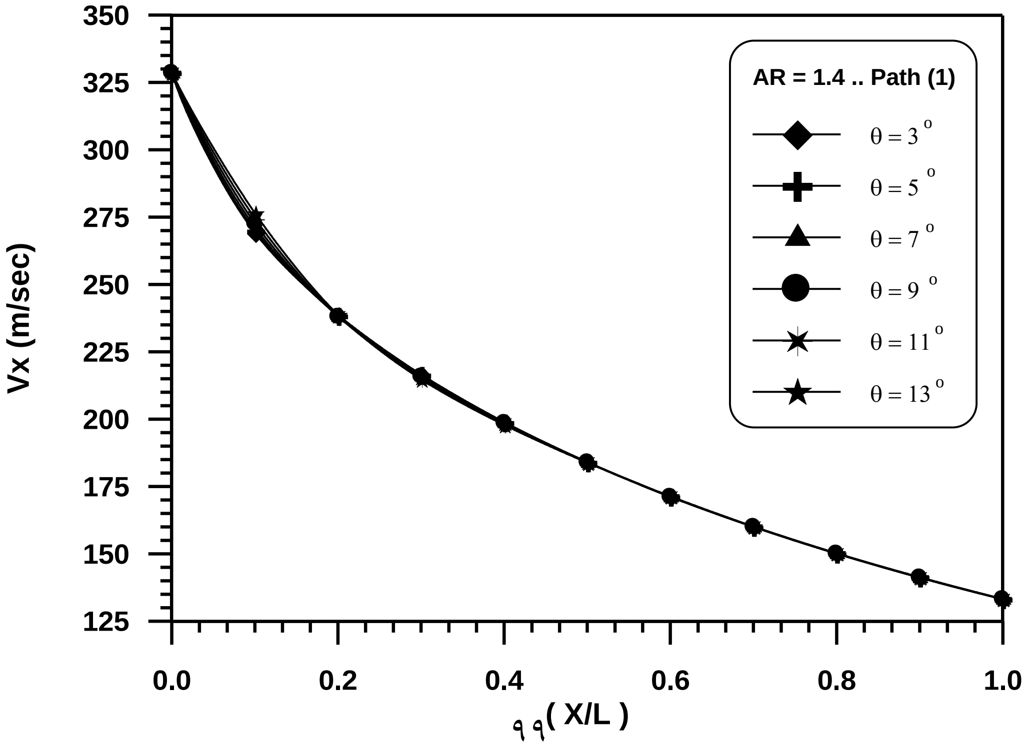

Fig. (٥.٣٢) Flow axial velocity component across the diverge portion of intake.

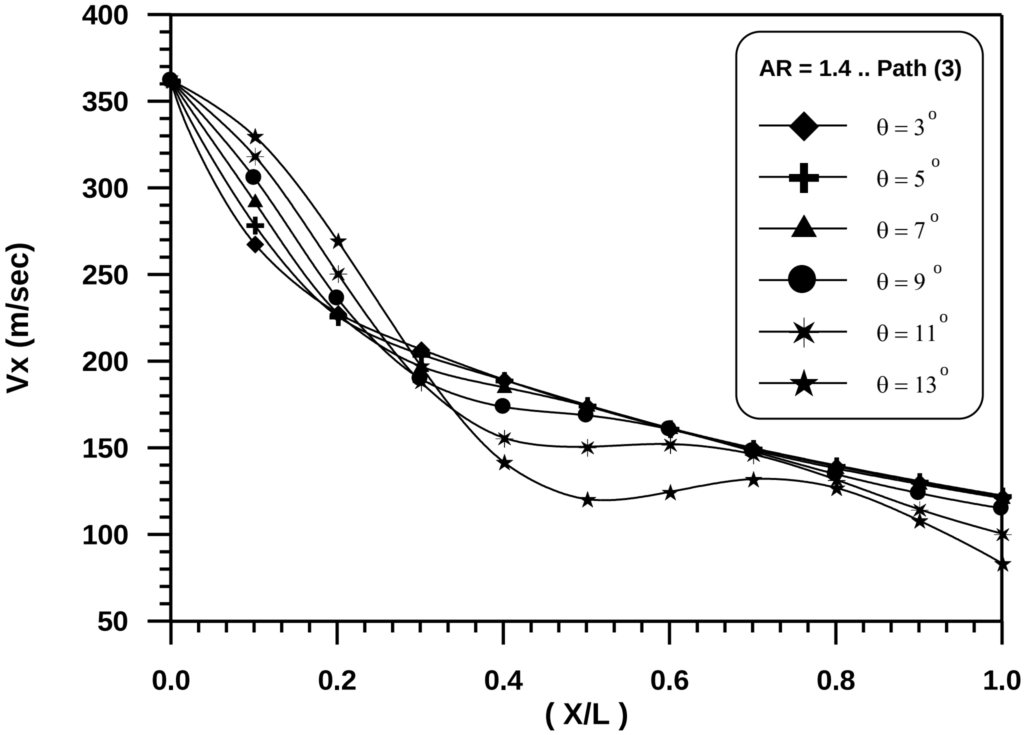

Fig. (٥.٣٤) Flow axial velocity component across the diverge portion of intake.

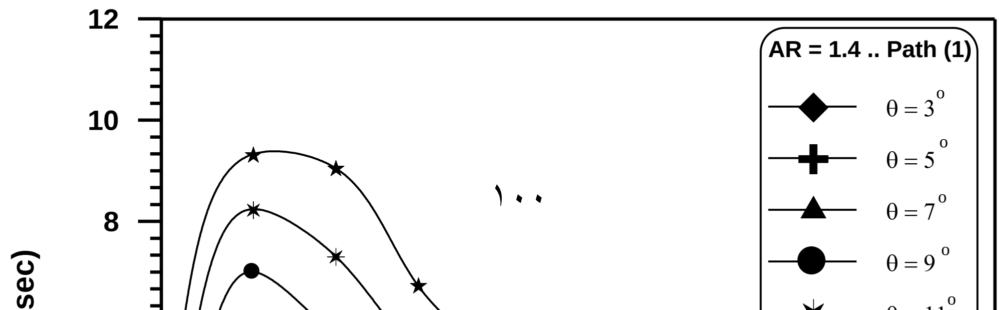

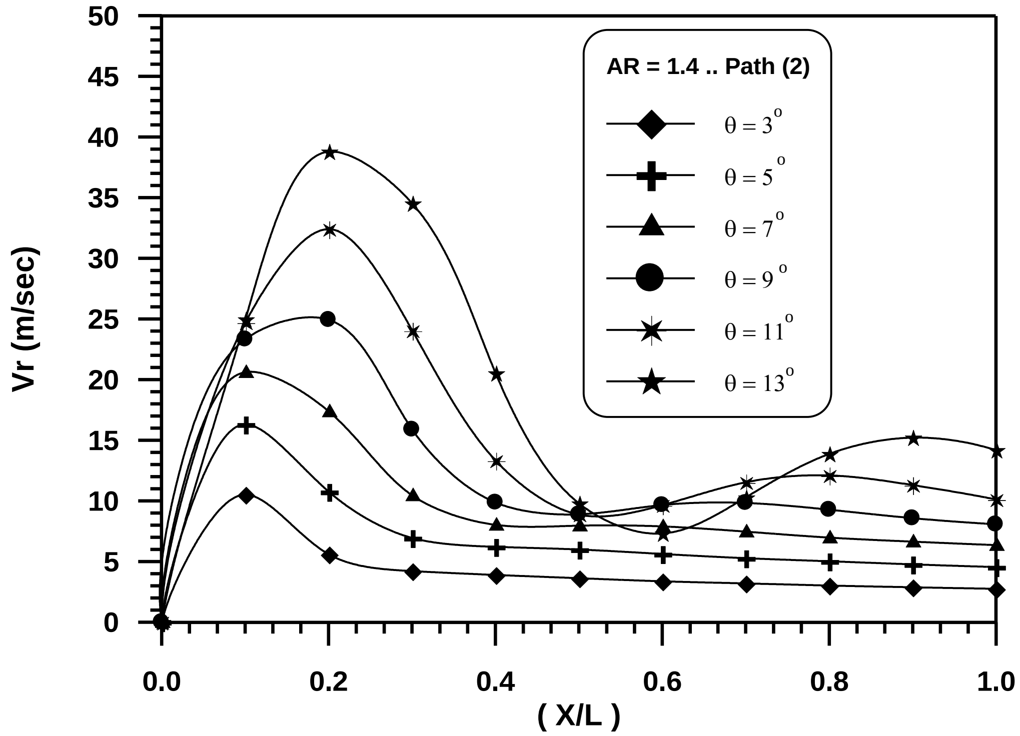

Fig. (٥.٣٦) Flow radial velocity component across the diverge portion of intake.

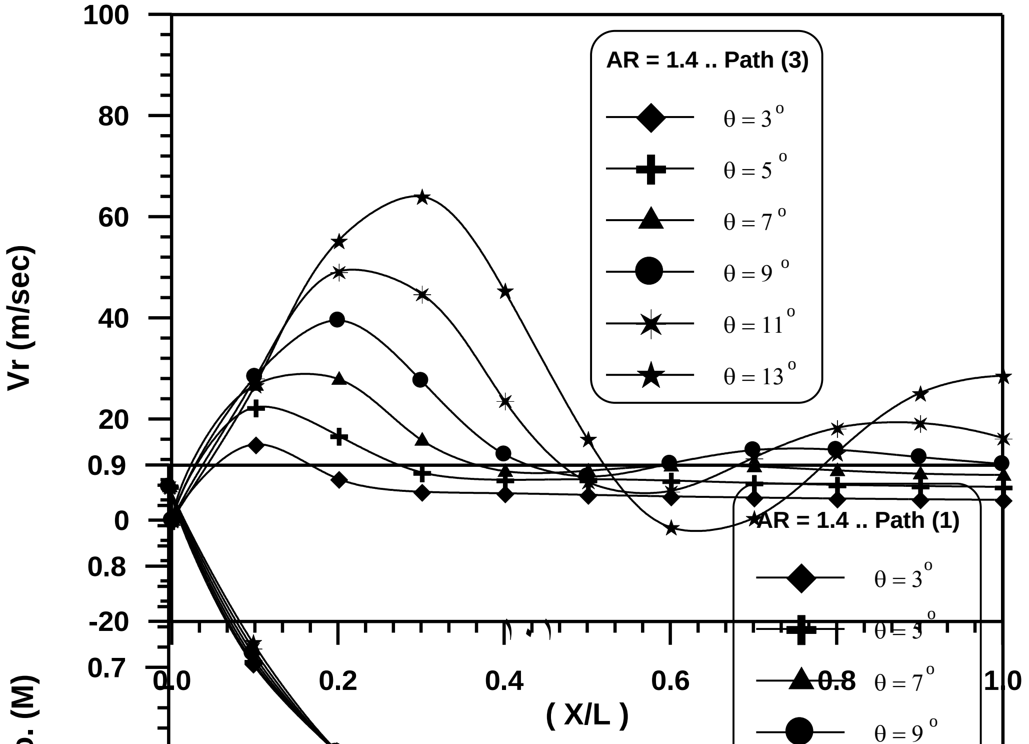

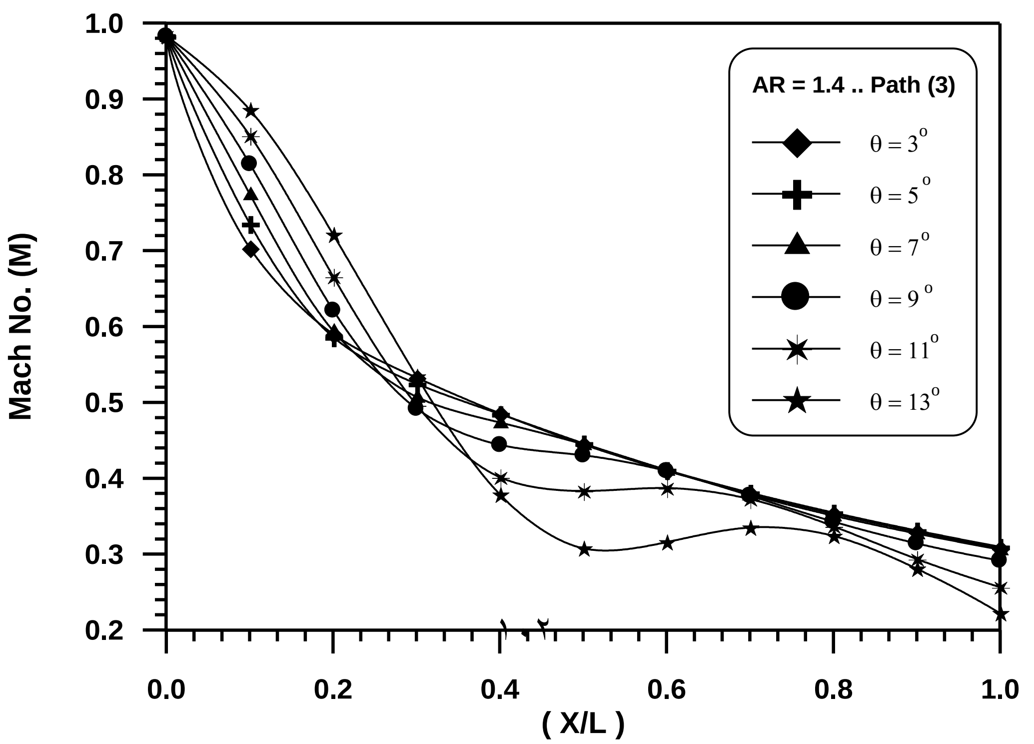
AR = 1.4 .. Path (3)
θ = 3°
θ = 5°
θ = 7°
θ = 9°
θ = 11°
θ = 13°
Mach No. (M)
(X/L)
0.2
0.3
0.4
0.5
0.6
0.7
0.8
0.9
1.0
0.0
0.2
0.4
0.6
0.8
1.0

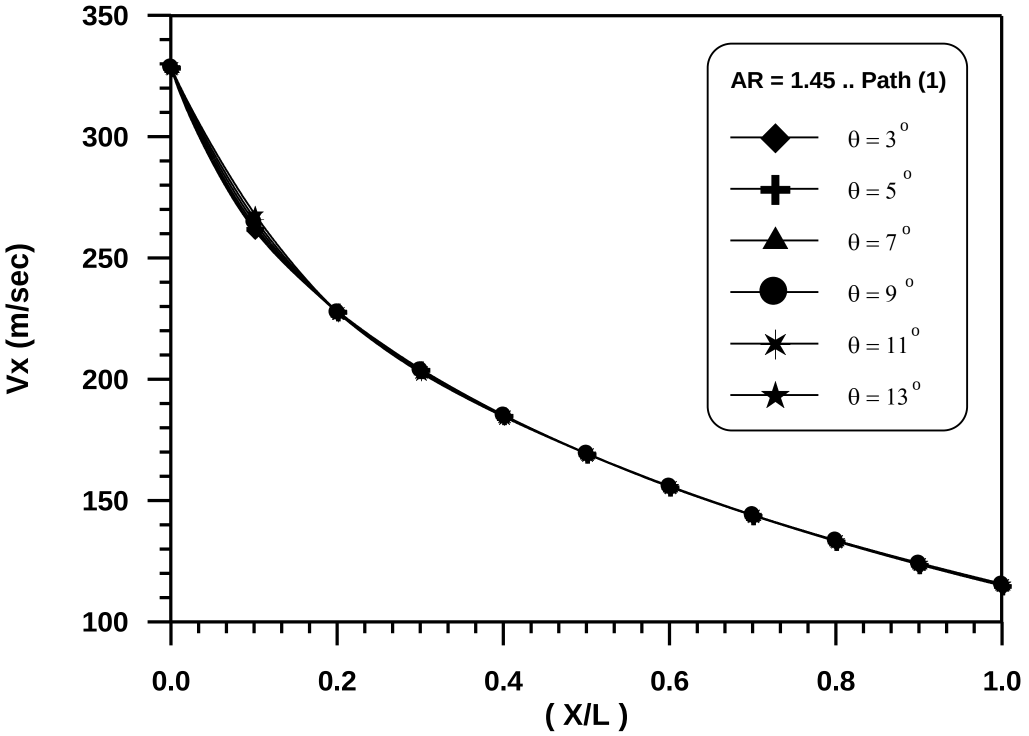

Fig. (٥.٤٢) Flow axial velocity component across the diverge portion of intake.

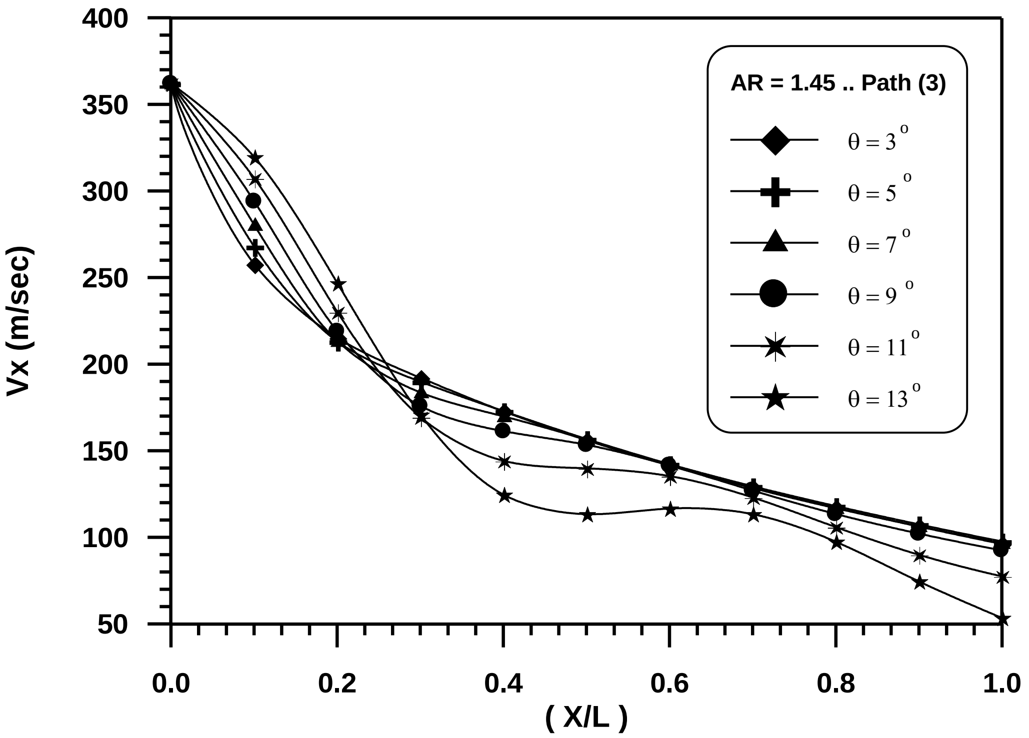

Fig. (٥.٤٤) Flow axial velocity component across the diverge portion of intake.

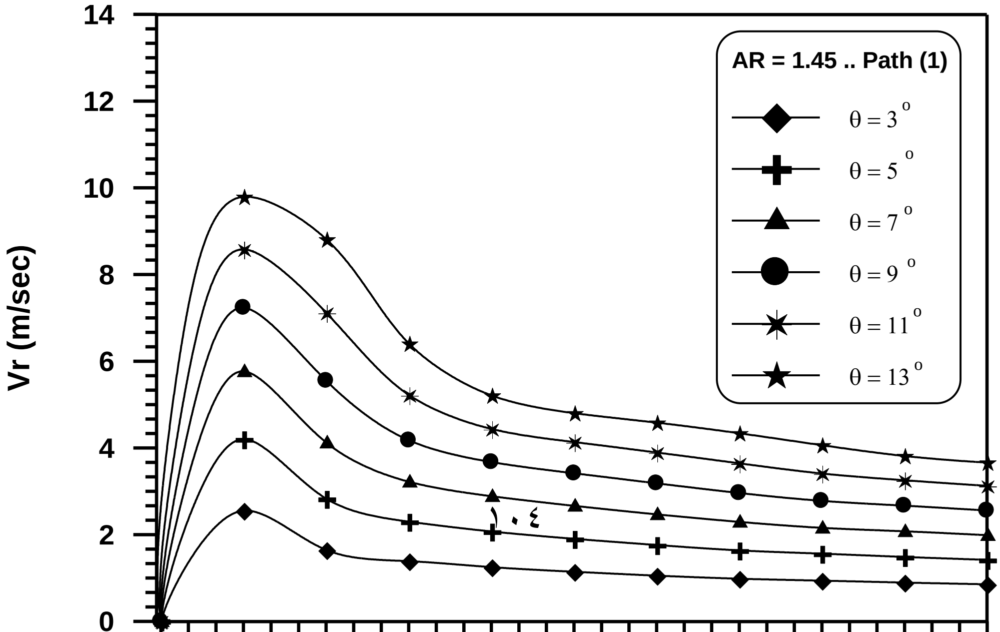

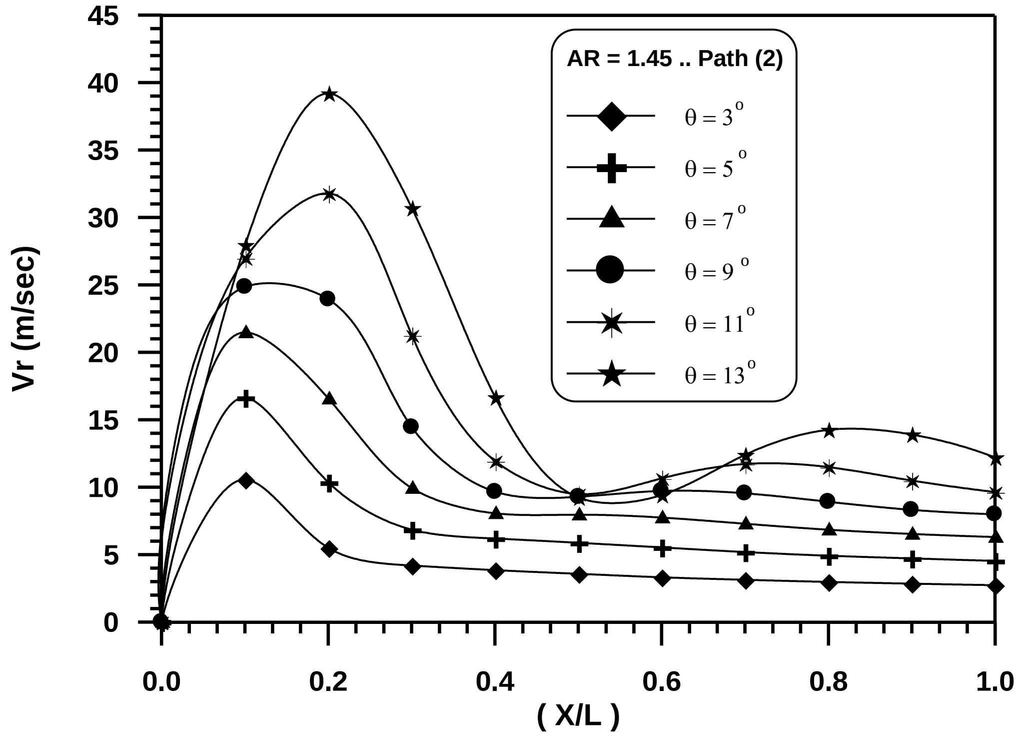

Fig. (٥.٤٦) Flow radial velocity component across the diverge portion of intake.

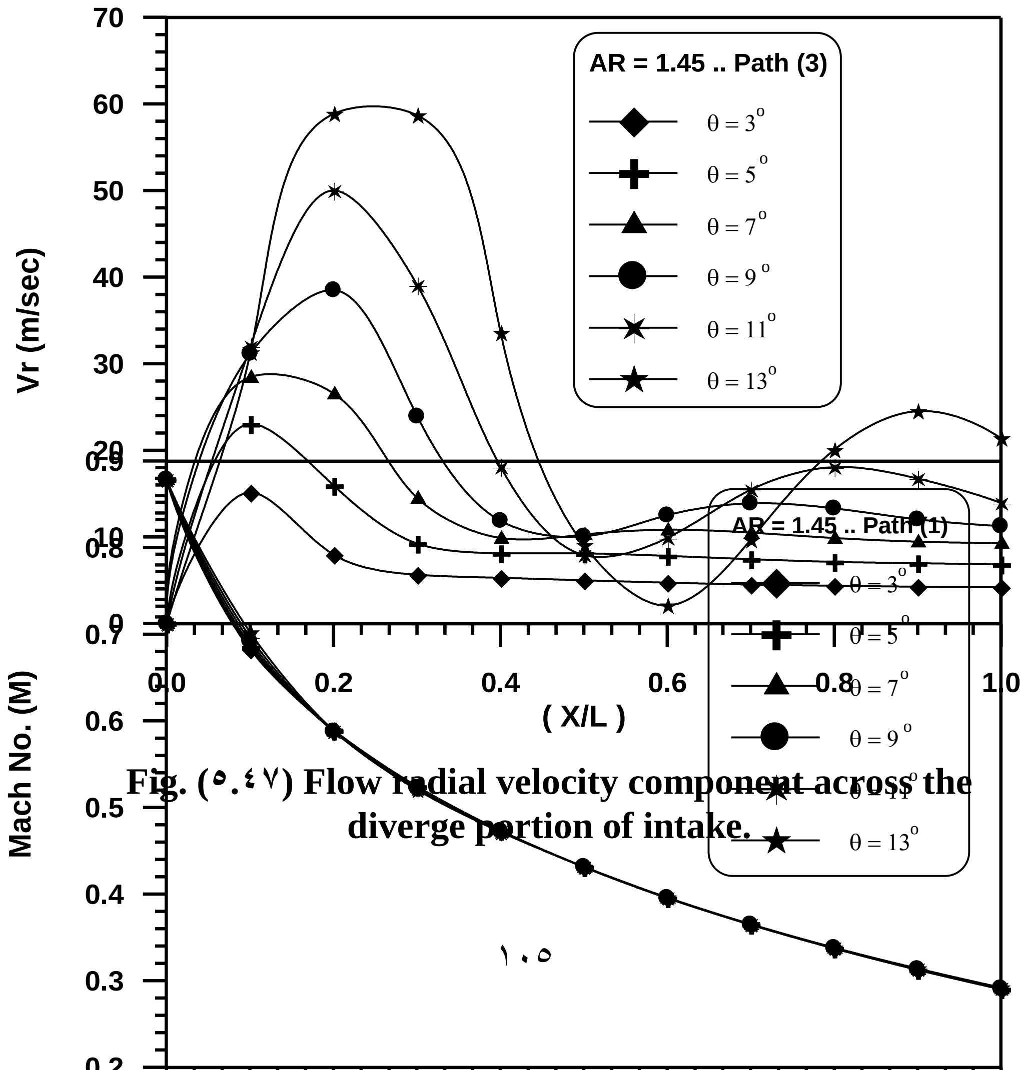

Fig. (٥.٤٧) Flow radial velocity component across the diverge portion of intake.

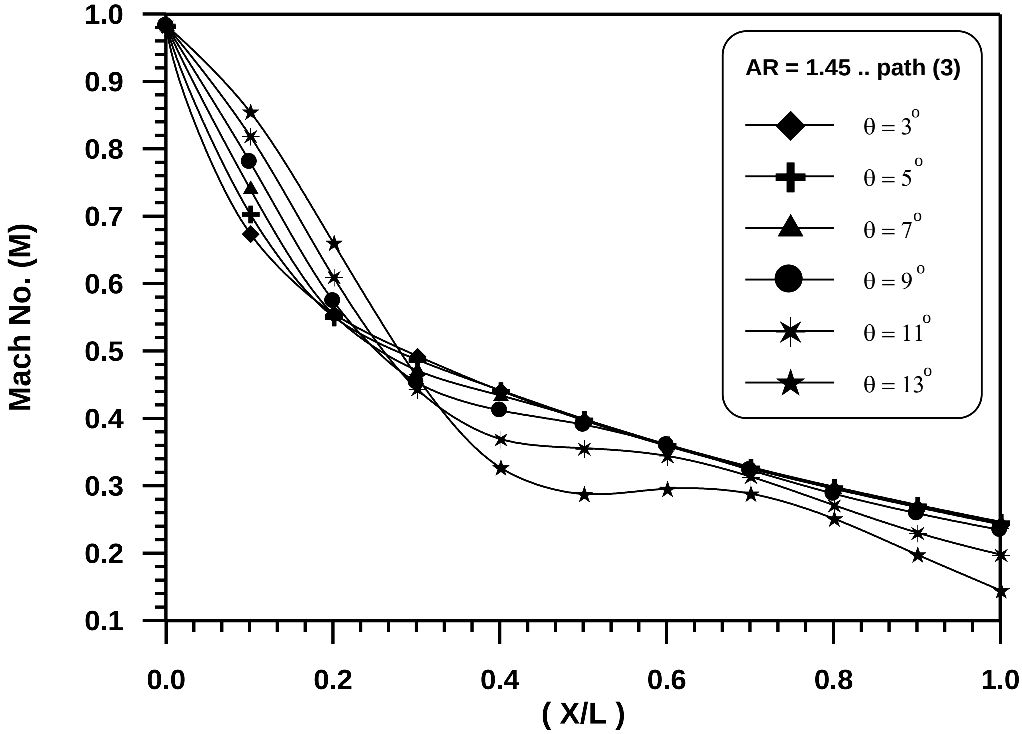

Fig. (٥.٥٠) Mach number distribution across the diverge portion of intake.

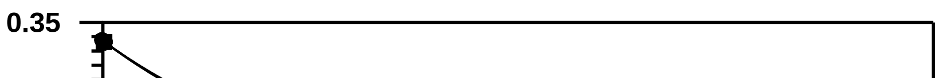

LIST OF CONTENTS

NOMENCLATURE

LATIN SYMBOLS		
SYMBOL	**DESCRIPTION**	**UNIT**
A	Area.	$m^{٢}$
a	Acoustic speed, (speed of sound).	m/sec
Cp	Specific heat ratio, taken as (١٠٠٥)	J/kg.ºK
det.	Determinant.	-
E.T	Error tolerance.	-
F_C	Continuity equation.	-
F_{MX}	Momentum equation in x-direction.	-
F_{Mr}	Momentum equation in r-direction.	-
F_E	Energy equation.	-
FDEs	Finite difference equations.	-
H	Altitude.	m
h	Step in Runge-Kutta integration method.	-
h_{CO}	Radius of intake cowl.	m
J	Jacobian.	-
$L_{١}$	Length of converge part of intake.	m
$L_{٢}$	Length of diverge part of intake.	m
L_N	Length of the spike.	m
L_{NW}	Length of the second cone.	m
L_W	Length of the first cone.	m
M	Mach number.	-
$\dot{m}$	Mass flow rate.	kg/sec
N	Steps number between the shock wave and the surface of cone.	-
P	Static pressure.	$N/m^{٢}$
PDEs	Abbreviated of (Partial differential equation)	-
P.E	Abbreviated of (Percent relative error).	-
R	Gas constant, taken as (٢٨٧).	J/kg.ºK
r	Radius.	m
$r_{١}$	Inlet gap of flow of intake.	m
$r_{٢}$	Exit gap of flow of intake.	m
r_{th}	Throat gap of flow of intake.	m

$r_W(x)$	Function describing the wall of a diffuser.	m
T	Static temperature.	ºK
TOL.	Abbreviated of (error tolerance).	
u	Velocity component with horizontal axis.	m/sec
v	Velocity component with vertical axis.	m/sec
V	Absolute velocity.	m/sec
v_r	Velocity component in r-direction (for external part intake).	m/sec
v_θ	Velocity component in θ-direction (for external part intake).	m/sec
v_x	Velocity component in x-direction (for internal part intake).	m/sec
v_r	Velocity component in r-direction (for internal part intake).	m/sec
x,r	Physical plane coordinate.	-
١	Region behind the first conical shock wave.	-
٢	Region behind the second conical shock wave.	-
٣	Region behind the normal shock wave.	-

GREEK SYMBOLS		
SYMBOL	DESCRIPTION	UNIT
γ	Specific heat ratio, taken as (١.٤).	-
θ	Ray angle (for external part), and diverge angle of diffuser (for internal part).	deg.
φ	Third dimension of spherical coordinate system.	deg.
Φ	Angle of direction of flow with horizontal axis.	deg.
β	Angle between shock wave and the flow direction immediately behind the shock wave.	deg.
α	Mach angle.	deg.
ø	Third dimension of cylindrical coordinate system.	deg.
∞	Free stream condition.	-
$\sigma_{١}$	First conical shock wave.	deg.
$\sigma_{٢}$	Second conical shock wave.	deg.
$\delta_{C١}$	First semi cone angle.	deg.
$\delta_{C٢}$	Second semi cone angle.	deg.
ρ	Density.	$kg/m^{٣}$
ξ,η	Computational plane coordinate.	-

SUBSCRIPT AND SUPERSCRIPT SYMBOLS		
SYMBOL	DESCRIPTION	UNIT
∞	Free stream condition.	-
s	Property immediately behind the shock wave.	-
c	Property in the surface of cone.	-
co	Abbreviated of (cowl).	-
act	Abbreviated of (actual).	-
o	Signifies stagnation state.	-
ξ,η	Derivative with respect to coordinates ξ,η respectively.	-
i, j	Grid points in x, r coordinates respectively.	-
*	Dimensionless property.	-

REFERENCES

١. Oswatitsch, K.L., " Der Druckruckgewinn bei Geschossen mit Ruckstossantrieb bei hohen Uberschallgeschwindigkeiten Cder Wirk ungsgrad vor Stossdiffusoren", Forchungen Und Entwicklungen des Heereswaffenamtes. Bericht. Nr. ١٠٠٥, ١٩٤٤.

٢. Brajnikoff, George B., "Pressure Recovery at Supersonic Speeds through Annular Duct Inlets Situated in A Region of Appreciable Boundary Layer. II. Effect of An Oblique Shock Wave Immediately A Heed of the Inlet", NACA. RM No. A٨C١١, ١٩٤٨.

٣. Ferri A., and Louis M. Nucci, "Theoretical and Experimental Analysis of Low-Drag Supersonic Inlets Having A Circular Cross Section and A Central body at Mach numbers of ٣.٣٠, ٢.٧٢, and ٢.٤٥", NACA Report ١١٨٩, ١٩٤٨.

٤. Ferri A., and Louis M. Nucci, "Preliminary Investigation of A New Type of Supersonic Inlets", NACA Report ١١٠٤, ١٩٥٢.

٥. Conners, James F., and Rudolph C. Meyer, "Performance Characteristics of Axisymmetric Two- Cone and Isentropic Nose Inlets at Mach number ١.٩٠", NACATN ٣٥٨٩, Jan. ١٩٥٦.

٦. McGregor, I., " Some Theoretical Parameters Relevant to the Performance of Rectangular Air Intakes with Double-Ramp Compression Surface at Supersonic Speed", AIAA Education Series, RAE Technical Report ٧١٢٣٧, ١٩٧١.

٧. Tindell r.H., "Inlet Drag and Stability Considerations for M = ٢.٠٠ Design", AIAA ٨٠-١١٠٥R, Vol. ١٨. No. ١١, Nov. ١٩٨١.

٨. Shaikh, A.H., M.V.K.V. Prasad, S.V. Rammana, M.P. Reddy, T.S. Rao, and B.S.S. Chandran, "Wind Tunnel Testing of ٢D Supersonic Air Intake", National Conference on Air Breathing Engines and Aerospace Propulsion (NCABE), Dec. ٢٠٠٠.

٩. Sandip chattopadhyay, B. Murugan, and J.K. Prasad, "Experimental Investigation of Flow Inside A Generic Ramjet Intake at M = ٢", (NCABE), Dec. ٢٠٠٠.

١٠. Conners, James F., and Rudolph C. Meyer, "Design Criteria for Axisymmetric and Two-Dimensional Supersonic Inlets and Exits", NACA TN ٣٥٨٩, ١٩٥٦.

١١. Steger, Joseph L., "Implicit Finite-Difference Simulation of Flow about Arbitrary Two- Dimensional Geometries", AIAA Journal, Vol. ١٦, No. ٧, July ١٩٧٨.

١٢. Chen, Lee-tzong and D.A. Caughey, "Calculation of Transonic Inlet Flow Field Using Generalized Coordinates", Aircraft Journal, Vol. ١٧, No. ٣, March ١٩٨٠.

١٣. Knight, Doyle D., "Calculation of High- Speed Inlet Flows Using the Navier-Stokes Equations", Aircraft Journal, Vol. ١٨, No. ٩, Sep. ١٩٨١.

١٤. Bangent, L.H., D.M. Santman, and L.D. Miller, "Some Effects of cruise Speed and Engine Matching on supersonic Inlet Design", Aircraft Journal, Vol. ١٩, No. ١, Jan. ١٩٨٢.

١٥. Shimabukuro, K.M., H.R. Welge, and A.C. Lee, "Inlet Design Studies for A Mach ٢.٢ Advanced Supersonic Cruise Vehicle", Aircraft Journal, Vol. ١٩, No. ٧, July ١٩٨٢.

١٦. Lavante E. von and W.T. Thompkins Jr., "An Implicit, Bidiagonal Numerical Method for Solving the Navier-Stokes Equations", AIAA Journal, Vol. ٢١, No. ٦, June ١٩٨٣.

١٧. Biringes, S., "Numerical Simulation of Two-Dimensional Inlet Flow fields", Aircraft Journal, Vol. ٢١, No. ٤, April ١٩٨٤.

١٨. Walters, R.W., Douglas L. Dwoyer, and H.A. Hassan, "A Strong Implicit Procedure for the Compressible Navier-Stokes Equations", AIAA Journal, Vol. ٢٤, No.١, Jan. ١٩٨٦.

١٩. Bradley, Pamela F., Douglas L. Dwoyer, and Jerry C. South Jr., "Vectorized Schemes for Conical Potential Flow Using the Artificial Density Method", AIAA Journal, Vol. ٢٤, No. ١, Jan. ١٩٨٦.

٢٠. Moretti, Gino, "Efficient Euler Solver with Many Applications", AIAA Journal, vol. ٢٦, No. ٦, June ١٩٨٨.

٢١. Gilding, B.H., "A Numerical Grid Generation Technique", Computers and Fluids, Pergamon Journals Ltd, Vol. ١٦, No. ١, PP. (٤٧-٥٨), ١٩٨٨.

٢٢. Dimitri P., "Diffuser Performance of Two-Stream Supersonic Wind Tunnels", AIAA Journal Vol. ٢٧, No. ٨, Aug. ١٩٨٩.

٢٣. Mittal, S., V. Jain, and R.K. Sullerey, "Numerical Investigation of Supersonic Mixed-Compression Inlet Using Euler Equation", NCABE, Dec. ٢٠٠٠.

٢٤. Singh Th.R., B.S.S. Chandran, V. Babu, and T. Sundaraajan, "Numerical Simulation of Supersonic Mixed Compression Axisymmetric Air Intakes", NCABE, Dec. ٢٠٠٠.

٢٥. Geetha, J.J., T.K. Ganesh A., and S. Panneerselvam, "Forbody Design for Aerodynamic Propulsion Requirements of An Airbreathing Hypersonic Research Vehicle", NCABE, Dec. ٢٠٠٠.

٢٦. Ferri, A., "Elements of aerodynamics of Supersonic Flow", Macmillan Co., New York, ١٩٤٩.

٢٧. Miles, Ed. R.C., "Supersonic Aerodynamics A Theoretical, Introduction", New York, McGraw-Hill Book Co., ١٩٤٩.

٢٨. Ames Research Staff, "Equations, Tables, and Charts for Compressible Flow", NACA Report ١١٣٥, ١٩٥٣.

٢٩. Hurd, R., "Supersonic Inlets", AGARDograph ١٢٠. The Avisory Group for Aerospace Research and Development. NATO. Aug. ١٩٦٩.

٣٠. Shapero, A.H., "The Dynamics and Thermodynamics of Compressible Fluid Flow", ٢Vol. Roland Press, New York, ١٩٥٣, ١٩٥٤.

٣١. Krasnov, N.F., "Aerodynamics of Bodies of Revolution", Rand Press, New York, ١٩٧٠.

٣٢. Thompson, P.A., “Compressible Fluid Dynamics”, McGraw-Hill Book Co., New York, ١٩٧٢.

٣٣. Zucrow M.J., J. D. Hoffman, “Gas Dynamics”, ٢Vol. John Wiley & Sons Co., New York, ١٩٧٦, ١٩٧٧.

٣٤. Schreier, S., “Compressible Flow”, John Wiley & Sons Co., New York, ١٩٨٢.

٣٥. Anderson Jr., J.D. ”Modern Compressible Flow with Historical Perspective”, McGraw-Hill Book Co., New York ١٩٨٢.

٣٦. Anderson, D.A., J.C. Tannehill, and R.H. Pletcher, “Computational Fluid Mechanics and Heat Transfer, Hemisphere Publishing”, New York, ١٩٨٤.

٣٧. Michel, A. Saad, “Compressible Fluid Flow”, Prentice-Hall Co., ١٩٨٥.

٣٨. Seedon, J. and E.L. Goldsmith, “Intake Aerodynamics”, Collins Professional and Technical Books, William Collins Sons & Co. Ltd. London, ١٩٨٥.

٣٩. Thomas Jr., A.N., “Inlets”, The Marguardt Co. Nuys, California, ١٩٨٥.

٤٠. Al-Khafaji, A.W. and J.R. Todey, “Numerical Method in Engineering Practice”, HRD International Education, New York, ١٩٨٦.

٤١. Hoffman, K.A., “Computational Fluid Dynamics for Engineers”, Engineering Education System, Austin, ١٩٨٩.

٤٢. Raymer, D.P., “Aircraft Design: A Conceptual Approach”, ٢nd Edition AIAA Education Series, Washington, ١٩٩٢.

٤٣. Hodge, B.K. and K. Koenig, “Compressible Fluid Dynamics, with Personal Computer Application”, Prentice-Hall Co., New Jersey, ١٩٩٥.

٤٤. Oosthuizen, P.H. and W.E. Carscallen, “Compressible Fluid Flow”, McGraw-Hill Book Co., ١٩٩٧.

٤٥. Chapra, S.C. and R.P. Canate, “Numerical Methods for Engineers, with Programing and Software Applications”, ٣rd Edition, McGraw-Hill Book Co., ١٩٩٨.

٤٦. Fox, R.W. and A.T. McDonald, “Introduction to Fluid Mechanics”, ٥th, John Wiley & Sons Co., ١٩٩٨.

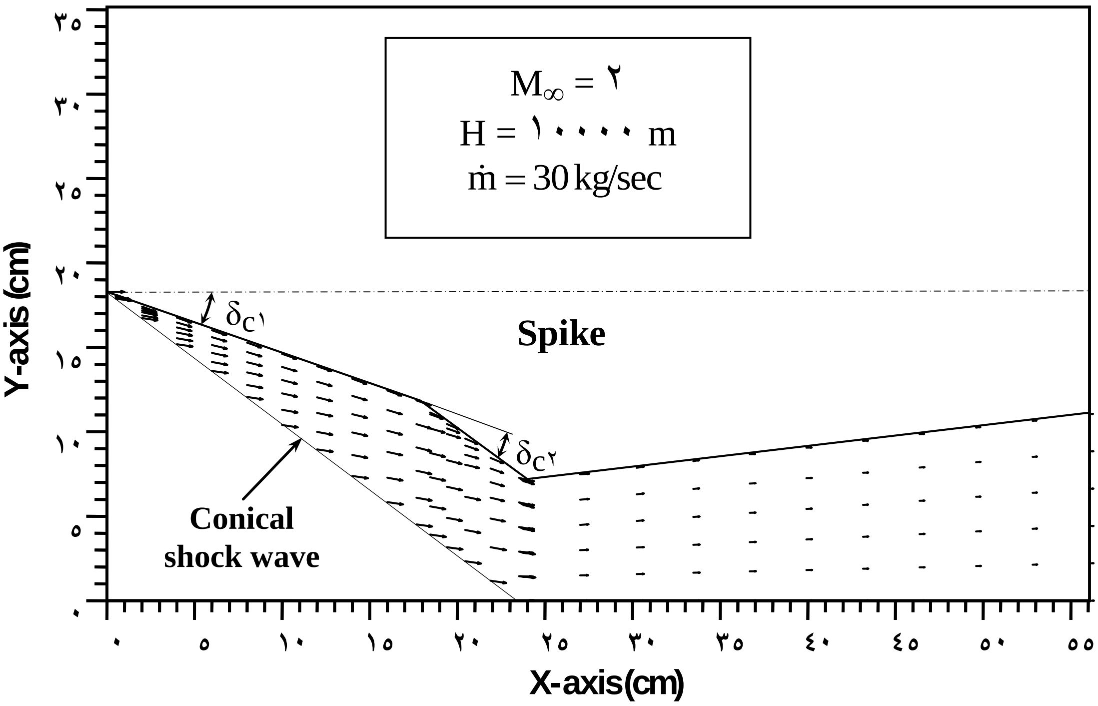

Fig. (٥.٥٢) Vector plot distribution along supersonic air intake.

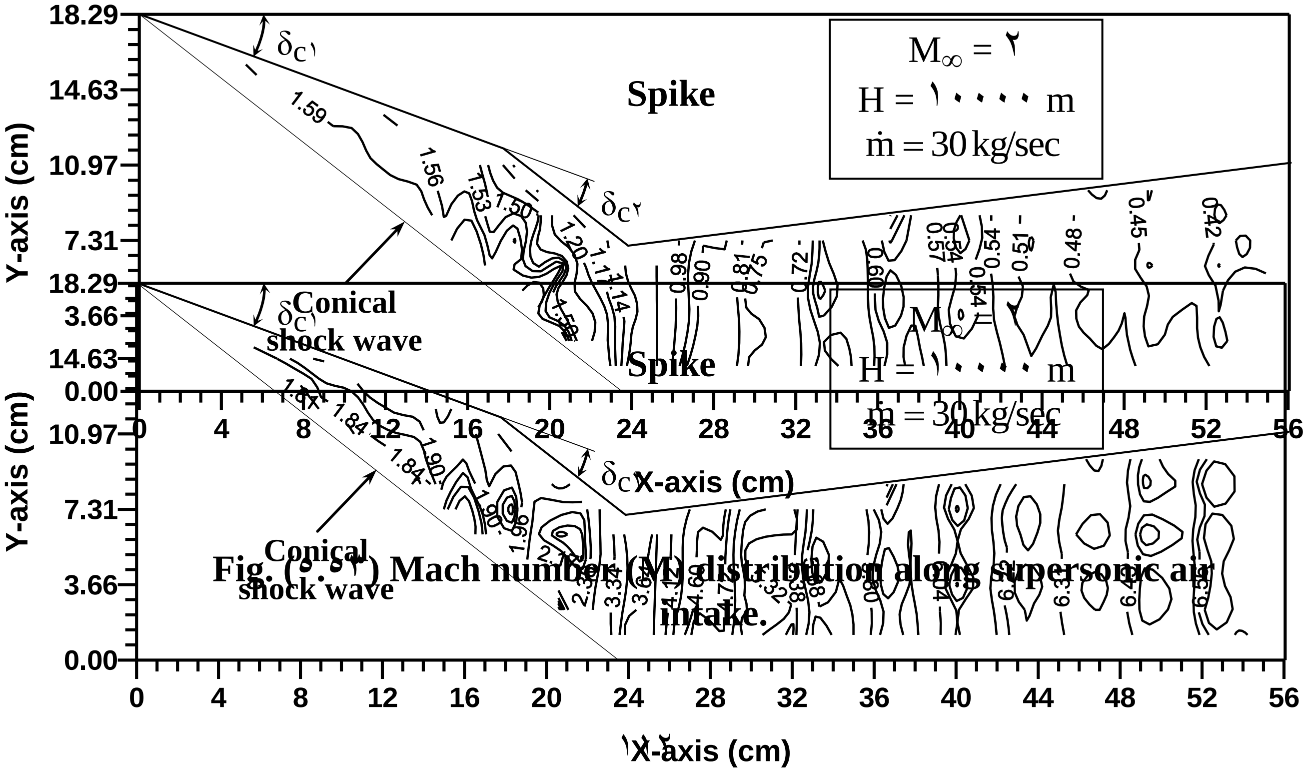

Fig. (٥.٥٣) Mach number (M) distribution along supersonic air intake.

Fig. (٥.٥٤) Pressure ratio (P ...) distribution along supersonic air

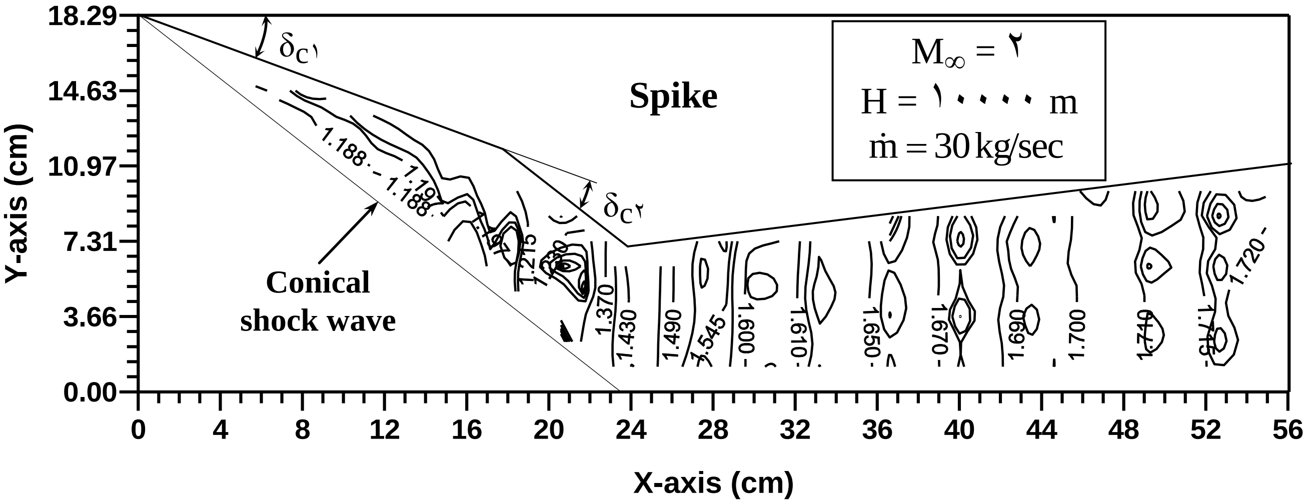

Fig. (٥.٥٥) Temperature ratio $\left(\frac{T}{T_\infty}\right)$ distribution along supersonic air intake.

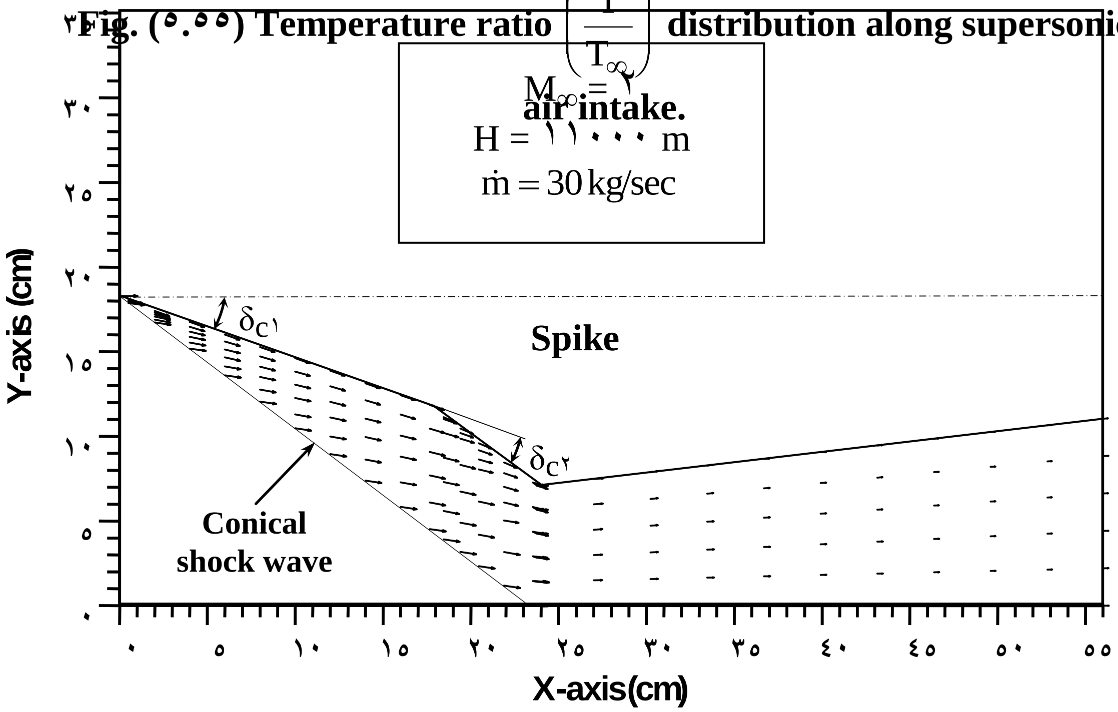

Fig. (٥.٥٦) Vector plot distribution along supersonic air intake.

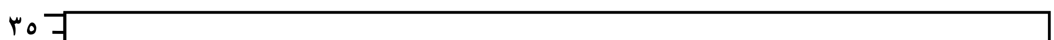

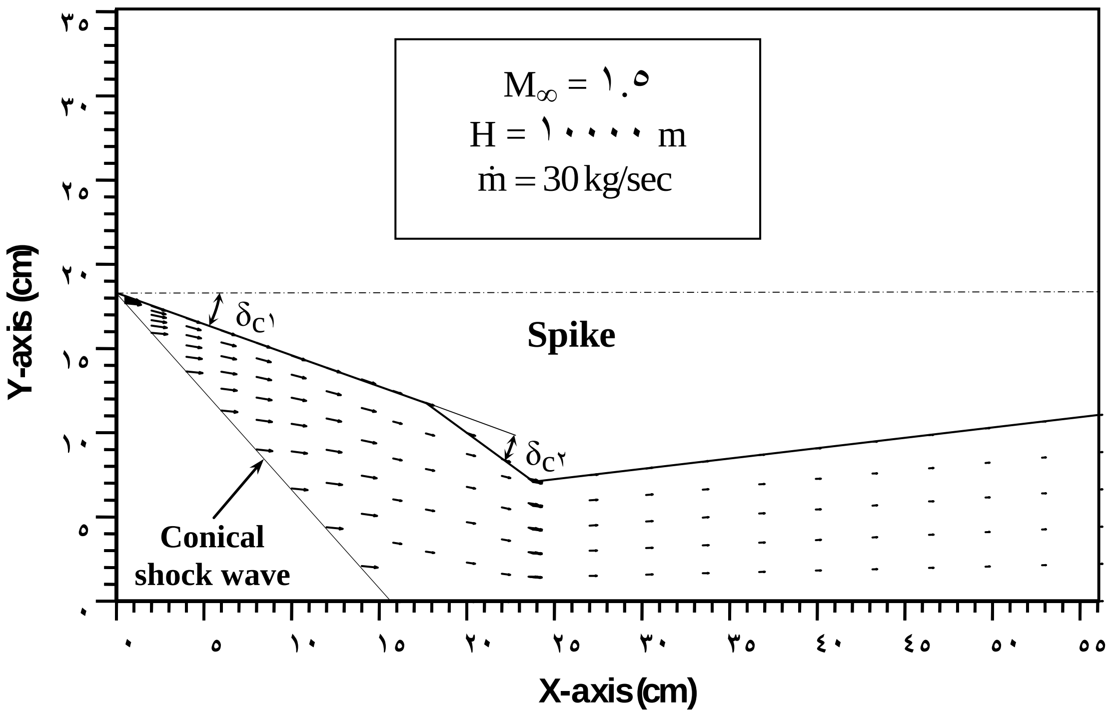

Fig. (٥.٥٨) Vector plot distribution along supersonic air intake.

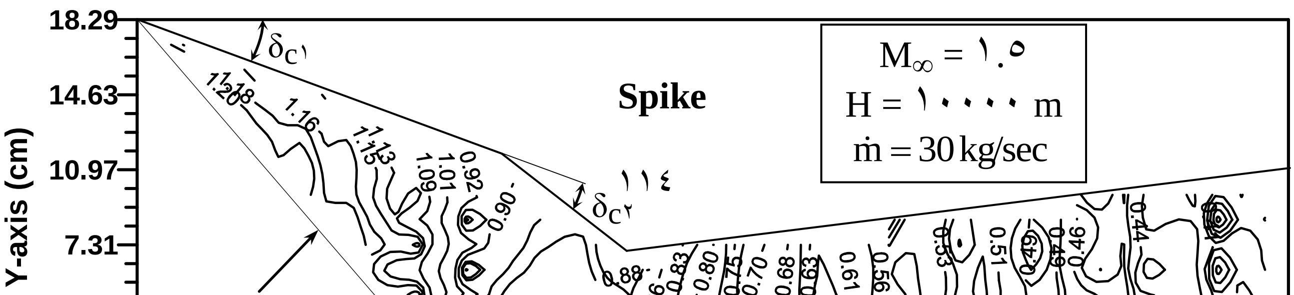

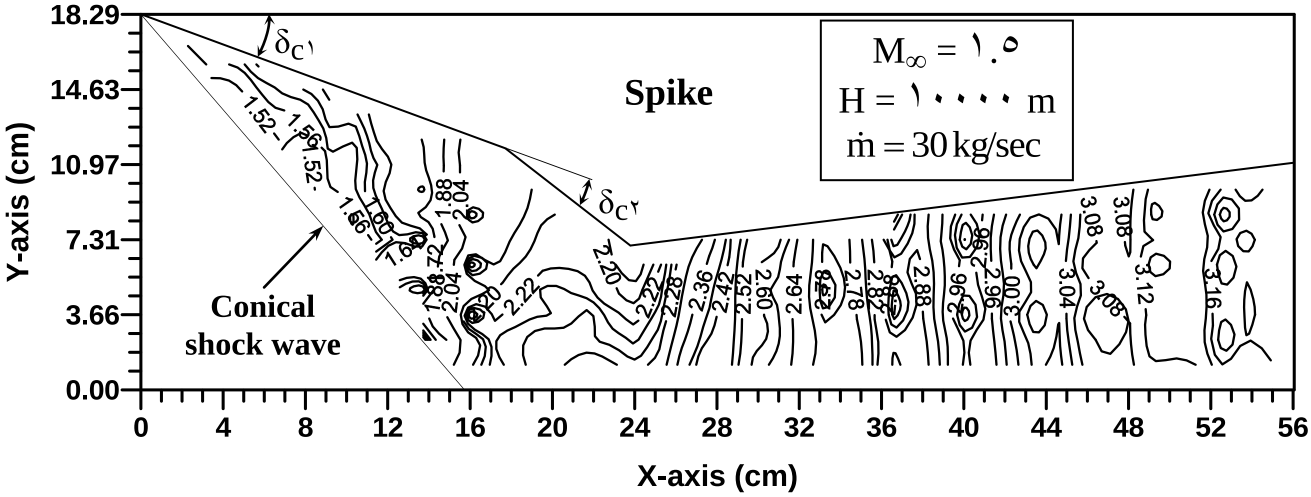

Fig. (٥.٦٠) Pressure ratio $\left(\frac{P}{P_\infty}\right)$ distribution along supersonic air intake.

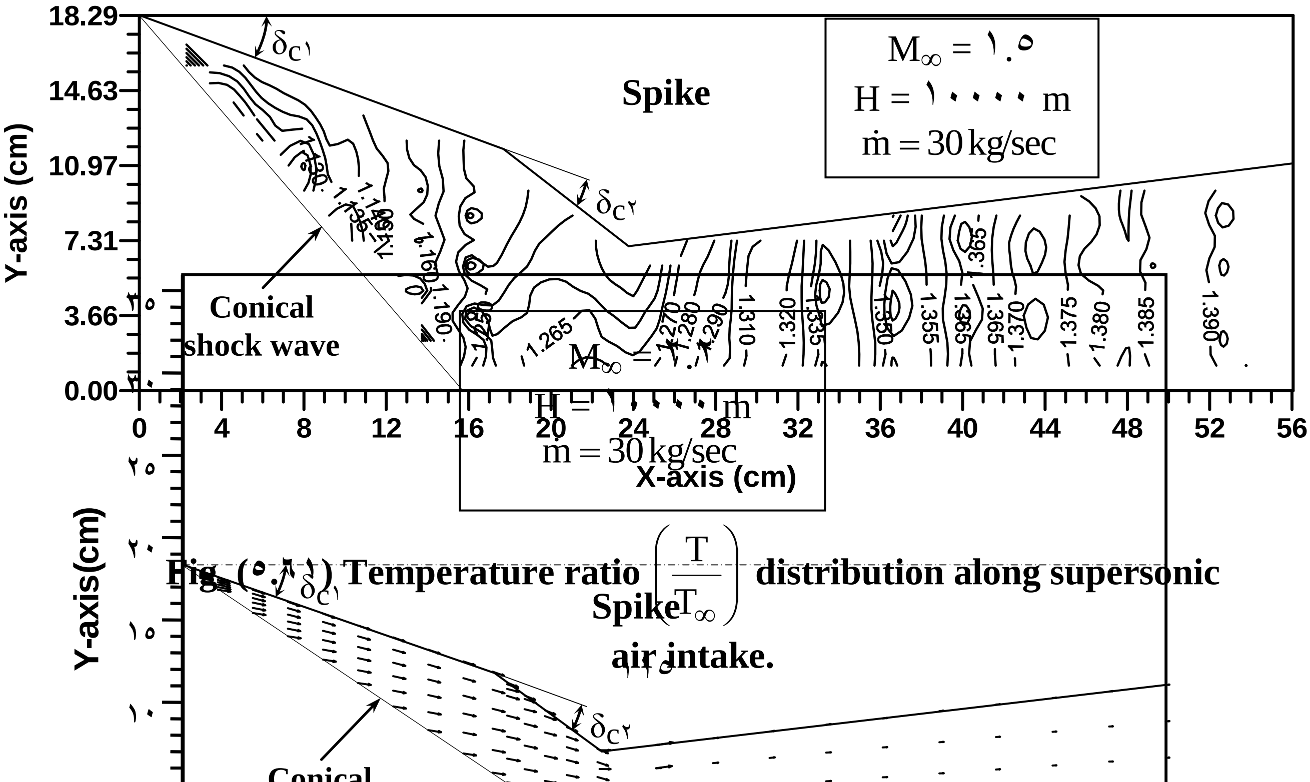

Fig. (٥.٦١) Temperature ratio $\left(\frac{T}{T_\infty}\right)$ distribution along supersonic air intake.

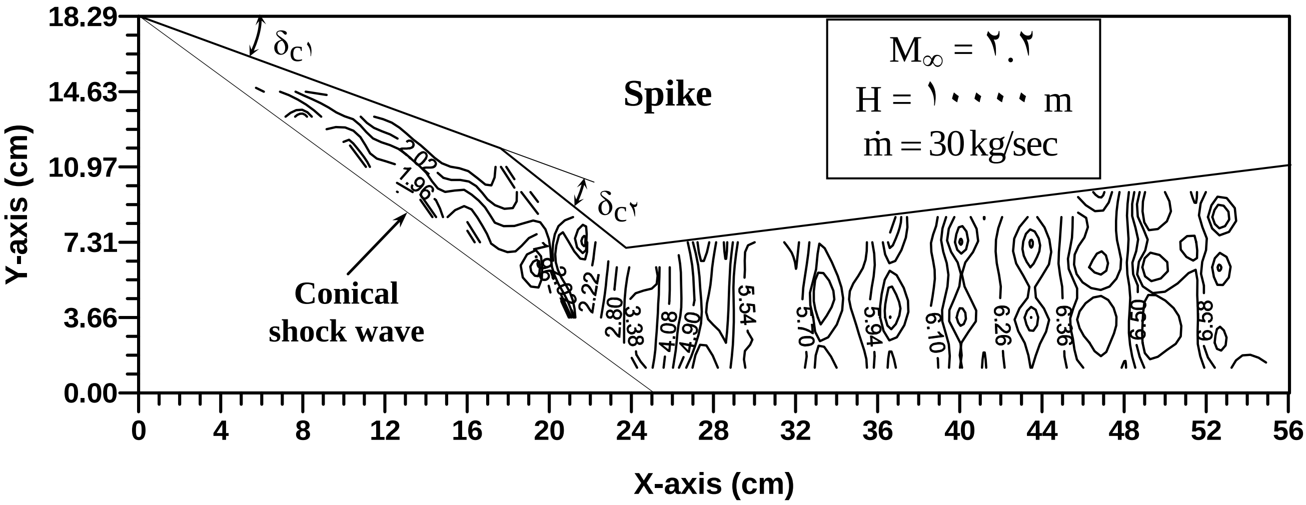

Fig. (٥.٦٤) Pressure ratio $\left(\frac{P}{P_\infty}\right)$ distribution along supersonic air intake.

Ministry of Higher Education and Scientific Research
Babylon University
College of Engineering
Department of Mechanical Engineering

Design of Axisymmetric Supersonic Air Intake

A Thesis

Submitted to the College of Engineering of the University of Babylon in Partial Fulfillment of the Requirements for the Degree of Master of Science in Mechanical Engineering

By

Hussain Kadhim Al-Shukri

B. SC. 2000

Supervisors

Dr. Arkan K. Al-Taie

Dr. Abdul Kareem A. Wahab

September 2003

1- Introduction: -

The supersonic intakes have been developed since the second World War, in parallel with the development of the jet engine itself, so due to this development supersonic intakes have many different shapes, but for the same basic function. The intake consists of a duct (rectangular, cylindrical or conical) as in Fig. (1) with fixed or variable geometry depending on the surface of compression or spike moving inside the intake Fig. (2).

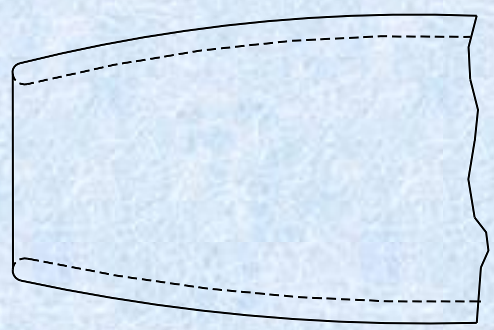

a- Pitot intake
(for subsonic aircraft).

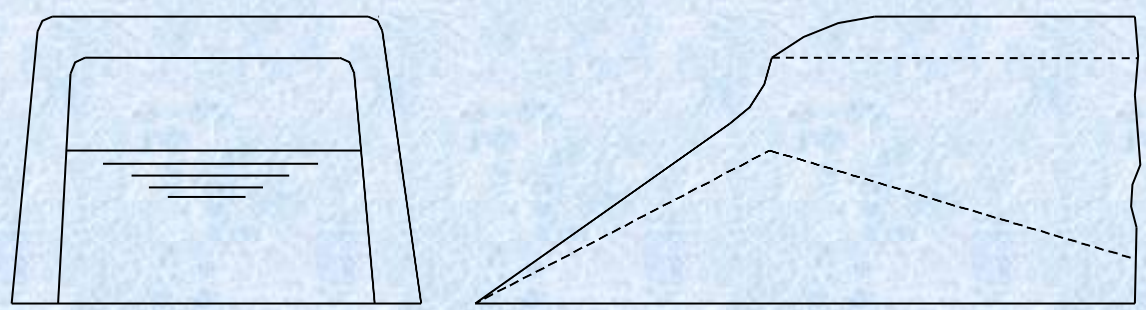

d- (2-Dimensions) intake.

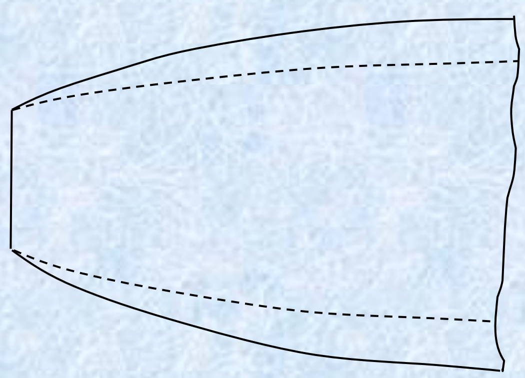

b- Pitot intake
(for supersonic aircraft).

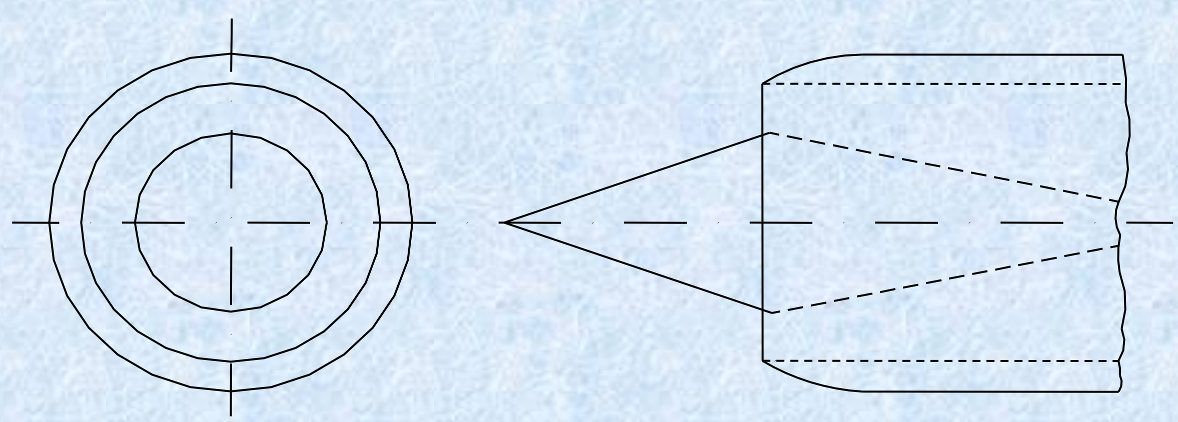

e-Conical or spike or round intake.

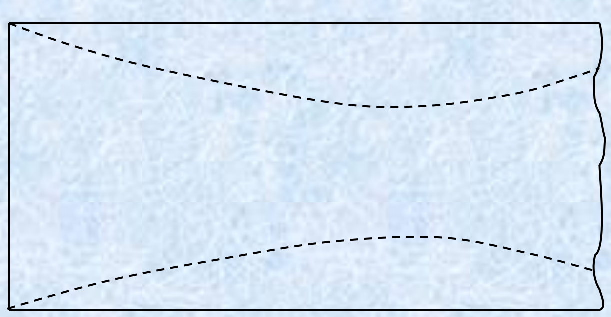

c- Internal compression intake.

Fig. (1) Intake types.

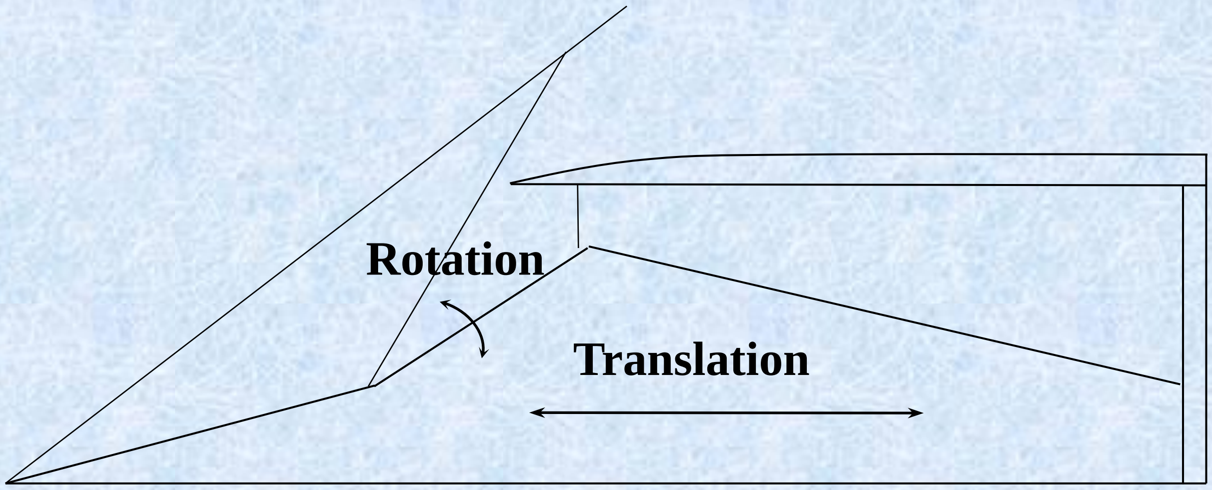

Fig. (2) Supersonic variable geometry intake.

Supersonic intake consists of two parts, supersonic part (shock wave part) which consists of number of shock waves (oblique or conical) and finished with a weak or a strong normal shock wave depending on its position from intake, the another is subsonic part (shockless part), where this part consists of divergent walls (diffuser). Where the subsonic flow will be further slowed down to the speed required by the engine. Thus, a diffuser is increasing in a cross-sectional area from front to back, as shown in Fig. (3).

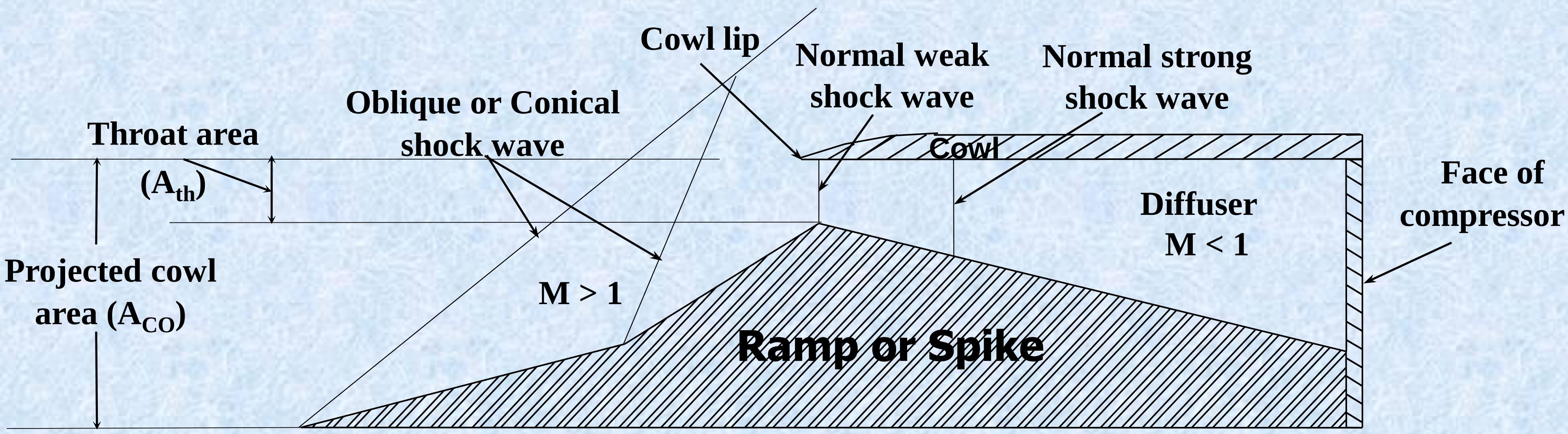

Fig. (3) Supersonic intake.

The basic function of a supersonic air intake is to supply the correct quantity and quality of air to the compressor face of the engine. The correct mass flow of air must be delivered to the compressor face at about Mach 0.3~0.5, with acceptable velocity distribution with as little loss of stagnation pressure (Po) as possible. Consequently the intake delivers air to the compressor at a static pressure considerably greater than ambient and it is, therefore, able to contribute significantly to the cycle compression process Fig. (4) [29], where the intake is required to do this at all flight conditions and at least weight, cost, and drag.

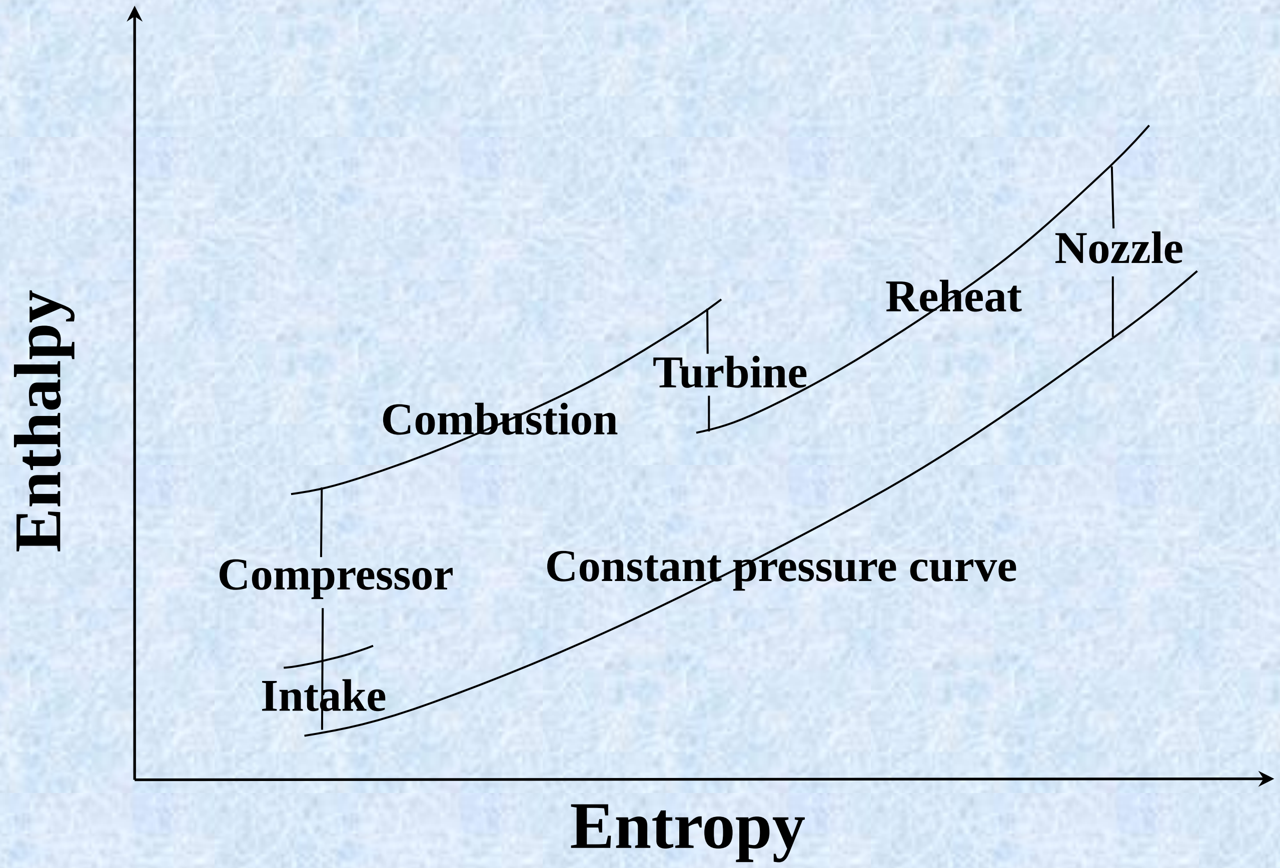

Fig. (4) Supersonic gas turbine cycle.

2- Supersonic Intake Under Study: -

The Supersonic intake type considered as a fixed geometry axisymmetric external compression with two cones (bicone) Fig. (5). Where running on-design Mach number, the supersonic part consists of two conical shock waves, followed by a normal shock wave.

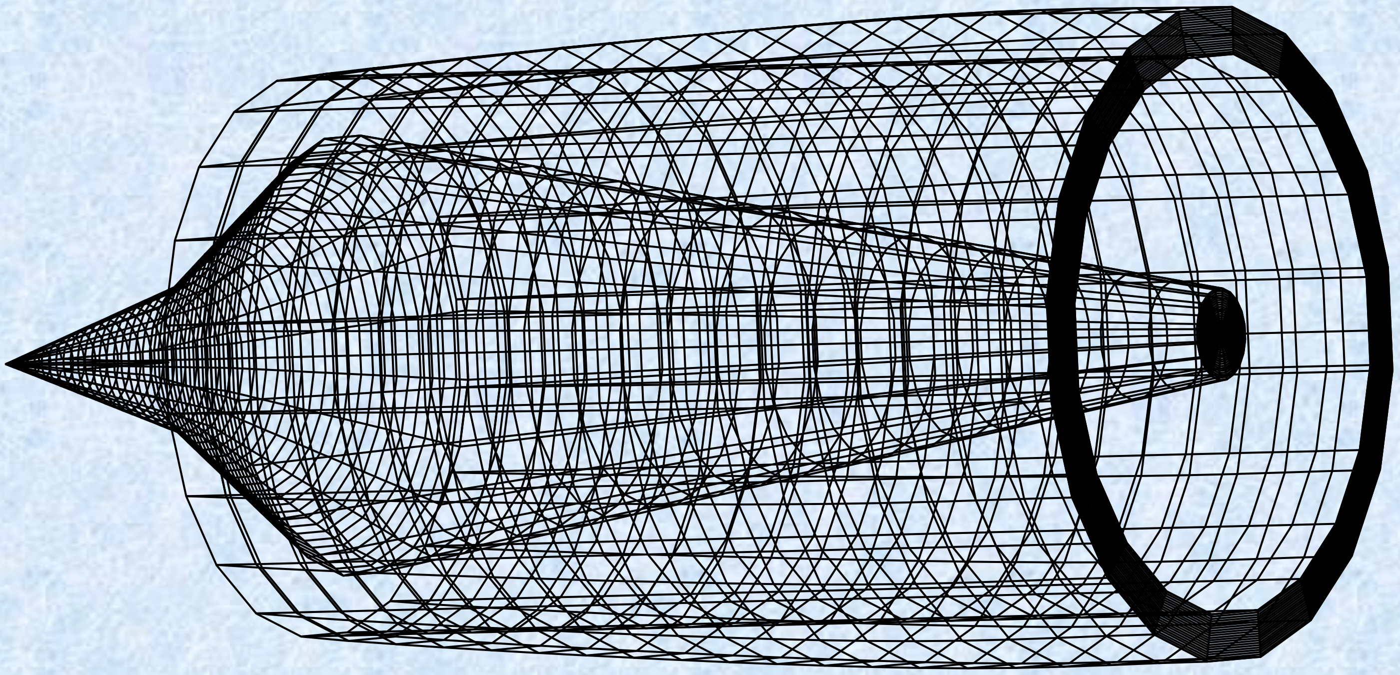

Fig. (5) External compression supersonic air intake.

3- The Aim Of The Work: -

A-The aim of the present work is to design an axisymmetric bicone supersonic air intake, as follows: -

1- Design the external part and analyze the supersonic flow around the cone by using Taylor-Maccoll method.

2- Design the internal part, a numerical solution will be employed based on a finite difference technique, where the set of equations governing the problem will be solved iteratevilly by using Newton-Raphson method.

B- Performance study: -

i- On design.

The on design conditions are Mach number (M = 2),($\dot{m} = 30$ kg/sec), and the flow properties are at an altitude of (H = 10 km).

ii- Off design.

The values of Mach number and flow properties are then changed to predict the intake flight envelope.

The results are to be obtained at a different flow Mach number, different angles of cone, different altitudes, and at different area ratios for subsonic portion, where optimization is the final goal.

4- External Part: -

This part consists of a sharp cone with semi-vertex angle (δ_{C1}), followed by a second cone with semi-angle (δ_{C2}) as in Fig. (6). The shocks generated due to the sharp cones in supersonic flow are called ‘conical shock waves’. The flow behind the conical shock wave is itself conical, and called as ‘conical flow’, in such flows, the flow properties are constant along rays from the vertex of a cone but varies along a streamline.

So For the conical flow it is convenient to express the governing equations in the spherical coordinate system.

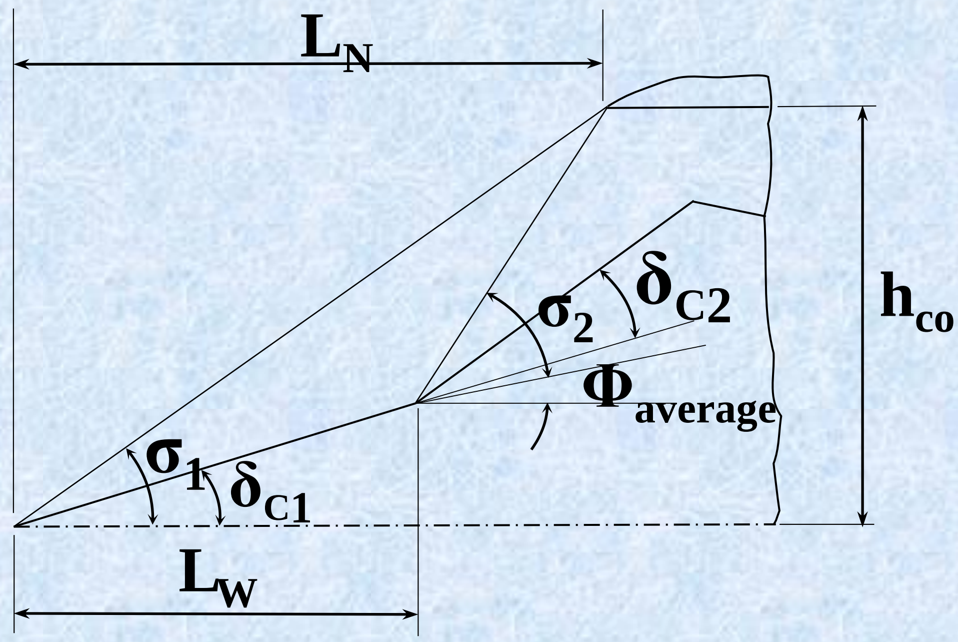

Fig. (6) External part geometry.

4.1- Assumptions: -

The following assumptions are made: -

1- The airflow is treated as a perfect gas.
2- Zero angle of attack (Axisymmetric flow).
3- Non-viscous flow.
4- The cone has straight surface.
5- Steady flow.

4.2- Limits Of Design: -

The design elements of this part are δ_{C1}, δ_{C2}, LW, LN, and hco, the geometric angles of first and second angles of cone may be optimized in terms of pressure recovery. Where all pressure recoveries are based on shock losses. In the intake under consideration the total pressure losses, occur across the two conical shock waves and the normal shock wave.

5- Internal Part: -

This part starting immediately downstream of the external part of intake, this part of intake has axisymmetric convergence-divergence form, as shown in Fig. (7). So it is convenient to express the governing equations in cylindrical coordinate system.

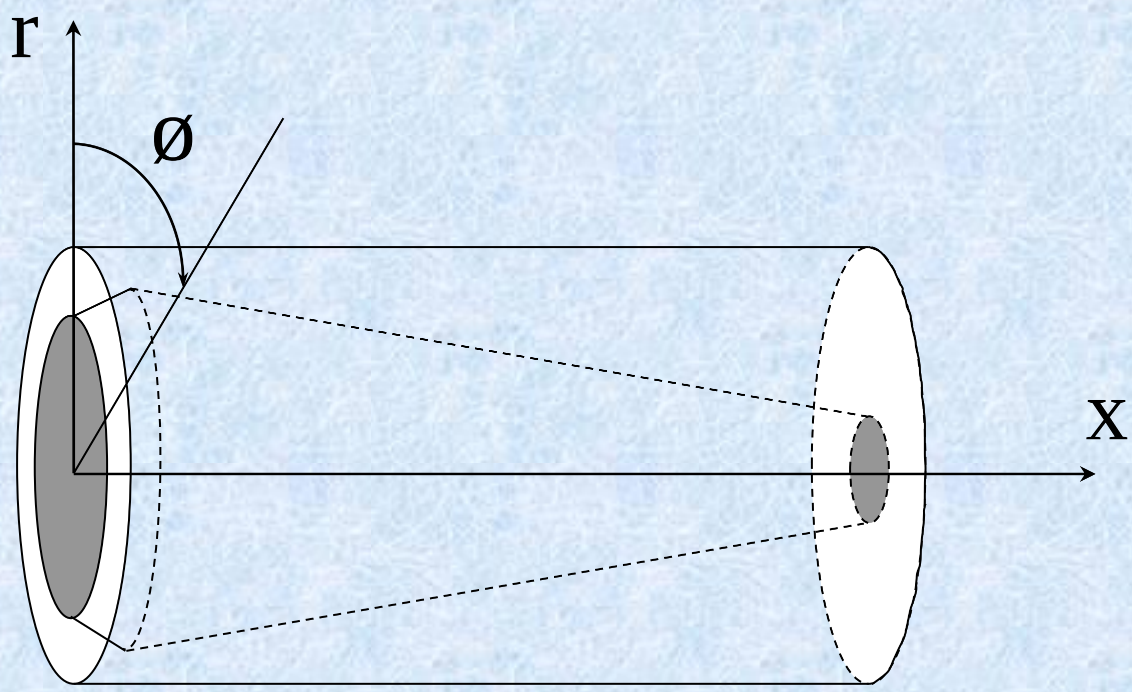

Fig. (7) Internal part of intake.

5.1- Assumptions: -

The following assumptions are made: -

1- The airflow is treated as a perfect gas.
2- The flow is treated as quasi-three dimensional (Axisymmetric flow).
3- Non-viscous flow.
4- The flow is Steady.

5.2- Limits Of Design: -

The design elements of this part are area ratio (AR), length (L2), and angle of inclination wall (θ). These elements must be optimized to get intake with the following characteristics: -

- Short enough to keep weight and drag to minimum.
- Long enough to give Mach equals to (0.3~0.5) at the face of compressor.
- The air has uniform flow with high-pressure ratios.

6-Results And Discussion: -

The results are the output of the computer programs. These computer programs are built to analyze and then design of the two-parts of intake (external and internal flow parts). Hence, so as to obtain deep understanding, the results will be presented for each two parts separately and then the collection takes place.

6.1-Results Of The External Part: -

A Taylor-Maccoll method was employed to analyze the supersonic inviscid flow around the cone by solves the equations of continuity and momentum in spherical coordinate system. The results are concerned on presented of flow properties over a cone in supersonic Mach number for different angle of cone (10^o to 50^o) with different free stream Mach number (~1.1 to 5). Finally the optimization takes place to design this part.

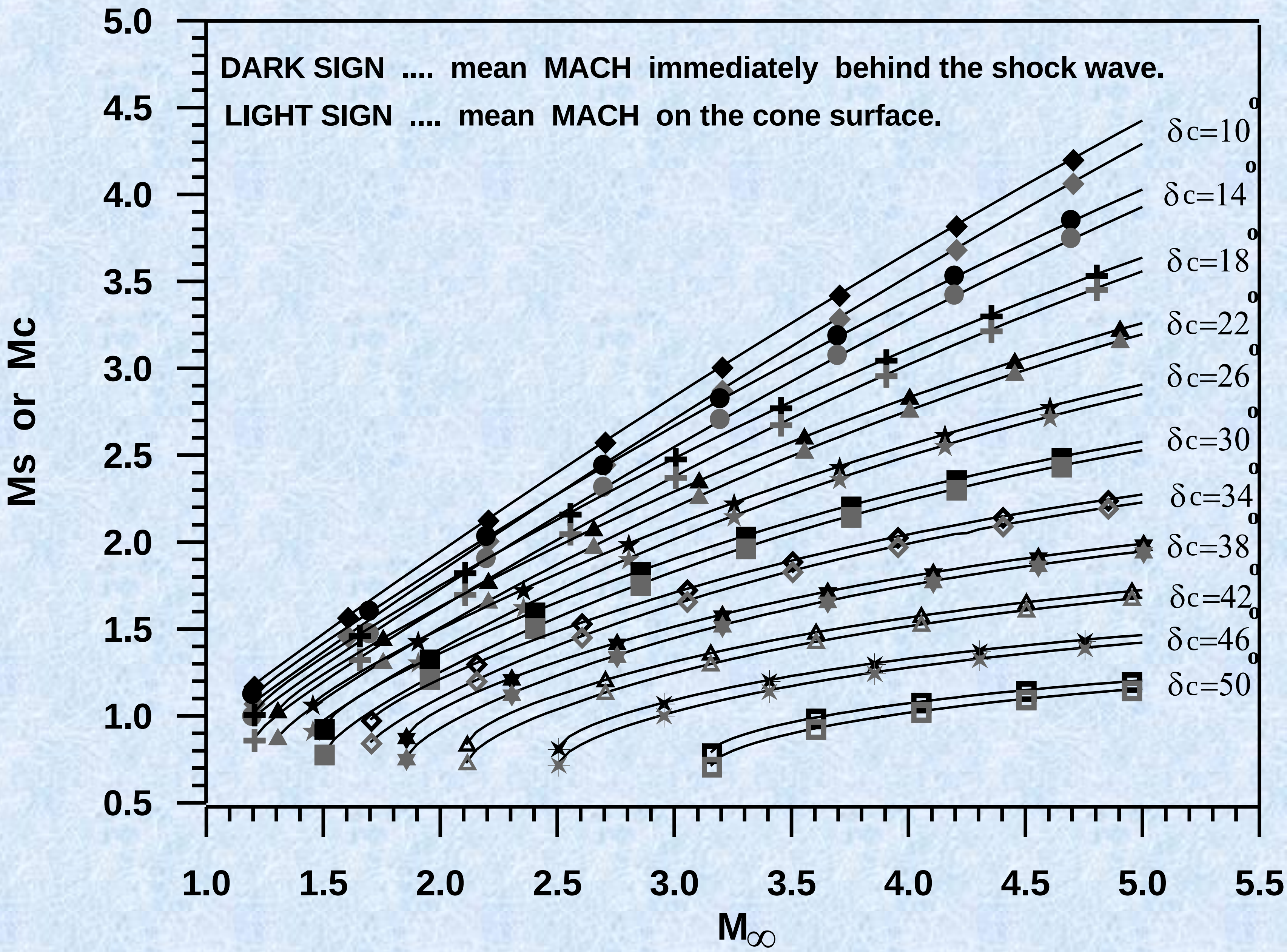

Fig. (8) Mach number behind the shock wave and at the surface of cone versus free stream Mach number for different cone angles.

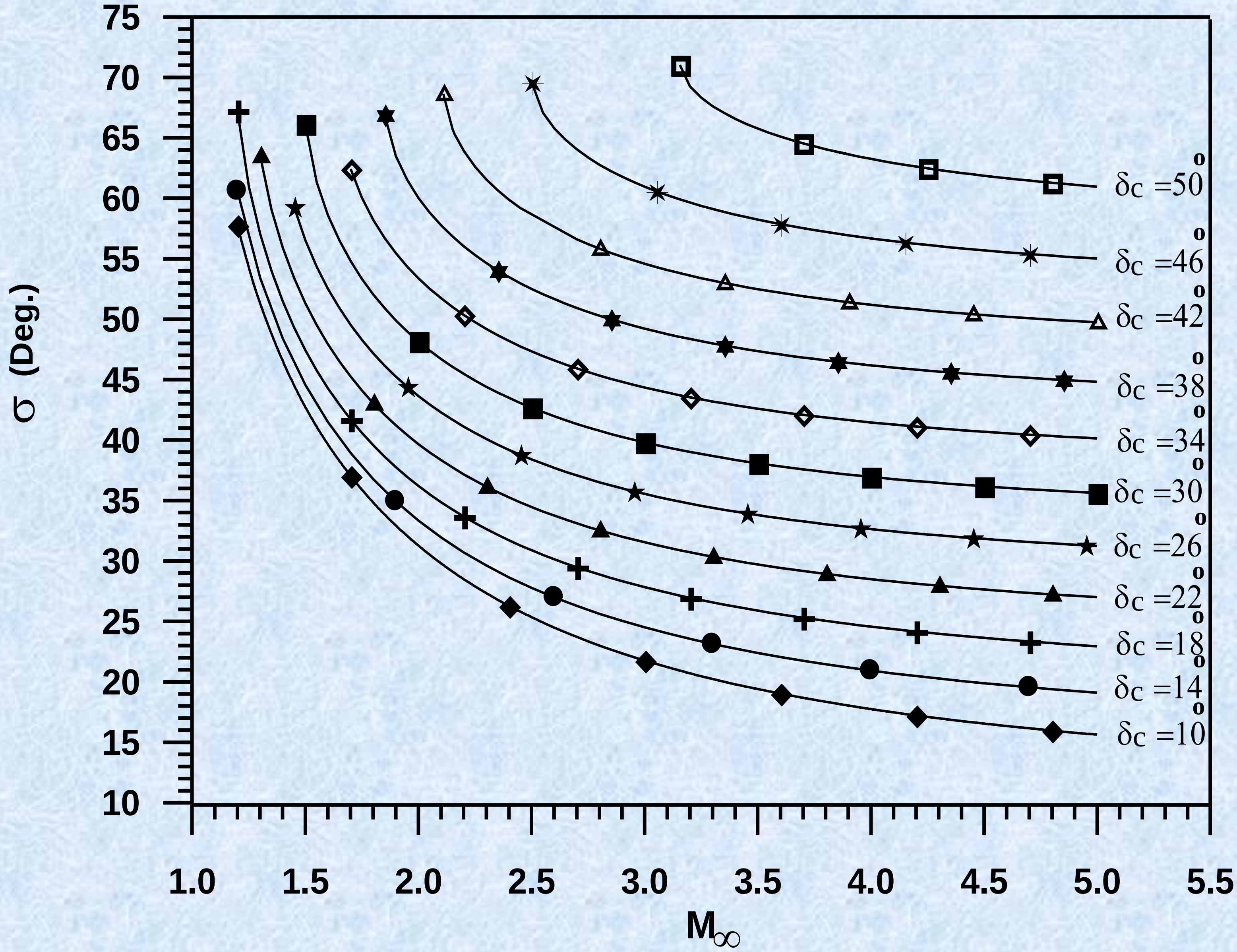

Fig. (9) Angle of the shock wave versus free stream Mach number for different cone angles.

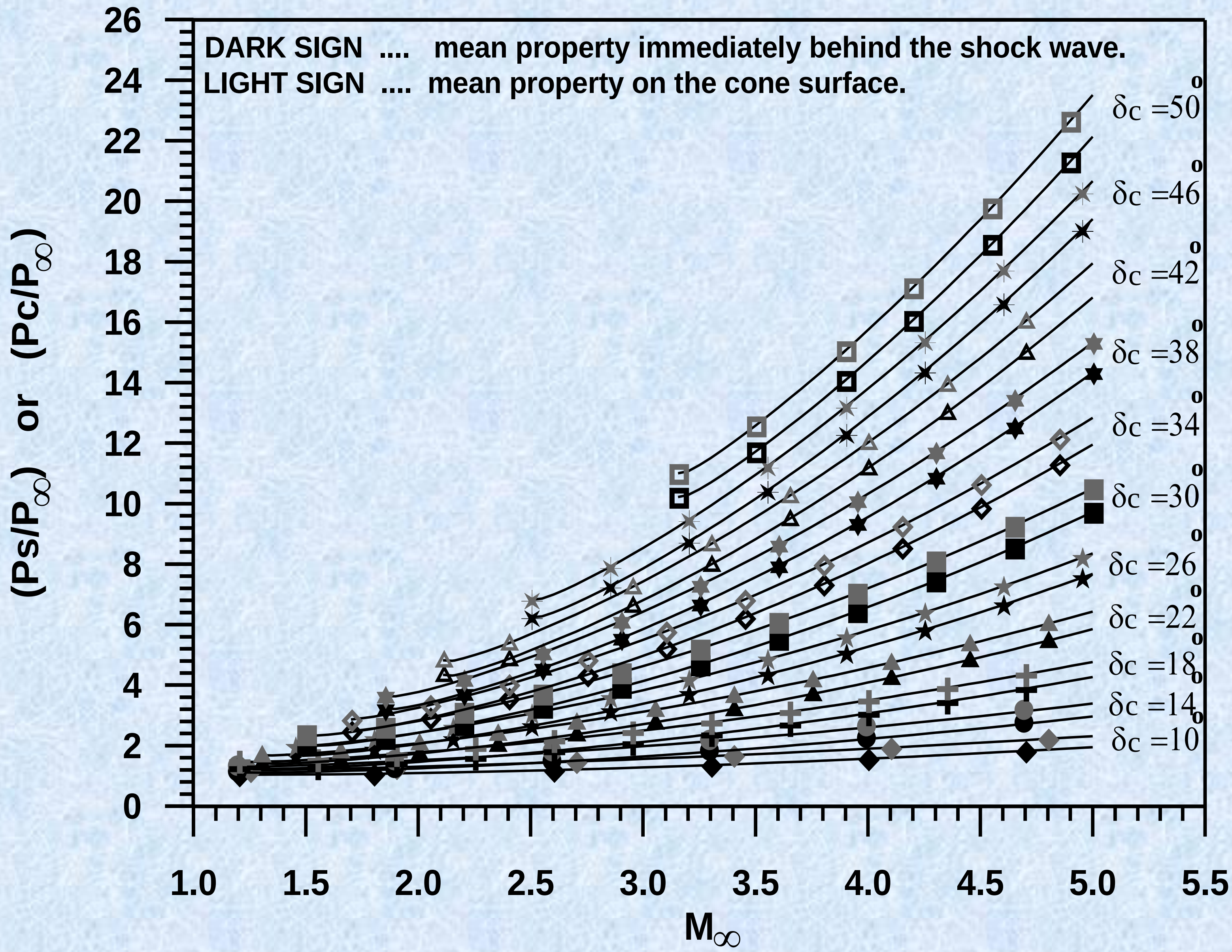

Fig. (10) Pressure ratio behind the shock wave and at the surface of cone versus free stream Mach number for different cone angles.

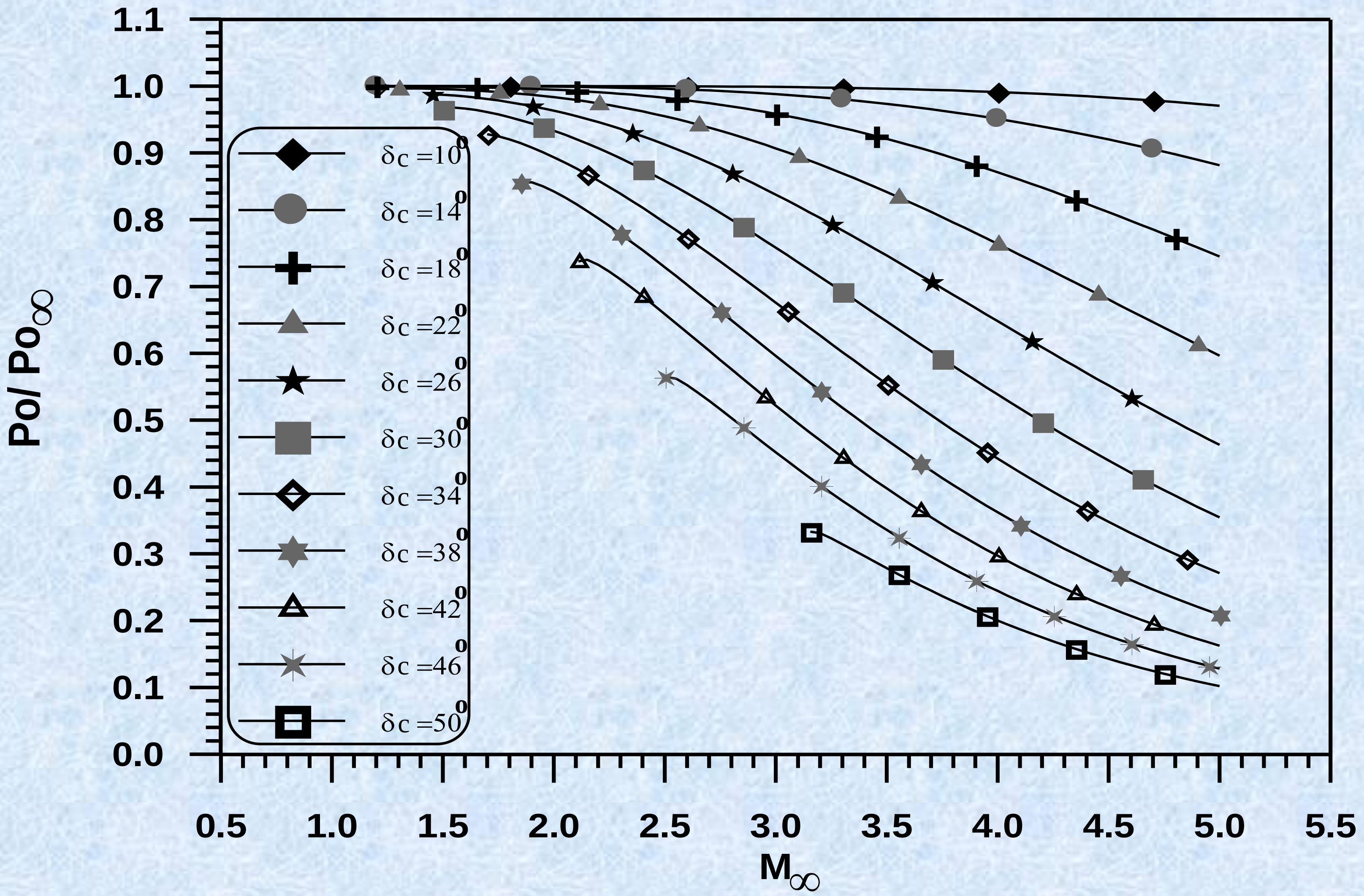

Fig. (11) Total Pressure ratio of total pressure behind the shock wave to free stream total pressure versus free stream Mach number for different cone angles.

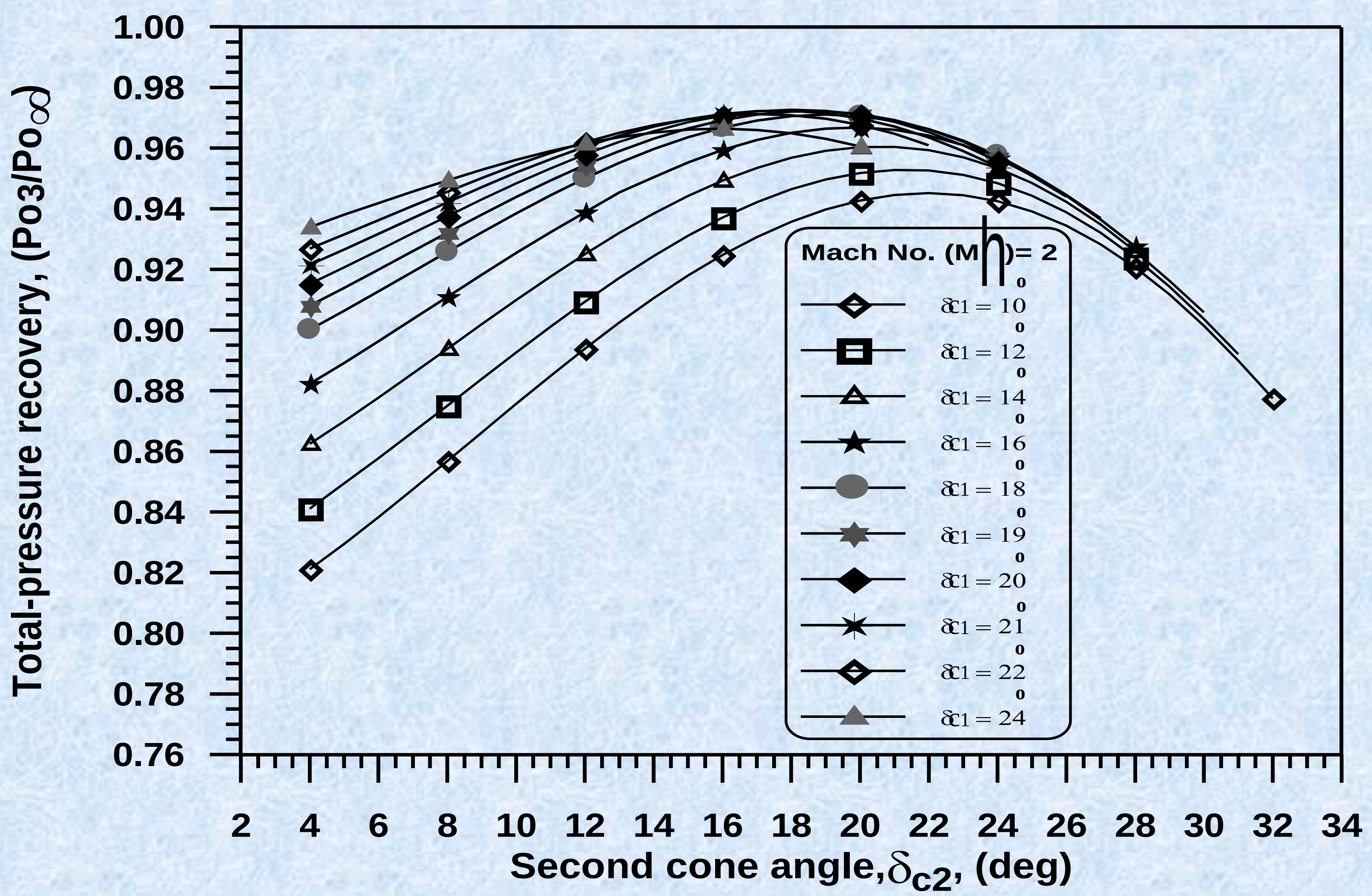

Fig. (12) Total pressure recovery of total pressure behind the normal shock to free stream total pressure versus second cone angle for different first cone angles.

The flow over cone may be supersonic, subsonic or mixing between supersonic and subsonic. The data presented in table (1) give the minimum values of the freestream Mach number for which flow between the cone and the shock remains supersonic. At lesser Mach numbers, subsonic regions appear and cause deviations from conical flow.

δ_C°	1	2	3
10	1.0538	1.0588	1.116
12.5	1.0828	1.0848	1.1645
15	1.1193	1.123	1.2187
17.5	1.1622	1.1688	1.2781
20	1.2115	1.2227	1.3428
22.5	1.2673	1.2853	1.4135
25	1.3301	1.3572	1.4911
30	1.482	1.5336	1.6736
35	1.6814	1.7686	1.9114
40	1.9582	2.0995	2.2486
45	2.321	2.6216	2.795
50	3.155	3.6791	3.9569

Notes: -

Col. 1: Minimum value of(M_∞) for which conical flow is possible.

Col. 2: Maximum value of (M_∞) for completely subsonic flow between the cone and the shock wave.

Col. 3: Minimum value of (M_∞) for completely supersonic flow between the cone and the shock wave.

Table (1) Values of freestream Mach number for various flow regimes for supersonic conical flow.

In order to validate the present study, some of empirical formulas, in which the properties of flow and the conical shock wave angle can be found with small different on the values that calculated from present study, are presented down, [31].

$$K_1 = M_\infty \sin\delta_c \qquad \ldots(1)$$

$$M_\infty \sin\theta_s = \left(1 + \frac{(\gamma+1)}{2} K_1\right)^2 \qquad \ldots(2)$$

$$\frac{P_c}{P_\infty} = 1.493(K_1)^{1.98} + 1.302 \qquad \ldots(3)$$

$$\frac{T_c}{T_\infty} = 0.2403(K_1)^{1.97} + 1.119 \qquad \ldots(4)$$

6.2-Results Of The Internal Part: -

A finite difference method was employed to solve the equations of continuity, momentum and energy for an axisymmetric flow. In this section the results of diverge part are presented. These results present the optimum design annular diverge part diffuser for several area ratios (AR) and angle of diverge wall (θ). For each area ratio the angle was increased until circulation takes place. And for each area ratio, Mach numbers distribution at the exit section for a series of angles are presented.

Fig. (13) shows the paths of results for a diverge portion of diffuser. Path (1) is at the row (J = 1), path (2) is at the row (J = 4), and path (3) is at the row (J = 5).

Fig. (13) Paths of diverge portion of supersonic air intake.

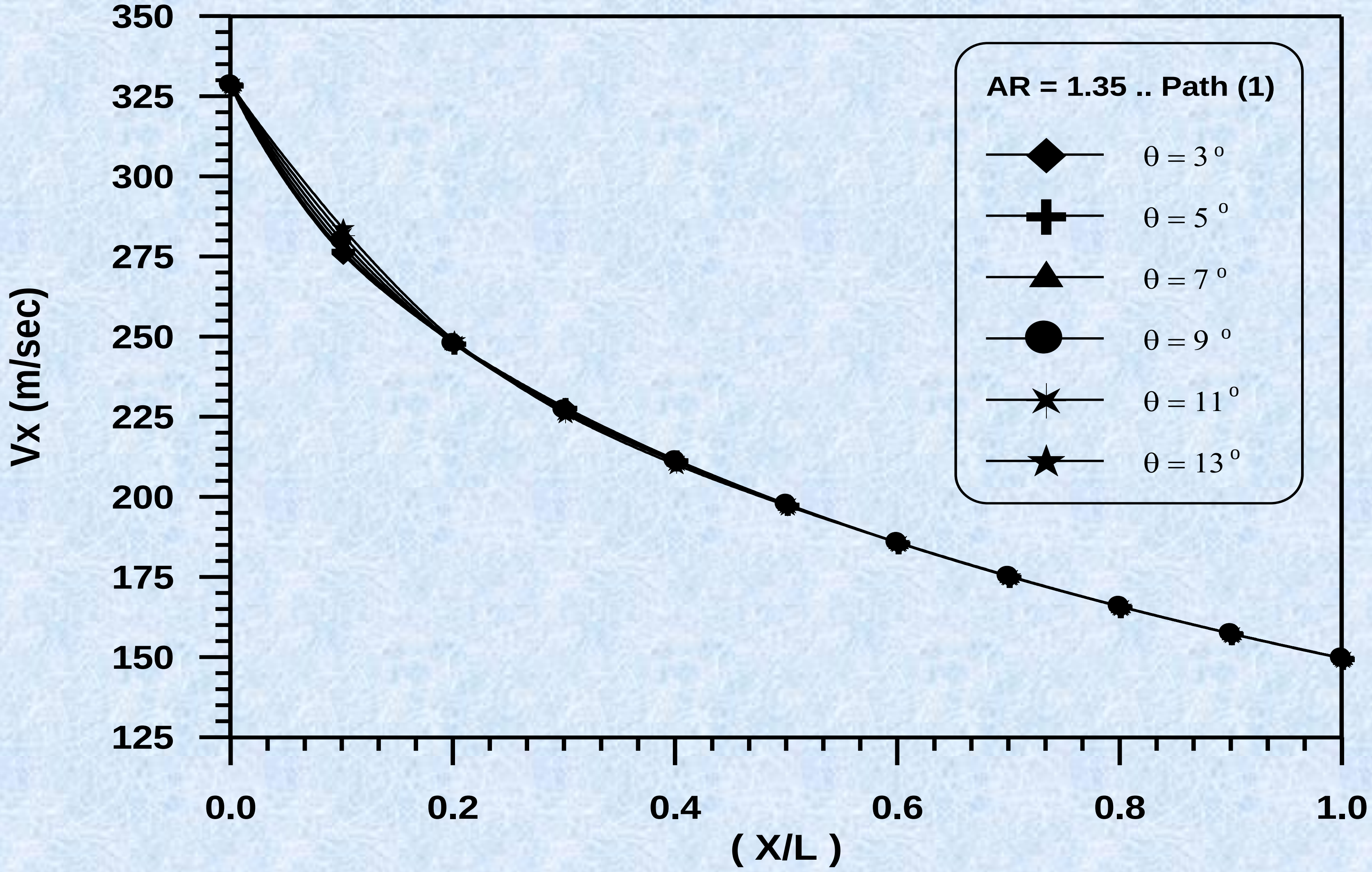

Fig. (14) Flow axial velocity component across the diverge portion of intake.

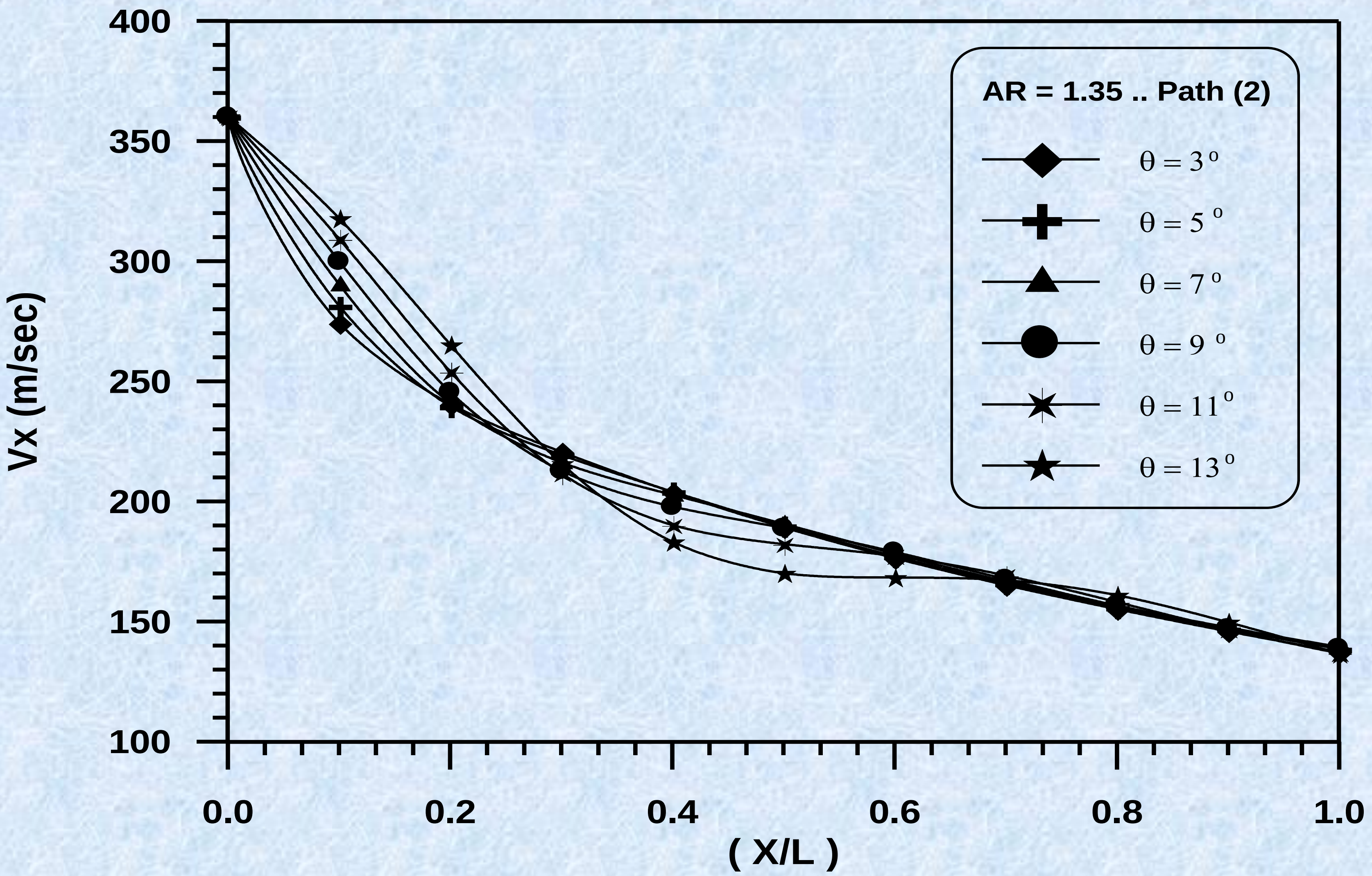

Fig. (15) Flow axial velocity component across the diverge portion of intake.

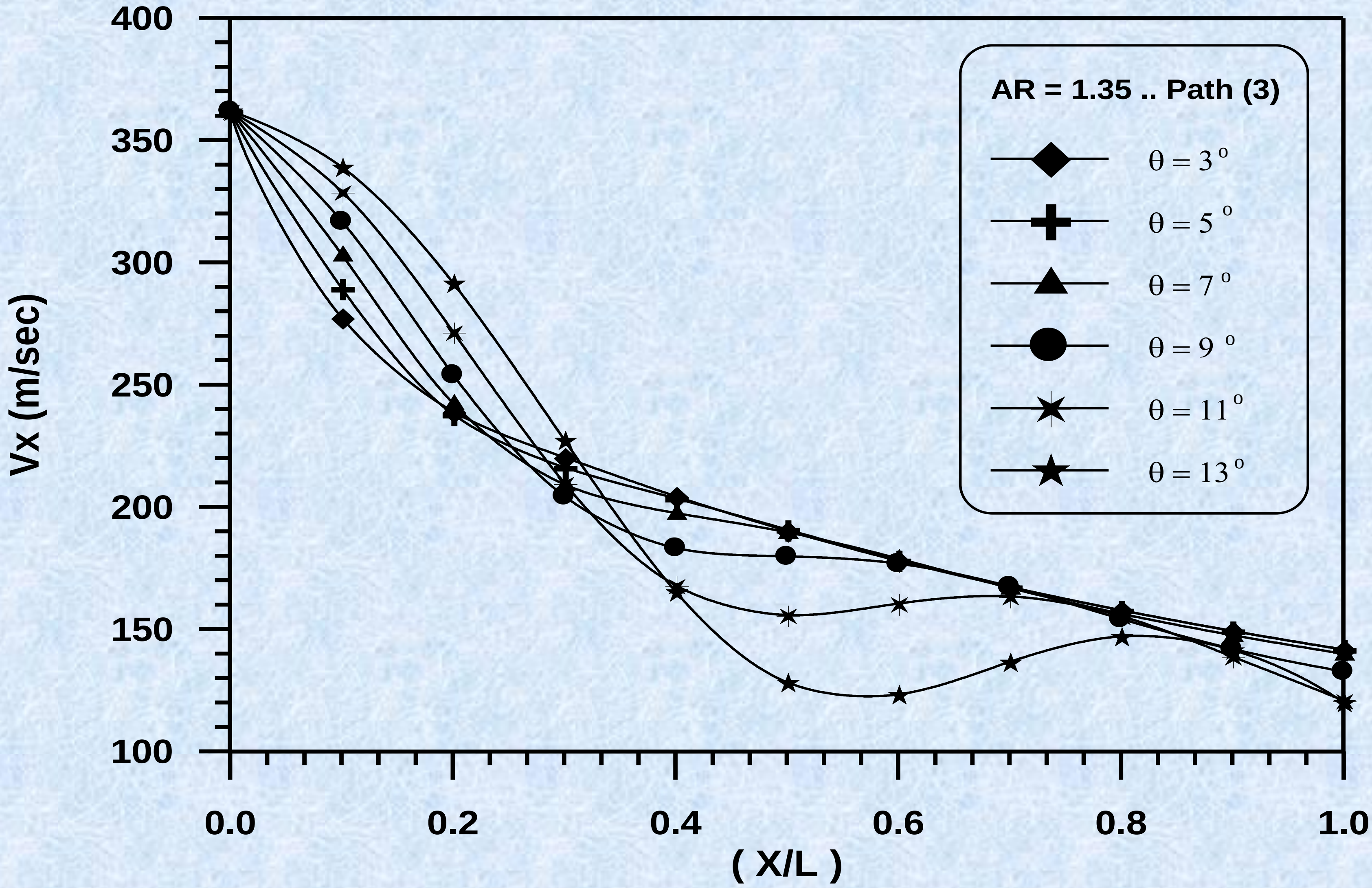

Fig. (16) Flow axial velocity component across the diverge portion of intake.

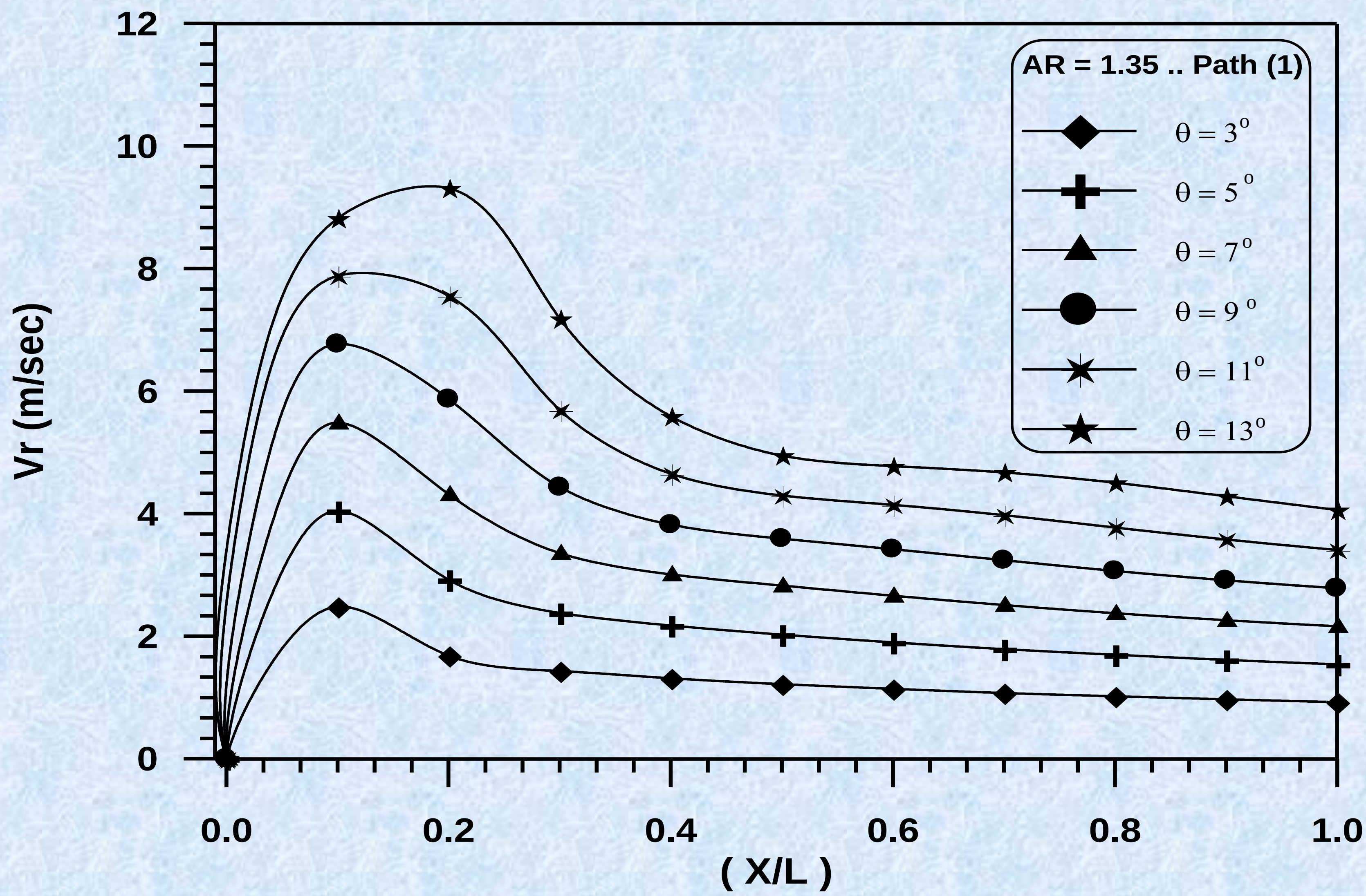

Fig. (17) Flow radial velocity component across the diverge portion of intake.

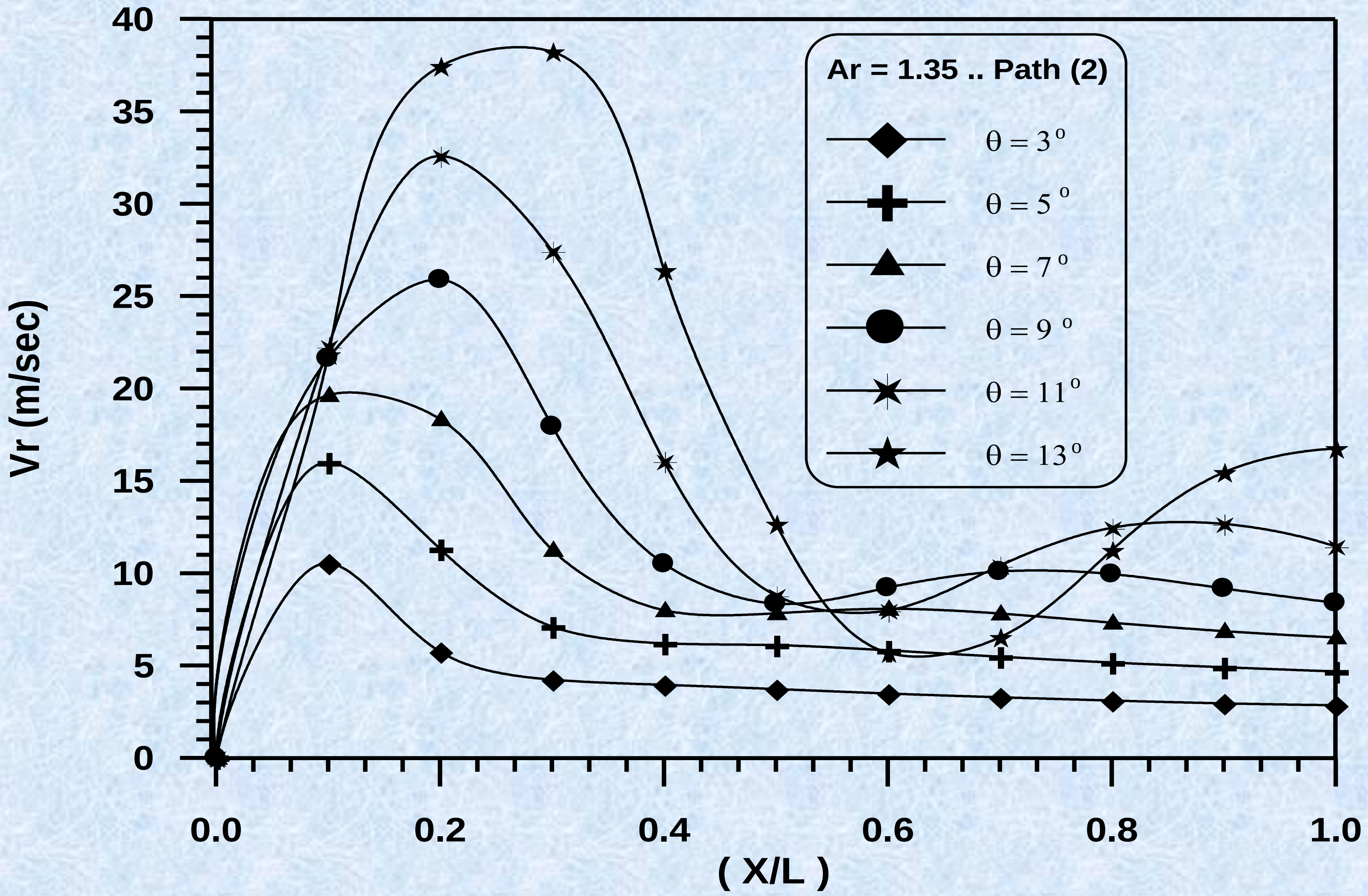

Fig. (18) Flow radial velocity component across the diverge portion of intake.

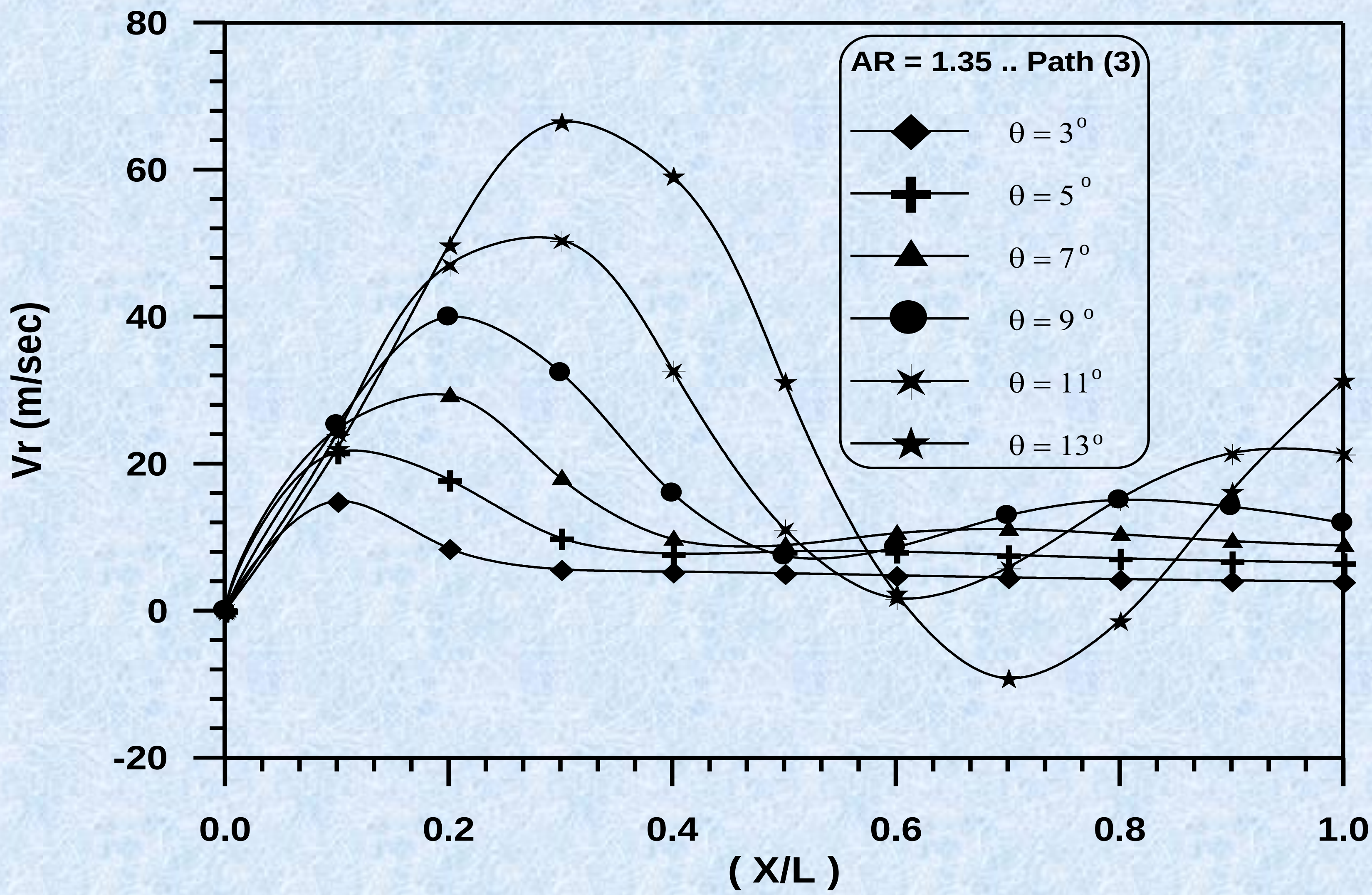

Fig. (19) Flow radial velocity component across the diverge portion of intake.

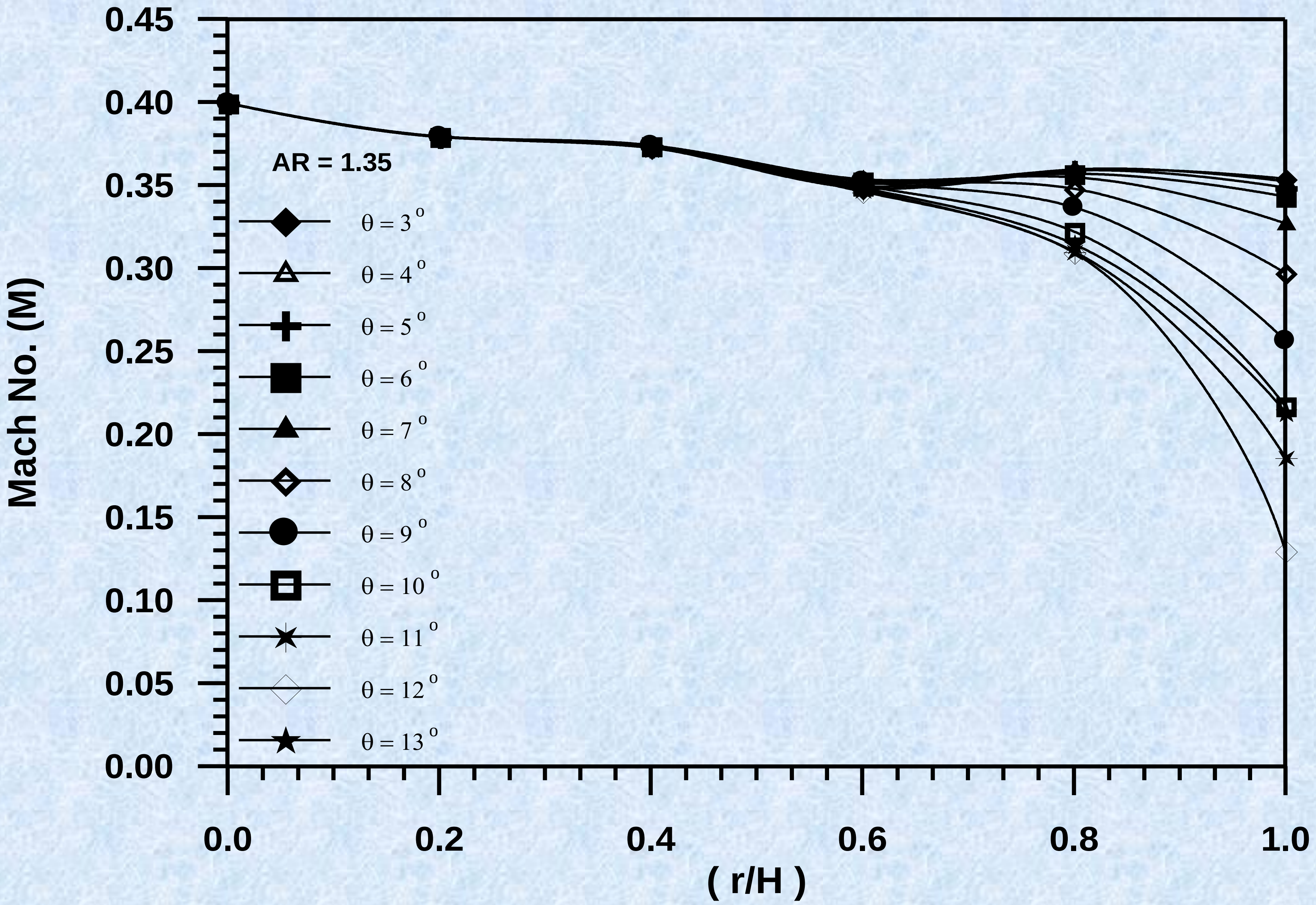

Fig. (20) Mach number distribution at the exit section.

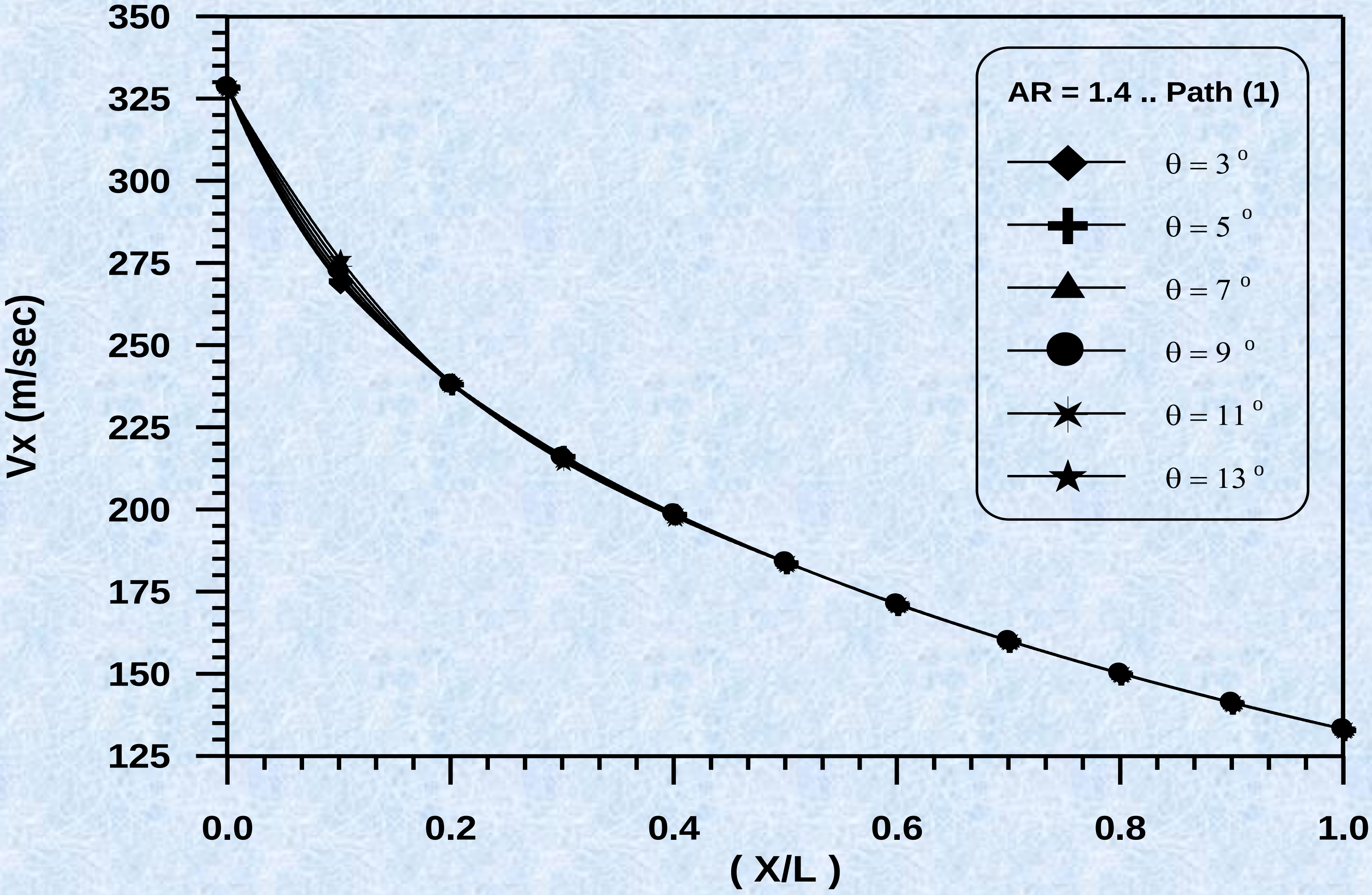

Fig. (21) Flow axial velocity component across the diverge portion of intake.

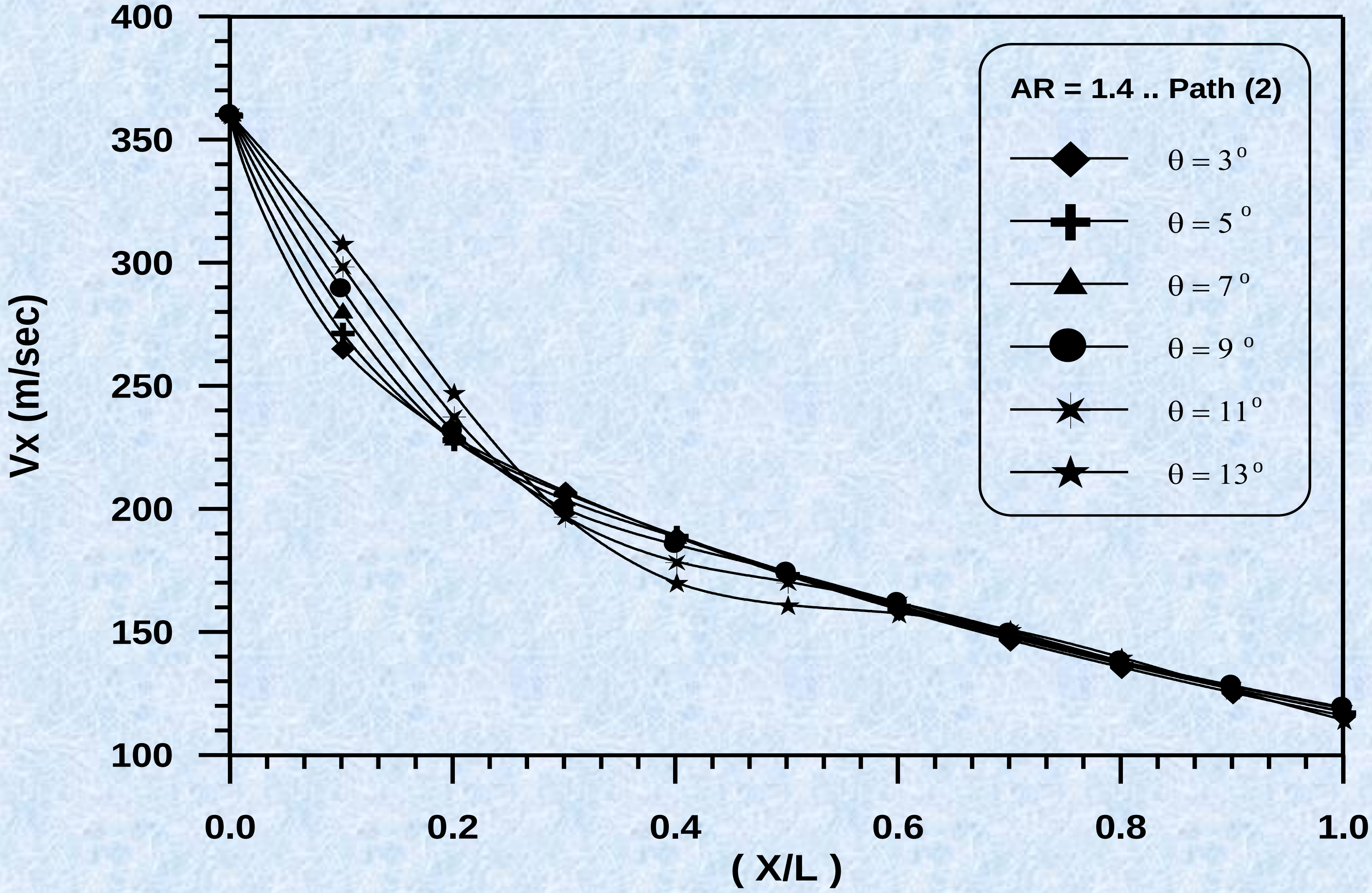

Fig. (22) Flow axial velocity component across the diverge portion of intake.

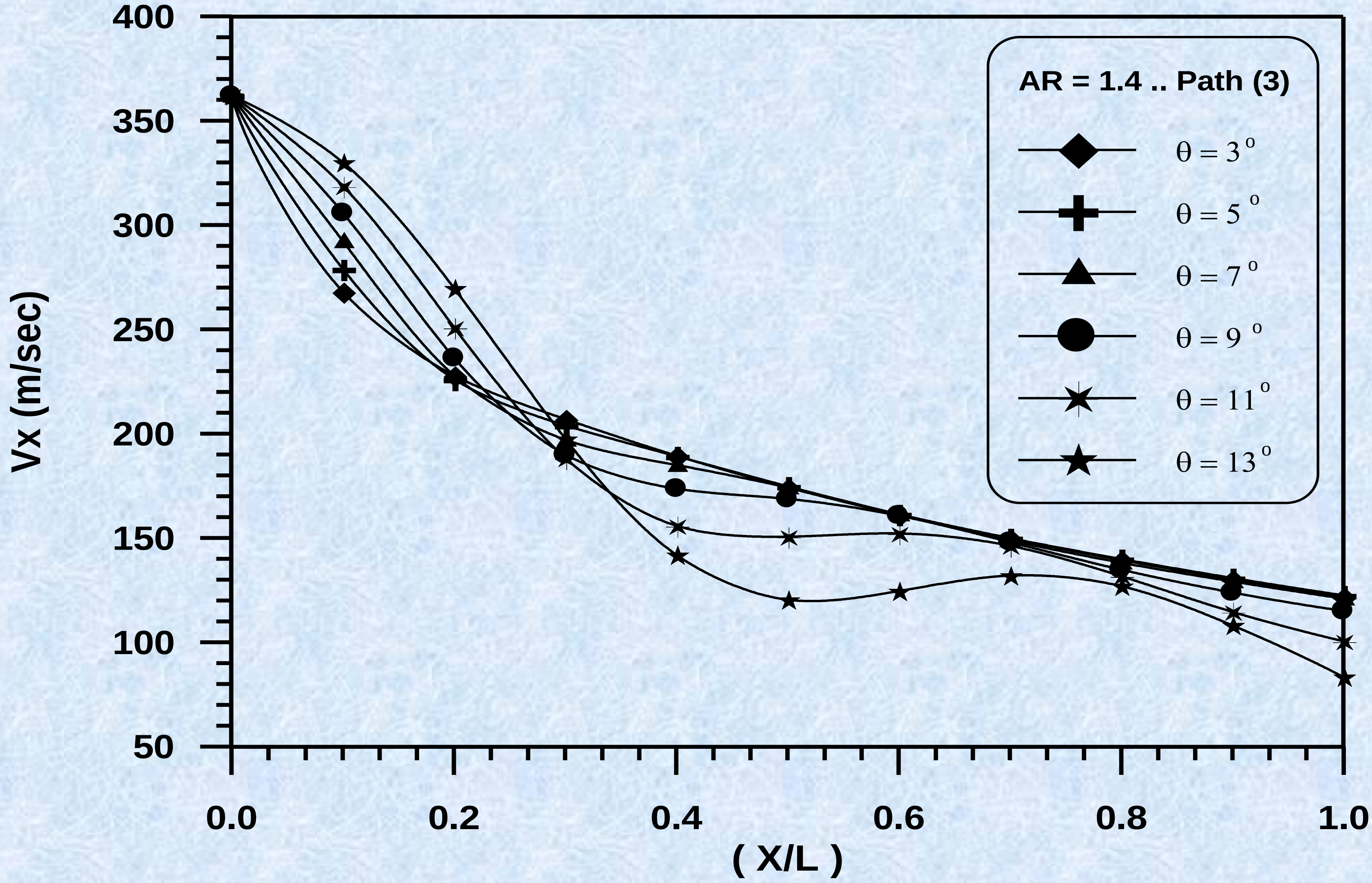

Fig. (23) Flow axial velocity component across the diverge portion of intake.

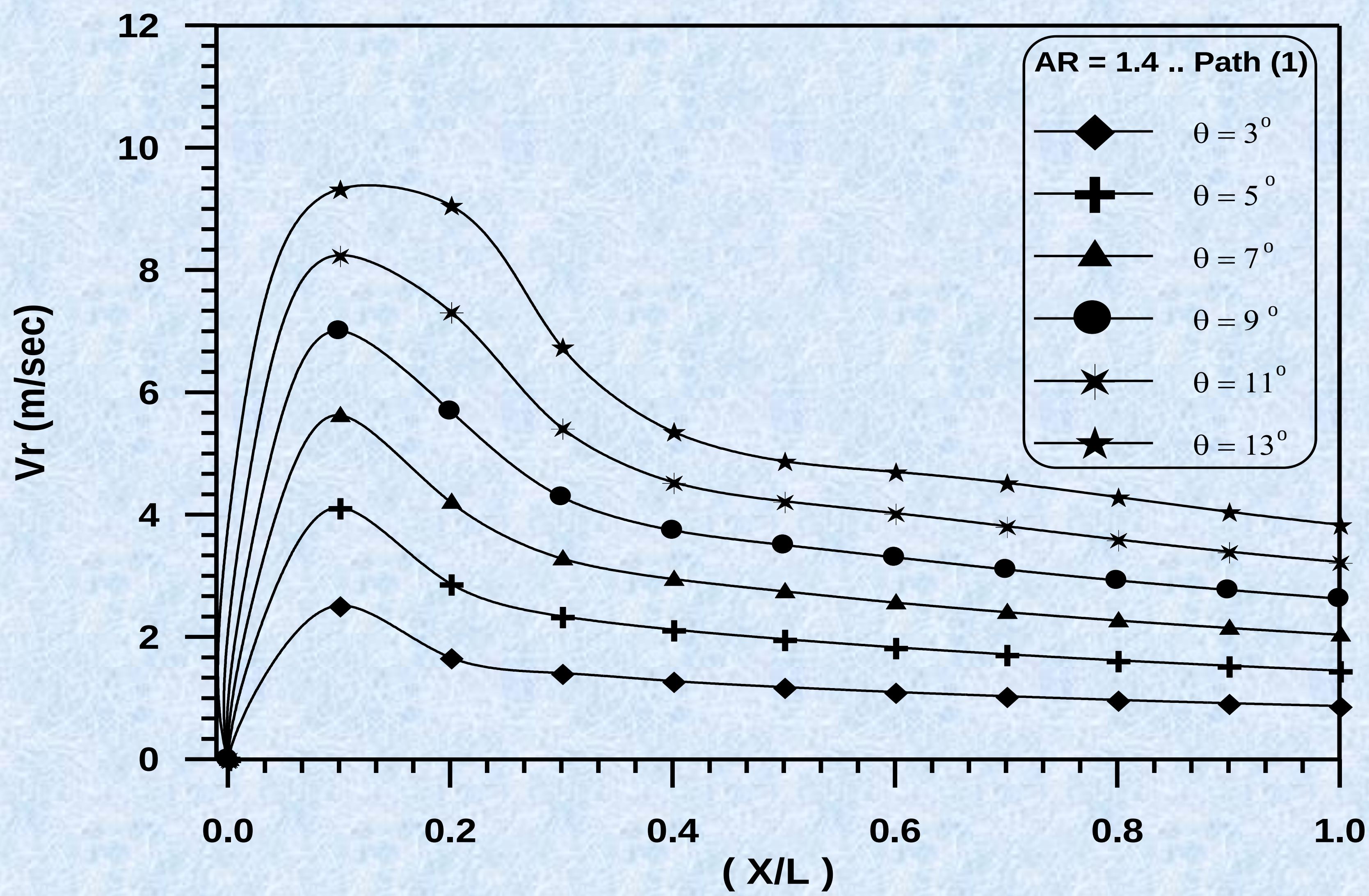

Fig. (24) Flow radial velocity component across the diverge portion of intake.

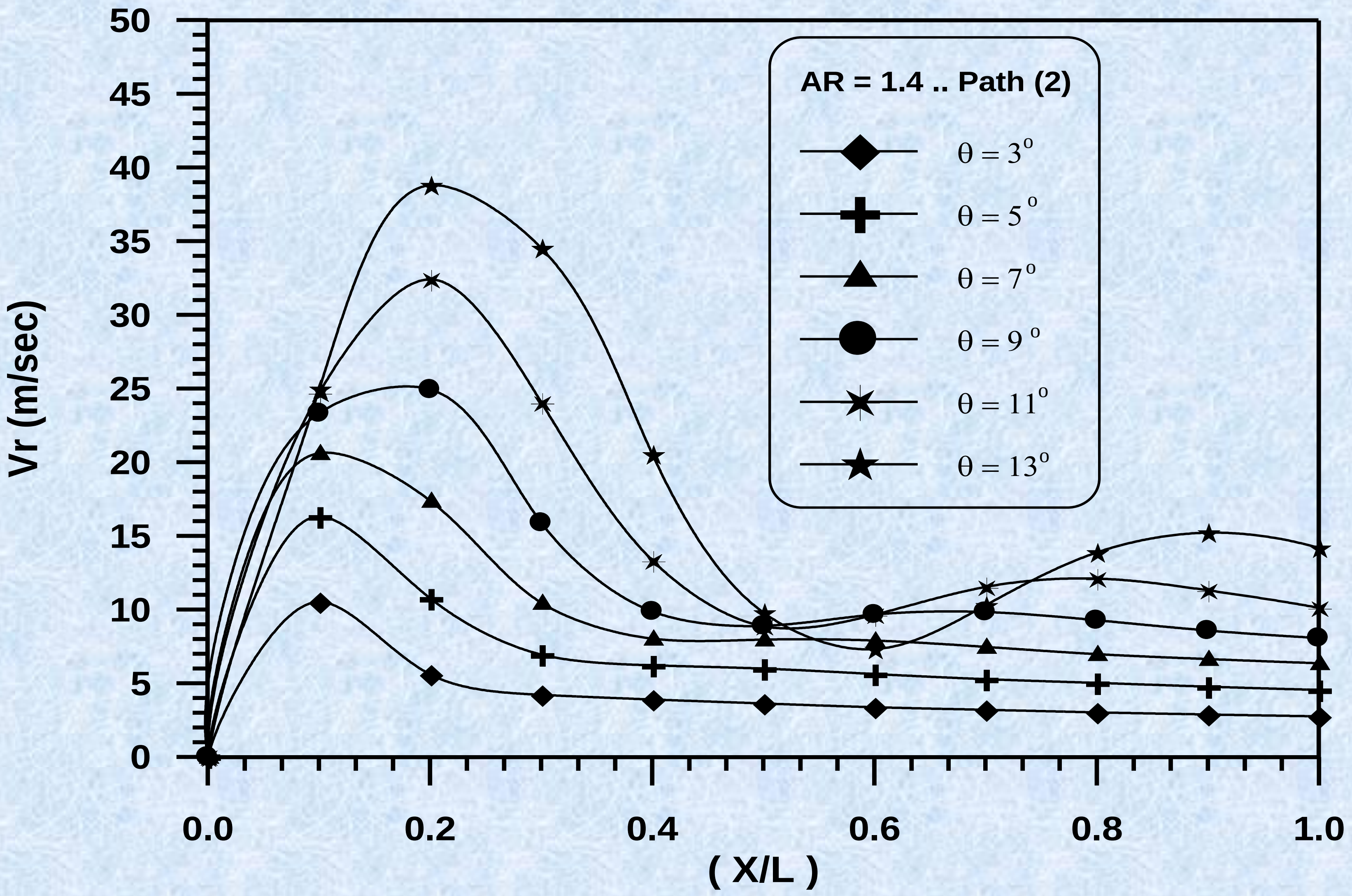

Fig. (25) Flow radial velocity component across the diverge portion of intake.

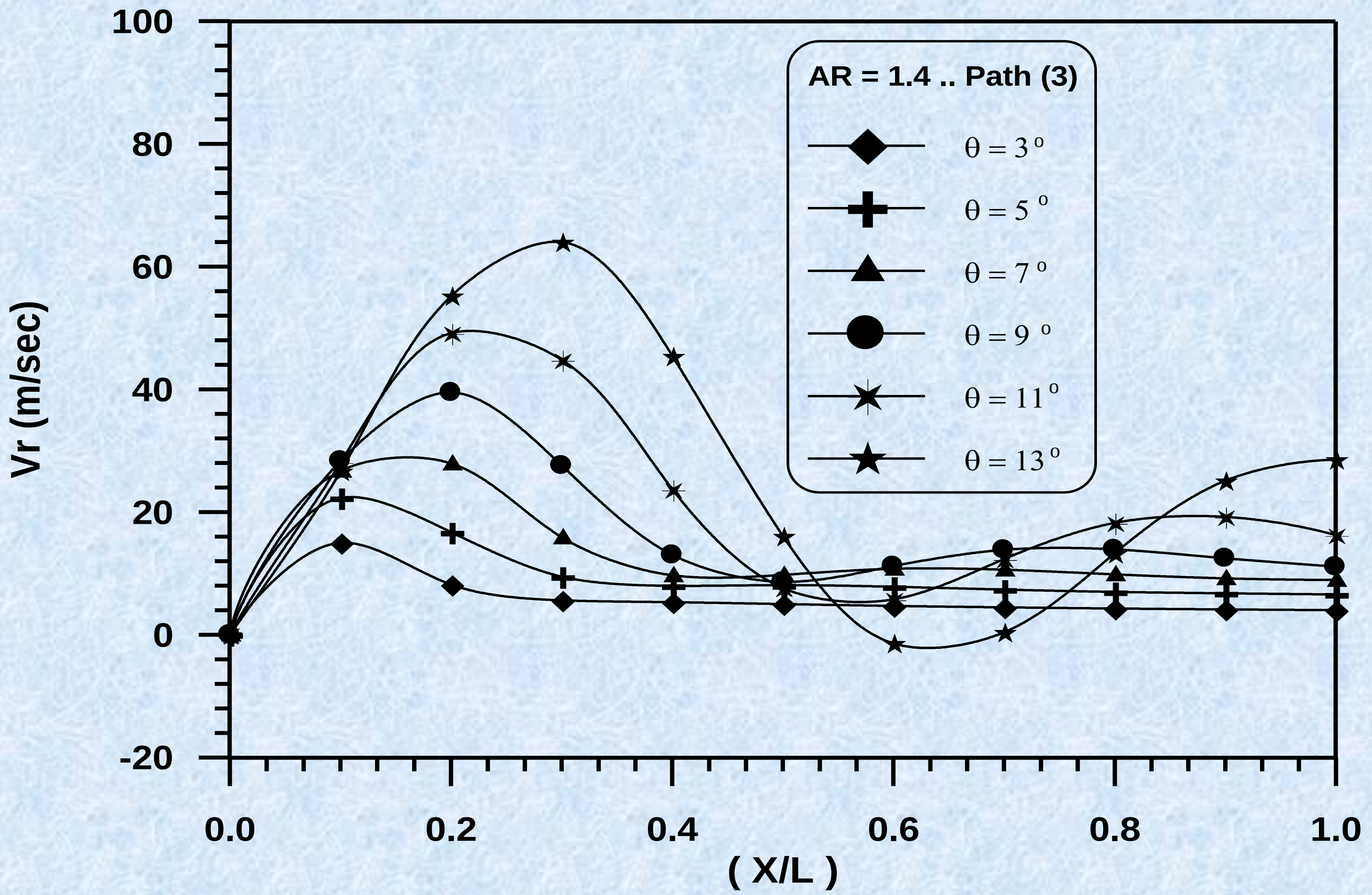

Fig. (26) Flow radial velocity component across the diverge portion of intake.

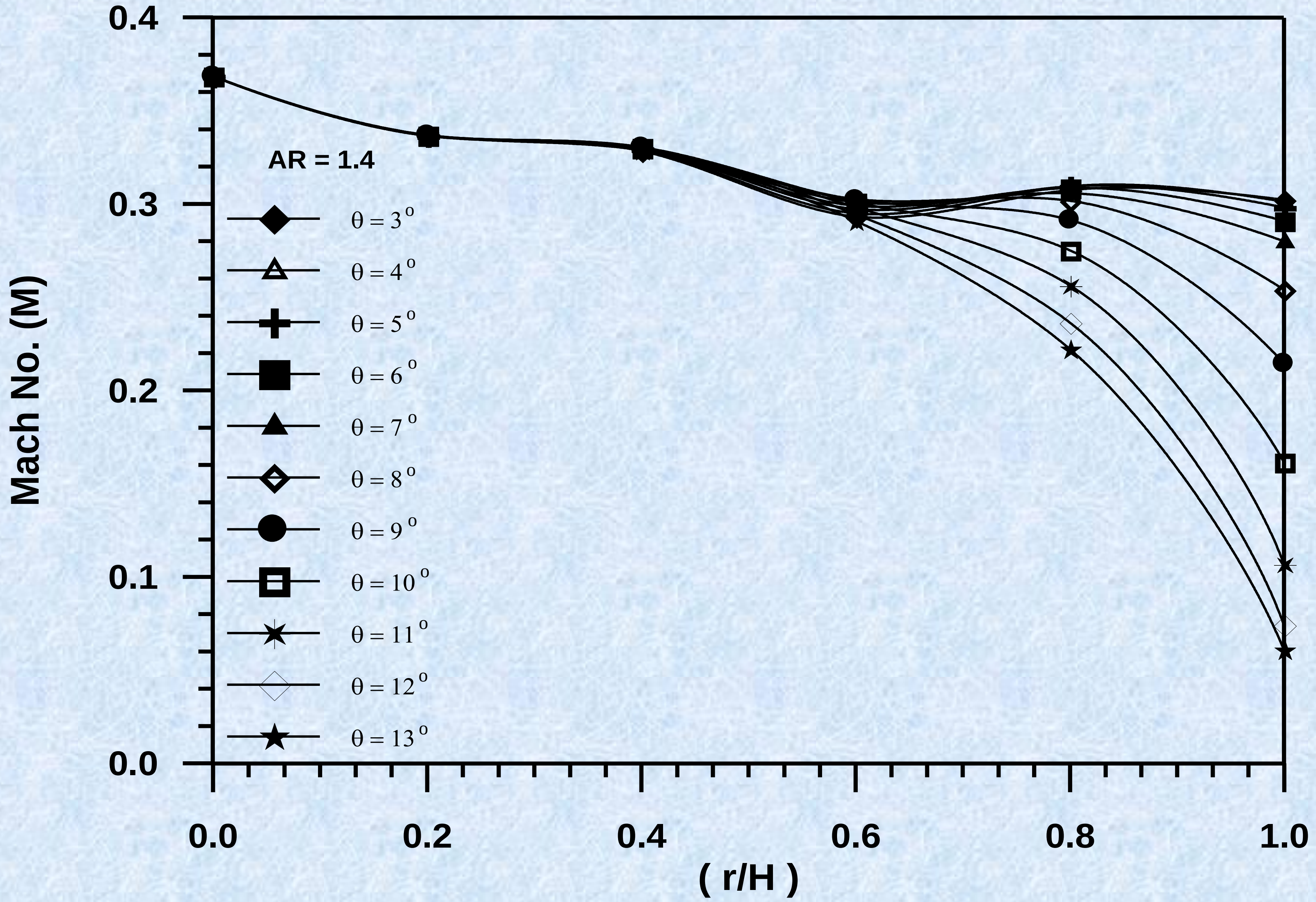

Fig. (27) Mach number distribution at the exit section.

7-Results Of Performance: -

The performance study was done at on and off design conditions by offer of properties of flow along the intake that designed in previous section.

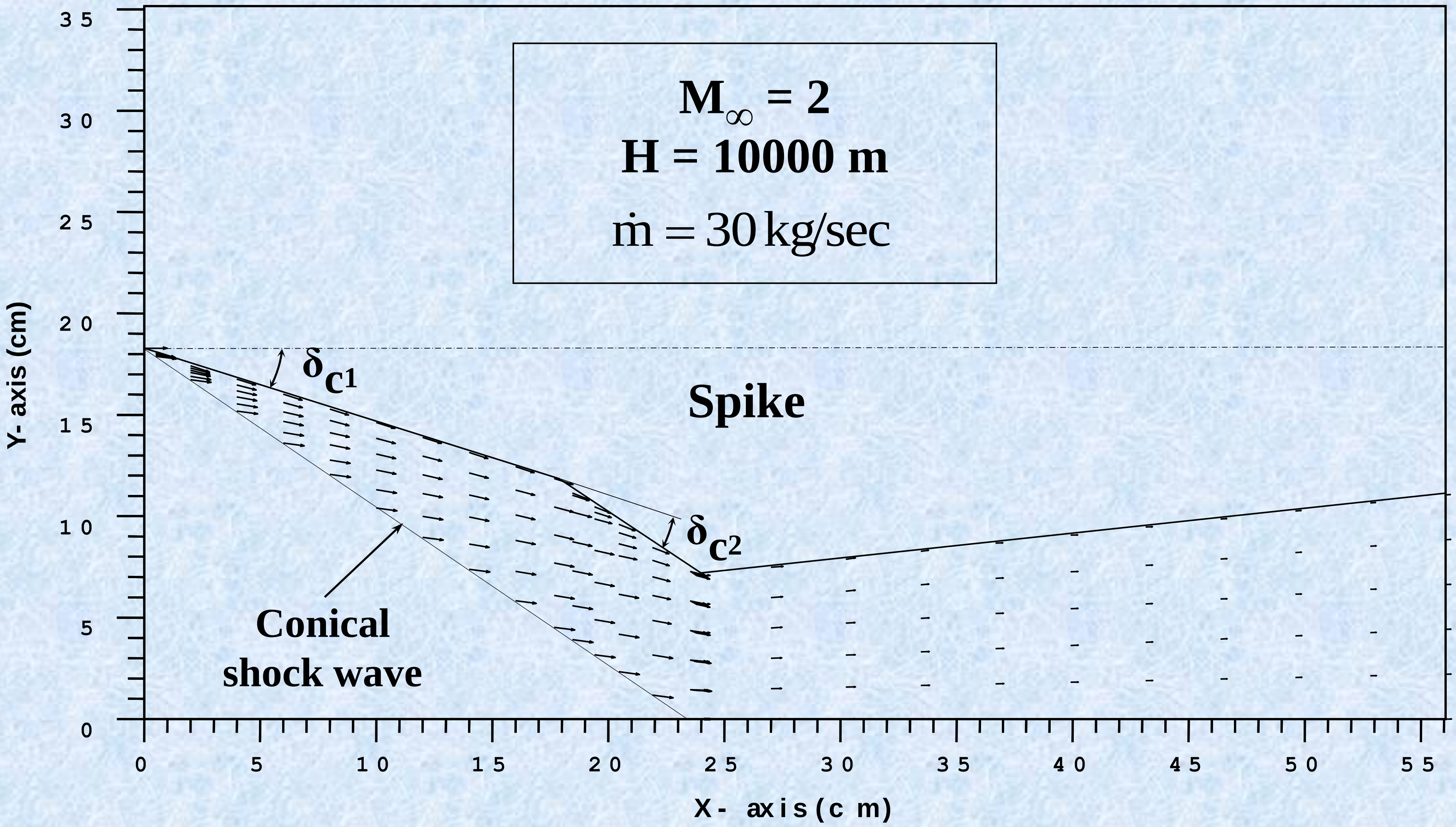

Fig. (28) Vector plot distribution along supersonic air intake.

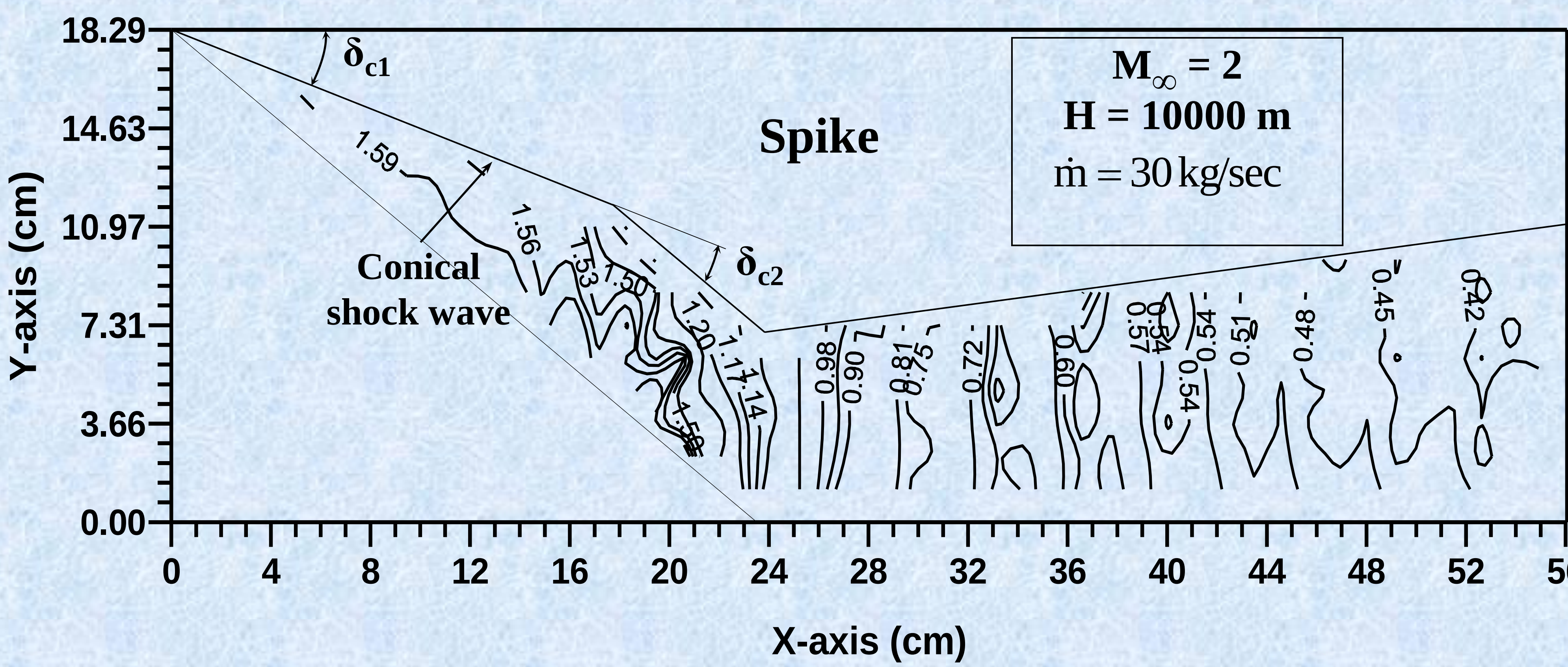

Fig. (29) Mach number (M) distribution along supersonic air intake.

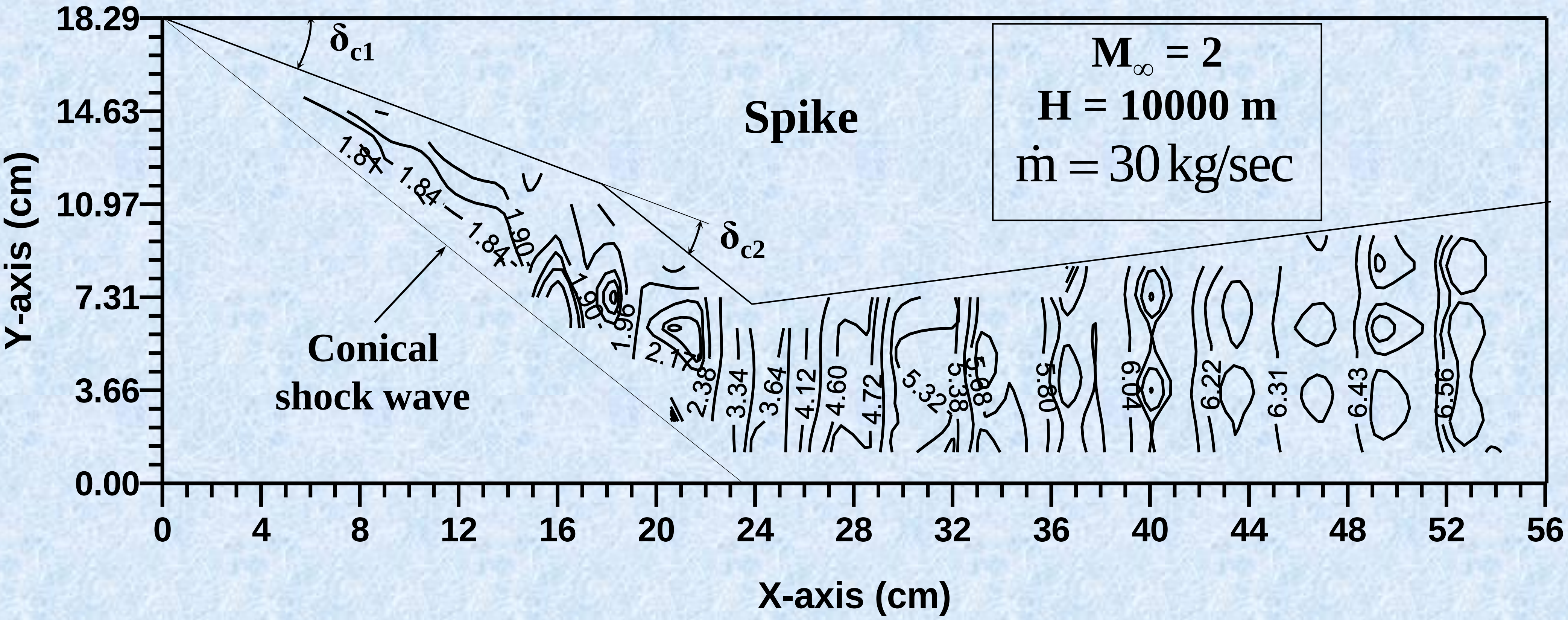

Fig. (30) Pressure ratio ($\frac{P}{P_\infty}$) distribution along supersonic air intake.

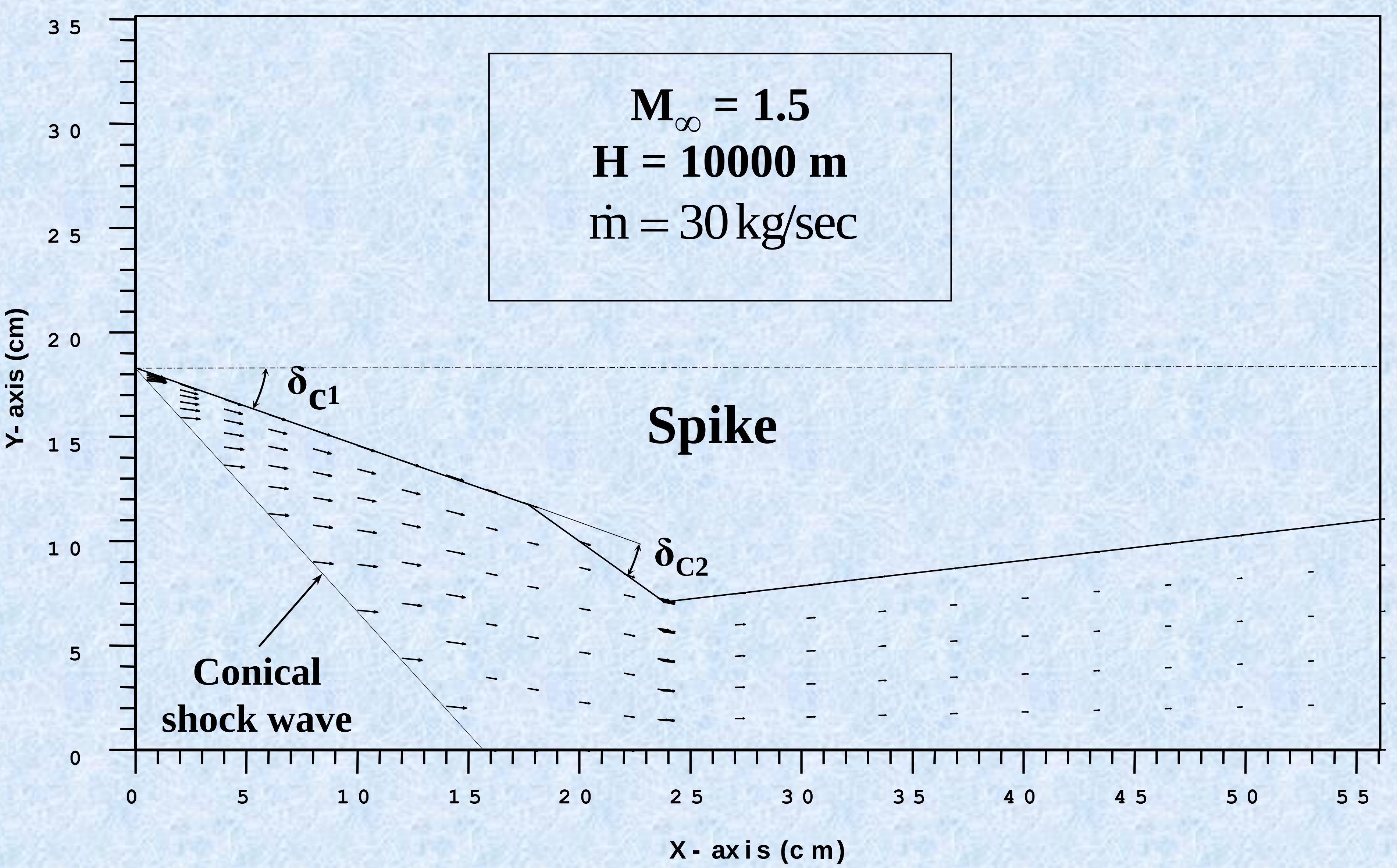

Fig. (31) Vector plot distribution along supersonic air intake.

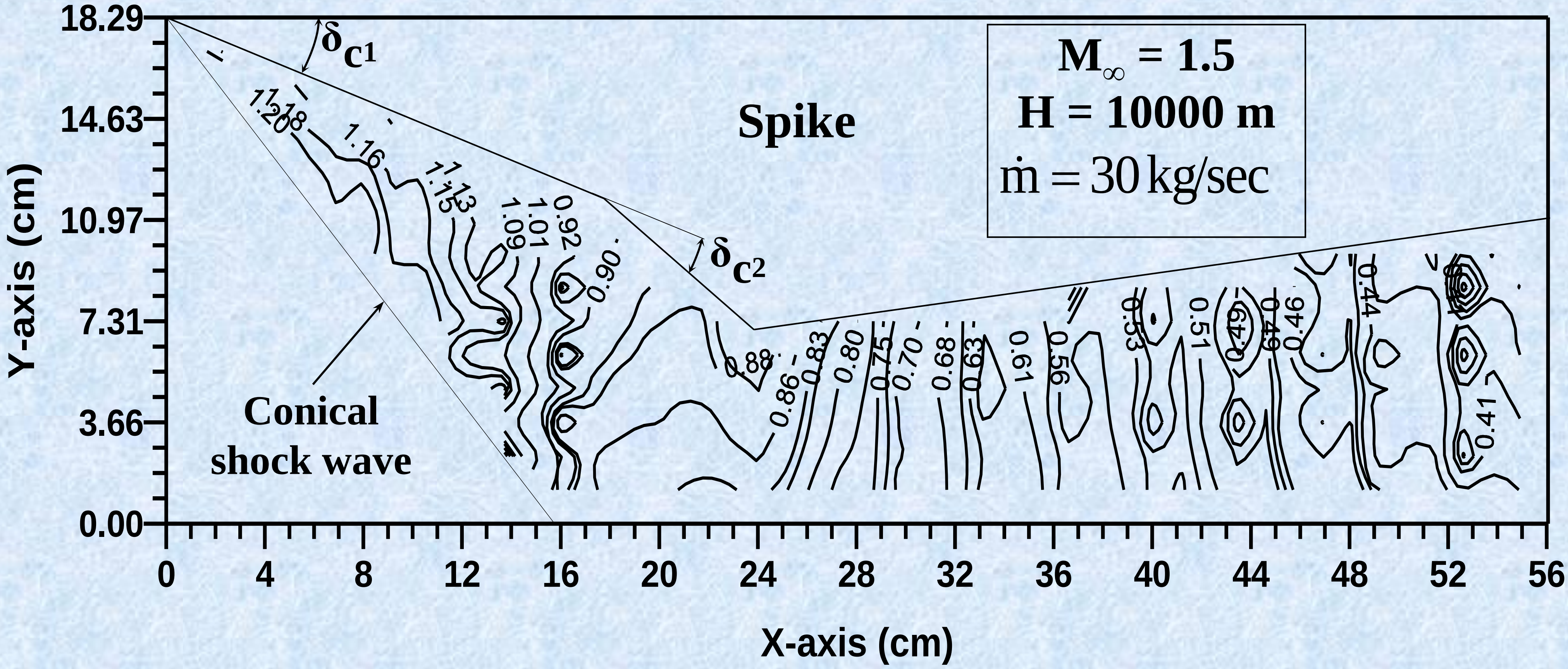

Fig. (32) Mach number (M) distribution along supersonic air intake.

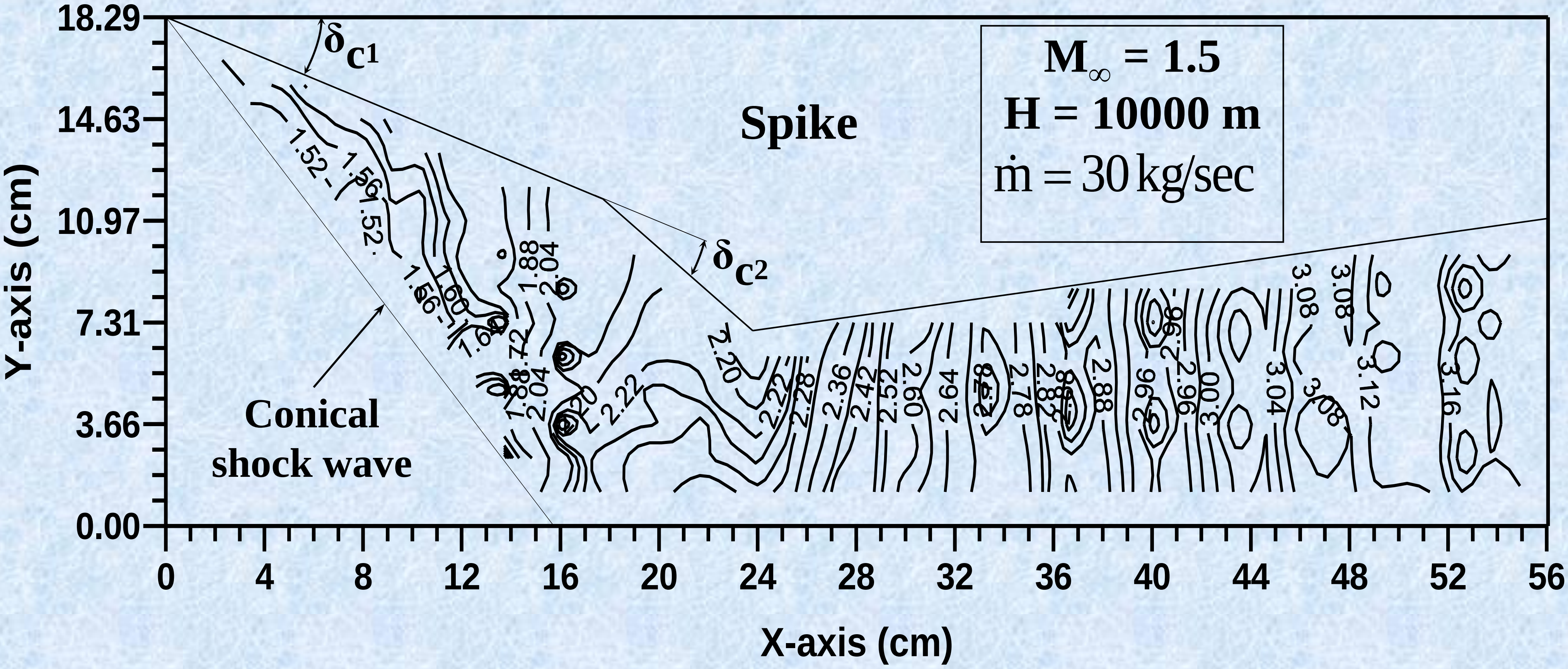

Fig. (33) Pressure ratio ($\frac{P}{P_\infty}$) distribution along supersonic air intake.

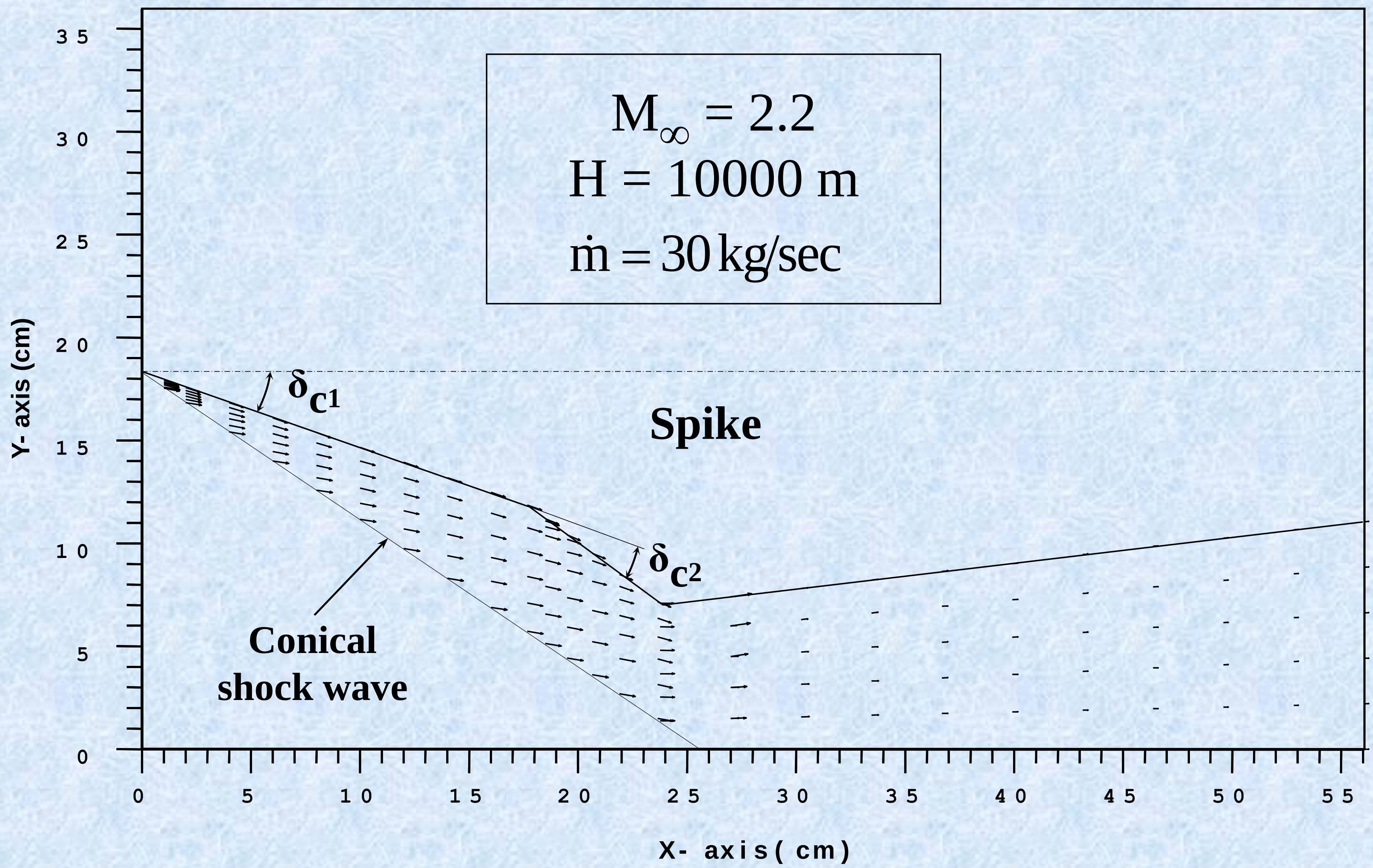

Fig. (34) Vector plot distribution along supersonic air intake.

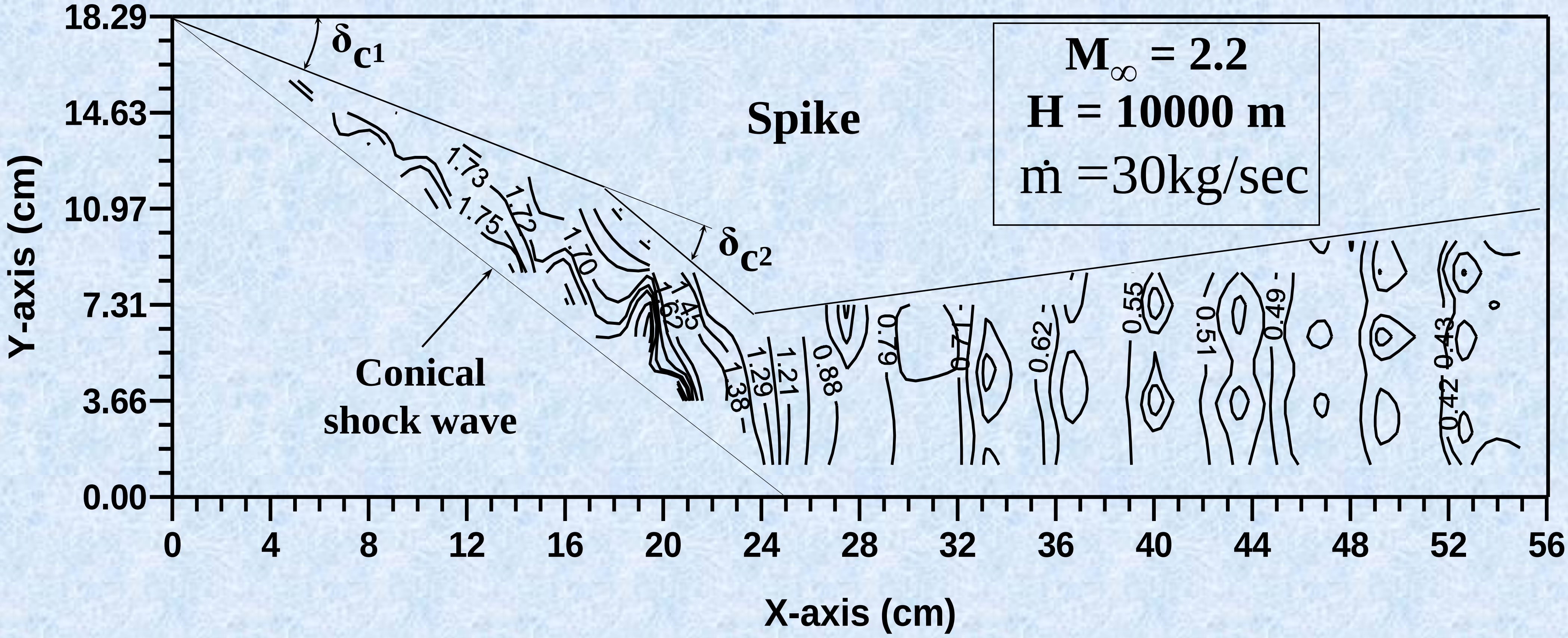

Fig. (35) Mach number (M) distribution along supersonic air intake.

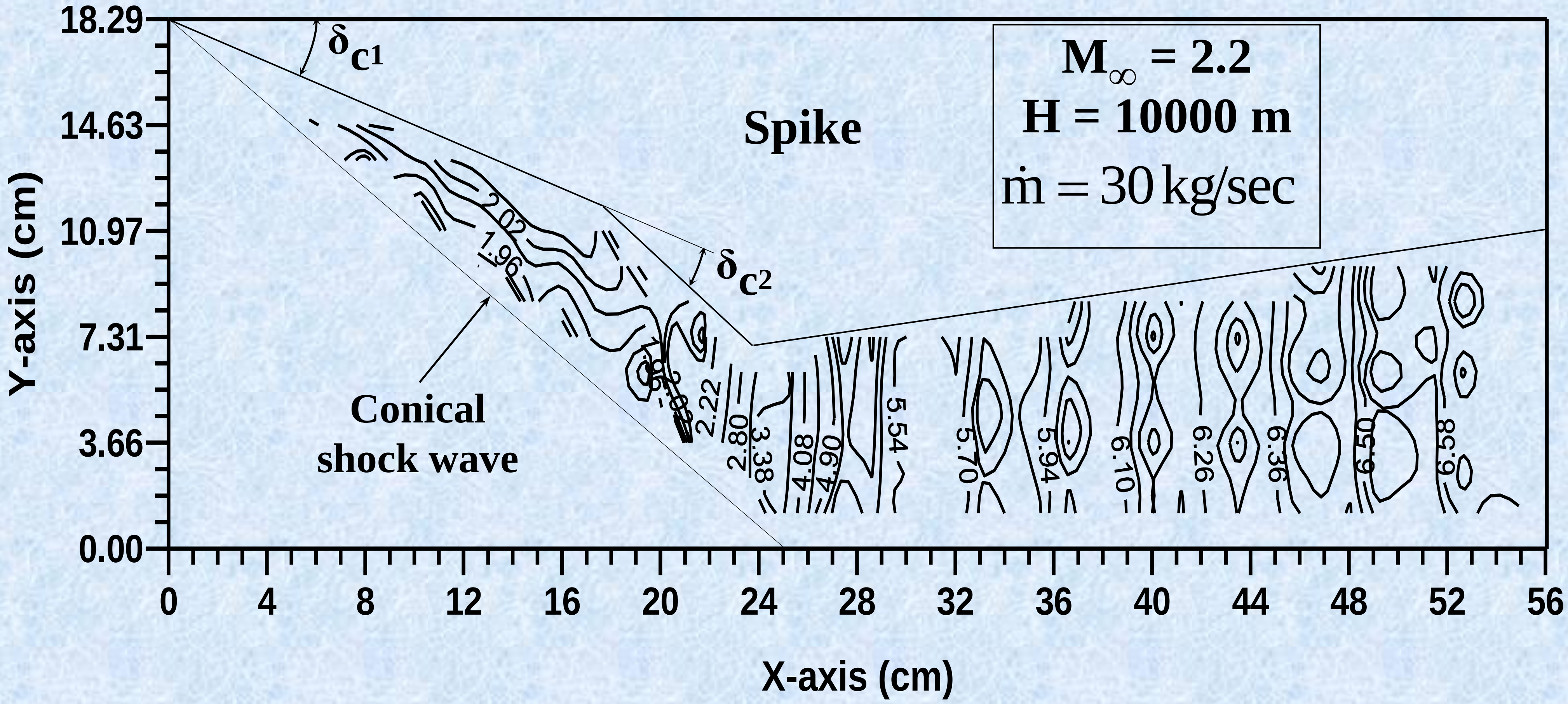

Fig. (36) Pressure ratio ($\frac{P}{P_\infty}$) distribution along supersonic air intake.

8-Conclusions: -

The conclusions of this study may be classified into two parts according to parts of intake under study: -

8.1- External Part: -

1. **The flow over the cone is complex, where this flow has curve form, so it is non-uniform, thus, its properties are non-uniform, so it needs to three dimensions to study (or quasi-three dimensions (axisymmetric)).**

2. **The program written was used successfully to solve equations (Momentum and continuity) for the compressible, steady state and quasi three-dimensional (axisymmetric (annular diffuser)) inviscid flow, to analyze the flow over the cone and predict the optimum design for the external part of supersonic air intake.**

3. **The flow which is initially supersonic just behind the shock front may either remain supersonic or go over to a subsonic flow at some surface (θ = constant (the sonic cone or sonic line)). Where in the latter case, the flow field is mixing supersonic and subsonic. Finally, a flow, which is initially subsonic behind the shock, will necessarily remain subsonic.**

4. **The total pressure recovery ($P_{o3}/P_{o\infty}$) increases with increasing the first cone angle for range ($10^o - 20^o$) for constant second cone angle until it reaches to maximum value then decreases for range ($21^o - 24^o$). Also total pressure recovery increases with increasing the second cone angle for constant first cone angle but at different range then drop. So the optimum first and second cone angle was (20^o) and (18^o) respectively, as shown in Fig. (12).**

8.2- Internal Part: -

1. **The program written was used successfully to solve equations (Momentum, continuity, energy, and state) for the compressible, steady state and quasi three-dimensional (axisymmetric) annular diffuser to analyze and predict the optimum design of this part.**

2. **The results indicated that the axial velocity component (v_x) for paths (1) and (2) decreases with distance and increases with increase of the angle for the same area ratio near inlet and approximately the same value at exit. Also these values decreases with the increase area ratio for the same angle. For path (3) and for angles ($3^o - 7^o$) the velocity behave as in paths (1) and (2), and for large than these angles the velocity decreases with the distance until it reaches to minimum value at large angle then increases to normal value at diffuser exit for the same area ratio. This behavior eliminates gradually with the increase area ratio for the same angle.**

3. The radial velocity component (v_r) for path (1) increases with distance until it reaches to maximum value near the inlet, then decreases then level out, at the same angle for all area ratio. Also the velocity increases with increase of the angle for the same area ratio. For paths (2) and (3) and for angle ($3^o - 7^o$) the velocity behaves as in path (1). For large than these angles the velocity increases with distance then decreases until it reaches minimum value at large angle then increases to normal value at diffuser exit for the same area ratio. This behavior eliminate gradually with increase of the area ratio for the same angle

4. Mach number (M) behaves as axial velocity in paragraph (2). Mach number at the exit section decreases from high to low values (subsonic) with the increase distance from straight to diverge wall.

5. From studying the results of the analysis of flow through the divergent portion for several models, the geometry data for optimum design found are: -

   AR = 1.35,

   $\theta = 7^o$

9- Geometry Data For Optimum Design Of Supersonic Air Intake: -

From studying the results of the analysis of the flow through the external and internal parts of supersonic air intake, for several models the geometry data for optimum design found are: -

δc1 = 20°.	hco = 23.525 cm.	L1 = 2.5 mm.
δc2 = 18°.	r1 = 7.27798 cm.	L2 = 32.28 cm.
LN = 23.5247 cm.	rth = 7.083 cm.	θ = 7°.
LW = 17.664 cm.	r2 = 11.046 cm.	Loverall = 56.056 cm.

10- Recommendation: -

The following recommendations are suggested for a further work to achieve a complete analysis and design of supersonic air intake: -

1. **Developing the work by employing non-zero angle of attack (non-axisymmetric).**

2. **Design of the transient section (Throat section), which includes the cowl lip and the surface of spike.**

3. **Developing the work by employing viscous flow, and comparing the results with the present (unviscous).**

4. **Change the geometry of the spike as the follows: -**

- **4-shock system (Three - cone).**
- **Isentropic compression system.**

5. **Employing another technique to solve the governing differential equations, such as characteristic method, finite element method and MacCormack method.**

Thank You for listen and

Iam ready to any Question